Norwegian University of Life Sciences
Faculty of Veterinary Medicine

Philosophiae Doctor (PhD)
Thesis 2023:49

Pulmonary micrometastasis and immunological pre-metastatic niche in dogs with osteosarcoma

Mikrometastatisk kreftspredning til lungene og immunologisk premetastatisk nisje hos hunder med beinkreft

Mikael Mathias Kolmannskog Kerboeuf

Pulmonary micrometastasis and immunological pre-metastatic niche in dogs with osteosarcoma

Mikrometastatisk kreftspredning til lungene og immunologisk premetastatisk nisje hos hunder med beinkreft

Philosophiae Doctor (PhD) Thesis

Mikael Kerboeuf

Norwegian University of Life Sciences
The PhD programme in Veterinary Sciences
at the
Faculty of Veterinary Medicine

Ås 2023

Thesis number 2023:49
ISSN 1894-6402
ISBN 978-82-575-2078-6

PhD Supervisors

Kristin P. Anfinsen, Cand.Med.Vet, MVetMed, PhD, DACVIM (SAIM), DECVIM-CA
Associate Professor
Department of Companion Animal Clinical Sciences
Faculty of Veterinary Medicine
Norwegian University of Life Sciences (NMBU), Ås, Norway

Lars Moe, Cand.Med.Vet, PhD
Professor Emeritus
Department of Companion Animal Clinical Sciences
Faculty of Veterinary Medicine
Norwegian University of Life Sciences (NMBU), Ås, Norway

Erling O. Koppang, Cand.Med.Vet, PhD
Professor
Department of Preclinical Sciences and Pathology
Faculty of Veterinary Medicine
Norwegian University of Life Sciences (NMBU), Ås, Norway

Preben Boysen, Cand.Med.Vet, PhD
Professor Department of Preclinical Sciences and Pathology
Faculty of Veterinary Medicine
Norwegian University of Life Sciences (NMBU), Ås, Norway

David Argyle, DVM, BVMS, PhD, DECVIM-CA. FRSE, FRSA, FRCVS
Professor
Royal (Dick) School of Veterinary Studies and Roslin Institute
The University of Edinburgh, Midlothian, Scotland.

Acknowledgements

The work contained within this thesis was carried out at the Department of Companion Animal Clinical Sciences, and the Department of Preclinical Sciences and Pathology, Faculty of Veterinary Science at the Norwegian University of Life Sciences (NMBU). Our collaborators at The Royal (Dick) School of Veterinary Studies and Roslin Institute, Edinburgh, and the Norwegian Radium Hospital have also contributed considerably to this project. The project was generously funded by the Faculty of Veterinary Medicine (NMBU, Norway), the Research Fund for Cancer in Dogs (Norway), the Norwegian Research Council (Norway), the Small Animal Practice Veterinary Association's (SVFs) Scientific and Professional Fund (Norway), the Astri and Birger Torsteds Foundation (Norway), and Agria and the Swedish Kennel Klub (SKK) Research Fund (Sweden). Before we embark on this thesis, I want to extend my deepest gratitude to everyone who has helped me on this journey.

First, I would like to thank **Lars Moe**, my original main supervisor. He always picks up the phone when I have questions and is never too busy to offer guidance and help. No matter the time of day (or night), he will always find time to look through whatever document or application I send him or participate in an evening necropsy of a newly recruited case. Without his support and dedication, this project would not have been possible.

Second, I would like to thank **Anita Haug Haaland**, who also, for a time, had the role of main supervisor. Her ability to concretize floating ideas and thoughts into solid plans and ideas has been important for defining a clear path for the project. Her skills in academic writing and critical thinking have been invaluable when writing and drawing conclusions from our results.

Third, I would like to thank **Kristin Paaske Anfinsen**, who agreed to take over the main supervisor torch, despite having a busy clinical schedule. Her immense work capacity and effectiveness have been paramount for finalising my thesis despite only being involved in the later stages of the project. Her skills in academic writing and ability to approach the subject matter from a different point of view have been very helpful and, hopefully, made my thesis more relatable to a broader audience.

I would also like to thank **Preben Boysen** and **Erling Olaf Koppang**, who helped me understand the laboratory methods that I used in the project. Thanks to both, I have been able to perform these methods autonomously and get a broader understanding of the available techniques in research. In addition, they both gladly answer the phone whenever I call and always have time to discuss design, methods, and results. Their contributions to the manuscripts are also much appreciated.

I would also like to thank **Øyvind Bruland** and **David Argyle**, who have contributed with material, tools, ideas, and discussions, which have been paramount for completing this project. Furthermore, I would also like to thank them for introducing me to new people I hope to work with in the future.

I would also like to extend my gratitude to the technicians working in the immunology (**Grethe Marie Johansen**) and pathology departments (**Aleksandra Bodura Göksu, Mari Katharina Aas Ådland, Soheir Chahine Al Taoyl,** and **Sigbjørn Lunner**). Whenever I needed help, they always had time to show me how to do things and suffered the mess I made while working. I would also like to thank the **veterinary technicians** in the clinic who helped me with the blood sampling of dogs.

I would also like to acknowledge **Kjetil Dahl** (deceased), who originally started this project with **Frode Lingaas** and **Lars Moe**. This project would not have existed had it not been for their contributions. Furthermore, their collaboration with Evidensia Oslo Animal Hospital was also vital for recruiting cases for the project.

Mikael Kerboeuf

Oslo, April 2023

Table of Contents

1 Abbreviations and definitions

AEC	3-amino-9-ethyl carbazole
Ang-2	Angiopoietin 2
APC	Allophycocyanin
AR	Antigen retrieval
Arg-1	Arginas-1
ATP	Adenosine triphosphate
BCG	Bacillus Calmette-Guérin
BMDC	Bone marrow-derived cell
BSA	Bovine serum albumin
CAF	Cancer-associated fibroblast
CCL	Chemokine C-C motif ligand
CD	Cluster of differentiation
cDNA	Complementary DNA
CDX	Cell line-derived xenograft
CFSE	Carboxyfluorescein succinimidyl ester
COX	Cyclooxygenase
CR	Complete regression
CSF-1	Macrophage-colony stimulating factor
CTLA4	Cytotoxic T-lymphocyte associated protein 4
CXCL	Chemokine C-X-C motif ligand
CX3CL	Chemokine C-X3-C motif ligand
DAB	Diaminobenzidine
DAPI	4',6-diamidino-2-phenylindole
DC-SIGN	Dendritic cell-specific C-type lectin
DEG	Differentially expressed gene
DFI	Disease-free interval
DYAR	Dog-years at risk
ECM	Extracellular matrix

EDTA	Ethylenediamine tetraacetic acid
ELISA	Enzyme-linked immunosorbent assay
EMT	Epithelial-mesenchymal transition
EV	Extracellular vesicle
FBS	Foetal bovine serum
Fc	Fragment crystallisable
FFPE	Formalin-fixed paraffin-embedded
FISH	Fluorescent *in situ* hybridization
FITC	Fluorescein isothiocyanate
FMO	Fluorescence minus one
FSC	Forward scatter
GEM	Genetically engineered mouse
GFP	Green fluorescent protein
G-CSF	Granulocyte-colony stimulating factor
HGF	Hepatocyte growth factor
HIAR	Heat-induced antigen retrieval
HIF1α	Hypoxia-inducible factor 1-α
HPF	High-power fields
IF	Immunofluorescence
IFN- γ	Interferon-γ
IHC	Immunohistochemistry
IL	Interleukin
iPSC	Induced pluripotent stem cell
iTreg	Induced regulatory T-Lymphocyte
LPS	Lipopolysaccharides
LYVE-1	Lymphatic vessel endothelial receptor 1
MARCO	Macrophage receptor with collagenous structure
MDSC	Myeloid-derived suppressor cells
MFG-E8	Milk fat globule-EGF factor 8
MFI	Mean fluorescent intensity
miRNA	MicroRNA
MMP	Matrix metalloproteinase

mRNA	Messenger RNA
MST	Median survival time
MTP	Muramyl tripeptide
M-CSF	Macrophage-colony stimulating factor
NF-κB	Nuclear factor kappa-light-chain-enhancer of activated B cells
NGS	Next-generation sequencing
NK	Natural killer
NOD2	Nucleotide-binding oligomerization domain 2
NSAID	Non-steroidal anti-inflammatory drug
nTreg	Natural regulatory T-Lymphocyte
OS	Osteosarcoma
PBMC	Peripheral blood mononuclear cells
PBS	Phosphate-buffered saline
PCR	Polymerase chain reaction
PD	Programmed cell death protein
PD-L	Programmed death-ligand
PDX	Patient-derived xenograft
PE	Phycoerythrin
PET	Positron emission tomography
PI	Propidium iodide
piRNA	Piwi-interacting RNA
PMN	Pre-metastatic niche
PNiPAAm	Poly(N-isopropylacrylamide)
P/S	Penicillin/streptomycin
qPCR	Quantitative polymerase chain reaction
RBC	Reb blood cell
RFP	Red fluorescent protein
RIN	RNA-integrity number
RNA-Seq	RNA-sequencing
ROS	Reactive oxygen species
RPMI	Roswell Park Memorial Institute
rRNA	Ribosomal RNA

SCC	Side scatter
TAM	Tumour-associated macrophage
TAN	Tumour-associated neutrophil
TBS	Tris-buffered saline
TCM	Tumour-conditioned media
TCMΦ	Tumour-conditioned macrophage
TCR	T-cell receptor
TGF-β	Transforming growth factor-β
Th	T helper lymphocyte
TLR	Toll-like receptor
TME	Tumour microenvironment
TNF-α	Tumour necrosis factor-α
TP-3	Tumour protein-3
Treg	Regulatory T-lymphocytes
TREM2	Triggering-receptor-expressed on myeloid cells 2
TRM	Tissue-resident macrophages
VCAM	Vascular cell adhesion molecule-1
VEGF	Vascular endothelial growth factor
VEGFR	Vascular endothelial growth factor receptor

2 List of papers

Early immunohistochemical detection of pulmonary micrometastases in dogs with osteosarcoma.
Mikael Kerboeuf, Erling Olaf Koppang, Anita Haug Haaland, Frode Lingaas, Øyvind Sverre Bruland, Jon Teige and Lars Moe, *Acta Vet Scand*, 41 (2021)
https://doi.org/10.1186/s13028-021-00608-9

Canine *in vitro* generated tumor-conditioned macrophages display an M2-skewed phenotype.
Mikael Kerboeuf, Anita Haug Haaland, Lars Moe, David Argyle, Seda Ozaydin, Maciej Parys and Preben Boysen
Manuscript in writing

Immunological premetastatic niche in dogs with naturally occurring osteosarcoma.
Mikael Kerboeuf, Kristin Paaske Anfinsen, Erling Olaf Koppang, Frode Lingaas, David Argyle, Jon Teige, Bente Kristin Sævik and Lars Moe
Manuscript in writing.

"No one man, however brilliant or well-informed, can come in one lifetime to such fullness of understanding as to safely judge and dismiss the customs or institutions of his society, for these are the wisdom of generations after centuries of experiments in the laboratory of history" - Will & Ariel Durant Eller

3 Abstract

Cancer is currently ranked as a leading cause of death in humans and dogs, most often due to metastatic disease. The pre-metastatic niche (PMN) represents the metastasis-supporting microenvironmental changes that occur in a distant target organ before metastasis. The primary tumour shapes the PMN in the metastatic target organ by releasing soluble factors and extracellular vesicles. PMN-formation is an essential step in metastatic development and drives organotropism. Osteosarcoma (OS) is the most common primary bone tumour in dogs and humans, with a high metastatic rate, despite a low metastatic prevalence at diagnosis. Although most dogs develop pulmonary metastases (>90%), the prevalence of micrometastases or PMN formation at diagnosis is unknown.

In this thesis, we assessed the prevalence of pulmonary micrometastases and PMN formation in dogs with OS without macroscopic metastases, focusing on macrophage and bone marrow-derived cell populations. In addition, we assessed the phenotype and transcriptomes of *in vitro*-generated canine monocyte-derived tumour-conditioned macrophages (TCMΦ) and compared them to classically (M1) and alternatively activated (M2) macrophages.

We prospectively enrolled dogs with treatment naïve OS (n=15), which we necropsied and sampled immediately after euthanasia. We divided these dogs into those with macroscopic metastases (n=5) and not (n=10). Control dogs without cancer (n=10), systemic inflammatory diseases, allergy, or atopy, and not receiving immunomodulating drugs were enrolled retrospectively from the pathology archives. Blood from healthy dogs (n=6) was collected to generate macrophages *in vitro*.

We performed chromogenic immunohistochemistry (IHC) with TP-3 to immunolabel micrometastasis in seven frozen lung samples from each dog with OS without metastases. We labelled samples from two dogs with OS with macroscopic metastases and two without cancer as controls. *In vitro* generated TCMΦ were compared to M1 and M2 macrophages using flow cytometry (CD206, CD209, CD11d,

FcεRI, and LYVE-1) and RNA-sequencing. A lung sample from each of the 15 dogs with OS and ten control dogs without cancer was immunolabelled using multiplex immunofluorescence (CD204, CD206 and CD11d) to identify macrophages, their phenotype, and bone marrow-derived cells.

The main findings were:

- Pulmonary micrometastases could be detected with TP-3 immunohistochemistry in a subset of dogs with OS before macroscopic metastases had developed. The prevalence of micrometastases (20%) was significantly lower than expected based on post-surgical metastatic rates.

- TCMΦ had a high expression of several M2-associated phenotypical markers on flow cytometry, while RNA-Seq showed upregulation of several additional M2-markers. TCMΦ had an M2-skewed cytokine and chemokine profile and exhibited several similarities to human and murine TCMΦ.

- The number of $CD204^+$ macrophages, $CD206^+$ macrophages and monocytes, and $CD11d^+$ bone marrow-derived cells (BMDCs) in the lungs of dogs with OS without metastases was significantly higher than in dogs without cancer. Similarly, the total nucleated cell count was higher in dogs with OS than in those without cancer. Dogs with established pulmonary metastases had significantly lower numbers of $CD11d^+$ BMDCs than dogs with OS without metastases.

In summary, this thesis provides new insight into the early phases of metastasis in dogs with OS. Furthermore, the results help bridge the knowledge gap between canine and human tumour immunology and provides new markers to study tumour-associated macrophages (TAMs) in dogs. In addition, our findings support the existence of an immunological PMN in a naturally occurring cancer model.

4 Norsk sammendrag

Kreft er i dag ansett som vanligste dødsårsaken hos både mennesker og hunder, som oftest som følge av spredning av kreftsykdommen (metastatisk sykdom). Den premetastatiske nisjen (PMN) defineres som de metastasefremmende endringene som skjer i mikromiljøet i et organ der det kommer til å utvikles spredninger. Primærsvulsten danner den PMN i slike målorganer ved hjelp av løselige stoffer og ekstracellulære vesikler som føres med blodet. PMN-dannelse anses som et viktig steg i utviklingen av spredninger og er med på å bestemme hvor svulsten sprer seg. Osteosarkom (OS) er den vanligste primærsvulsten som oppstår i knoklene hos både mennesker og hunder, og har en stor evne til å metastasere på tross av en lav metastaseforekomst ved diagnosetidspunktet. Selv om de fleste hunder med OS utvikler lungemetastaser (>90%), er forekomsten av mikrometastaser og PMN dannelse ved diagnosetidspunktet ukjente.

I denne avhandlingen har vi undersøkt forekomsten av mikrometastaser og PMN dannelse, med fokus på makrofager og celler fra beinmargen, hos hunder med OS uten synlige metastaser. I tillegg har vi undersøkt fenotypiske egenskaper og genuttrykket til *in vitro*-produserte tumorkondisjonerte makrofager (TCMΦ). Disse makrofagene ble sammenliknet med klassisk aktiverte (M1) og alternativt aktiverte (M2) makrofager.

Vi rekrutterte hunder med OS som ikke hadde fått noen form for kreftbehandling (n=15) prospektivt og obduserte og samlet prøver fra disse umiddelbart etter avliving. Disse hundene ble så delt inn i to grupper; de med synlige metastaser (n=5) og de uten (n=10). Vi rekrutterte også kontrollhunder (n=10) retrospektivt fra patologiarkivene. Disse kontrollhundene var frie for systemiske inflammatoriske sykdommer og allergier, og hadde ikke stått på medisiner som kunne påvirke immunforsvaret. Vi samlet også blod fra friske hunder (n=6) for å produsere makrofager *in vitro*.

Vi gjennomførte immunhistokjemisk (IHC) farging, med TP-3, av syv nedfryste lungeprøver fra hver av hundene med OS uten metastaser for å identifisere

mikrometastaser. I tillegg farget vi prøver fra to hunder med OS med metastaser og to hunder uten kreft som kontroller. *In vitro*-produserte TCMΦ ble sammenliknet med M1 og M2 makrofager ved hjelp av flowcytometri (med følgende markører: CD206, CD209, CD11d, FcεRI og LYVE-1) og RNA sekvensering. Én lungevevsprøve fra hver av de 15 hundene med OS og fra de 10 kontrollhundene uten kreft ble farget ved hjelp av immunfluoresens med følgende markører: CD204, CD206 og CD11d, for å kartlegge forekomsten av makrofager og deres fenotype, samt forekomsten av celler fra beinmargen (beinmargsderiverte celler, BMDCs).

Hovedfunnene våre var:

-Vi påviste mikrometastaser i lungene hos kun en liten andel av hundene med OS før de hadde utviklet synlige lungemetastaser ved hjelp av TP-3 immunhistokjemi. Forekomsten av lungemikrometastaser (20%) var betydelig lavere enn forventet basert på forekomsten av lungemetastaser etter fullstendig kirurgisk fjerning av primærsvulsten.

-TCMΦ hadde et høyt uttrykk av flere M2-typiske fenotypiske overflatemarkører ved flowcytometri. RNA-sekvensering viste i tillegg at ytterligere M2-typiske markører var oppregulerte i TCMΦ. Cytokin- og kjemokinprofilene til TCMΦ liknet på dem hos M2 makrofager og også på dem hos TCMΦ fra mennesker og mus.

-Forekomsten av $CD204^+$ makrofager, $CD206^+$ makrofager og monocytter, og $CD11d^+$ BMDCs var høyere i lungene til hundene med OS uten metastaser enn hos hundene uten kreft. I tillegg var det totale antallet kjerneholdige celler høyere hos hunder med OS enn hos dem uten kreft. Hundene med etablerte lungemetastaser hadde betydelig lavere antall $CD11d^+$ BMDCs i lungene enn hundene med OS uten synlige metastaser.

Resultatene i denne avhandlingen bidrar med ny kunnskap om de tidlige fasene av den metastatiske utviklingen hos hunder med OS. De bidrar også til å belyse kunnskapshull i tumorimmunologien hos hund, og vi har funnet nye markører som kan brukes til å studere TAMs hos hund. Funnene våre gir gode holdepunkter for å si at en immunologisk PMN faktisk forekommer hos en modell med naturlig oppstått kreftsykdom.

5 Synopsis

5.1 Introduction

5.1.1 Osteosarcoma

5.1.1.1 Incidence

Osteosarcoma (OS) is the most common primary bone tumour in dogs (Dorfman et al., 1977, Spodnick et al., 1992, Ehrhart, 2013). Accounting for up to 85% of all canine primary bone tumours, OS has an incidence rate of 13.9 to 27.2/100.000 dog-years at risk (DYAR), depending on geographic location, and a lifetime risk of 0.19-10.7% depending on the breed (Egenvall et al., 2007, Anfinsen et al., 2011, Sapierzyński and Czopowicz, 2017). Some large to giant breed dogs have the highest risk of developing OS, such as Saint Bernard dogs, Great Danes, Irish setters, Doberman pinschers, Rottweilers, German Shepherds, Labradors, Boxers, Irish Wolfhounds, Scottish deerhounds, Greyhounds and Leonbergers (Misdorp and Hart, 1979, Spodnick et al., 1992, Ru et al., 1998, Cavalcanti et al., 2004b, Egenvall et al., 2007, Ehrhart, 2013). OS usually affects middle-aged to older dogs (mean age of 7 to 8 years) (Brodey et al., 1963, Misdorp and Hart, 1979, Spodnick et al., 1992, Cavalcanti et al., 2004a, Cavalcanti et al., 2004b, Egenvall et al., 2007, Ehrhart, 2013). A bimodal age distribution has been observed, with a small peak reported at 18-24 months and a larger one at 7-9 years. Most reports indicate that male dogs are more commonly affected than females, yet some have shown the opposite, especially for OS of the axial skeleton (Brodey et al., 1963, Brodey and Riser, 1969, Brodey and Abt, 1976, Misdorp and Hart, 1979, Mauldin et al., 1988, Heyman et al., 1992, Spodnick et al., 1992, Cavalcanti et al., 2004a, Egenvall et al., 2007). Neutering has also been shown to be a risk factor (Ru et al., 1998, Cooley et al., 2002). Most OS tumours arise in the appendicular skeleton (75.0-81,9%), especially in the metaphysis and epiphysis of the long bones, while the rest mainly occur in the axial skeleton (17.1-22,3%) (Brodey et al., 1963, Dorfman et al., 1977, Misdorp and Hart, 1979, Cavalcanti et al., 2004a).

5.1.1.2 Clinical presentation and behaviour

Dogs with appendicular OS usually present with lameness and swelling of the affected limb, while those with OS of the axial skeleton will show variable clinical signs depending on the location (including local swelling, lameness, dysphagia, exophthalmos, facial deformities, and nasal discharge) (Brodey et al., 1959, Brodey et al., 1963, Ling et al., 1974, Ehrhart, 2013). The diagnosis is usually made based on a combination of physical examination findings, diagnostic imaging results (radiographs, computer tomography and magnetic resonance imaging) and evaluation of fine needle aspirates or bone biopsies (Brodey et al., 1959, Brodey et al., 1963, Ling et al., 1974, Davis et al., 2002, Loukopoulos et al., 2005, Neihaus et al., 2011, Karnik et al., 2012, Ehrhart, 2013, Sabattini et al., 2017). Although radiographically detectable metastases are uncommon at presentation (<15-17.1%), most dogs will eventually develop pulmonary (>90%) and osseous metastases when treated with surgery alone, with the majority of dogs (72.5%) being euthanized or succumbing due to metastasis (Ling et al., 1974, Spodnick et al., 1992, Cavalcanti et al., 2004a).

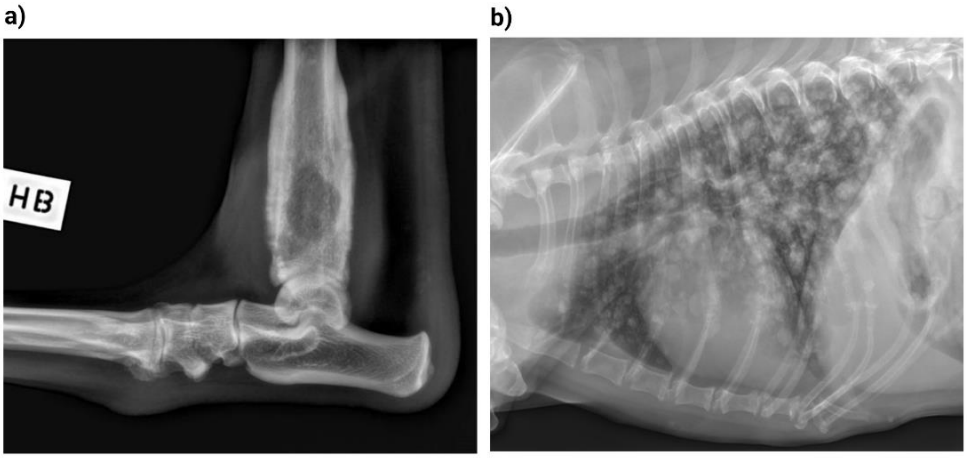

Figure 1: Radiographs of dogs with osteosarcoma (OS). ***a)*** *Radiograph of the right hock from a dog with non-metastatic OS. There is a mixed pattern of central osteolysis of the medullary and cortical bone of the distal tibia and peripheral osteoproliferation over the cortical bone.* ***b)*** *Thoracic radiograph of a dog with OS with pulmonary metastases. There is a multifocal structured interstitial pattern compatible with metastatic nodules (Images by the author).*

5.1.1.3 Traditional therapy

The median survival time (MST) of dogs with appendicular OS treated with surgery alone is between 19.2-25 weeks (Mauldin et al., 1988, Spodnick et al., 1992, Thompson and Fugent, 1992). The current treatment recommendation for OS relies on a combination of surgical removal of the tumour, either limb amputation or limb-sparing surgery, adjuvant chemotherapy and/or radiation therapy (Ehrhart, 2013). Adjuvant chemotherapy protocols using cisplatin, carboplatin or doxorubicin can prolong the survival times of dogs with OS, with an MST ranging from 241 to 413 days (Mauldin et al., 1988, Kraegel et al., 1991, Thompson and Fugent, 1992, Berg et al., 1995, Bergman et al., 1996, Boston et al., 2006, Selmic et al., 2014). Dogs that present with distant metastases show poor treatment outcomes, with a reported MST of only 76 days.

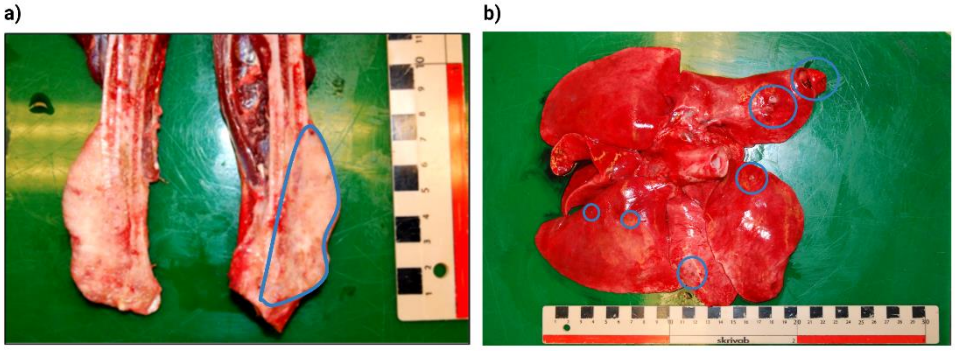

Figure 2: Macroscopic findings at necropsy from a dog with osteosarcoma (OS). ***a)*** *Sagital section of the radius and ulna from a dog with OS. The cortical and medullary bone at the distal end the the radius is destroyed and replaced by tumour tissue. The tumour is outlined with a blue line.* ***b)*** *Macrospopic view of the dorsal aspect of the lungs from a dog with metastatic OS. Macroscopic metastases are outlined with blue circles (Images by the author).*

5.1.1.4 Immunotherapy

Several immunotherapies have also proven effective against canine OS. Immunotherapeutic strategies used to treat canine OS stem from the observation that some patients with surgical site infections survive longer than those without. In a study evaluating pre-operative radiation therapy before limb-sparing surgery for OS, dogs that developed surgical site infections had significantly longer survival

times than those who did not (MST of 11 versus five months) (Thrall et al., 1990). Similarly, Lascelles et al. (2005) showed that dogs who developed surgical site infections after limb-sparing surgery and chemotherapy had an MST of 252 days longer than those without. The use of the Bacillus Calmette-Guérin (BCG) vaccine, alone or in combination with irradiated autologous tumour cells, also significantly improved survival in dogs with OS when given after surgery (MST of 51 versus 14 weeks) (Owen et al., 1975). Similarly, the macrophage-repolarizing drug muramyl tripeptide (MTP) significantly improved survival in dogs with OS after surgical removal of the primary tumour (median survival time of 222 versus 77 days) (MacEwen et al., 1989). Interleukin (IL)-2 is a potent stimulator of cytotoxic $CD4^+$ and $CD8^+$ T-cell differentiation, expansion, and effector functions (Spolski et al., 2018). When treated with nebulized liposomal human Il-2, two out of four dogs with established pulmonary metastases experienced long-lasting (>one year) complete regression (CR) of all metastatic lesions (Khanna et al., 1996). Similarly, intravenous administration of cationic liposomal-DNA complexes coding for canine IL-2 resulted in CR or partial regression in 3/20 and stable disease in 4/20 dogs with OS with pulmonary metastases (Dow et al., 2005). Cancer vaccines have also shown promising results in canine OS. In a phase I clinical trial assessing the safety and efficacy of a recombinant *Listeria monocytogenes* vaccine expressing a chimeric human epidermal growth factor receptor 2 (HER2/neu) construct given after surgery and standard chemotherapy, disease-free interval (DFI) and MST was significantly improved (Mason et al., 2016). Dogs treated with the vaccine had an MST of 738 days, significantly longer than historical controls treated with amputation and carboplatin alone (MST of 207-321 days). Despite the early success, a later trial showed that some dogs developed *Listeria* infections, which in addition to being a serious adverse effect for the patient, also posed a zoonotic risk for the healthcare workers and families caring for the dogs (Musser et al., 2021). Although most of these therapies are not used regularly in the clinic, they show the potential for immunotherapies for treating dogs with OS.

5.1.1.5 Osteosarcoma micrometastasis

OS is highly metastatic in dogs, and most eventually develop pulmonary metastases. Although >90% of dogs develop pulmonary metastasis after complete surgical removal of their tumour, radiographically detectable metastases are relatively rare at the time of diagnosis (>15-17%) (Ling et al., 1974, Spodnick et al., 1992,

Cavalcanti et al., 2004b, Selmic et al., 2014, Skorupski et al., 2016). This has led to the assumption that >90% of dogs with OS have micrometastases at the time of diagnosis (Ehrhart, 2013). However, where these micrometastases reside remains unknown. Bruland et al. (2005) examined the prevalence of micrometastases in the bone marrow of human patients with OS. They found that 63% of patients had tumour cells in the bone marrow at presentation. Among those presenting with visible metastases, the prevalence of tumour cells in the bone marrow was 92%. However, no studies have evaluated the incidence of pulmonary micrometastases at diagnosis, neither in humans nor dogs. Considering that bones and lungs are the main target organs for distant metastases in both humans and dogs, knowing whether micrometastases are present in the lungs might have implications for future treatment strategies (Brodey et al., 1963, Brodey and Riser, 1969, Ling et al., 1974, Spodnick et al., 1992, Federman et al., 2009).

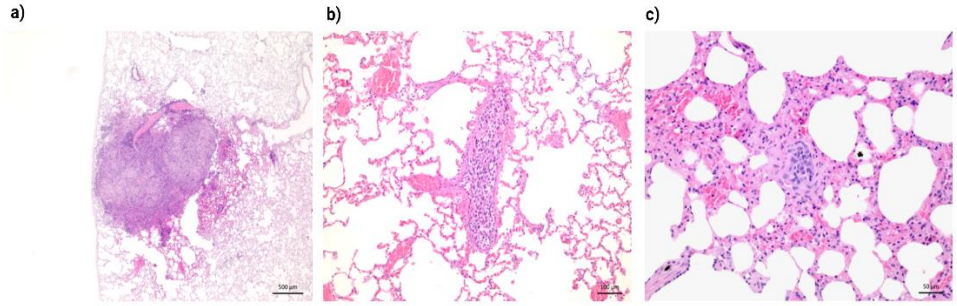

Figure 3: Histologic sections of metastases of different sizes in the lungs of dogs with OS. ***a)*** *Image of a macroscopically visible metastasis, hematoxylin and eosin (H&E) stain, 25x magnification.* ***b)*** *Image of a microscopic metastasis within a pulmonry arteriole, H&E stain, 100x magnification.* ***c)*** *Image of a micrometastasis lodged in the alveolar septa, H&E stain, 200x magnification (Images by the author).*

5.1.1.6 Tumour protein-3

Bruland et al. created the monoclonal antibody tumour protein-3 (TP-3), which binds specifically to a sarcoma-associated cell membrane antigen (Bruland et al., 1986, Bruland et al., 1988). TP-3 binds to a monomeric polypeptide with a molecular weight of 80 kDa, later identified as an isoform of placental alkaline phosphatase (oral communication Walchli et al. 2022). TP-3 binds to various human sarcomas, including all cases of OS examined, many synovial cell sarcomas,

malignant fibrous histiocytomas, hemangiopericytomas, chondrosarcomas and other undifferentiated sarcomas. TP-3 has failed to bind to any non-sarcoma malignancies in humans. As in humans, TP-3 was shown to bind to all OS tumours examined in dogs, as well as some chondrosarcomas, but also multiple cases of carcinomas, including lung carcinomas, squamous cell carcinomas, thyroid carcinomas, and prostatic carcinomas (Haines and Bruland, 1989, Page et al., 1994). TP-3 also binds to some normal canine tissues, including myoepithelial cells in the mammary glands, the brush border of the ciliated respiratory epithelium, and the endothelium in some normal organs (placenta and proximal renal tubules). The relatively low abundance of the epitope of TP-3 under physiological conditions makes it an ideal candidate for studying microscopic disease and as a therapeutic target.

5.1.2 Pre-metastatic niche

5.1.2.1 Historic perspective – Seed-and-soil hypothesis

In 1889, Dr Stephen Paget (1889) published an article describing how secondary growths of cancer, or metastases, seemingly occurred in specific organs. He noted that breast cancer had a much higher chance of metastasising to the liver than other organs and that this pattern differed from the formation of abscesses in empyema, meaning it was not random. He compared cancer cells to plant "seeds", containing the information necessary to grow into metastases, and referred to the site of metastasis as the "soil". Like plant seeds, which will only grow under the right conditions in their preferred soil, cancer cells had to encounter the right conditions to grow into metastases. This became known as "the seed and soil" hypothesis and was the first description of what later became known as organotropism (Gao et al., 2019).

The underlying mechanism for organotropism remained a mystery for over a century after Paget published his paper. In 2005, Kaplan et al. (2005) described how bone marrow-derived haematopoietic progenitor cells homed to sites of future metastases before cancer cells arrived. Furthermore, tumour-derived factors also increased fibronectin production at these sites, facilitating the haematopoietic progenitor cells recruitment and creating a tumour-permissive environment. These microenvironmental changes could be induced in non-tumour-bearing mice by giving them tumour-conditioned media and occurred in the organs to which the specific cell lines usually metastasized. Moreover, they could inhibit the development of metastases by removing or depleting these haematopoietic progenitor cells from the bone marrow of the mice. This phenomenon was coined the pre-metastatic niche (PMN) formation and paved the way for a new research field. To reiterate Paget's hypothesis, it was not enough for the seed to land on fertile soil; the soil had to have been "fertilized" by the plant from which it came before the seed could grow.

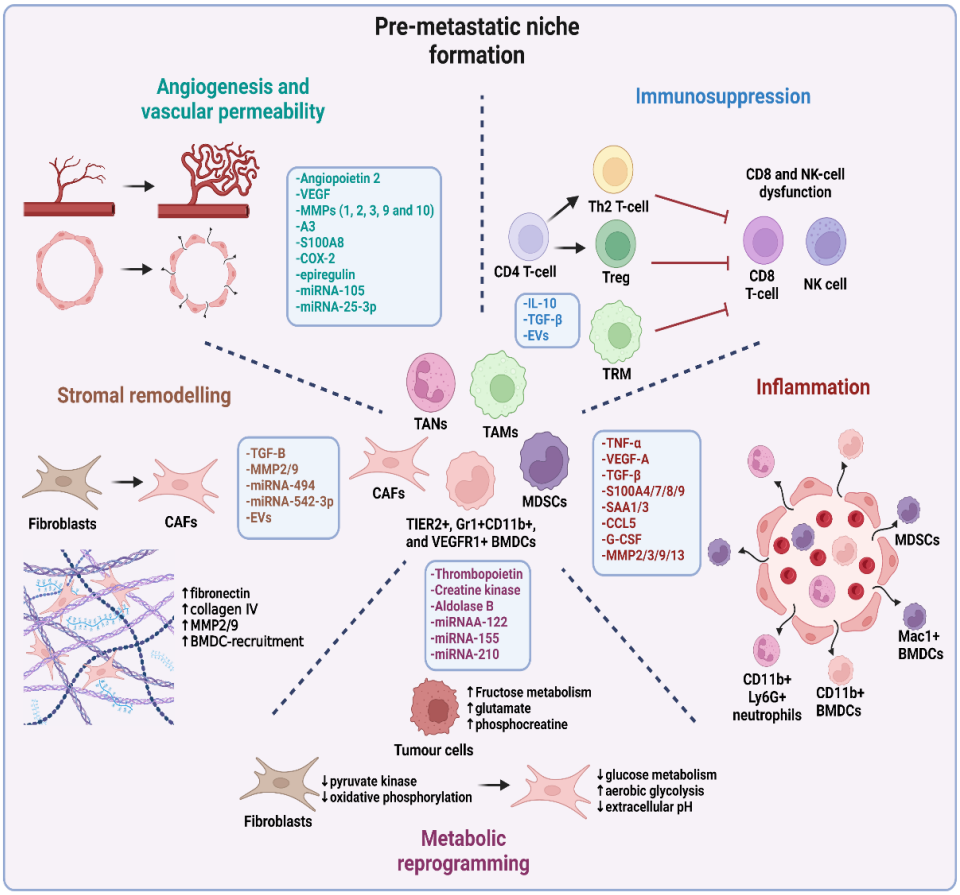

Figure 6: Schematic overview of some mechanisms involved in pre-metastatic niche formation. Boxes with blue frames indicate tumour-derived mediators responsible for each aspect of pre-metastatic niche formation (Figure by the author, created using BioRender©, 2023).

5.1.2.2 Definition

The PMN encompasses the metastasis-supporting microenvironmental changes that occur in a distant target organ before metastasis (Liu and Cao, 2016). Since Kaplan et al. introduced the term, PMN-formation has been described in several cancer forms and different metastatic target organs (Liu and Cao, 2016, Dong et al., 2021, Wang et al., 2021). These microenvironmental changes include vascular permeability and angiogenesis, immunosuppression, inflammation, and stromal and metabolic reprogramming (Liu and Cao, 2016, Wang et al., 2021). Primary tumour-

derived soluble factors and extracellular vesicles (EVs, which include exosomes) are responsible for inducing these changes.

PMN formation has almost exclusively been studied in pre-clinical murine models. Tumour-draining lymph nodes from human cancer patients show local changes compatible with PMN formation (Gillot et al., 2021). However, there are no papers describing PMN formation in distant metastatic target organs in humans and dogs.

5.1.2.3 Organotropism

An increasing number of studies have begun attributing the organotropism of metastases to the successful establishment of a PMN in specific organs. For instance, vascular endothelial growth factors (VEGFs) and exosomes released from primary breast cancer tumours can trigger an inflammatory response, bone marrow-derived cell (BMDC) recruitment, and immunosuppression in the lungs before metastasis occurs (Liu et al., 2014, Wen et al., 2016). When conditioned with exosomes from a highly metastatic mammary cancer cell line, naïve mice developed the same microenvironmental changes in the lungs and liver, which were also the sites in which metastases usually developed when transplanted with that line (Wen et al., 2016). The microenvironmental changes did not occur when they treated mice with exosomes from a non-metastatic mammary cancer cell line. Similarly, mice injected with Lewis lung carcinoma cells developed BMDC clusters in the liver and lungs, while those injected with melanoma cells developed them in the lungs, liver, testis, spleen, and kidneys (Kaplan et al., 2005). In both cases, the BMDC clusters only developed in organs that were common sites for metastases for the cancer cell lines used. In murine models of melanoma, cancer cell-derived exosomes were retained in the organs to which they preferentially metastasise, resulting in PMN formation (Peinado et al., 2012, Plebanek et al., 2017). Furthermore, the number and size of pulmonary metastases increased when they transplanted mice with bone marrow pre-treated with exosomes from a highly metastatic melanoma cell line (Peinado et al., 2012). When mice were pre-treated with exosomes from a non-metastatic melanoma line, metastatic development was blocked (Plebanek et al., 2017).

Integrins, which are ubiquitously expressed by all cells, are central mediators for inter-cellular and cell-to-extracellular matrix (ECM) interactions (Anderson et al., 2014). Integrins on the surface of tumour-derived exosomes are partly responsible

for the organotropism of their uptake (Hoshino et al., 2015). Exosomes that expressed the integrin αVβ5 were preferentially taken up by Kupffer cells in the liver, mediating liver tropism, while those expressing α6β4 and α6β1 bound to pulmonary fibroblast and epithelial cells, resulting in lung tropism.

5.1.2.4 Vascular permeability and angiogenesis

Vascular destabilisation in the PMN is driven by several factors and promotes the extravasation of tumour cells and metastasis. In the premetastatic lung, Angiopoietin 2 (Ang-2), matrix metalloproteinase (MMP) 3, and MMP10 are upregulated and help disrupt vascular integrity, facilitating metastasis (Huang et al., 2009). Recruited $TIE2^+$ monocytes and $Gr1^+CD11b^+$ BMDCs also create a pro-angiogenetic and vascular remodelling environment (Yan et al., 2010, Saharinen et al., 2011, Hiratsuka et al., 2013). These cells secrete VEGFs, angiopoietin, MMP9, A3, and S100A8, which promote angiogenesis, disrupt endothelial cell-to-cell junctions and result in vascular leakiness. Human renal cancer cell-derived $CD105^+$ micro-vesicles, melanoma-derived exosomes, and $CEMIP^+$ exosomes from patients with brain metastases can also stimulate angiogenesis at pre-metastatic sites (Grange et al., 2011, Peinado et al., 2012, Rodrigues et al., 2019). Furthermore, miRNA-105, epiregulin, cyclooxygenase-2 (COX-2), MMP1, and MMP2 contribute to vascular permeability and promote metastases in breast cancer models (Gupta et al., 2007, Zhou et al., 2014). Similarly, miRNA-25-3p in exosomes from colorectal cancer cells can regulate the expression of VEGFR2, zona occludens-1, occludin, and claudin-5 in endothelial cells, resulting in metastasis-promoting vascular changes (Zeng et al., 2018). Primary tumours can also induce lymphangiogenesis in the pre-metastatic lymph node and promote lymph node metastasis (Gillot et al., 2021). Tumour-derived VEGF-A, VEGF-C, integrins, and erythropoietin can mediate tumour-driven lymphangiogenesis.

5.1.2.5 Immunosuppression

Before colonizing cancer cells can grow in the metastatic target organ, the immunological microenvironment must become immunosuppressive and tumour-permissive. The primary tumour accomplished this by preconditioning tissue-resident immune cells and recruiting immunosuppressive BMDCs to the pre-

metastatic niche. Recruited Gr^+CD11b^+ myeloid cells and myeloid-derived suppressor cells (MDSC) can produce the immunosuppressive cytokines IL-10 and transforming growth factor-β (TGF-β) (Yan et al., 2010, Sceneay et al., 2012, Vadrevu et al., 2014, Wang et al., 2016b). This results in the induction of regulatory T-lymphocytes (Tregs), Th2 cells, $CD8^+$ T-cell dysfunction and reduced natural killer (NK) cell effector function. The primary tumour can also directly condition tissue-resident macrophages in the metastatic target organ. Breast cancer-conditioned alveolar macrophages and microglia cells have upregulated immunosuppressive cytokines such as TGF-β, which inhibit T-cell proliferation and can inhibit Th1 and induce Th2 polarization (Sharma et al., 2015, Xing et al., 2018). Additionally, tumour-derived EVs can directly suppress anti-tumour T-cells and NK-cells at the pre-metastatic site (Wen et al., 2016, Zhao et al., 2019). Together, these modifications result in tumour-permissive immunological reprogramming at the pre-metastatic site.

5.1.2.6 Inflammation

Another key aspect of PMN formation is inflammation. Tumour-derived factors can induce an inflammatory state which results in the recruitment of BMDCs and facilitates tumour-cell recruitment. Tumour necrosis factor- α (TNF-α), VEGF-A, and TGF-β from the tumour can stimulate pro-inflammatory S100A8 and S100A9 production in the pre-metastatic lung, resulting in serum amyloid A (SAA) 3 production (Hiratsuka et al., 2006, Hiratsuka et al., 2008, Tomita et al., 2010). SAA3 can then activate NF- κB through toll-like receptor (TLR) 4 on endothelial cells, macrophages, and Clara cells (Club cells), which results in TNF-α production and recruitment of $CD11b^+$ and $Mac1^+$ BMDCs and MDSCs to the pre-metastatic lung. Another S100 family protein, S100A4, can induce SAA1, SAA3, RANTES (CCL5), G-CSF, MMP2, MMP3, MMP9, MMP13, S100A8 and S100A9 production in the pre-metastatic liver through the same pathway (Hansen et al., 2015). These mediators enhance tumour cell adhesion, migration, and invasion, resulting in metastasis and immune cell infiltrates. Furthermore, S100A7 can promote fibrosis and BMDC recruitment to the pre-metastatic niche (Padilla et al., 2017). $CD11b^+Ly6G^+$ neutrophils recruited to the pre-metastatic lungs can also support colonization and metastasis thru the production of pro-inflammatory leukotrienes (Wculek and Malanchi, 2015).

5.1.2.7 Metabolic reprogramming

Metabolic dysregulation is a hallmark of cancer, and metastatic tumour cells require specific nutritional and energetic conditions in their new microenvironment to compete with resident cells (Wang et al., 2021). Differences in metabolic programming have been shown to influence the organotropism of metastasis. Thrombopoietin can promote liver metastasis in colorectal cancer by increasing lysine catabolism, triggering Wtn-signalling and glutamate synthesis in colonizing tumour cells (Wu et al., 2015). Breast cancer-derived miRNA-122 can suppress glucose metabolism by downregulating pyruvate kinase in tissue-resident cells in the PMN, promoting metastasis (Fong et al., 2015). Similarly, melanoma-derived miRNA-155 and 210 can suppress oxidative phosphorylation and induce aerobic glycolysis in fibroblasts, resulting in extracellular acidification (Shu et al., 2018). Colorectal cancer cells can secrete creatine kinase into the extracellular space when encountering hepatic hypoxia, resulting in phosphocreatine production, which can be used by cancer cells to generate adenosine triphosphate (ATP) and sustain metastatic growth (Loo et al., 2015). Similarly, colorectal cancer cells can upregulate aldolase B during metastasis, which supports fructose metabolism as an energy source during metastatic proliferation (Bu et al., 2018).

5.1.2.8 Stromal remodelling

Another important step in PMN formation is ECM remodelling. This remodelling provides adhesion for incoming cancer cells and BMDCs and increases matrix stiffness (Dong et al., 2021). Exosomes from pancreatic cancer cells are taken up by Kupffer cells, resulting in the TGF-β-mediated production of fibronectin by stellate cells in the liver (Costa-Silva et al., 2015, Yu et al., 2017). Fibronectin facilitates the recruitment of bone marrow-derived macrophages and neutrophils. Similarly, EVs from melanoma cells can induce pulmonary fibronectin deposits, resulting in $CD45^+$ cell accumulation (Ghoshal et al., 2019). Exosomes from prostate cancer cells can also upregulate fibronectin and collagen IV and the ECM-remodelling enzymes MMP2 and MMP9 in several metastatic organs (Deep et al., 2020). Exosomes derived from rat pancreatic adenocarcinoma can induce the upregulation of several MMPs in stromal cells in lymph nodes and fibroblast in the lungs before metastasis thru miRNA-494 and 542-3p (Rana et al., 2013). Since fibroblasts are the important producers of ECM components, several studies have assessed the effect of tumour-

derived EVs on their phenotype. EVs from nasopharyngeal carcinoma, colorectal cancer, hepatocellular carcinoma, and OS can activate fibroblasts into cancer-associated fibroblasts (CAFs) (Fang et al., 2018, Ji et al., 2020, Mazumdar et al., 2020b, Wu et al., 2020). CAFs have a high production of fibronectin, VEGF receptors, and pro-inflammatory mediators, such as S100A8, IL-6, and IL-8, that promote metastasis.

5.1.3 Tumour-associated macrophages

5.1.3.1 Tumour microenvironment

The tumour microenvironment (TME) is highly complex and heterogeneous and is composed of cellular and acellular components. There is no consensus for defining the TME, but Laplane et al. (2018) proposed a spatially delineated TME model depending on proximity to the tumour. They divided the TME into six distinctive layers, namely 1) the tumour cell-only environment, 2) the niche, 3) the confined, 4) the proximal, 5) the peripheral, and 6) the organismal TME. The peripheral layer refers to distally located lymphatic tissues, and the organismal layer, the microbiota and exosomes. These two layers have not been included in the conventional definition of the TME (Jin and Jin, 2020). The first four TME layers contain non-malignant cells, vessels, regional lymphoid organs and lymph nodes, nerves, intercellular components, and metabolites in the tumour centre, margin, and vicinity. The cellular constituents of the TME include tumour cells, T-lymphocytes, B-lymphocytes, NK-cells, tumour-associated macrophages (TAMs), MDSCs, granulocytes, tumour-associated neutrophils (TANs), dendritic cells, mast cells, CAFs, adipocytes, vascular endothelial cells, and pericytes (Anderson and Simon, 2020, Jin and Jin, 2020). Within the conventional definition (the first four layers), the TME can be divided into six distinctive specialized niches, although they are highly intertwined and cross-talk. They include 1) the hypoxic niche, 2) the immune microenvironment, 3) the metabolic microenvironment, 4) the acidic niche, 5) the innervated niche, and 6) the mechanical microenvironment. Since we investigated the role of macrophages within the TME and pre-metastatic niche in this thesis, we will focus on the immune microenvironment.

Immune cells play a central role in the TME, and depending on the context, they can either suppress or promote tumour growth. Tregs, MDSCs, TAMs, and $Ly6G^+$ neutrophils help build an immunosuppressive and tumour-permissive environment in the pre-metastatic niche and tumour tissues. TAMs are the most prevalent cellular constituents of the TME and play a central role in this immunosuppression and tumour progression in general (Cendrowicz et al., 2021, Feng et al., 2022). To understand their role in the TME, we must first explore their biology and functions.

5.1.3.2 Macrophage polarization

Macrophages are a heterogeneous population of immune cells belonging to the mononuclear phagocytic system (Gordon, 2007, Hume et al., 2019). They originate from embryonic yolk sac precursors, foetal liver precursors, and bone marrow-derived monocytes (Stremmel et al., 2018, Hume et al., 2019). Macrophages help maintain tissue homeostasis by removing dead cells, regulating iron metabolism, and sensing oxygen levels and osmolarity (Kotas and Medzhitov, 2015, Soares and Hamza, 2016, Gordon and Martinez-Pomares, 2017). In addition, macrophages have a central role in the innate immune system serving as a first-line defence against pathogens and as a link between the innate and adaptive immune systems (Arango Duque and Descoteaux, 2014). They have been implicated in numerous diseases, from atherosclerosis to autoimmune disease and cancer (Moore et al., 2013, Ma et al., 2019, Beltraminelli and De Palma, 2020).

Depending on the microenvironmental cues, macrophages can take on different phenotypical characteristics. The notion of M1 (classically activated) and M2 (alternatively activated) macrophages was introduced by Mills et al. (2000). Similarly to $CD4^+$ T helper cells, which can take on a Th1 and Th2 phenotype, Mills suggested that macrophages could take on an M1 or M2 phenotype in response to signalling cues from Th1 and Th2 cells, respectively. M1 macrophages are associated with pro-inflammatory functions, pathogen killing-abilities, production of reactive oxygen species (ROS), and secretion of pro-inflammatory cytokines (such as TNF-α, Il-1β, IL-2, IL-6, IL-8, IL-12, and IL-23) (Martinez and Gordon, 2014, Murray et al., 2014). M1 macrophages can be generated *in vitro* when stimulated with interferon-γ (IFN-γ) and lipopolysaccharides (LPS). M2 macrophages are associated with anti-inflammatory functions and highly phagocytic capabilities. They play an important role in tissue remodelling, angiogenesis, and anti-parasitic immune responses and secrete anti-inflammatory cytokines (such as IL-10 and TGF-β). Similarly to M1, M2 macrophages can be generated *in vitro* when stimulated with IL-4, IL-10, IL-13, or TGF-β, alone or in combination. Although there is a relatively good overlap between *in vivo* and *in vitro* M1 macrophages, the overlap for M2 macrophages is poor (Cendrowicz et al., 2021).

However, this M1/M2 dichotomy quickly falls short when trying to recapitulate the complexity of macrophage polarization. Therefore, Mantovani et al. (2004) suggested further subclassification of M2 macrophages into M2a, M2b, and M2c,

depending on which activating cues are used (M2d was also added later) (Ferrante et al., 2013). Even with the addition of these subtypes, the classification system could not fully cover all different polarizations (Martinez and Gordon, 2014). Therefore, Murray et al. (2014) introduced experimental guidelines for *in vitro*-generated macrophages. They suggested that experiments should include the source of macrophages, which activating signals were used, and also proposed a collection of markers describing macrophage activation. Furthermore, they noted phenotypical and functional differences for different phenotypes between species, further complicating the system. It has become increasingly clear that macrophages are highly plastic cells which can adopt different phenotypes within the same tissues (Gordon et al., 2014, Martinez and Gordon, 2014, Murray, 2017). *In vitro* macrophage models are unable to fully replicate the *in vivo* complexity (maturation of cells, adhesion, extracellular matrix, chemotactic signalling). Recent studies adopting more sophisticated tools such as single-cell RNA-sequencing and mass cytometry have shown that *in vivo* macrophages could not be classified within the traditional M1/M2 system, neither as discrete states nor along a spectrum of alternative polarization trajectory (Chevrier et al., 2017, Lavin et al., 2017, Azizi et al., 2018, Wagner et al., 2019, Zilionis et al., 2019).

5.1.3.3 Macrophage phenotypes in dogs

There are phenotypical and functional differences in macrophage phenotypes between humans and mice, and between humans and dogs (Murray et al., 2014, Heinrich et al., 2017). Heinrich et al. and Herrmann et al. characterized canine *in vitro*-generated M1 and M2 macrophages (Heinrich et al., 2017, Herrmann et al., 2018). They shared some common traits with the human *in vitro*-generated macrophages, including morphological features and a high expression of FcεRI and CD206 in M2 macrophages. However, several markers considered M1 or M2-specific in humans and mice could not differentiate these phenotypes in dogs. CD16, CD32, iNOS, MCH class II, CD80, and CD86 (M1-specific), or CD163 and Arginase-1 (Arg-1) (M2-specific) were not differentially expressed between canine M1 and M2 macrophages. Furthermore, the transcriptomic overlap between human and canine M1 and M2 macrophages was relatively poor. These findings underline the need for better characterization of canine macrophage polarization as there are significant inter-species differences. A larger arsenal of phenotypical markers is needed to perform in-depth *in situ* and *in vivo* characterization of macrophage populations.

5.1.3.4 Tumour-associated macrophages

TAMs represent one of the main cellular constituents of the TME and play a central role in its regulation (Cendrowicz et al., 2021, Feng et al., 2022). They can promote tumour progression, remodel the TME extracellular matrix, promote angiogenesis, regulate tumour metabolism, and have an immunomodulatory effect on the adaptive immune response. Furthermore, TAMs can facilitate invasion, intravasation, lymphoinvasion, survival in circulation, and extravasation of cancer cells.

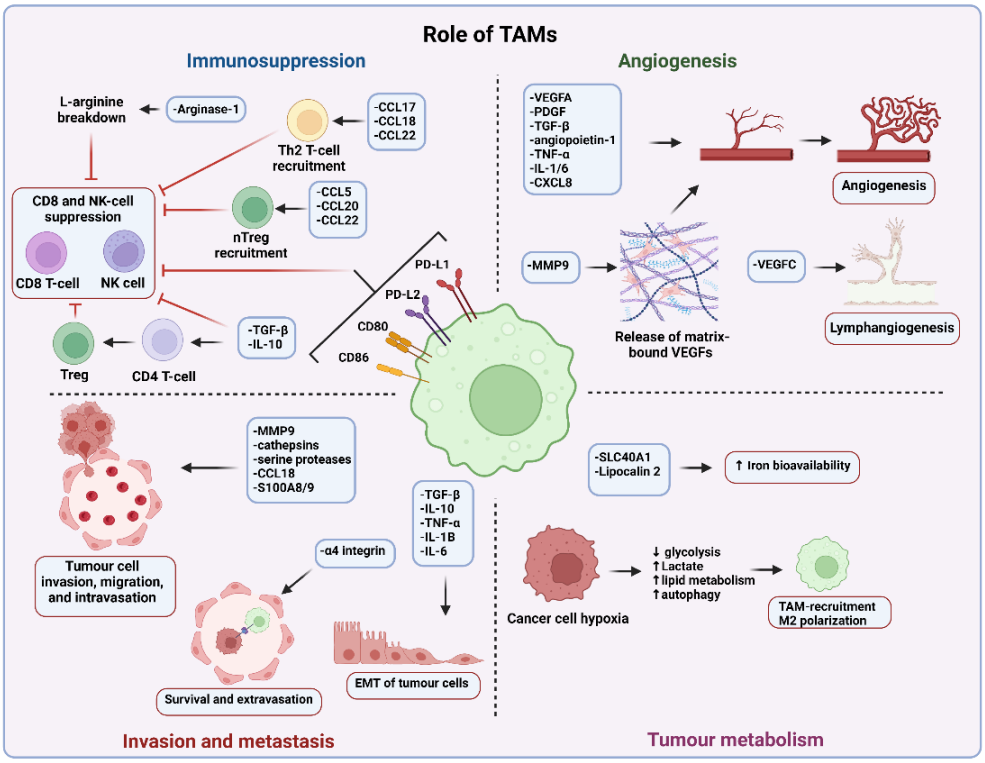

Figure 5: Schematic overview of some tumour-associated macrophage (TAMs) functions in cancer. Boxes with blue frames indicate mediators responsible for their functions, while boxes with red frames indicate their functions (Figure by the author, created using BioRender©, 2023).

5.1.3.4.1 TAMs – Phenotype

TAMs are often characterized as having a predominantly M2-skewed phenotype, meaning they are anti-inflammatory and tumour-permissive (Beltraminelli and De Palma, 2020, Cendrowicz et al., 2021, Hourani et al., 2021). Despite what we know regarding *in vivo* macrophage polarization and their non-conformity to the classic M1/M2 dichotomy, this nomenclature is commonly used in TAM research. As stated previously, we know that macrophages within a given microenvironment can express both M1 and M2-associated traits, such as within tumours (Chevrier et al., 2017, Lavin et al., 2017, Azizi et al., 2018, Wagner et al., 2019, Zilionis et al., 2019). In fact, several clusters of myeloid cells (including TAMs) exist within tumours and cannot be divided into M1 and M2 macrophages. TAMs can express both cytokines and chemokine usually associated with M1 macrophages (such as TNF-a, IL-1b, IL-6, chemokine C-C motif ligand (CCL) 2, CCL5, CCL17, CCL18, CCL20 and CCL22), but also those associated with M2 macrophages (IL-10, TGF-β, VEGFs, and MMPs) (Chen et al., 2019, Beltraminelli and De Palma, 2020). However, TAMs generally share many main functional characteristics with M2 macrophages, such as immunosuppression, matrix remodelling, and angiogenesis. Furthermore, several studies have found that higher numbers of TAMs expressing M2-associated markers correlate with a poor prognosis in cancer patients (Kubota et al., 2017, Lee et al., 2019, Jamiyan et al., 2020, Debacker et al., 2021, Iwicka et al., 2022). Additionally, therapies aimed at inducing an M1-shift in TAMs have also been proven effective in the treatment of cancer, further supporting the notion that TAMs have pro-tumoural functions (van Dalen et al., 2018, Sun et al., 2021, Iwicka et al., 2022).

5.1.3.4.2 TAMs – Origin and recruitment

TAMs originate from self-renewing yolk sack-derived tissue-resident macrophages (TRM) and recruited bone marrow-derived circulating monocytic cells (Hourani et al., 2021). The relative contribution of each population to the total TAM pool can vary depending on the time point of tumour progression (Casanova-Acebes et al., 2021, Pombo Antunes et al., 2021). In the early phase of tumour progression, TRMs are the primary source of TAMs, while monocyte-derived macrophages dominate in the later stages. Although both populations contribute to the total pool of TAMs, most derive from circulating monocytes in human tumours (Cassetta et al., 2019).

Several cytokines, chemokines and growth factors are involved in the recruitment of monocytes and expansion of TRMs in cancer. Macrophage-colony stimulating factor (M-CSF, or CSF-1), a haematopoietic growth factor, is highly expressed in many tumours (Lee et al., 2013, Van Overmeire et al., 2016, Hourani et al., 2021). M-CSF is involved in the recruitment of monocytes to the tumour, stimulates the expansion of local TRMs, and can induce a pro-tumoral phenotype. The CCL2 is overexpressed in many cancers and is a potent chemoattractant for monocyte recruitment to tumour tissues (Hourani et al., 2021). CCL3, CCL5, CCL8, and C-X3-C motif ligand 1 (CX3CL1) also contribute to monocyte recruitment to tumours (Lee et al., 2013, Hourani et al., 2021). The expression level of several of these chemokines also correlates with the number of infiltrating TAMs and a poor prognosis in several cancers. IL-34 is also involved in the recruitment and pro-tumoral polarization of monocytes in tumour tissues and is highly expressed in many cancers (Lee et al., 2013).

Hypoxia within the tumour tissue also results in a high expression of VEFG-A, which has a chemotactic effect on monocytes (Sawano et al., 2001, Kerber et al., 2008). Besides cytokines and chemokines, tumour-derived microRNA-375, in combination with oxidized low-density lipoproteins, was shown to induce migration and repolarization of monocytes to breast cancer tissues (Frank et al., 2019). The diversity of mechanisms responsible for TAM expansion and recruitment reflects inter- and intra-tumour heterogeneity and explains why therapeutic strategies aimed at blocking this process have not proven very effective (Beltraminelli and De Palma, 2020).

5.1.3.4.3 TAMs – Immunosuppression

One of the main functions of TAMs is suppressing the adaptive immune response in mounting a robust anti-tumour response. They accomplish this by secreting anti-inflammatory cytokines, expressing immune checkpoint ligands, and metabolizing amino acids vital for T-cell functions.

TAMs secrete the immunosuppressive cytokines IL-10 TGF-β, which modulate T-cell and NK-cell functions (Oh and Li, 2013, Wang et al., 2019). They thereby inhibit the cytotoxic activity of $CD8^+$ T-cells and NK-cells and induce $CD4^+$ regulatory T-cells (induced regulatory T-cells, iTregs) that suppress effector T-cells. Furthermore, TAMs secrete CCL5, CCL20 and CCL22, resulting in the recruitment of natural Tregs

(nTregs) to the tumour (Curiel et al., 2004, Liu et al., 2011, Shimizu et al., 2018). By secreting CCL17, CCL18, and CCL22, TAMs are responsible for recruiting naïve and T helper (Th) 2 lymphocytes (Erreni et al., 2011). Th2 lymphocytes are immunosuppressive and secret IL-4 and IL-13, resulting in pro-tumoral immunosuppressive macrophage polarization (DeNardo et al., 2009).

The immunosuppressive function of TAMs is also mediated directly by cell-to-cell contact through immune checkpoint ligands. TAMs have a high expression of programmed death-ligand (PD-L) 1, which interacts with programmed cell death protein 1 (PD-1), resulting in the inhibition of cytokine production and T-cell receptor (TCR) signalling (Kuang et al., 2009, Intlekofer and Thompson, 2013, Petty et al., 2021). This modulates T-cell function and inhibits anti-tumour T-cell responses. Additionally, TAMs have a high expression of PD-L2 and cytotoxic T-lymphocyte associated protein 4 (CTLA4) ligands CD80 and CD86, which inhibit normal cytotoxic T-cell functions when activated (Vandenborre et al., 1999, Umezu et al., 2019, Cendrowicz et al., 2021).

Finally, TAMs can metabolize certain amino acids, effectively starving T-cells of nutrients essential for their function. They have a high production of Arg-1, which breaks down L-arginine and reduces its availability to T-cells (Popovic et al., 2007, Rodriguez et al., 2007, Czystowska-Kuzmicz et al., 2019, Nakamura and Smyth, 2020). This results in the inhibition of T-cell proliferation, TCR-complex expression, and development of immunological memory.

5.1.3.4.4 TAMs – Angiogenesis

Another essential function of TAMs is their contribution to the angiogenesis of growing tumours. TAMs infiltrate hypoxic regions of the tumour through CCL2, CCL5, and CSF-1 mediated chemotaxis, and upregulation of the hypoxia-inducible factor 1-α (HIF1α) in TAMs results in increased production of VEGFs (Palazon et al., 2017, Chen et al., 2019, Cendrowicz et al., 2021). In addition to VEGFs, TAMs also secrete platelet-derived growth factor (PDGF), TGF-β, and angiopoietin-1, which facilitate angiogenesis by promoting endothelial cell proliferation and maturation, as well as pericyte infiltration (Lewis et al., 2000, Ribatti et al., 2007, Riabov et al., 2014, Thijssen et al., 2018). TAMs also secrete MMP9, which can induce angiogenesis by releasing matrix-bound VEGFs (Qian and Pollard, 2010). The pro-

inflammatory TAM-derived cytokines TNF-α IL-1, and IL-6, and chemokine C-X-C motif ligand 8 (CXCL8) also contribute to tumour angiogenesis (Qian and Pollard, 2010, Tamura et al., 2018). TAMs also seem to play a role in lymphangiogenesis, as they can produce VEGF-C, which promotes tumour lymphangiogenesis, and integrins that interact with lymphatic vessels (Bieniasz-Krzywiec et al., 2019, Tacconi et al., 2019).

5.1.3.4.5 TAMs – Invasion and metastasis

TAMs can promote cancer cell migration, invasion, and metastasis by secreting several matrix-remodelling enzymes. They secrete cathepsins, MMP9, and serine proteases capable of disrupting basal membranes and cell-to-cell junctions, facilitating invasion, migration and intravasation of cancer cells (Ngambenjawong et al., 2017). In addition to promoting invasion, cathepsins promote cancer cell growth and metastasis (Vasiljeva et al., 2006). TAMs also secrete CCL18 and S100A8/A9, which can also promote cancer cell migration and invasion (Chen et al., 2011a, Lim et al., 2016). It has also been shown that TAMs play a role in the epithelial-mesenchymal transition (EMT) of cancer cells, which is a central process in cancer invasion and metastasis (Liu et al., 2013, Aras and Zaidi, 2017, Yao et al., 2018, Cai et al., 2019). They accomplish this by secreting TGF-β, IL-10, TNF-a, IL-1B, and IL-6, which results in the loss of cell-to-cell junction between cancer cells and the gain of mesenchymal phenotypes. Lastly, TAMs can directly support the survival of cancer cells in circulation and facilitate their extravasation at distant metastatic sites (Cendrowicz et al., 2021). The α4 integrin on TAMs interacts with vascular cell adhesion molecule-1 (VCAM-1) on cancer cells which triggers PI3K/Akt signalling and protects cancer cells from death signals (Chen et al., 2011b). Furthermore, the interaction between α4 integrin and VCAM-1 facilitates the extravasation of cancer cells to the lungs.

5.1.3.4.6 TAMs – Regulation of tumour metabolism

Within the TME, hypoxia and abnormal metabolism result in strenuous conditions for cancer cells. Hypoxic tumours mainly produce energy through anaerobic glycolysis due to poor oxygen availability, which results in lactate production (Pillai et al., 2019). TAMs tend to accumulate in hypoxic regions of the tumours and in

close contact with sprouting blood vessels (Beltraminelli and De Palma, 2020). Lactate produced by cancer cells contributes to polarizing TAMs towards an M2-skewed phenotype (Colegio et al., 2014). Furthermore, reduced glycolytic metabolism and increased lipid metabolism in TAMs can induce M2-skewed polarization (Xiang et al., 2018, Wu et al., 2019). Cancer cell autophagy, the process of degrading cellular constituents for energy production under nutrient-deficient conditions, has also been shown to play a role in TAM recruitment and M2-skewed polarization (Yang et al., 2014, Sanjurjo et al., 2018, Guo et al., 2019). Hypoxia can also upregulate soluble carrier family 40, member 1, and lipocalin 2 expressions in TAMs, which can increase iron bioavailability and uptake by cancer cells (Mertens et al., 2016, Ören et al., 2016).

5.1.3.4.7 TAMs – Resistance to chemotherapy and radiation therapy

Both radiation therapy and chemotherapy generally increase TAM numbers within tumours after treatment (Larionova et al., 2019, Beltraminelli and De Palma, 2020). There is evidence that TAMs are directly involved in resistance to these therapies, and depletion of TAMs can attenuate tumour resistance to chemotherapy and radiotherapy (Paulus et al., 2006, Xu et al., 2013, Shiao et al., 2015). Through secretion of IL-6, TAMs can induce chemotherapy resistance by activating the STAT3 pathways in cancer cells (Yin et al., 2017, Zhu et al., 2017, Xu et al., 2019). Additionally, TAM-derived IL-10, IL-34, hepatocyte growth factor (HGF), cathepsin B and S, and milk fat globule-EGF factor 8 protein (MFG-E8) have all been shown to mediate chemotherapy resistance in several tumours (Jinushi et al., 2011, Shree et al., 2011, Quail and Joyce, 2013, Ruffell et al., 2014, Baghdadi et al., 2016). By secreting CSF-1 and IL-4, TAMs have also been implicated in radiation therapy resistance in some cancer forms (Xu et al., 2013, Shiao et al., 2015). Moreover, there is evidence that TAM-derived miRNA-21 can suppress apoptosis through activating PI3K/Akt signalling in cancer cells and confer resistance to cisplatin (Zheng et al., 2017).

5.1.3.4.8 TAMs in dogs

Only a few studies have investigated TAMs in dogs with cancer. Studies have found a correlation between high numbers of TAMs and poor survival times or high histologic grades in dogs with mammary tumours, soft tissue sarcoma, melanoma, and lymphoma (Raposo et al., 2015, Seung et al., 2018, Finotello et al., 2021, Parisi et al., 2021, Vázquez et al., 2021, Porcellato et al., 2022). Counterintuitively, high $CD204^+$ TAM numbers, a marker for tissue-resident and monocyte-derived macrophages, were associated with a longer DFI in dogs with OS (Withers et al., 2019a). The number of $CD204^+$ TAMs in pulmonary metastases was higher than in primary tumours of dogs with OS (Withers et al., 2019b). Monteiro et al. showed that virtually all macrophages within canine mammary tumours express the M2-associated marker CD206 (Monteiro et al., 2018). Similarly, a large proportion of TAMs within canine malignant melanomas express the M2-associated marker CD163, although this marker has not been validated as M2-specific in dogs (Porcellato et al., 2022). Few mechanistic studies have been done on canine TAMs. However, canine hemangiosarcoma cells produce CCL2 *in vitro*, stimulating monocyte migration and recruitment (Regan et al., 2017).

5.1.4 Cancer models

Pre-clinical model systems are extensively used in biomedical research and are instrumental in exploring biological mechanisms. Cancer research relies heavily on model systems to study biochemical and genetic pathways involved in cancer and to assess new cancer therapies (Sajjad et al., 2021). Each model system has its advantages and disadvantages. The cancer models used in research include *in vitro*, *in vivo*, and *in silico* models. Although each of these systems aims to mimic some features of cancer, none can fully recapitulate naturally occurring cancer. The inability of these models to recreate the heterogeneity of naturally occurring cancer, the TME, and the interactions with the host's immune system impedes our complete understanding of cancer pathogenesis and therapeutic development. Here, we will focus on *in vitro* and *in vivo* models and not *in silico* models, which are based on computer models to predict physiological and pharmacological processes.

5.1.4.1 *In vitro* models

Most *in vitro* cancer research relies on the 2D growth of cancer cell lines. These are easy to manage, inexpensive, immortalized, multiply quickly, amenable to high throughput testing of therapeutic agents, and have a low cellular heterogeneity (Sajjad et al., 2021). Moreover, they exhibit similar genetic and intrinsic features to that of primary tumours of humans (Domcke et al., 2013, Goodspeed et al., 2016). However, cancer cell lines have several limitations. When culturing cancer cells, there is a lack of stromal components, such as ECM, associated immune cells, lymphatic and blood vessels, and fibroblasts (Goodspeed et al., 2016). Furthermore, the culture media composition, growth surface, use of foetal bovine serum, and lack of tumour hypoxia further differ from *in vivo* conditions (Sharma et al., 2010). Additionally, genetic drift at high passaging numbers, risk of cross-contamination or mislabelling of cell lines, and lack of cell lines for some cancer subtypes are other limitations associated with their use (Sajjad et al., 2021).

To reduce some of the limitations of 2D-cultured cell lines, 3D-cancer spheroid and organoid models have been developed over the past decade. Some advantages of spheroids over traditional 2D cultures include their structural organization and oxygen, pH, and nutritional gradients (Han et al., 2021). They have an external proliferating zone, an internal quiescent zone, and a necrotic core. Additionally,

their growth kinetics, metabolic rates, and resistance to chemotherapy and radiotherapy are similar to that of i*n vivo* solid tumours. Organoids, which contain organ-specific cells and exhibit organ-specific functionalities, are also used in cancer research to provide insight into the pathophysiology of tumour development. However, these models also share several limitations with the 2D cultures and have their own unique limitations. Depending on the technique used to generate spheroids and organoids, the composition of the culture medium, use of ECM additives, choice of cell lines, and size of the spheroids at the time-point of the essay, to name some, can have implications for the study outcomes (Han et al., 2021). However, the fidelity of these *in vitro* models is improving, and cancer spheroids co-cultured with CAFs and patient-derived immune cells are promising platforms for high throughput screening of new therapies (Rausch et al., 2021, Poon and Ailles, 2022).

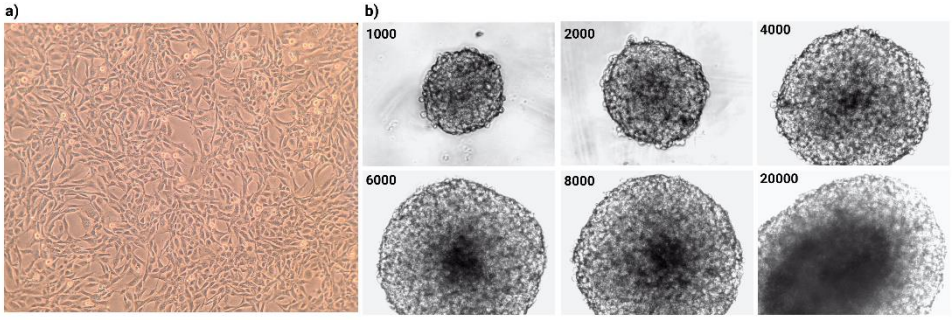

Figure 4: Inverted light microscopy images of in vitro cultured canine osteosarcoma cells (D17). ***a)*** *2D-cultured adherent D17 cells cultured on tissue-treated plastic showing typical spindeloid morphology.* ***b)*** *3D-cultured D17 cells forming spheroids after 72 hours in culture on ultra-low attachment plastic. The size and structure of the spheroids depend on the initial number of seeded cells (from 1000 to 20.000/well). A dark necrotic centre is visible in the larger spheroids.* ***(Images by the author)***

5.1.4.2 *In vivo* models

Since *in vitro* models cannot address all aspects of cancer research, it is also necessary to use *in vivo* models. Organisms such as mice, *Drosophila melanogaster (D. melanogaster)*, zebrafish, and *Caenorhabditis elegans* (*C. elegans*) are commonly used in cancer research (Day et al., 2015, Sajjad et al., 2021). *D. melanogaster*, zebrafish, and *C. elegans* have been used extensively to study molecular and

biochemical cancer biology as well as therapeutic drug discovery. Some of the advantages of these models include their small size, low cost, and easy propagation. Additionally, rapid ex-utero development and embryonic transparency facilitate imaging. Furthermore, they can easily be genetically modified and transplanted with human and murine xenografts. However, due to rudimentary haematopoietic systems, differences in lymphatic systems, and inappropriate tumour-host interactions (xenotransplantation), to name a few, their translational value is limited.

Murine models have been used extensively in cancer research since the 1950s (Day et al., 2015). Syngeneic murine cancer models were developed and used in the 1960s and 1970s (Talmadge et al., 2007, DeVita and Chu, 2008). These models rely on transplanting allographs from murine tumours into immunocompetent inbred strains of mice with the same genetic background. Later, in the 1970s and 80s, cell line-derived xenograft (CDX) models were developed, where *in vitro*-established human cancer cell lines were injected into immunocompromised mice. However, CDX models have failed to predict the efficacy of targeted therapies, and most (95%) drugs that succeed in mice fail when reaching human clinical trials (Sharpless and Depinho, 2006). CDX models do not recreate an appropriate tumour-host interaction and lack the tumour heterogeneity of naturally occurring cancer. To improve their translational value, more sophisticated murine models have been developed, including patient-derived xenograft (PDX) models, humanized murine models, and genetically engineered mouse (GEM) models (Day et al., 2015). PDX models rely on implanting immunocompromised mice with surgical patient-derived tumour samples (Koga and Ochiai, 2019). PDX models preserve tumour architecture, stromal composition, and molecular heterogeneity seen in patients. However, the human stromal component is maintained only for 2-3 passages before the mice stromal components become dominant. Moreover, these models rely on heavily immunocompromised mice, making immunomodulating therapies challenging to assess in these models. Strategies have been developed to improve their translational value for immunotherapeutic development. The mice can be "humanized" by transplanting them with $CD34^+$ human haematopoietic stem cells, or peripheral blood mononuclear cells (PMBCs), to generate a humanized immune response to the PDX. Although these strategies may create a more natural interaction between the immune system and the tumour, they still cannot reproduce a natural tumour-host interaction. GEM models, on the other hand, provide a system where cancer evolves within its natural microenvironment (Day et al., 2015). They

also replicate inter- and intra-tumour heterogeneity and provide a platform for evaluating immunomodulating therapies. However, their use can be challenging: Inter-species differences, such as different immune properties between humans and mice, make extrapolations difficult. Additionally, only a few genes can be studied simultaneously. Regardless of the choice of murine model, there are also inherent species differences between mice and humans. Pharmacokinetics, pharmacodynamics, and maximum tolerated doses of drugs vary between the two species (Day et al., 2015). The field of murine models is constantly changing, and hopefully, more sophisticated models will become available and affordable with time. However, regardless of how sophisticated they become, limitations such as lack of genetic diversity due to inbreeding, housing in specific-pathogen-free conditions, and lack of variation in diet and microbiome will remain unless radical changes are made to how experimental animals are used and kept.

Pigs are also sometimes used in cancer research due to their anatomical, physiological, and genetic similarities with humans. They have been used to model leukaemia, lymphoma, soft tissue sarcoma, pancreatic ductal carcinoma, hepatocellular carcinoma, breast cancer, and colorectal cancer (Schook et al., 2015, Watson et al., 2016, Kalla et al., 2020). However, cancer research involving this species is uncommon, despite the advantages of the pig model. This is probably due to high cost, housing requirements, lack of species-specific reagents, duration of experiments, and ethical considerations.

5.1.4.3 Dogs as cancer models

As in humans, cancer is one of the leading causes of death among family-owned dogs (Bonnett et al., 1997, Proschowsky et al., 2003, Adams et al., 2010, Inoue et al., 2015, Wang et al., 2016a). Veterinarians and translational researchers have advocated for dogs with cancer as models for their human counterparts for over 50 years (Prier and Brodey, 1963, MacEwen, 1990, Mottolese et al., 1994, Knapp and Waters, 1997, Vail and MacEwen, 2000). It is estimated that 4.2 million dogs are diagnosed with cancer annually in the United States (representing an incidence rate of approximately 5.300/100.000 DYAR) (Schiffman and Breen, 2015). In comparison, 1.66 million humans are diagnosed with cancer (representing an annual incidence rate of approximately 500/100.000 years at risk). This remarkably high number of dogs with cancer represents a largely untapped resource in cancer research. There

is, however, a clear difference in the types of tumours most commonly seen in the two species (Schiffman and Breen, 2015). While humans primarily develop carcinomas, dogs have a much high incidence of sarcomas. This is believed to be a result of the selective breeding of dogs over the past two to three centuries, which is estimated to have resulted in a sevenfold reduction in genetic diversity. This selective breeding, primarily aimed at phenotypical characteristics and appearance, has probably resulted in higher frequencies of specific cancers in specific breeds we see today. Furthermore, differences in exposure to known carcinogens, such as alcohol and tobacco, may also contribute to the differences in cancer types between the two species. The restricted genetic variation in dogs also allows for easier identification of the genetic basis of certain inherited diseases, like cancer.

The canine cancer model does not have the same limitations as murine models (Park et al., 2016). Issues related to xenotransplantation, lack of genetic diversity, inter- and intra-tumour heterogeneity, natural host-tumour interaction (interactions with the tumour stroma and immune system), and exposure to a natural living environment (microbiome diversity, educated immune system, dietary differences) are not present when using dogs with naturally occurring cancer. Additionally, due to the relatively short lifespan of dogs, lack of established "standard-of-care" treatment for many cancers, and willingness of many owners to participate in clinical trials (due to lack of effective treatment options or financial reasons), clinical trials are often less cumbersome and expensive than in humans (Park et al., 2016). Canine drug trials are estimated to be 10 to 100 times less costly than human trials (Burton and Khanna, 2014). Although variation in the incidence of different cancers could be viewed as a limitation of the canine model, it also offers a unique opportunity to study rare human cancer forms that are common in dogs, such as OS. However, there are still some limitations when using dogs as cancer models. Running clinical trials in dogs remains significantly more expensive than in mice, there are stricter ethical regulations to consider, it is impossible to control all experimental variables, there are fewer canine-specific reagents available compared to murine ones, and there is a larger inter- and intra-tumour heterogeneity requiring larger sample sizes than in murine trial (Park and Shin, 2016).

5.1.4.4 Canine osteosarcoma as a model for human osteosarcoma

Dogs with naturally occurring OS are considered excellent models for their human companions (Brodey, 1979, Withrow et al., 1991, Mueller et al., 2007, Withrow and Wilkins, 2010, Simpson et al., 2017). In addition to being the most common primary bone tumour in both species, they have remarkably similar clinical, pathological, molecular, and genetic features (Withrow et al., 1991, Federman et al., 2009, Simpson et al., 2017, Zhao et al., 2021). Additionally, the incidence rate of OS in dogs is estimated to be between 27-75 times higher than in humans, making it much easier to recruit cases for trials and research (Schiffman and Breen, 2015, Simpson et al., 2017). In contrast to humans, OS generally develops in middle-aged to older dogs (mean age of 7-8 years), although a bimodal distribution has been observed (Brodey et al., 1963, Misdorp and Hart, 1979, Spodnick et al., 1992, Cavalcanti et al., 2004b). In humans, on the other hand, OS is primarily seen in adolescent patients (during the second decade of life), with a smaller peak seen after 60 years of age (Zhao et al., 2021). Several studies have shown that genetic driver mutations and copy number alterations in human and canine OS are similar (Mendoza et al., 1998, Kirpensteijn et al., 2008, Angstadt et al., 2012). The OS-associated genes *TP53, CDC5L, MYC, RUNX2*, *CDKN2A/B, ADAM15, CTC1, MEN1, CDK7,* and others have been shown to be implicated in OS development in both species. Treatment strategies are also similar between the species and rely mainly on surgery, chemotherapy, and radiation therapy (Withrow et al., 1991, Federman et al., 2009, Simpson et al., 2017). Despite the many comparative studies and programs to date, no studies have investigated the potential of dogs with OS as models to study the pre-metastatic niche.

5.1.5 Immunohistochemistry and immunofluorescence

5.1.5.1 Immunohistochemistry

Immunohistochemistry (IHC) is a laboratory method that exploits the specific binding of an antibody to an antigen to detect and localize antigens in cells and tissues (Magaki et al., 2019). IHC can be used to determine cell types, their phenotypes, or organ of origin. Enzyme-conjugated (peroxidase) antibody-based IHC was developed in the 1960s (Avrameas and Uriel, 1966, Nakane and Pierce, 1966, Nakane, 1968). The method further evolved in the following decades, and alkaline phosphatase-conjugated antibodies became available (Mason and Sammons, 1978b, Mason and Sammons, 1978a, Cordell et al., 1984). Today IHC is used routinely in research, pathological, and anatomical laboratories. It is used as a histopathological diagnostic tool to discriminate benign from malignant lesions, subclassify neoplasia, as a prognostic tool, identify therapeutic targets, and more (Matos et al., 2010). Formalin-fixed and paraffin-embedded (FFPE) tissues are mainly used for IHC staining since they can easily be stored long-term (Magaki et al., 2019). Frozen and plastic-embedded tissues can also be used for IHC. The sequential steps in IHC (for FFPE tissues) can be summarized as: 1) Deparaffinization and rehydration, 2) antigen retrieval, 3) blocking, 4) addition of primary antibody, 5) application of secondary antibody, 6) application of detection reagent, and 7) counterstaining (Magaki et al., 2019).

1) FFPE tissues are surrounded by paraffin which can interfere with the IHC labelling and must be removed. After slicing the FFPE-tissue blocks and applying them on tissue slides, paraffin is removed by transferring the slides to a xylene bath. The tissues are rehydrated in an ethanol gradient (from 100 to 95 to 80, then 70% ethanol) and transferred to deionized water.

2) Formalin fixation enables long-term stable tissue storage with minimal tissue degradation by cross-linking proteins. Before applying the primary antibodies, this cross-linking should be abolished to make epitopes more accessible for antibody binding. To retrieve antigens masked by fixation, antigen retrieval (AR) can be performed using either chemical or physical methods. Chemical methods include enzymatic digestion and denaturing treatment, while physical methods include heat and ultrasound. Usually, a combination of heat (heat-induced antigen retrieval, HIAR) and chemical treatment is used. The rehydrated slides are placed in a buffer

(such as citrate or EDTA at low, neutral, or high pH) and then heated using a microwave oven, water bath, pressure cooker, or autoclave.

3) When using a peroxidase-conjugate system for IHC, endogenous peroxidase activity should be quenched before adding the primary antibody. Some tissues and cells have a high endogenous peroxidase activity, which can result in unspecific chromogen precipitation unless it is blocked. Quenching is commonly performed by submerging the slides in a hydrogen peroxide bath (usually 3%). Additionally, to reduce the unspecific binding of antibodies, blocking with serum (from the species in which the secondary antibody originates) or a universal blocking buffer should be performed before adding the primary antibody.

4) When choosing which primary antibody to use in IHC, there are several aspects to consider. The primary antibody can be monoclonal or polyclonal (the former usually results in less background staining), and different dilution factors can be used. Usually, different dilutions should be assessed for each species and given tissue, as the ideal concentration of an antibody to optimize contrast between positive staining and nonspecific background staining can vary widely.

5) Although a reporter enzyme can be conjugated directly to primary antibodies, this is uncommon since it requires each antibody to be conjugated and does not allow signal amplification. A reporter enzyme converts a colourless chromogen substrate into a coloured and visible product. Therefore, the enzyme is usually conjugated with the secondary antibody. Commonly used enzymes include horseradish peroxidase or alkaline phosphatase. Polymer-based methods using many peroxidase molecules and secondary antibodies attached to a dextran backbone are also available, allowing for increased signal strength and sensitivity.

6) When a chromogenic substrate is added to the tissues, like diaminobenzidine (DAB) or 3-amino-9-ethyl carbazole (AEC), the enzyme conjugated to the secondary antibody creates a coloured product. This results in staining of the epitope of interest.

7) Finally, the slides are counterstained to visualize the tissues and then mounted with a cover glass.

Whenever performing IHC staining, running relevant controls in parallel with the investigated tissues is essential. A positive control should contain tissues that express the antigen of interest known to stain with the antibody used. Negative controls from the sample should be run in parallel to ensure no unspecific binding of antibodies. These should undergo the exact same staining protocol, but the primary antibody must be omitted or replaced with a non-immune antibody from the same species (isotype control).

There are many considerations when performing IHC, such as which antibodies to use, which AR methods to use, and the effect of storage condition and length on epitopes. These have been reviewed elsewhere and will not be further discussed here (Matos et al., 2010).

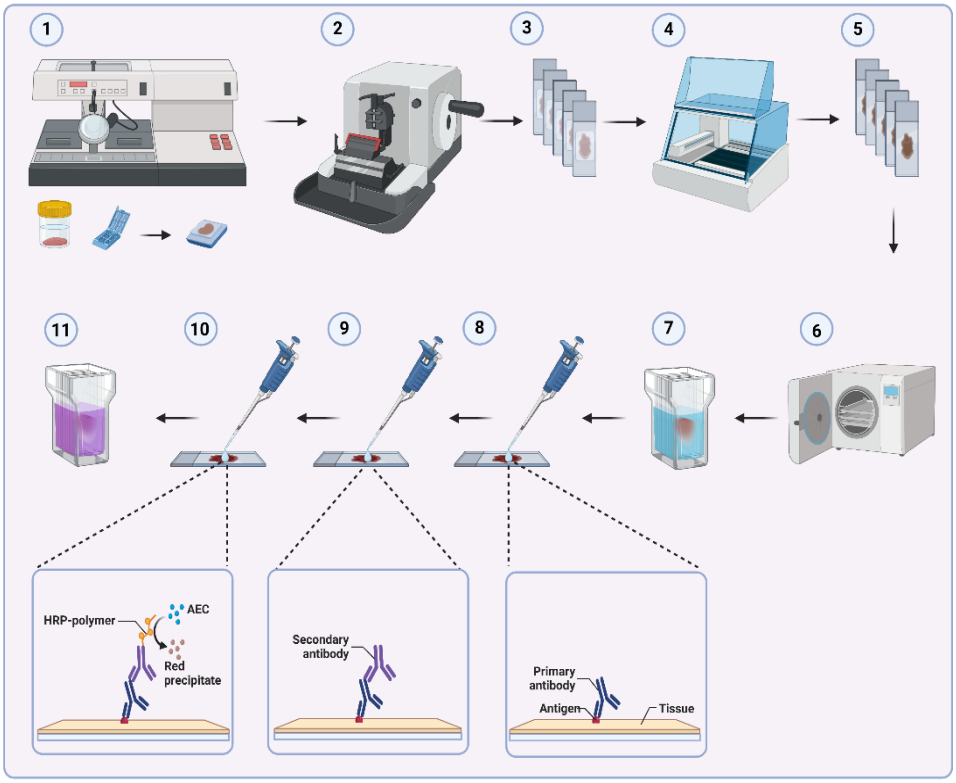

Figure 7: Schematic representation of the sequential immunohistochemical (IHC) labelling steps. 1) Formalin-fixed tissues are embedded into paraffin blocks. 2) Tissue sections are made from the paraffin blocks using a microtome. 3) Tissue sections are placed on microscopy slides, dried, and stored at 4°C until labelling. 4) Slides are deparaffinized and rehydrated using xylene and alcohol baths. 5) Slides are placed in deionized water and ready for IHC labelling. 6) Heat-induced epitope retrieval is performed by placing the slides in a denaturing buffer and heating using an autoclave, pressure cooker, water bath, or microwave. 7) Endogenous peroxidase activity is blocked by submerging the slides in 3% hydrogen peroxide, and the tissues are blocked for non-specific binding using serum or a universal blocking buffer. 8) The primary antibody is added and binds to its epitope. 9) The secondary antibody is added and binds to the primary antibody. 10) The chromogen substrate is added and precipitates into a coloured product when in contact with the antibody-bound enzyme. 11) The tissues are visualized using haematoxylin counterstain, then mounted and left to dry (Figure by the author, created using BioRender©, 2023).

5.1.5.2 Immunofluorescence

Like IHC, immunofluorescence (IF) exploits the specific binding of antibodies to antigens to detect and localize them (Robertson et al., 2008, Im et al., 2019). Contrary to IHC, IF allows multiplexing to visualize many antigens simultaneously. Additionally, IF can label a variety of samples, from cell cultures to tissues (frozen or FFPE) to entire organisms. The sequential steps of IF are similar to the ones described for IHC but with some differences. As there is no enzymatic chromogen reaction to visualize the antibody labelling, there is no need to quench the endogenous peroxidase activity. IF relies on the labelling of an antigen with an antibody conjugated to a fluorophore (direct or primary IF) or the recognition of a primary antibody with a secondary antibody conjugated to a fluorophore (indirect or secondary IF). As with IHC, indirect IF is the most widely used method as it allows signal amplification (several secondary antibodies bind to the primary antibody), increasing sensitivity. IF also provides better resolution than IHC, which is advantageous when labelling subcellular structures. Fluorophore-conjugated antibodies emit light upon excitation by light of a shorter wavelength. Each fluorophore has a specific excitation and emission wavelength peak. They also have different extinction coefficients and quantum yields, which influence the brightness of a fluorophore, and excitation-emission times, which can be used to separate signals with overlapping emission spectra. The choice of fluorophores depends on several factors. Bright fluorophores should be used for low-abundance antigens. Fluorophores with minimal spectral overlap should be used when several antigens are labelled. Fluorophores with the least spectral overlap with tissue autofluorescence should be used to avoid background noise. Additionally, photobleaching of fluorophores can result in loss of signal over time, which can be avoided by choosing photostable fluorophores, mounting tissues in antifade mounting media, and storing slides in the dark and cold.

Whereas IHC-labelled tissues are imaged using bright field microscopy, fluorescent imaging requires an epifluorescent or confocal microscope. Traditionally, epifluorescent microscopy has been used to image IF-labelled tissues, which has limited the use of FFPE tissue since they exhibit high levels of autofluorescence. Confocal microscopy collects a thin optical section (0.5 µm) of the tissues, while epifluorescent imaging collects the entire thickness of a tissue section (3-6 µm) (Robertson et al., 2008). Thin optical sections reduce the contribution of autofluorescence to the image in confocal microscopy. Additionally, confocal

microscopy uses lasers to produce light, meaning the excitation bandwidth is much narrower (<5 nm) than conventional mercury vapour lamps used in epifluorescent microscopy. The intensity of each laser can also be regulated individually, allowing the ideal signal-to-background for each fluorophore. Confocal microscopy also permits the user to set numerically defined collection windows for each fluorophore, resulting in better control than dichroic and trichroic glass filters used in epifluorescent imaging. Finally, confocal microscopy allows for sequential imaging, meaning lasers and collection windows can be operated individually.

5.1.6 Flow cytometry

Whereas IHC and IF detect antigens in fixed tissues and cells, flow cytometry can analyse single cells or particles in a suspension. Traditionally, flow cytometry consists of three systems: 1) fluidics, 2) optics, and 3) electronics (McKinnon, 2018). The fluidic system delivers and focuses the sample to the interrogation point in front of the lasers by using pressurized sheath fluid (buffered salt-based solution). The optic system consists of lasers, dichroic and bandpass filters that steer the fluorescent light signal to specific detectors, and collection optics consisting of photomultiplier tubes and photodiodes. The electronic system converts the signals from the detectors into digital signals. Modern flow cytometers also use ultrasonic waves for acoustic focusing instead of only pressurized sheath fluid, which allows for better focusing of cells for laser interrogation.

Flow cytometry has several applications in many fields of study. In immunology, it is used for immunophenotyping, to study antigen-specific immune responses, and measure intracellular cytokines, cell proliferation, phagocytosis, and apoptosis. Additionally, flow cytometry can be used for cell cycle analysis, signal transduction analysis, fluorescent *in situ* hybridization (FISH), and more.

Each particle is analysed for its visible light scatter and fluorescent signals. Light scatter is measured as forward scatter (FSC, in the forward direction) and side scatter (SCC, at 90^{o}). FSC indicates the relative particle size, while SCC indicates the internal complexity or granularity. Most flow cytometers today have several laser and fluorescent detectors, allowing for many parameters to be analysed. The most used lasers include ultraviolet (355 nm), violet (405 nm), blue (488 nm), green (532 and 552 nm), green-yellow (561 nm), and red (640). Cells and particles can be prepared for fluorescent measurements through transfection and expression of fluorescent proteins (such as green or red fluorescent protein, GFP and RFP), fluorescent dyes (nucleic acid dyes such as propidium iodide (PI) and DAPI), proliferation dyes (such as carboxyfluorescein succinimidyl ester (CFSE)), viability dyes (such as Live/Dead™ reagents), and calcium indicator dyes (such as indo-1), or fluorescently conjugated antibodies or RNA-probes. Fluorophore-conjugated antibodies are commonly used in flow cytometry, and many fluorophores are available. These include phycobiliproteins such as phycoerythrin (PE) and allophycocyanin (APC), quantum dots (semiconductor nanocrystals), polymer dyes

such as Brilliant Violet™ and Blue™, and tandem dyes such as small organic fluorophores (Cy3, Cy5, and Cy7) coupled with phycobiliproteins or polymer dyes.

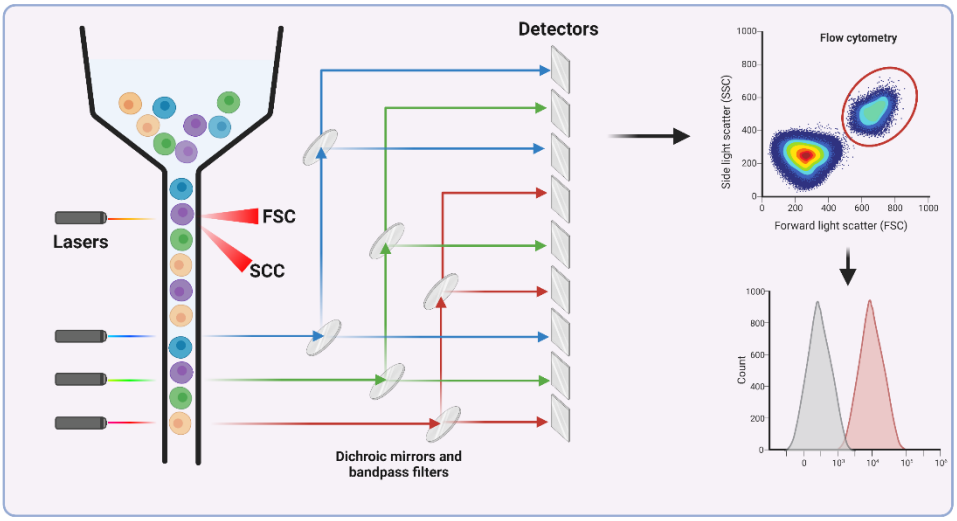

Figure 8: Schematic representation of the inner workings of a flow cytometer. The cells in suspensions are delivered and focused to the interrogation point in front of the laser by pressurized sheath fluid. Visible light signals are recorded as forward scatter (FSC) and side scatter (SSC). Fluorescent signals are guided through a series of dichroic mirrors and bandpass filters before reaching the photomultiplier tubes and detectors (Figure by the author, created using BioRender©, 2023).

As with IHC and IF, running appropriate controls is essential when performing flow cytometry (Cossarizza et al., 2021). Unstained negative controls can provide information regarding cellular autofluorescence, while isotype controls can provide information regarding unspecific antibody binding. Whenever cells with high numbers of Fc-receptors are analysed using flow cytometry, such as macrophages and dendritic cells, an Fc-blocker or species-specific IgG should be used to limit unspecific binding (Andersen et al., 2016). When several fluorophores are used simultaneously, there will usually be some spectral overlap. Therefore, single controls should be included, where the interrogated cells or antibody-capture beads are stained using only one of the antibodies/fluorophores (Cossarizza et al., 2021). These readings are used to set the correct compensation values for the fluorophore panel to compensate for any bleed-through from one fluorophore into the other channels. Lastly, fluorescence minus one (FMO) controls should be used to set the appropriate gates when performing multiplex flow cytometry. FMO controls are

stained using all the fluorophores in the panel minus the one of interest. These controls permit the setting of appropriate gates taking into account autofluorescence and spectral overlap from the other fluorophores. Additionally, biological controls (positive and negative controls) should be included. They provide biologically relevant comparisons related to different treatments or stimuli.

5.1.7 RNA-sequencing

RNA-sequencing (RNA-Seq) is a high-throughput sequencing method that provides information into the transcriptome of cells (Kukurba and Montgomery, 2015). Compared to older methods such as Sanger-sequencing and microarray methods, RNA-Seq gives higher coverage and better resolution. The transcriptome is highly complex and encompasses several types of coding and non-coding RNAs. Coding RNA is known as messenger RNA (mRNA), while non-coding RNA includes ribosomal RNA (rRNA), transfer RNA, small nuclear RNA, microRNA (miRNA), piwi-interacting RNA (piRNA), long non-coding RNA, and others, each with different roles. RNA-Seq provides a detailed and quantitative view of gene expression, alternative splicing, and allele-specific expression.

For RNA-Seq, RNA is first isolated from a sample. The quality of the RNA should be assessed to ensure it is not too degraded. RNA-integrity is usually measured as an RNA-integrity number (RIN) from 1 to 10, 1 being the lowest quality, and RIN values of <6 significantly affect the sequencing results. RIN values can be measured using a bioanalyzer, and the software calculates the values based on, among others, the ratio of 28S to 18S ribosomal bands. Next, sequencing libraries are prepared by reverse-transcribing the RNA to complementary DNA (cDNA). Several library constructions are available, which can isolate desired RNA molecules (Poly-A selection or Ribodepletion for sequencing mRNA, size selection for sequencing miRNA, piRNA, and silencing RNA), fragment or amplify random primed cDNA molecules, and ligate sequencing adaptors. Once libraries are ready, the cDNA is sequenced using a next-generation sequencing (NGS) platform. Most RNA-Seq experiments today use the Illumina™ platform, which applies an ensemble-based sequencing-by-synthesis approach. DNA molecules are clonally amplified using fluorescently labelled reversible-terminator nucleotides. Since Illumina™ platforms clonally amplify the DNA, they provide relative RNA expression levels of genes.

After cDNA sequencing, the reads (e.g., DNA sequences) can be mapped to a reference genome. The reads are aligned, mapped, and assembled into transcripts. The quality of the raw sequencing data and the mapped reads should be assessed for biases (can be introduced at any point of the experimental pipeline; RNA extraction, sample preparation, library preparation, sequencing, and read mapping). Once the transcriptome has been constructed, differential gene expression between

conditions can be evaluated. Several statistical methods have been developed to assess differential gene expression but will not be reviewed here.

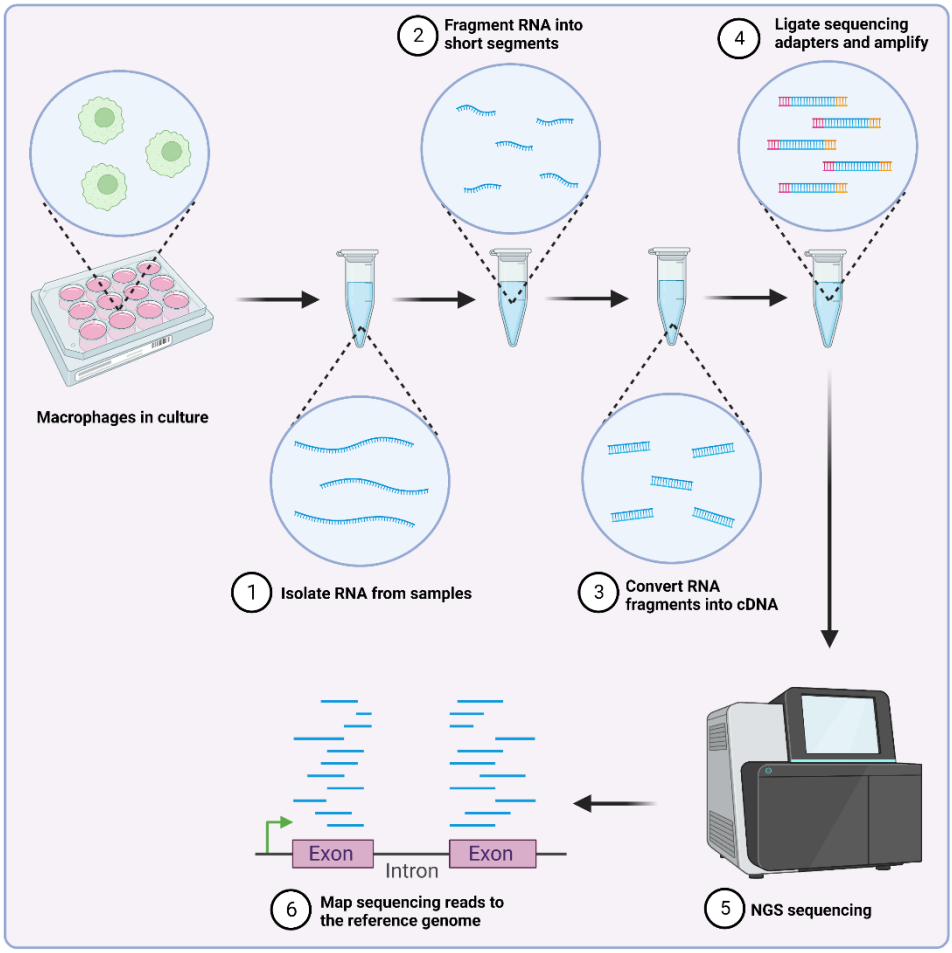

Figure 9: Schematic representation of the sequential steps of RNA-sequencing. ***1)*** *RNA is isolated from a biological sample, such as cells in a culture, using a commercially available RNA-isolation kit. After ensuring the RNA is of good quality,* ***2)*** *it can be fragmented, and* ***3)*** *converted to cDNA using reverse transcriptase.* ***4)*** *cDNA fragments are then ligated to adaptors and clonally amplified.* ***5)*** *cDNA is then sequenced using a next-generation sequencing (NGS) platform.* ***6)*** *The reads (DNA sequences) are then aligned and mapped to a reference genome, and the transcriptome is assembled (Figure by the author, created using BioRender©, 2023).*

5.1.8 Knowledge gaps

Although dogs with cancer are considered excellent research models for their human counterparts among some researchers, their potential for studying several aspects of cancer progression remains unexploited. This includes the early processes of metastases, such as micrometastatic development and PMN formation. Furthermore, since dogs develop cancer naturally, they do not have the same limitations as most murine models. Therefore, dogs have great potential in translational immunotherapy research that remains largely untapped. Despite extensive knowledge of immune cell phenotypes and functions in mice and humans, canine cancer immunology is a poorly studied field.

Although radiographically detectable metastases are uncommon at presentation (<15-17%), most dogs with OS (>90%) eventually develop metastatic disease despite surgical removal of the primary tumour. Where the disseminated cancer cells reside before macroscopic metastases develop remains unknown. The lungs and bones are the main target organs for metastatic OS in humans and dogs. Bruland *et al*. found tumour cells in the bone marrow in 63% of human OS patients at presentation. Amongst those presenting with overt metastases, the prevalence was 92%. To our knowledge, pulmonary micrometastases have not been studied in human or canine OS. **What is the prevalence of pulmonary micrometastases in dogs with OS without visible metastases?**

Despite knowledge of TAMs in humans and mice, we know little about their role in dogs. Several reports have shown that macrophages are present in the primary tumour and metastatic lesions in several cancer forms in dogs, such as OS and mammary carcinomas. Furthermore, their numbers seem to correlate with histologic grade and survival. Only a few studies have evaluated phenotypical and transcriptomic characteristics of canine macrophages *in vitro*. There is also a lack of validated canine phenotypical macrophage markers for *in situ* and *in vivo* research of TAMs and knowledge about TAM functions in general. **Are canine *in vitro*-generated monocyte-derived tumour-conditioned macrophages phenotypically and transcriptomically similar to M2 macrophages?**

PMN formation has almost exclusively been studied in preclinical murine models. However, the limited translational value of these models, mentioned previously, could bring the validity of these findings into question. One of the main challenges

when studying PMN formation in humans is the inability to access material and tissues from healthy organs before they develop metastases. Here, veterinary medicine presents a unique opportunity, as many dogs with cancer are euthanized before they develop metastases. As such, they could represent a relevant naturally occurring cancer model to study PMN formation and serve as a bridge between preclinical science and humans. **Do dogs with OS have immunological changes in the lungs compatible with PMN formation before they develop metastasis?**

5.1.9 Aims

The overall aim was to show that dogs with OS can serve as naturally occurring cancer models to study early metastasis and PMN formation. We wanted to accomplish this through the specific objectives of each paper included in the thesis:

- To evaluate the prevalence of pulmonary micrometastases in dogs with osteosarcoma before visible metastases have developed. **(Paper I)**

- To characterize canine *in vitro*-generated monocyte-derived tumour-conditioned macrophages and compare them with classically (M1) and alternatively (M2) activated macrophages. **(Paper II)**

- To study the prevalence and phenotype of macrophages and bone marrow-derived cells in the pre-metastatic lungs of dogs with OS before visible metastasis has occurred. Thereby we wanted to provide evidence of an immunological pre-metastatic niche. **(Paper III)**

5.2 Materials and Methods

A summary of the material and methods used in the papers is presented here. For further details, please see the specific article.

Material

The studies included in this thesis consisted of two prospective non-randomized case-control studies (**paper I and III**) and one laboratory study (**paper II**).

The cases included in **papers I and III** were the same and were recruited from the University Small Animal Hospital (NMBU) and private practice (Evidensia Oslo Dyresykehus) between 2012 and 2019. Owners signed a written consent form before euthanasia of the dogs included. Only those with treatment naïve OS (OS+, n=15) were included as cases. Based on necropsy findings, dogs with OS were divided into those with macroscopic metastases (OS+/Met+, n=5) and those without (OS+/Met-, n=10). Control cases (OS-/Met-, n=10) were enrolled retrospectively from the pathology archives based on pathology reports and clinical records.

None of the included dogs could have any current or previous neoplastic disease other than OS. They could not have received treatment (chemotherapy, radiation therapy, or immunomodulating therapy) or have any other condition (fulminant allergy, atopic dermatitis, or systemic inflammatory conditions, either infectious or immune-mediated) at the time of euthanasia which could interfere with macrophage phenotypes. Both cases and control dogs could be of any breed, age, weight, sex, and neutering status.

Routine necropsy and standard tissue sampling for formalin fixation and paraffin embedding were performed in all dogs. In addition, tissue samples were collected from any suspected pathological lesions, including the tumour. Tissues were stained with haematoxylin & eosin and evaluated microscopically by a pathologist. Two tissue samples, one from the peripheral and one from the central areas of the lung lobes, from each of the seven lung lobes, were collected and formalin-fixed (n=14 in total). An identical set of tissue samples were snap frozen (n=14) and stored at -80^{o}C from all dogs with OS (n=15) and two of the control cases (n=2).

Dogs included in **paper II** (n=6) were recruited from the University Small Animal Hospital (NMBU), had to be clinically healthy, have no clinically detectable disease,

or receive any treatment known to interfere with macrophage phenotype. They could be of any breed, age, weight, sex, and neutering status and had to have a body weight of over 10 kg. Each dog had a serum biochemistry profile and a complete blood count analysed to ensure they had no underlying disease.

***Table 1**: Overview of clinical characteristics, white blood cell counts, and monocyte counts in dogs included in **Paper II**. Sex male (M) and female (F), age in years, body weight in kg, neutered yes (Y) and no (N).*

Case	Age	Sex	breed	Body weight	Neutered	White blood cell count/L	Monocyte count/L
1	7	F	English setter	19.2	N	5.7 $x10^9$	0.3 $x10^9$
2	1	F	English setter	16.3	N	9.6 $x10^9$	0.4 $x10^9$
3	2	F	Labrador retriever	22.8	Y	8.7 $x10^9$	0.2 $x10^9$
4	4	F	Labrador retriever	28.1	Y	7.1 $x10^9$	0.3 $x10^9$
5	8	M	Labrador retriever	25.4	N	5.8 $x10^9$	0.2 $x10^9$
6	1	M	Labrador retriever	28.5	N	9.0 $x10^9$	0.5 $x10^9$

*Table 2: Overview of clinical characteristics and pathological findings in dogs included in **Papers I and III**. Sex male (M) and female (F), age in years.*

Case	Group	Breed	Sex	Age	Sampling year	Cause of euthanasia
1	OS+/MET+	Mixed breed	M	1	2012	Osteosarcoma, left distal radius
2	OS+/MET+	Schnauzer	F	8	2013	Osteosarcoma, right distal radius
3	OS+/MET+	Irish wolfhound	F	7	2014	Osteosarcoma, right proximal humerus
4	OS+/MET+	Rottweiler	M	9	2013	Osteosarcoma, left distal ulna
5	OS+/MET+	Tervuren	F	8	2014	Osteosarcoma, left distal radius
6	OS+/MET-	Newfoundland dog	M	8	2018	Osteosarcoma, left distal radius
7	OS+/MET-	Siberian husky	M	3	2013	Osteosarcoma, left proximal humerus
8	OS+/MET-	Irish wolfhound	F	6	2013	Osteosarcoma, right distal tibia
9	OS+/MET-	English setter	M	8	2018	Osteosarcoma, right distal ulna
10	OS+/MET-	Pointer	F	4	2016	Osteosarcoma, left distal tibia
11	OS+/MET-	Shar Pei	M	11	2013	Osteosarcoma, right proximal humerus
12	OS+/MET-	Rottweiler	F	9	2015	Osteosarcoma, left proximal humerus
13	OS+/MET-	German shepherd	F	3	2013	Osteosarcoma, left distal radius
14	OS+/MET-	Flat-coated retriever	M	3	2015	Osteosarcoma, left distal radius
15	OS+/MET-	Leonberger	M	6	2016	Osteosarcoma, left distal radius
16	OS-/MET-	Dalmatian	M	8	2016	Urolithiasis
17	OS-/MET-	Shetland Sheepdog	F	1	2020	Behavioral problems
18	OS-/MET-	Chihuahua	M	7	2017	Idiopathic epilepsy
19	OS-/MET-	Jack Russell terrier	M	6	2018	Road traffic accident (hip fracture, tail fracture, perforation jejunum and rectum, perforation bladder)
20	OS-/MET-	Australian shepherd	F	1	2019	Behavioral problems
21	OS-/MET-	Dachshund	M	6	2014	Intervertebral disc disease
22	OS-/MET-	Malinois	M	4	2016	Intervertebral disc disease
23	OS-/MET-	Lagotto Romagnolo	M	1	2018	Vertebral fracture
24	OS-/MET-	Spanish Greyhound	F	4	2015	Behavioral problems
25	OS-/MET-	Dachshund	F	5	2014	Road traffic accident (multiple hip and sacral bone fractures, subcutaneous, intramuscular, and retroperitoneal bleeding)

Paper I

Early immunohistochemical detection of pulmonary micrometastases in dogs with osteosarcoma.

Overview

In this paper, we performed TP-3 IHC on frozen tissue sections to identify microscopic metastases, micrometastases and TP-3 positive single cells. A total of 14 dogs were included in this study, ten dogs with OS without metastases (OS+/Met-), two dogs with OS with metastases (OS+/Met+), and two without cancer (OS-/Met-). The OS+/Met+ dogs served as positive controls, while the OS-/Met- dogs served as negative controls. Seven of the 14 snap frozen lung tissue samples (six from the peripheral areas and one from the central areas) were randomly chosen and evaluated in each dog.

Immunohistochemical staining

We based the IHC protocol on work from Bruland et al. but with several modifications (Bruland et al., 1985). Briefly, we sliced snap-frozen tissues into 7µm sections with a cryostat. We then mounted tissue sections on poly-lysin-coated slides (Superfrost™ Plus), dried them at room temperature, and kept them at -80 °C until further use. IHC sections were labelled using the peroxidase-conjugated immune-polymer method (EnVision™+). The EnVision™+ kit uses an indirect IHC method, with secondary antibodies conjugated to a polymer linked to many reporter enzymes, allowing for greater signal amplification (Sabattini et al., 1998). The kit uses horseradish peroxidase as the reporter enzyme. We fixed the tissue sections in cold acetone (-20°C) and air-dried them. We tried several other fixatives, but they all resulted in signal loss. Endogenous peroxidase activity was inhibited by immersing the slides in a cold (4°C) 0.3% H_2O_2 solution in phosphate-buffered saline (PBS). Using methanol as the solvent for H_20_2 resulted in the loss of signal. We blocked the sections using a 1:50 solution of normal goat serum in 5% bovine serum albumin in tris-buffered saline (BSA/TBS) to prevent non-specific antibody binding. We then incubated the sections with the primary antibody (TP-3, monoclonal IgG 2A, mouse anti-human) diluted in 1% BSA/TBS. Next, we incubated the sections with the secondary antibody from the kit (EnVision™). Finally, we developed the immunolabelled tissues using AEC substrate chromogen and then counterstained them with Mayer's haematoxylin. The slides were mounted with coverslips using a water-soluble mounting medium. We labelled negative controls using the same

protocol while omitting the primary antibody. We used a section containing micrometastases and macroscopic metastases as a positive control for each run.

Microscopic evaluation

We assessed each slide manually for microscopic metastases, micrometastases and TP-3-positive single cells. Micrometastases were defined as clusters of ≥5 and ≤50 TP-3 positive cells. Clusters of>50 cells were defined as microscopic metastases, while <5 TP-3 positive cells were defined as TP-3 positive single cells. When present, we counted the total number of microscopic metastases and micrometastases in each section. We also counted the number of TP-3-positive single cells in 10 high-power fields (HPF, defined as one field at 400x, equivalent to 0.196 mm2 for the microscope used) for each section.

Statistics

We compared the mean number of TP-3-positive cells per 10 HPF per lung lobe between groups using an unpaired Kruskal-Wallis test and Wilcoxon rank-sum tests between group pairs. We also compared the mean numbers of TP-3-positive cells per 10 HPF between different lung lobes between all dogs combined and in between groups using the same statistical tests. The prevalence of micrometastases in the OS+/Met- group was tested against the expected prevalence (>90%) using a binomial test. P-values <0.05 were considered statistically significant.

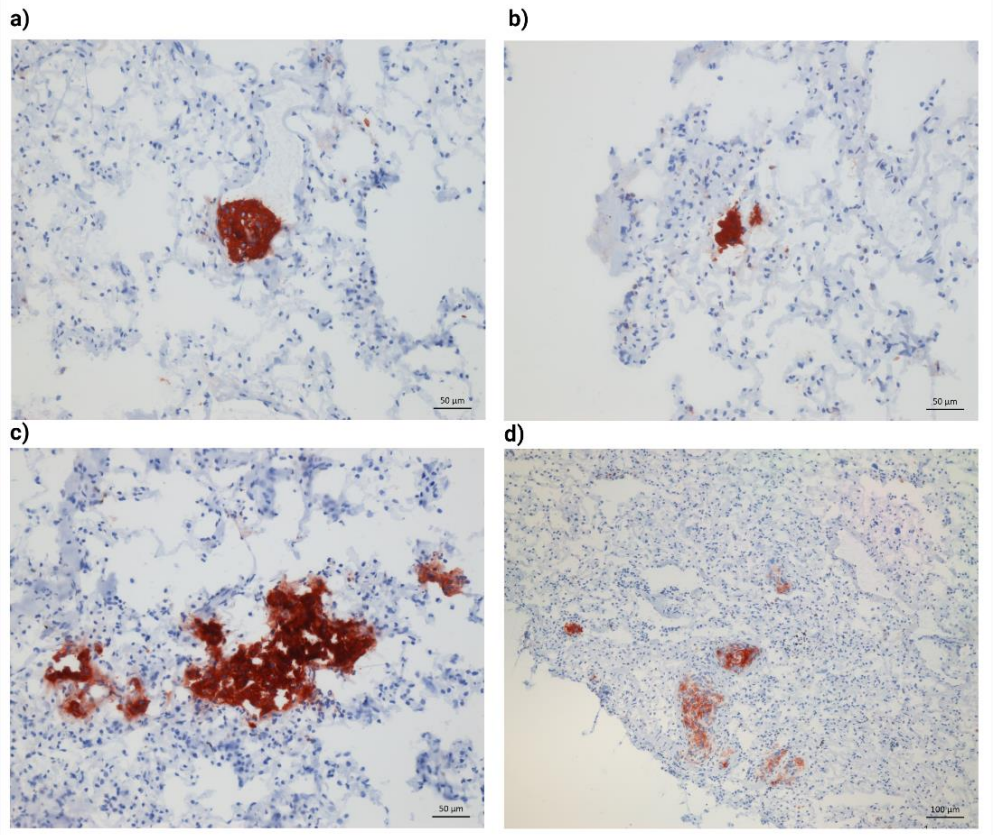

Figure 10: Immunohistochemical labelling of canine lung tissues of dogs with OS using TP-3. Images show pulmonary micrometastases and microscopic metastases from OS. ***a)*** *and* ***b)*** *show micrometastases, while* ***c)*** *shows a microscopic metastasis (200x magnification).* ***d)*** *shows both micrometastases and a microscopic metastasis (100x magnification).*

Paper II

Canine *in vitro* generated tumour-conditioned macrophages display an M2-like phenotype.

Overview

In this paper, we generated tumour-conditioned monocyte-derived macrophages (TCMΦ) *in vitro* and compared them phenotypically and transcriptomically to M1 and M2 macrophages. Their expression of various surface markers was assessed using flow cytometry, while RNA-Seq was used to compare their transcriptomes.

Monocyte isolation

We isolated peripheral blood mononuclear cells (PBMCs) from EDTA blood samples using density gradient centrifugation. Density gradient centrifugation permits easy isolation of mononuclear cells from red blood cells and granulocytes based on their relative density (Turner et al., 2020). Briefly, we diluted blood 1:2 in dPBS containing 2% foetal bovine serum (FBS) and 1% penicillin/streptomycin (P/S), then transferred it to a SepMate™ tube (StemCell Technologies) containing 15 mL of room-tempered Lymphoprep (1.077 g/mL, StemCell Technologies) and centrifuged it for 10 minutes (1200xg at 20°C). We harvested PBMCs by pouring the top layer off, leaving red blood cells and granulocytes in the tube. We washed the cells twice, lysed the remaining red blood cells using cold (4°C) distilled water, and then washed them once more.

We isolated monocytes from PBMCs using MACS CD14 MicroBeads (Miltenyi Biotec) and MACS LS columns coupled with a MidiMACS™ magnet separator, according to the manufacturer's instructions. Briefly, we incubated PBMCs with MACS CD14 MicroBeads in MACS buffer on ice for 15 minutes, then washed them once before applying them to a pre-rinsed MACS LS column placed in a MidiMACS™ magnet. After washing the column three times, we removed it from the magnet separator, and $CD14^+$ cells were washed out and collected, then washed twice more.

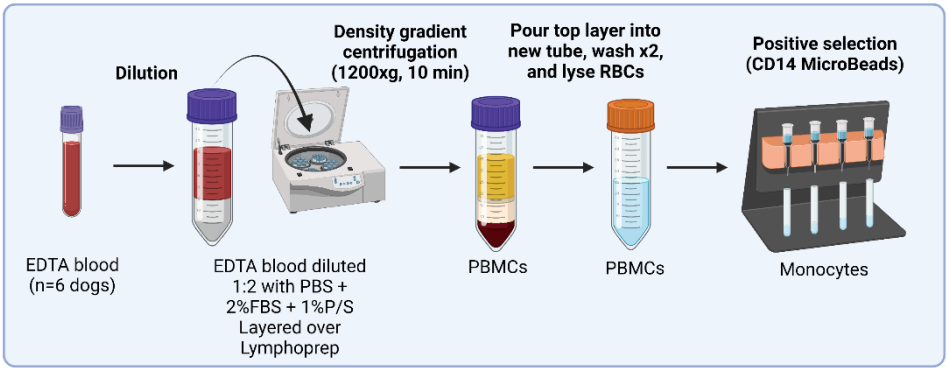

Figure 11: Schematic representation of peripheral blood mononuclear cell (PBMC) and monocyte isolation from canine blood. Red blood cells (RBCs), foetal bovine serum (FBS), penicillin/streptomycin (P/S) (Figure by the author, created using BioRender©, 2023).

Macrophage generation

We resuspended monocytes in Roswell Park Memorial Institute (RPMI)-1640 medium with GlutaMAX™ containing 10% FBS and 1% P/S (complete medium) and seeded them on 12-well Nunc™ Multidishes with UpCell™ surface (Thermo Fisher Scientific). We generated M1 and M2 macrophages according to the same protocol used by Heinrich et al. (Heinrich et al., 2017). Briefly, M1 macrophages were differentiated over five days using granulocyte-macrophage colony-stimulating factor (GM-CSF, 5 ng/mL), followed by stimulation with lipopolysaccharide (LPS, 100 ng/mL), interferon-gamma (IFN-γ, 20 ng/mL) and GM-CSF over 2 days. M2 macrophages were differentiated over five days using macrophage colony-stimulating factor (M-CSF, 25 ng/mL), followed by stimulation with interleukin 4 (IL-4, 20 ng/mL) and M-CSF for two days.

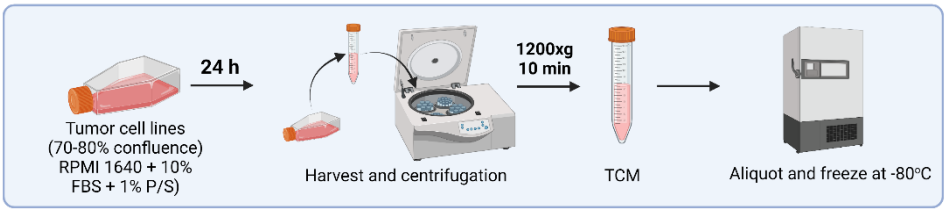

Figure 12: Schematic overview of the generation of tumour conditioned media (TCM). Roswell Park Memorial Institute (RPMI), foetal bovine serum (FBS), penicillin/streptomycin (P/S) (Figure by the author, created using BioRender©, 2023).

We generated three TCMΦ populations using tumour-conditioned media (TCM) from three different canine cancer cell lines, D17 (OS), KTOSA5 (OS), and REM134 (mammary carcinoma). We used the same protocol as Solinas et al. to generate TCM (Solinas et al., 2010). We generated the three TCMΦ populations (TAM(D17), TAM(KTOSA5), and TAM(REM134)) by incubating monocytes in 1:1 TCM to complete medium and M-CSF over 7 days.

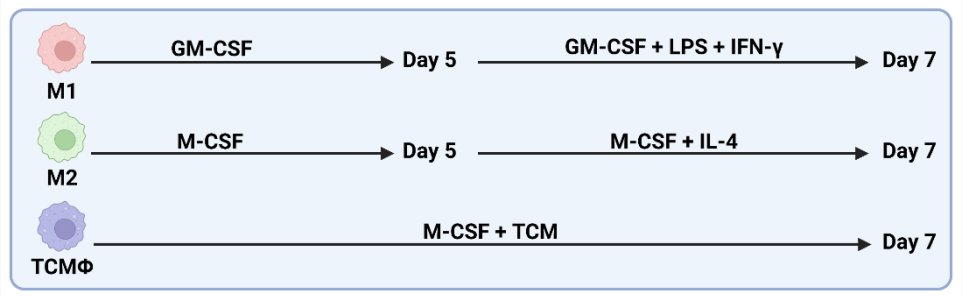

Figure 13: Schematic overview of the differentiation protocol used to generate each macrophage population in vitro. Granulocyte-macrophage colony-stimulating factor (GM-CSF), macrophage colony-stimulating factor (M-CSF), lipopolysaccharide (LPS), interferon-gamma (IFN-γ), interleukin-4 (IL-4), tumour-conditioned media (TCM), tumour-conditioned macrophages (TCMΦ). (Figure by the author, created using BioRender©, 2023).

All cultures were maintained under standard culture conditions (5% CO_2, 37°C) and inspected daily. Half of the culture medium was replaced every 2-3 days, and fresh growth factors were added.

Flow cytometry

After seven days, we removed the medium, washed the wells with dPBS, and filled them with complete medium. Due to the temperature-sensitive surface of the plates, harvesting was easily accomplished by placing the cells at room temperature for 30 minutes and gentle pipetting, as cells detach when the temperature falls below 32°C. We transferred approximately 1 x10^5 cells per condition to a 96-well u-bottom plate for staining. First, we stained dead cells using the LIVE/DEAD™ fixable yellow staining kit (Invitrogen) according to the manufacturer's instructions. Next, we incubated the cell with a canine Fc-receptor binding inhibitor (Invitrogen), diluted

in flow buffer (dPBS containing 0.5% BSA and 0.005% sodium azide) to inhibit unspecific antibody binding. Since our panel contained many antibodies, we performed direct labelling with fluorophore-conjugated primary antibodies. The following antibodies to were used to label the generated macrophages: Pacific blue anti-CD14 1:100, FITC anti-LYVE-1 1:50, APC anti-CD11d 1:50, Pacific blue anti-FcεRI 1:50, PE/Cy7 anti-CD206 1:50, and PE-anti-CD209a 1:50. After labelling, we fixed the cells using 1x BD FACS™ Lysing Solution (BD Biosciences) and resuspended them in flow buffer before analysis. We recorded at least 10.000 gated events for each staining using the Gallios flow cytometer (Beckman Coulter), equipped with the Kaluza G software (Beckman Coulter). Data were analysed using Kaluza analyser software v.2.1 (Beckman Coulter).

We assessed the purity of macrophages using CD14 staining. Furthermore, we used fluorescence minus one (FMO) controls to set the gates. Additionally, we performed single staining controls using UltraComp eBeads™ (Invitrogen) to adjust compensation. We ran unstained samples to record autofluorescence and isotype controls as part of the protocol optimization to control for unspecific binding. We calculated the Δ mean fluorescent intensity (MFI) for each reading by subtracting the FMO control MFI from the measure MFI of a given population.

RNA-Seq

We isolated total RNA using the RNeasy Mini Kit (Qiagen) according to the manufacturer's instructions. We used the Agilent 2200 Tape station system and software (Agilent) to measure RNA integrity according to the manufacturer's instructions. Library preparation and sequencing were performed at a commercial laboratory (The Norwegian Sequencing Centre, Oslo). Briefly, cDNA libraries were generated using the TruSeq stranded mRNA prep kit (Illumina™) according to the manufacturer's instructions. Samples were sequenced on the NovaSeq 6000 (Illumina™) using a NovaSeq 6000 SP flow cell (Illumina™) with resulting 100bp single-end reads.

Bioinformatic analysis

We assessed raw RNA sequences for quality using FastQC (version 0.11.9). We removed low-quality regions and trimmed adapters using Trimmomatic (version 0.39). Finally, we mapped high-quality reads using Kallisto (version 0.44.0) using reference transcriptome ROS_Cfam_1.0 (GCA_014441545.1) with a k-mer length of

31 (Broad Institute, Cambridge, MA, released June 2021; downloaded from Ensemble release 105).

Statistics

For flow cytometric data, we compared groups using one-way ANOVA, with post hoc testing using Tukey tests for comparison between groups. We performed differentially expressed gene (DEG) analysis using Degust (version 4.1.1)/R (version 4.2.2) to compare gene expression between conditions. The significance level was set at P=0.05.

Paper III

Immunological pre-metastatic niche in dogs with osteosarcoma

Overview

In paper III, we used multiplex immunofluorescence (IF) on FFPE tissue sections to identify macrophages, monocytes, and BMDCs. We included a total of 25 dogs for this study, ten dogs with OS without metastases (OS+/Met-), five dogs with OS with metastases (OS+/Met+), and ten without cancer (OS-/Met-). We randomly chose one of the peripheral FFPE lung samples if the dog had a complete set of samples, while we used the available lung tissue sample from dogs with only one.

Immunohistochemical staining

We compared IHC and IF labelling of FFPE tissues to ensure chromogenic and fluorescent signals were identical during protocol optimisation. Briefly, we deparaffinised the tissue sections (cut at 4 μm thickness) in xylene and rehydrated them through an ethanol gradient in an automated slide stainer. We performed heat-induced epitope retrieval (HIER) by placing the slides in Diva Decloaker (Biocare Medical) and heated them using a pressure cooker (110°C for 10 minutes). Next, we inhibited endogenous peroxidase activity using 3% H_2O_2 in methanol and blocked the sections using a 1:50 solution of normal goat serum in 5% BSA/TBS. We immunolabelled the sections using the same kit and protocol as in paper I (EnVision™+). Slides were labelled using antibodies against CD204 (1:100, mouse anti-human), CD206 (1:1600, rabbit anti-human), and CD11d (1:20, mouse anti-dog).

Immunofluorescent staining

We sectioned tissue for IF staining from FFPE blocks (cut at 4 μm thickness). First, we deparaffinised and performed HIER as described for the IHC staining. We then performed the IF labelling according to the protocol by Robertson et el. with some modifications (Robertson et al., 2008). We blocked sections using 1:50 normal goat serum in 5% BSA/TBS, then incubated them with the primary antibodies diluted in IF-buffer (PBS + 1%BSA + 2% FBS). We used CD206 (1:1600) and CD204 (1:100), or CD206 (1.1600) and CD11d (1:50) for labelling. Next, we incubated the sections with secondary antibodies diluted in IF-buffer (Alexa fluor 647 goat-anti mouse IgG1 and Alexa fluor 750 goat anti-rabbit, both at 1:1000). We added 4',6-diamidino-2-phenylindole (DAPI, 1.43 μM, 1:10.000) in the IF-buffer for the last three washing steps for nuclear staining. Finally, we mounted the slides using ProLong™ Diamond to prevent photobleaching, stored them at 4°C, and imaged them within a week.

We labelled negative controls using the same protocol while omitting the primary antibodies. As part of the protocol optimisation, we also included FMO controls where one fluorophore was omitted from the panel and single controls using only one of the fluorophores at the time. We used these controls to set the acquisition settings for the confocal microscope. To ensure there was no cross-reactivity, we also included single controls where one or both secondary antibodies were applied. We also ran isotype controls to ensure there was no unspecific binding. We labelled a section from healthy splenic tissue in each run as a positive control.

Quantification of labelled cells

We assessed the IHC sections using bright field microscopy and a confocal microscope to image IF sections. The confocal microscope we used (Leica Stellaris 8) has a white laser, meaning the user can set the excitation point for each channel at their discretion. We chose the settings for the laser and collection windows using the single and FMO controls to limit unspecific background, optimise signal strength, and ensure no spectral overlap between channels. Ten images were taken randomly from each sample at 200x (equivalent to 0.276mm^2), and immunolabelled cells were automatically quantified using ImageJ 1.51K.

We opened images in ImageJ, adjusted the intensity and contrast, and then converted them to 8-bit grayscale images. Then we adjusted the threshold to remove background noise and inverted them to allow the software to quantify cells. Finally, we used the particle analysis tool to quantify cells. The number of DAPI$^+$,

$CD204^+$, $CD206^+$, $CD11d^+$, $CD204^-CD206^+$, $CD204^+CD206^-$, and $CD204^+CD206^+$ were recorded.

Statistics

We compared the mean number of $CD204^+$, $CD206^+$, $CD204^+CD206^-$, $CD204^+CD206^+$, $CD204^-CD206^+$, $CD11d^+$, and DAPI positive cells per 10 HPF, as well as the number of positive cells normalized to the total nucleated cell count (DAPI positive) between groups using Wilcoxon rank-sum tests for each pair and an unpaired Kruskal-Wallis test. We compared the age between groups using Student t-tests and sex distribution using a Chi-square test. P-values <0.05 were considered statistically significant for statistical testing.

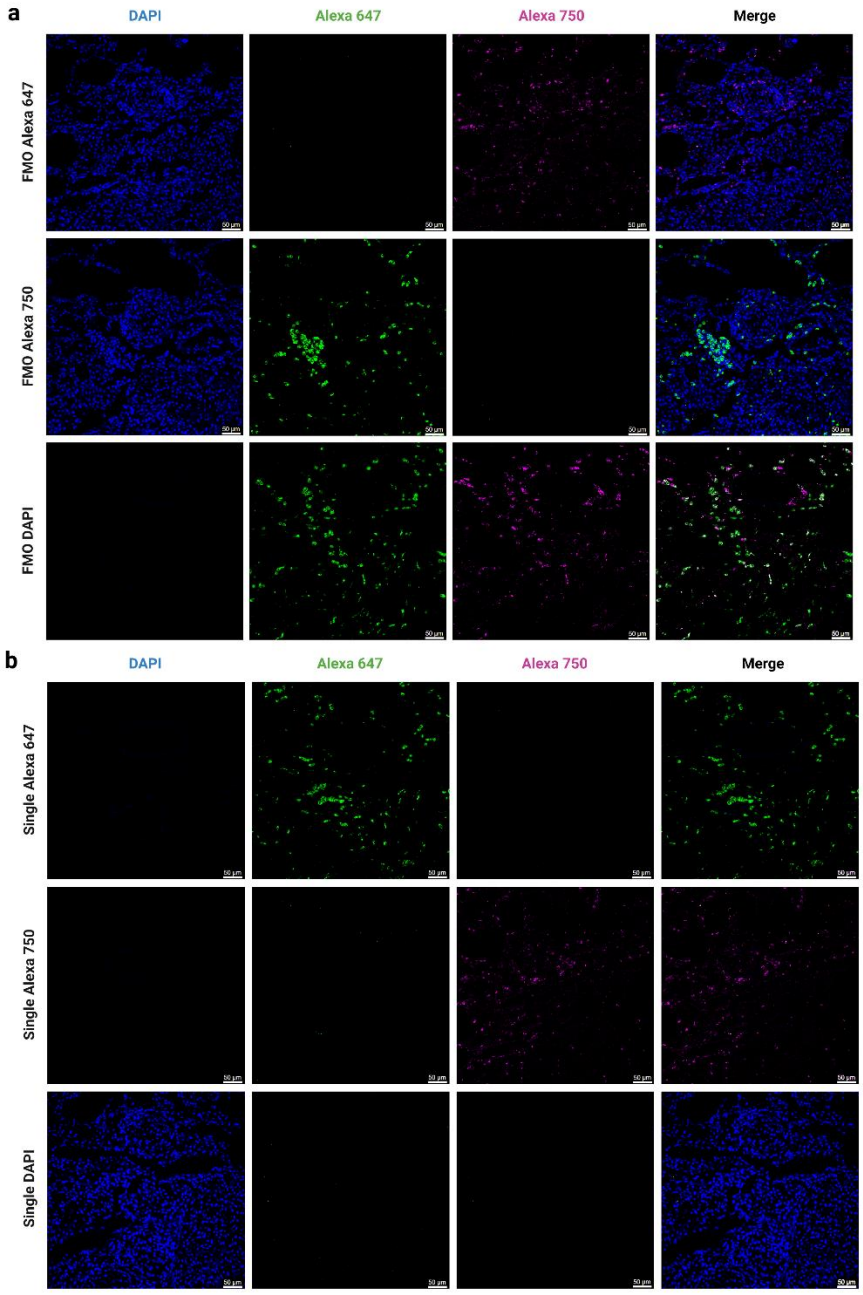

Figure 14: Immunofluorescent labelled lung tissues from a dog with metastatic OS. ***a)*** *shows fluorescence minus one (FMO) controls, labelled with all fluorophores minus one* ***b)*** *shows single controls, labelled with a single fluorophore at the time.*

5.3 Results

Paper I

Early immunohistochemical detection of pulmonary micrometastases in dogs with osteosarcoma.

Mikael Kerboeuf, Erling Olaf Koppang, Anita Haug Haaland, Frode Lingaas, Øyvind Sverre Bruland, Jon Teige, Lars Moe

Acta Veterinaria Scandinavica, 2021, DOI: 10.1186/s13028-021-00608-9

Canine osteosarcoma (OS) is a highly aggressive cancer, and most dogs (>90%) develop metastases despite a low overt metastatic prevalence (>15%) at the time of surgery. This study aimed to investigate the prevalence of pulmonary micrometastases in dogs with OS without macroscopic metastases. A tissue sample from each of the seven lung lobes was immunolabelled with TP-3 to identify micrometastases (defined as clusters of 5-50 tumour cells), microscopic metastases (defined as clusters of >50 tumour cells), and TP-3 positive single cells (defined as clusters of <5 tumour cells). We found that micrometastases easily overseen on routine histology could be detected with TP-3 immunohistochemistry. Furthermore, pulmonary micrometastases and microscopic metastases were only present in two out of ten (20%) dogs with OS without macroscopic metastases. This prevalence was significantly lower than the expected prevalence of >90% ($P<0.0001$). The micrometastatic and microscopic metastatic occurrences were relatively high in dogs where they were present. Micrometastases were found in three (43%) and four (57%) of the seven samples from each of the two dogs, with a mean of 0.6 and 1.7 micrometastases per sample. Microscopic metastases were found in one (14%) and four (57%) of the seven tissue samples in the same two dogs, with a mean of 0.14 and 1.0 microscopic metastases per sample. Only four (57%) and two (29%) of the seven tissue samples from these two dogs had neither micrometastases nor micrometastases present. The mean numbers of TP-3 positive cells were not significantly different between the OS+/Met+, OS+/Met-, and OS-/Met- groups. The ciliated bronchial epithelium was also labelled by TP-3, often all the way down to the terminal bronchioles. Snap-frozen tissues often result in poor tissue morphology, and cells can easily dislodge from their original location. Most TP-3 positive single cells represented dislodged epithelial cells, making the distinction between epithelial cells and tumour cells impossible. In conclusion, pulmonary micrometastases could be detected with TP-3 in a subset of dogs with OS before macroscopic metastases had developed. The prevalence of pulmonary

micrometastases was significantly lower than expected based on the high pulmonary metastatic rate.

Paper II

Canine *in vitro* generated tumour-conditioned macrophages display an M2-like phenotype.

Mikael Kerboeuf, Lars Moe, David Argyle, Seda Ozaydin, Anita Haug Haaland, Preben Boysen.

Tumour-associated macrophages (TAMs) are abundantly present in the tumour stroma and play a central role in regulating the tumour microenvironment (TME). They are important for tumour progression, invasion, intra- and extravasation of tumour cells, angiogenesis, extracellular matrix remodelling, and immunosuppression. This study aimed to phenotypically and transcriptomically characterize *in vitro* generated tumour-conditioned macrophages (TCMΦ) and compare them to M1 and M2 macrophages. Freshly isolated monocytes were differentiated into M1, M2, and three different TCMΦ populations *in vitro*. Surface marker expression was assessed using flow cytometry and transcriptomes generated using RNA-Seq. Morphologically, TCMΦ had a heterogeneous appearance but were more similar to M2 than M1 macrophages. All TCMΦ had an increased expression of the M2-associated markers CD209 and FcεRI, while 2/3 TCMΦ also had an increased expression of two additional M2 markers (CD206 and CD11d). Transcriptomically, only CD209 and FcεRI were upregulated in All TCMΦ compared to M1 macrophages. Several additional M2-associated surface markers were also upregulated in TCMΦ on RNA-Seq (CD36, CD163, CD204, TREM2, and MARCO). M1 associated cytokines, such as TNFα , IL1a, IL6, IL15, IL27, and IL34, and chemokines, such as CCL4, CCL5, and CCL22 were downregulated in TCMΦ. M2-associated cytokines and chemokines, such as TGF-β, CCL23, and MMP9, were upregulated in TCMΦ. The pro-inflammatory mediators S100A8, S100A9, and S100A13 were also upregulated in TCMΦ, compared to M1 and M2 macrophages. Given the high heterogeneity of TAMs *in vivo*, these results should be interpreted carefully and verified *in situ* and *in vivo*. The inability to recapitulate the complex interactions in the TME and tumour hypoxia limits the translation value of *in vitro* experimental studies such as this one. In conclusion, canine *in vitro*-generated TCMΦ exhibit several M2-associated pro-tumoural traits. Canine and human TCMΦ share many similarities, further warranting the use of dogs as research models to study TAMs. Furthermore, we identified several new M2-associated canine macrophage markers.

Paper III

Immunological pre-metastatic niche in dogs with osteosarcoma

Mikael Kerboeuf, Kristin Paaske Anfinsen, Erling Olaf Koppang, Frode Lingaas, David Argyle, Jon Teige, Bente Sævik, Lars Moe.

Pre-metastatic niche (PMN) formation is essential for metastatic development and drives metastatic organotropism. However, our knowledge of PMN formation stems primarily from studying pre-clinical models, and no studies have investigated PMN in veterinary medicine. This study aimed to investigate macrophage numbers and phenotypes and the presence of bone marrow-derived cells (BMDCs) in the pre-metastatic lungs of dogs with OS. A pulmonary tissue sample from each dog was immunofluorescently labelled to identify macrophages (CD204), M2-skewed macrophages and monocytes (CD206), and BMDCs (CD11d). The mean number of cells per 10 high-power fields was compared between dogs with OS, with and without metastases and dogs without cancer. The number of $CD204^+$ macrophages, $CD206^+$ macrophages and monocytes, and $CD11d^+$ BMCDs was significantly higher in the pre-metastatic lungs of dogs with OS than in dogs without cancer. The total nucleated cell density ($DAPI^+$) was higher among the dogs with OS than those without. Dogs with established OS metastases had comparable numbers of $CD204^+$ and $CD206^+$ cells as those without metastases. However, the number of $CD11d^+$ BMDCs was significantly lower among dogs with OS with established metastases than those without. The results were also the same when the counts were normalized to the total nucleated cell counts, aside from the number of $CD204^+$ cells, which did not reach statistical significance. The ratio of M2-skewed macrophages ($CD206^+CD204^+/CD204^+$) was similar between the groups. Although most dogs would likely have developed pulmonary metastases, this is not certain and therefore represents a limitation. In conclusion, our results provide evidence of PMN formation in a naturally occurring cancer model similar to those observed in pre-clinical murine models. Furthermore, they support using dogs with naturally occurring cancer as models to assess new PMN-targeting therapies.

5.4 Discussion

5.4.1 Methodical considerations

5.4.1.1 Selection bias

The primary aim of research is to study the association or the effect of some exposure on a particular outcome. Although the ultimate goal of any study is to make inferences about some association or causation to the broader population of interest (study population), one can seldom sample the entire population. Therefore, researchers rely on studying a smaller group of individuals from the study population and hope that this group is representative of the larger population. When this is not the case, and the selected individuals do not represent the study population, it results in selection bias (Tripepi et al., 2010).

There are several potential selection biases in this thesis. First, the dogs with OS we included might not represent the dogs in the study population (all dogs with appendicular OS). Since the owners had declined tumour-specific treatment (surgery, chemotherapy, radiation therapy, bisphosphonates, or immunotherapy), most dogs received pain relief until euthanasia. As a result, most dogs were euthanized shortly after diagnosis, while some achieved a good quality of life for a prolonged period until euthanasia (up to 155 days after diagnosis). Since our goal was to study the prevalence of pulmonary micrometastases at the time of clinical diagnosis or when surgery usually would have been performed, this may have influenced the results. The pulmonary micrometastatic prevalence might have been even lower if all the dogs had been euthanized shortly after diagnosis. However, seven out of 10 (70%) dogs with OS without macroscopic metastases were euthanized within two weeks after presentation, meaning they were probably representative of dogs at the time of surgery. On the other hand, one of the two dogs (50%) with OS without macroscopic metastases where micrometastases were present was euthanized 155 days after diagnosis, meaning it might not have had pulmonary micrometastases at diagnosis. This protracted time from diagnosis to euthanasia might also have influenced how far PMN formation had progressed. The changes compatible with immunological PMN formation we observed might not have been as pronounced at the time of diagnosis. However, this may have been beneficial in our case, given our small sample size, since more pronounced changes would be easier to identify. Regardless, it does not change the fact that PMN formation precedes metastasis in dogs with OS.

Furthermore, the dogs in the control group without cancer should ideally have been healthy with no concurrent disease. However, collecting lung tissues from healthy dogs would be ethically challenging, as it would entail collecting surgical lung biopsies or euthanizing healthy dogs. Dogs in the control group without cancer were all selected based on strict exclusion criteria to minimize potential confounding factors. However, it is unclear how different disease processes, trauma, and behavioural problems might interfere with macrophages and their phenotype, as well as BMDC recruitment to the lungs. Some drugs, such as chemotherapy and immunomodulating drugs, have been shown to influence macrophage phenotypes (Bryniarski et al., 2009, Mantovani and Allavena, 2015, Heath et al., 2021). For practical reasons, dogs receiving non-steroidal anti-inflammatory drugs (NSAIDs) were allowed in our studies. Since most dogs with OS had been receiving NSAIDs until and after presentation as pain relief, excluding those would have made it impossible to recruit enough cases. Similarly, dogs in the control group were also not excluded for having received NSAIDs, which some had. NSAIDs have been shown to induce both pro-inflammatory and anti-inflammatory skewing of macrophages, depending on the broadness of their spectrum (cyclooxygenase (COX)-1 and COX-2) and duration of therapy (Gilroy et al., 1999, Na et al., 2015). Moreover, NSAIDs can prolong survival and reduce metastatic development in several human and some canine carcinomas (de et al., 2009, Algra and Rothwell, 2012, Knapp et al., 2016, Zhao et al., 2017). Therefore, NSAIDs could potentially interfere with PMN formation and make the changes less pronounced. However, we still found significant differences between the groups. Surgery has also been shown to affect macrophage phenotype and numbers in the lungs and can induce the recruitment of MDSCs to tumour tissues (Mathenge et al., 2014, Tham et al., 2015, Kallis et al., 2020). Two of our control dogs had recently been through significant physical trauma (road traffic accidents), which could have interfered with macrophage phenotype and numbers in the lungs and BMDCs recruitment. However, this would probably have resulted in higher numbers of macrophages and BMDCs and M2-skewing of macrophages, resulting in changes more similar to those with OS. Despite including these dogs, there were still significant differences between the dogs with OS and the control group.

Although age and sex were not significantly different between the OS and control group without cancer, breed composition varied. Different breeds might show different responses to immunological challenges such as cancer. There is a lack of

published research assessing breed differences in macrophage of BMDC responses in dogs. Therefore, it is difficult to predict how this may have interfered with our results. Finding eligible control dogs was challenging enough, and breed matching would, in any case, not have been feasible.

5.4.1.2 Sample size

Recruiting enough cases for studies can be challenging, especially for rare diseases like OS. Strict exclusion criteria further complicate case recruitment. Many owners chose to treat their dogs when diagnosed with OS, precluding their enrolment in our study. Additionally, it can be hard to motivate owners to enrol their dogs for research when there is no incentive for them to do so other than increasing knowledge, such as the opportunity to try a new treatment. Therefore, the sample size is relatively small, making inferences about the micrometastatic prevalence in the study population less reliable. Changes compatible with PMN formation were still significant between groups, despite the small sample size, which could indicate that this is a common phenomenon at this stage of the disease. However, larger studies are warranted to confirm our results.

5.4.1.3 Morphological methods to identify micrometastases

Morphological methods such as IHC rely on processing and examining thin sections from tissue biopsies. If a disease process is diffusely present within an organ, changes in the tissue section will probably reflect the changes in the organ from which it came. However, this is not always the case if a disease process is focal or multifocal. One of the main concerns when using morphological methods to detect micrometastases is the relatively small proportion of tissue examined. In dogs where we found micrometastases, these were present in three (43%) and four (57%) of the seven lung lobes examined. This finding seemingly indicates that the micrometastatic burden is relatively high once micrometastases have developed. However, our protocol might not be sensitive enough to detect micrometastases in dogs with a lower micrometastatic burden. Micrometastases have been studied in several metastatic target organs in humans, such as lymph nodes, bone marrow, lungs, liver, pleural or peritoneal cavities, and peripheral blood (Huvos et al., 1971, Hashimoto et al., 1976, Nakajima et al., 1978, Sloane et al., 1980, Kondo et al., 1989,

Nanko et al., 1998, Bruland et al., 2005, Zhang et al., 2005, Gibson et al., 2018, Fossmark et al., 2019). Most of these studies used morphological methods, although some employed more sensitive ones, such as polymerase chain reaction (PCR)-based methods and tumour cell enrichment using magnetic beads. Lymph node micrometastasis detected morphologically is included in the staging systems of certain human cancers, such as breast cancer (Singletary et al., 2002). When using morphological methods, sections are usually made at three to five levels of the investigated lymph node (Fournier et al., 2004). This approach enables the investigator to assess a higher proportion of the investigated tissues than we could in our study. In a study examining the prevalence of micrometastases in seemingly unaffected lung tissues of humans with primary lung cancer, only 7.7% of evaluated microscopy slides contained micrometastases, with 47% of patients having micrometastases in total (Hashimoto et al., 1976). Their findings suggest several biopsies should be examined when searching for micrometastases, although this was a different setting and cancer form.

Other methods, such as PCR, are more sensitive for detecting micrometastases than morphological ones (Okami et al., 2000, Gillanders et al., 2004). However, information regarding appearance, size, and location is lost when using these methods. We could have used molecular techniques in parallel with morphological ones, but finding and validating OS-specific genes not expressed in healthy lung tissues is challenging and time-consuming. Other methods might have been more appropriate, such as enzymatic tissue dissociation followed by magnetic bead isolation and visual inspection, as performed by Bruland et al. (Bruland et al., 2005). Flow cytometric detection of micrometastasis in sentinel lymph nodes has also proven more sensitive than morphological methods (Ito et al., 2005, Hartana et al., 2016, Häyry et al., 2018). Although more sensitive and able to process larger tissue volumes, this method requires each sample to be processed immediately after euthanasia. Therefore, we could not have used the pre-collected frozen tissues and would have had to rely on newly enrolled cases.

5.4.1.4 How methods can interfere with results in *in vitro* research

When performing *in vitro* research, the experimental setup can significantly impact the study outcomes. For this reason, Murray et al. introduced guidelines for *in vitro* macrophage research (Murray et al., 2014).

The starting material used to generate macrophages can result in phenotypical and functional differences. Macrophages can be generated from patient-derived samples, such as monocytes from blood or BMDCs from a bone marrow sample, or from established monocyte-macrophage cells lines (such as canine DH82 and human THP-1 or SC), or pluripotent stem cells (iPSCs, which are induced from somatic cells). Both human and canine macrophage-monocyte cell lines can exhibit differences in surface marker expression and cytokine production compared to monocyte-derived macrophages when activated using the same growth factors and cytokines (Herrmann et al., 2018, Duweb et al., 2022). For example, the M2-associated marker FcεRI was upregulated in M2 vs M1 canine monocyte-derived macrophages, while DH82 cell line-derived macrophages showed the opposite (Herrmann et al., 2018). Similarly, the M2-associated markers CD163 and CD206 are not upregulated in the human THP-1 and SC cell line-derived macrophages when stimulated with IL4/IL13, whereas IL4/IL13 induce a higher expression of these markers in human monocyte-derived macrophages (Duweb et al., 2022). Macrophages can also be generated from BMDCs and iPSCs (Cao et al., 2019, Luque-Martin et al., 2021). The resulting macrophages are more similar to monocyte-derived macrophages than cell line-derived macrophages, yet some transcriptomic and functional differences exist. iPSC-derived macrophages have some benefits, as they are transcriptomically more similar to tissue-resident macrophages, which can be beneficial if these are the ones the investigator is interested in modelling (Cao et al., 2019). Furthermore, they are easy to manipulate genetically and can expand *in vitro*. However, generating macrophages from BMDCs and iPSCs requires more invasive sampling procedures. Furthermore, generating macrophages from iPSCs is technically challenging, time-consuming, and costly compared to using blood-derived monocytes. We used blood-derived monocytes to generate macrophages. In addition to being more representative of *in vivo* macrophages than cell-line-derived macrophages, a substantial proportion of TAMs are monocyte-derived, suggesting they might be better at modelling TAMs (Hourani et al., 2021).

When generating macrophages from blood-derived monocytes, the technique used to isolate monocyte from PBMCs can affect the resulting macrophage phenotype. Monocytes isolated using plastic adhesion result in macrophages that are M1-skewed (Nielsen et al., 2020). This method takes advantage of the ability of monocytes to adhere to the plastic surface of the culture vessel, which allows easy removal of the non-adherent fraction of PBMCs (lymphocytes and NK-cells). This

method also results in monocyte loss and low monocyte purity. On the other hand, monocyte isolation using negative selection results in M2-skewed macrophages. This method relies on labelling all other cells than the ones of interest with antibody-coated paramagnetic beads and collecting the cells that are not attracted by the magnet (in this case, monocytes). Monocyte isolation using positive selection with anti-CD14 coated paramagnetic beads interferes the least with downstream macrophage phenotype and results in the highest monocyte yield and purity. This method relies on only labelling the cells of interest while the unwanted cells are washed through the magnet. Therefore, we chose positive selection since it interferes the least with macrophage phenotypes.

Harvesting and detachment methods can also affect the expression of phenotypic surface markers and the functionality of macrophages (Chen et al., 2015). Enzymatic detachment reagents, like trypsin and Accutase™, can reduce M2-marker levels on macrophages, such as CD163 and CD206, compared to non-enzymatic methods. These reagents rely on the cleavage of extracellular and surface proteins to detach cells, which can also cleave surface receptors. Furthermore, they can reduce the phagocytic capabilities of macrophages. Therefore, enzymatic detachment methods can interfere with results and any downstream essays or applications of the resulting macrophages. Physical or chemical detachment methods affect macrophages less but can decrease viability if done incorrectly. Physical detachment methods include scraping and cooling, while chemical methods use reagents such as EDTA. We used temperature-responsive plastic to culture our macrophages, which enabled gentle harvesting and high viability. Thermo-responsive plastic interferes little with phenotypical marker expression and functionality (Rennert et al., 2017). The plastic is coated with a layer of poly(N-isopropylacrylamide) (PNiPAAm), which is slightly hydrophobic at culture temperatures (37^{o}C) but becomes hydrophilic at temperatures below 32^{o}C. The cells are gently detached by placing the plates at room temperature for a short time (20-30 minutes).

The combination of cytokines and growth factors used to generate specific macrophage phenotypes can affect the results. Therefore, Murray et al. advocated that authors must clearly state which cytokines they used to differentiate different macrophage phenotypes (Murray et al., 2014). M2 macrophages can be generated using IL-4, IL-10, IL-13, or TGF-β, alone or in combination and will result in different phenotypes. We chose the classical M2 activation protocol, using M-CSF and IL-4, which was used by Heinrich et al. as this protocol uses the least cytokines and,

therefore, introduces fewer variables (Heinrich et al., 2017). Similarly, tumour-conditioned macrophages can be generated *in vitro* using different protocols. Since M-CSF is an important growth factor for TAM differentiation *in vivo*, and since most cancer cell lines do not secret it, it is usually added when differentiating tumour-conditioned macrophages (Solinas et al., 2010, Grugan et al., 2012, Benner et al., 2019). Most protocols use tumour-conditioned media as it contains tumour-derived secretory factors and EVs. However, this results in a lack of cell-to-cell interaction. Since using tumour-conditioned media is commonplace in human and murine studies, we chose to use it over a co-culture setup, as it is more practical and easier to standardise.

Another factor which can interfere with *in vitro* experiments is microbiological contamination of reagents and cell lines (Segeritz and Vallier, 2017). Bacterial or fungal growth in the culture medium can profoundly affect cell culture experiments and take a long time to detect. Endotoxin measurements, bacteriologic or fungal cultures, pathogen-specific PCR, or enzyme-linked immunosorbent assay (ELISA) should be analysed when suspecting such contamination or as a routine procedure. Although we did not run any such assays, the cultures were inspected visually and under an inverted microscope daily.

5.4.1.5 Interspecies differences

One of the major hurdles when doing research in veterinary medicine is the lack of species-specific reagents. Many antibodies used in veterinary research were developed for human or murine antigens but cross-react with the canine epitope. For example, Moreira et al. showed that only 11 of 17 antibodies against human cytokines cross-reacted with the canine ones (Moreira et al., 2015). Therefore, one should be vigilant when adopting new essays and antibodies and validate them for canine applications. TP-3 recognizes a human tumour antigen but also labels canine OS on IHC and *in vivo* using positron emission tomography (PET) scans (Bruland et al., 1985, Haines and Bruland, 1989, Page et al., 1994). However, we should have considered additional validation steps to ensure that TP-3 binds to the same antigen. We could have performed western blotting to see if TP-3 binds to the same peptide as in humans, and the peptide could have been sequenced (Hnasko and Hnasko, 2015). Also, frozen tissue samples from the primary tumours should have been collected simultaneously with the lung samples to ensure they expressed the

TP-3 binding epitope. Without doing this, there is a chance that some tumours did not express the epitope, and neither would the micrometastases. However, we found no suspected micrometastases upon microscopy that were not labelled with TP-3.

5.4.1.6 Validating RNA-Seq findings

Traditionally, results from transcriptomic analyses were often validated using methods like quantitative PCR (qPCR) (Coenye, 2021). When transcriptomes were generated using older methods like microarray analyses, there were concerns regarding reproducibility and biases. However, modern RNA-Seq analyses use next-generation sequencing platforms (Illumina™) that do not suffer from the same issues and correlate well with qPCR results. We chose not to perform any validation of sequencing data in our study, both because of the fidelity of RNA-Seq and a lack of available RNA (it was all used for sequencing). Furthermore, the mRNA expression in cells does not necessarily accurately reflect protein abundance at a given time point (Reimegård et al., 2021). Proteins have a higher stability than mRNA, meaning they degrade less quickly, and proteins are often present in orders of magnitude higher than mRNA within cells. In our case, there was a good correlation between transcriptomic and flow-cytometric data for some markers, while others did not show a similar correlation.

5.4.2 General discussion

5.4.2.1 Osteosarcoma micrometastases – where are they?

Since most dogs with OS (>90%) develop pulmonary metastases after complete surgical removal of the primary tumour, it is generally accepted that >90% have micrometastases at this time. However, where these micrometastases reside at the time of surgery remains unanswered. In Paper I, we found pulmonary micrometastases and microscopic metastases in only 20% of the dogs with OS before macroscopic metastases had developed. Among human patients with OS, the prevalence of tumour cells in the bone marrow at presentation was shown to be 63%, while in those with visible metastases, it was 92% (Bruland et al., 2005). Although this relates to human patients, it would be reasonable to assume similar results in dogs. As in dogs, there is a relatively low metastatic prevalence at diagnosis (18%), and before the era of chemotherapy, over 80% of patients developed metastases after surgery (Marko et al., 2016, Misaghi et al., 2018). If the pulmonary micrometastatic prevalence found among our dogs is representative, it is substantially lower than what Bruland et al. found in the bone marrow of humans. A possible explanation could be that the bone marrow functions as a temporary nest for disseminated cancer cells until they eventually metastasize to the lungs. Indeed, human prostate and breast cancer cells can disseminate to the bone marrow using mechanisms similar to those used by homing hematopoietic stem cells (Müller et al., 2001, Taichman et al., 2002, Shiozawa et al., 2015, Allocca et al., 2019). It has been suggested that these tumour cells can lay dormant in the bone marrow niche, remaining quiescent for several years until metastases develop. Unpublished data from our group indicates that the micrometastatic prevalence in the bone marrow of dogs with OS is substantially higher than in the lungs. Several of the dogs included in Paper I were also assessed using the same method employed by Bruland et al. (2005), and all dogs with OS had bone marrow micrometastases. Further studies using different methods for identifying micrometastases are warranted to validate these findings. By improving our understanding of the metastatic chain of events, specific processes in metastatic development might be targeted, such as targeting the bone marrow niche or the PMN in the lungs.

5.4.2.2 Tumour conditioned macrophages and M2 macrophages – surface markers

It has become clear that the M1/M2 dichotomy represents two extremes of a complex and dynamic polarization spectrum. Single-cell RNA-Seq of TAMs further shows that they cannot be classified within this system (Chevrier et al., 2017, Lavin et al., 2017, Azizi et al., 2018, Wagner et al., 2019, Zilionis et al., 2019). In our *in vitro* study (Paper II), TCMΦ shared many similarities with M2 macrophages. However, we showed that they exhibit a distinctive phenotype, with several differences from M2 macrophages.

In paper II, we showed that *in vitro* generated TCMΦ had a high expression of several M2-associated markers. We found that surface receptor CD209, also known as dendritic cell-specific C-type lectin (DC-SIGN), was highly expressed among all TCMΦ populations and M2 macrophages, compared to M1. CD209 was also upregulated at the transcriptomic level. In line with our findings, human M2 macrophages, *in vitro* generated TCMΦ, and TAMs have been shown to have a high CD209 expression (Domínguez-Soto et al., 2011, Shao et al., 2019, Valeta-Magara et al., 2019, Hu et al., 2020, He et al., 2021). We also found that TCMΦ had a high expression of the M2-associated high-affinity IgE receptor FcεRI on flow cytometry and RNA-Seq, similar to M2 macrophages. In humans, FcεRI-expression by macrophages has been poorly characterized, but *in vitro*-generated human M2 macrophages have been shown to have a high FcεRI-expression (Pellizzari et al., 2019). We also found that our osteosarcoma TCMΦ, but not our mammary carcinoma TCMΦ, had an intermediately high expression of the M2-associated mannose receptor CD206. CD206 is a well-established M2-marker in humans and mice and has been shown to be highly expressed by most TAMs in these species (Mantovani et al., 2004, Smith et al., 2016, Yang et al., 2018, Hourani et al., 2021). As mentioned in the introduction, canine TAMs within mammary tumours have been shown to express CD206 (Monteiro et al., 2018). We also found that CD11d expression was intermediately high in our osteosarcoma TCMΦ but not in our mammary carcinoma TCMΦ. Furthermore, CD11d was highly expressed in M2 macrophages compared to M1. However, this was not the case on the transcriptomic level, as CD11d was neither upregulated in TCMΦ nor M2 macrophages. CD11d, or β2-integrin, was first identified in dogs and is expressed on a subset of bone marrow macrophages, splenic red pulp macrophages, and lymph node medullary macrophages, as well as a subset of $CD8^+$ lymphocytes (Danilenko et al., 1995).

Contrary to our findings, CD11d has been shown to be upregulated in murine M1 macrophages compared to M2 and was highly expressed by macrophages within atherosclerotic plaques (Aziz et al., 2017). Additionally, CD11d expression by tissues-resident leukocytes under physiologic conditions varies between mice, humans, and dogs, further complicating comparisons (Danilenko et al., 1995, Miyazaki et al., 2014). Moreover, we found that lymphatic vessel endothelial receptor 1 (LYVE-1) was upregulated in M2 versus M1 macrophages, but the expression among TCMΦ was more variable. In mice, LYVE-1 was shown to be expressed by M2-skewed tissue-resident macrophages, *in vitro* generated M2 macrophages, and TAMs in melanoma (Dollt et al., 2017, Lim et al., 2018, Chakarov et al., 2019, Kieu et al., 2022).

In addition to the markers we assessed by flow cytometry, several other M2-associated surface markers were upregulated in the TCMΦ on RNA-Seq. In humans, CD36 has been shown to be highly expressed in several cancers and TAMs and plays a role in tumour growth regulation, metastasis, and drug resistance (Ruan et al., 2022). Similarly, our TCMΦ had a high expression of CD36 on RNA-Seq. CD163, a well-established M2 marker in humans, is highly expressed by human TAMs (Chen et al., 2019). Similarly, we found that our TCMΦ had a high expression of CD163 on RNA-Seq. Additionally, human M2-like TAMs have been shown to have a high expression of CD204 (Ohtaki et al., 2010, Kurahara et al., 2011, Miyasato et al., 2017). In Paper II, our TCMΦ also showed a high CD204-expression on RNA-Seq. Interestingly, we found that triggering-receptor-expressed on myeloid cells 2 (TREM2) was upregulated in TCMΦ compared to M1 and M2 macrophages. TREM2 has been shown to be a marker for immunosuppressive TAMs and tumour-infiltrating monocytes within human tumours (Katzenelenbogen et al., 2020, Nakamura and Smyth, 2020). Similarly, macrophage receptor with collagenous structure (MARCO) was also highly upregulated in our TCMΦ compared to M1 and M2 macrophages. Immunosuppressive TAMs in murine models of breast cancer, melanoma, and colon cancer have been shown to express MARCO, and in humans, MARCO has been shown to be highly expressed by a subset of human TAMs and *in vitro* generated TCMΦ (Georgoudaki et al., 2016, La Fleur et al., 2021).

Our findings support the notion that canine TCMΦ, like TAMs, share many phenotypical characteristics with M2 macrophages, as in humans and mice. Furthermore, these new canine phenotypical macrophage markers should be helpful for the in-depth multi-marker characterization of canine TAMs *in situ*.

5.4.2.3 Tumour conditioned macrophages and M2 macrophages – cytokines and chemokines

One of the main functions of TAMs within tumours is to suppress the adaptive immune response. We found that the immunosuppressive cytokine TGF-β was upregulated in M2 and TCMΦ compared to M1 macrophages. TGF-β can inhibit $CD8^+$ and $CD4^+$ T-cell functions and induce and recruit Tregs that can inhibit effector T-cells, as mentioned in the introduction. Additionally, we found that the chemokine CCL23 was upregulated in TCMΦ, which in humans has been shown to induce exhausted T-cell phenotypes with a high expression of immune checkpoint proteins and promote cancer cell migration in ovarian cancer (Kamat et al., 2022). However, other immunosuppressive cytokines and chemokines associated with M2 macrophages and TAMs, such as IL10 and CCL13, were not significantly upregulated in our TCMΦ. There was no increase in Arg-1 expression in our TCMΦ, which does not support any immunomodulatory function through arginine metabolism. In line with our findings, human M2 macrophages also do not exhibit the same Arg-1 upregulation as in mice, supporting the notion of inter-species differences in certain aspects of macrophage functions (Murray et al., 2014). Furthermore, the immunomodulating checkpoint ligand PD-L1 was not upregulated in either our TCMΦ or M2 macrophages. On the other hand, we found that the CTLA-4 ligand CD86 was upregulated in TCMΦ compared to M1 and M2, which in humans has been shown to inhibit T-cell cytotoxic functions (Vandenborre et al., 1999).

Another central function of TAMs is their role in cancer cell migration, invasion, and metastasis. We found that the matrix-remodelling protease MMP9 was upregulated in TCMΦ. MMP9 has been shown to modify cell-to-cell junctions and disrupt basal membranes, thereby promoting cancer cell migration, invasion, and metastasis (Chen et al., 2019). Furthermore, the α4 integrin was upregulated in our TCMΦ compared to M1 and M2 macrophages. This integrin has been shown to promote survival and extravasation of cancer cells in murine models of breast cancer (Chen et al., 2011b).

Interestingly, we found that the M1-associated pro-inflammatory interleukins and cytokines were downregulated in TCMΦ. In humans, TAMs have been shown to produce several pro-inflammatory cytokines such as TNFα, IL1b, IL6, and

chemokines, and they are central contributors to angiogenesis, cell migration, and immunosuppression (Chen et al., 2019). Similarly, human *in vitro* generated TCMΦ have been shown to produce IL-6 and CCL2 (Solinas et al., 2010, Benner et al., 2019). Whether these differences in the expression of pro-inflammatory mediators are due to biological differences between dogs and humans and that different mechanisms are responsible for the same function remains unclear. Another possibility is that the cancer cell lines we used do not induce this response in macrophages *in vitro*. Additionally, as mentioned previously, mRNA levels do not always reflect protein expression, and additional essays, such as ELISA, could have been run to investigate further. On the other hand, we found that the pro-inflammatory mediators S100A8, S100A9, and S100A13 were upregulated in TCMΦ compared to both M1 and M2 macrophages. As mentioned previously, S100A8/9 have been shown to play a central role in pulmonary PMN inflammation. By inducing SAA3 production, and down-stream activation of the NF-κB pathway, S100A8/9 can induce pro-inflammatory cytokine production and BMDCs and MDCS recruitment (Hiratsuka et al., 2006, Hiratsuka et al., 2008, Tomita et al., 2010). Furthermore, S100A8/9 have been shown to promote cancer cell migration and invasion (Chen et al., 2019).

Lastly, none of the VEGFs were upregulated in our TCMΦ. Similarly, human TCMΦ have not been shown to have increased production of VEGFs when generated *in vitro* using TCM (Benner et al., 2019). Whether this is due to the lack of hypoxia or other reasons remains unclear. However, TGF-β and MMP9 have been shown to be central contributors to angiogenesis and were upregulated in our TCMΦ (Ribatti et al., 2007, Qian and Pollard, 2010, Riabov et al., 2014).

Although our TCMΦ exhibited a more M2-skewed phenotype than human TCMΦ, they still share many similarities. These results should be interpreted carefully, as this *in vitro* model does not fully recapitulate the complexity of *in vivo* macrophage polarization. However, the result may provide a basis for future *in vivo* and *in situ* studies, and this model could be used to assess macrophage-repolarizing drugs before *in vivo* studies.

5.4.2.4 Pre-metastatic niche

Despite being extensively studied in murine models, distant PMN-formation has not been studied in naturally occurring cancer. Due to the inherent limitations of murine

models, as described in the introduction, results from PMN research in this species may not be directly transferable to humans or dogs. We found evidence of microenvironmental changes in the lungs of dogs with OS without metastasis supporting the existence of such an immunological PMN in dogs.

5.4.2.4.1 CD11d$^+$ bone marrow derived cells

One of the most striking changes in murine PMN models is the recruitment of CD11b$^+$ BMDCs to the pre-metastatic lungs (Liu and Cao, 2016, Dong et al., 2021). These cells include Gr1$^+$, VLA-4$^+$, and VEGFR1$^+$ BMDCs, MDSC, macrophages, and monocytes. In murine models, recruited BMDCs are vital for creating a pro-angiogenetic environment, vascular leakiness, and immunosuppression. In Paper III, we found an increased number of CD11d$^+$ cells in the lungs of dogs with OS without metastases compared to dogs without cancer. Canine granulocytic and dendritic cells do not express CD11d, which suggests these positive cells were not neutrophils, but rather macrophage precursors (Danilenko et al., 1995). Furthermore, it has been shown that leukocytes in the alveoli and alveolar septa do not express CD11d under physiologic conditions in dogs, but they do so in humans (Danilenko et al., 1995, Miyazaki et al., 2014). Most human myeloid cells, such as circulating monocytes, monocyte-derived macrophages, tissue-resident macrophages, dendritic cells, and neutrophilic granulocytes, express CD11d. Since tissue-resident leukocytes in healthy canine lungs do not express CD11d, but bone marrow-derived macrophages and their precursors do, it is an ideal candidate to study BMDC recruitment to the pre-metastatic lungs. Since human tissue-resident pulmonary leukocytes express CD11d, it would not be useful as a BMDC-specific marker. Considering that a large proportion of CD11b$^+$ BMDCs in humans and mice are granulocytes and granulocytic MDSCs, we would not expect these cells to express CD11d in dogs, as it is considered macrophage-specific (Yan et al., 2010, Sceneay et al., 2012, Vadrevu et al., 2014, Wang et al., 2016b, Mazumdar et al., 2020a). However, adoptive transfer of MDSCs in mice has shown that most Gr1$^+$CD11b$^+$ MDSCs (granulocytic MDSC) differentiate into F4/80$^+$CD11b$^+$ macrophages in tumour tissues (Corzo et al., 2010). Therefore, it might not be surprising if these cells, which might have a granulocytic origin, express the macrophage-specific marker CD11d after extravasation to the lungs. Furthermore, the other subset of MDSCs, the monocytic MDSCs (CD11b$^+$Ly6C^{high}Ly6G$^-$), would be more likely to express CD11d than the granulocytic fraction (Chioda et al., 2011). In

paper II, we found that monocyte-derived osteosarcoma TCMΦ had an intermediately high expression of CD11d. The $CD11d^+$ cells we found among the dogs with OS without metastases in Paper III might also have expressed CD11b, but formalin fixation destroys the epitope in dogs and could not be assessed.

Interestingly, we found that the number of $CD11d^+$ cells was higher among the dogs with OS without metastases than those with established metastases. These results suggest that this $CD11d^+$ cell recruitment is a transient event, which occurs before metastasis but halters once metastases have developed. Whether these cells die and disappear or differentiate into macrophages remains unclear. Interestingly, the same phenomenon was observed in mice by Kaplan et al., with the percentage of BMDCs decreasing when the number of tumour cells in the metastatic site increased (Kaplan et al., 2005). They had transplanted the mice with BMDCs from green fluorescent protein (GFP)-transgenic mice before being injected with tumour cells. Their findings may suggest that the recruited BMDCs do not remain in the lungs after extravasation, as they would still express GFP after differentiation. Their results imply that this recruitment is transient and that the BMDCs are removed or die once metastases begin to establish.

5.4.2.4.2 Macrophages and monocytes

In Paper III, we also found an increased number of $CD204^+$ macrophages in the lungs of dogs with OS without metastases compared to dogs without cancer. Canine tissue-resident alveolar and interstitial macrophages express CD204 under physiological conditions (Kato et al., 2013). Furthermore, monocyte-derived macrophages also express CD204 shortly after extravasation. Whether the increase in $CD204^+$ macrophages we observed reflects a local expansion of tissue-resident macrophages or is due to recruited monocytes that differentiate into macrophages is unclear. Murine models of pancreatic cancer and salivary cystic carcinoma have shown that tumour-derived exosomes induce increased $F4/80^+$ macrophage numbers in the pre-metastatic liver and lungs, respectively (Costa-Silva et al., 2015, Yang et al., 2017). Our observations are in line with their results.

Similarly, we found that the number of cells expressing the M2-associated marker CD206 was higher in dogs with OS without metastases than in those without cancer. A large proportion of the $CD204^+$ macrophages were also $CD206^+$, meaning the

increased numbers of macrophages had an immunosuppressive tumour-permissive phenotype. Additionally, we found that $CD204^{-}CD206^{+}$ cell numbers were higher among OS dogs without metastases than those without cancer. These cells mostly had a morphology compatible with undifferentiated monocytes, which would explain their lack of CD204-expression. Similarly, in murine melanoma models of PMN-formation, monocytes have been shown to be recruited to the pre-metastatic lungs by tumour-derived exosomes (Plebanek et al., 2017). This may suggest that the increased numbers of macrophages are partly due to the recruitment and differentiation of monocytes.

The ratio of $CD206^{+}CD204^{+}/CD204^{+}$ positive cells, which reflects the percentage of M2-skewed macrophages, was comparable between our dogs with OS and dogs without cancer. As has been reported in humans, most alveolar and interstitial macrophages in healthy lungs expressed CD206 and can be considered M2-skewed under physiologic conditions (Mitsi et al., 2018). Since the lungs are in continuous contact with the environment through the inspiratory air, it would make sense that the macrophages here would not induce an inflammatory response to all antigens they encounter. Thereby, one could argue that one of the reasons why the lungs are a common site for metastases could be due to the high percentage of M2-skewed macrophages here. As mentioned in the introduction, M2-skewed macrophages are highly phagocytic, and M2-associated surface receptors such as MARCO can mediate the binding and internalization of extracellular particles such as exosomes (Martinez and Gordon, 2014, Kanno et al., 2020). If tumour-derived extracellular vesicles are preferentially internalized by M2-skewed macrophages in the lungs, we might also expect PMN formation to occur here since extracellular vesicles are the chief mediators of PMN formation.

There were no appreciable differences in the number of $CD204^{+}$ and $CD206^{+}$ cells between our dogs with OS with and without metastases. These results suggest this increase is not transient, like the $CD11d^{+}$ cell recruitment.

5.4.2.4.3 Total nucleated cell density

To reduce the effect of tissue density variation between dogs, we chose to normalize the cell counts to the total nucleated cell count in each HPF. Interestingly, we found that dogs with OS (both with and without metastases) had significantly more

nucleated cells per HPF than dogs without cancer. The variation in tissue density was more pronounced between the OS and control groups than between dogs within the same group. This increase was of such a magnitude that it could not be attributed to the increased numbers of macrophages, monocytes, and $CD11d^+$ BMDCs alone. Other BMDC fractions, such as granulocytes, granulocytic MDSCs, MDCS, Tregs, and stromal cells such as fibroblast, might explain the gap.

5.4.2.4.4 Other aspects of PMN formation

Angiogenesis and vascular leakiness are challenging to study in an *in situ* setting after euthanasia. However, M2-skewed macrophages have been shown to secrete matrix remodelling enzymes such as MMP 1,9, and 12, which can both induce angiogenesis and result in vascular leakiness (Jetten et al., 2014, Nakagomi et al., 2015, Jager et al., 2016, Liu and Cao, 2016). Indeed, in paper II, we showed that canine OS TCMΦ had a high expression of the M2-associated marker CD206 and upregulation of TGF-β, MMP9, and S100A8/9, which can induce angiogenesis and vascular permeability. Then, in Paper III, we found more $CD206^+$ macrophages in the pre-metastatic lungs of dogs with OS than in those without cancer. Additionally, MMPs play a central role in remodelling the extracellular matrix at the pre-metastatic site. However, we did not explore extracellular remodelling further in our dogs with OS.

We did not directly assess NK-cell dysfunction, hampered $CD8^+$ T cell cytotoxicity, or Treg recruitment. However, M2-skewed macrophages and TCMΦ have been shown to interfere with NK-cell and $CD8^+$ T cell responses (Oishi et al., 2016, Benner et al., 2019, Pu et al., 2021). Similarly, we showed in Paper II that canine OS TCMΦ had a high expression of TGF-β, CCL23, and the CTLA-4 ligand CD86, which can interfere with these responses. In murine models, MDSCs can inhibit NK-cell mediated cytotoxicity, antigen-presentation by dendritic cells and macrophages, and convert effector T-cells to Tregs (Li et al., 2009, Beury et al., 2014, Zoso et al., 2014). Whether the $CD11d^+$ BMDCs are capable of the same in our dogs with OS remains unanswered.

5.4.2.5 Dogs as models for TAM repolarizing and PMN targeting treatments

As mentioned in the introduction, the translational value of murine models for immunotherapies is limited (Olson et al., 2018). On the other hand, dogs with cancer represent ideal candidates for assessing immunomodulating drugs, as pointed out in previous work (Dow, 2019). We have found that canine TCMΦ exhibit an immunosuppressive and tumour-permissive phenotype, like in humans, suggesting dogs would be ideal candidates to study macrophage-repolarizing drugs in cancer therapy. Additionally, having found evidence of PMN existence, dogs with OS could also serve as models to study PMN-targeting drugs. In fact, the immunomodulating drug MTP was first assessed in dogs with OS before being used in human trials (MacEwen et al., 1989). In addition to improving outcomes in dogs with OS, MTP significantly prolonged survival in dogs with hemangiosarcoma when given after surgery (Vail et al., 1995). MTP binds to the intracellular nucleotide-binding oligomerization domain 2 (NOD2) receptor of macrophages, dendritic cells, monocytes, and Paneth cells (Inohara et al., 2003, Ogawa et al., 2011). NOD2 binding results in the activation of the NF-κB pathway, which results in the downstream production of pro-inflammatory cytokines like TNF-α, IL-6, IL-8, and IL-12. These cytokines are associated with M1-skewed macrophages, and MTP-treated macrophages show increased tumoricidal activity against cancer cells *in vitro* (Fidler et al., 1981). In the case of canine OS and hemangiosarcoma, MTP was given right after surgery, when dogs usually do not have macroscopically visible metastases. In the case of OS, we now know that dogs have increased numbers of M2-skewed macrophages and $CD11d^+$ BMDCs in the pre-metastatic lung. Whether MTP's clinical benefit is due to the reprogramming of TAMs within micrometastases and small metastases, the reprogramming of the immunosuppressive PMN, or both is unclear. As previously mentioned, MTP was later found to have a clinical benefit in human patients with OS (Meyers and Chou, 2014). These findings underline the usefulness of dogs with cancer as models to study these kinds of therapies. Dogs with cancer may therefore serve as a bridge between murine models and humans for assessing new immunomodulating and PMN-targeting drugs.

5.5 Identified knowledge gaps for future studies

The results from this research project have helped answer some questions regarding OS cancer biology, but many remain unanswered, and several new ones have appeared:

5.5.1 Osteosarcoma micrometastases

Our results indicate that the pulmonary micrometastatic prevalence at clinical diagnosis is relatively low. The results should be interpreted carefully, considering the method used to identify micrometastases. Future studies should use different identification methods, such as qPCR or flow cytometry-based techniques. Additionally, such studies should include more dogs to improve the micrometastatic prevalence estimate, given the likely low prevalence. Furthermore, micrometastases should be studied in other metastatic target organs, such as the bone marrow. These results will help shed light on the metastatic chain of events in dogs with OS.

5.5.2 TP-3 as a biomarker for tumour burden

Since the TP-3-associated antigen is considered a tumour-specific antigen with low expression under physiological conditions, it could serve as a serum biomarker to reflect disease burden. Future studies should assess whether ELISA-based assays using TP-3 could identify free soluble TP-3-associated antigens in serum and their diagnostic and prognostic value in dogs with OS. Other isoforms of alkaline phosphatase are easily measurable in serum. Whether the alkaline phosphatase isoform that binds to TP-3 is detectable in serum is unknown.

5.5.3 Canine tumour-associated macrophage markers

In paper II, we showed that TCMΦ had a high expression of several M2-associated markers on flow cytometry. Furthermore, additional M2-associated surface markers were upregulated at the transcriptomic level. Future studies should aim to assess these markers in canine TAMs *in situ* and *in vivo* to provide an in-depth mapping of

the macrophage landscape in dogs with cancer. Clinical outcome data could be compared with marker expression on TAMs in tumour biopsies to assess their potential prognostic value. Additionally, M2-associated markers expression on myeloid cell populations in peripheral blood could potentially provide prognostic and minimal residual disease information.

5.5.4 Functional characterisation of canine tumour-associated macrophages

With new and sophisticated methods such as single-cell RNA-Seq, it has become possible to study the immune landscape of tumours in detail. To further improve our understanding of canine TAMs and their similarities to human TAMs, single-cell RNA-Seq would provide an excellent ground for comparison. Furthermore, patient-derived TAMs could be isolated from tumours to assess their effects on T-cell proliferation, $CD4^+$ T-cell polarization, and $CD8^+$ T-cell and NK-cell cytotoxicity *in vitro*. Such setups would also provide better platforms to test TAM-repolarizing drugs *in vitro*.

5.5.5 Pre-metastatic niche

To our knowledge, there has not been any previous work describing PMN formation in veterinary oncology. Our results may therefore lay the ground for many future PMN studies using dogs with cancer as models. Dogs with other highly metastatic tumours, such as hemangiosarcoma, histiocytic sarcoma and melanoma, could potentially also be used as naturally occurring models to study PMN formation. Other aspects of PMN formation, such as metabolic and stromal remodelling, could also be studied in dogs. In-depth characterization of the immune landscape of the PMN using multi-marker immunofluorescent labelling and single-cell RNA-Seq may provide important information regarding naturally occurring PMN. Specific immune cell subsets could be isolated from pre-metastatic sites for further *in vitro* functional studies. Although we found evidence of PMN formation in the lungs, we did not investigate other typical metastatic and non-metastatic organs. Future studies should examine several organs to assess if PMN formation only occurs in common metastatic target organs. Additionally, patient-derived EVs could be isolated and

characterized, which may provide prognostic and diagnostic biomarkers and new therapeutic targets. In light of our findings, dogs with OS may serve as models to assess new PMN-targeting drugs.

5.6 Conclusions

The main findings from this project are:

- Pulmonary micrometastases can be detected in a subset of dogs with osteosarcoma without macroscopic metastases using TP-3 immunohistochemistry.

- The prevalence of pulmonary micrometastases was substantially lower than expected based on post-surgical metastatic rates.

- Several new canine M2 macrophage phenotypical markers were identified.

- Canine *in vitro*-generated tumour-conditioned macrophages had an intermediate to high expression of several M2-associated surface markers on flow cytometry and RNA-Sequencing.

- Canine *in vitro* generated tumour conditioned macrophages have an M2-skewed cytokine and chemokine profile, although some pro-inflammatory mediators were upregulated.

- Canine and human tumour-conditioned macrophages share several characteristics.

- Dogs with osteosarcoma without metastases have significantly higher numbers of $CD204^+$ macrophages, $CD206^+$ macrophages and monocytes, and $CD11d^+$ bone marrow-derived cells in the lungs than dogs without cancer.

- Dogs with established osteosarcoma pulmonary metastases have significantly lower numbers of $CD11d^+$ bone marrow-derived cells in the lungs than osteosarcoma dogs without metastases.

- Dogs with osteosarcoma have a significantly higher total nucleated cell density in the lungs than dogs without cancer.

- ❖ Dogs with osteosarcoma without pulmonary metastases show evidence of an immunological pre-metastatic niche, supporting the existence of distant pre-metastatic niche formation in naturally occurring cancer.

6 References

ADAMS, V. J., EVANS, K. M., SAMPSON, J. & WOOD, J. L. N. 2010. Methods and mortality results of a health survey of purebred dogs in the UK. *J Small Anim Pract,* 51**,** 512-524.

ALGRA, A. M. & ROTHWELL, P. M. 2012. Effects of regular aspirin on long-term cancer incidence and metastasis: a systematic comparison of evidence from observational studies versus randomised trials. *Lancet Oncol,* 13**,** 518-27.

ALLOCCA, G., HUGHES, R., WANG, N., BROWN, H. K., OTTEWELL, P. D., BROWN, N. J. & HOLEN, I. 2019. The bone metastasis niche in breast cancer-potential overlap with the haematopoietic stem cell niche in vivo. *J Bone Oncol,* 17**,** 100244.

ANDERSEN, M. N., AL-KARRADI, S. N., KRAGSTRUP, T. W. & HOKLAND, M. 2016. Elimination of erroneous results in flow cytometry caused by antibody binding to Fc receptors on human monocytes and macrophages. *Cytometry A,* 89**,** 1001-1009.

ANDERSON, L. R., OWENS, T. W. & NAYLOR, M. J. 2014. Structural and mechanical functions of integrins. *Biophys Rev,* 6**,** 203-213.

ANDERSON, N. M. & SIMON, M. C. 2020. The tumor microenvironment. *Curr Biol,* 30**,** R921-r925.

ANFINSEN, K. P., GROTMOL, T., BRULAND, O. S. & JONASDOTTIR, T. J. 2011. Breed-specific incidence rates of canine primary bone tumors--a population based survey of dogs in Norway. *Can J Vet Res,* 75**,** 209-15.

ANGSTADT, A. Y., THAYANITHY, V., SUBRAMANIAN, S., MODIANO, J. F. & BREEN, M. 2012. A genome-wide approach to comparative oncology: high-resolution oligonucleotide aCGH of canine and human osteosarcoma pinpoints shared microaberrations. *Cancer Genet,* 205**,** 572-87.

ARANGO DUQUE, G. & DESCOTEAUX, A. 2014. Macrophage cytokines: involvement in immunity and infectious diseases. *Front Immunol,* 5**,** 491.

ARAS, S. & ZAIDI, M. R. 2017. TAMeless traitors: macrophages in cancer progression and metastasis. *Br J Cancer,* 117**,** 1583-1591.

AVRAMEAS, S. & URIEL, J. 1966. [Method of antigen and antibody labelling with enzymes and its immunodiffusion application]. *C R Acad Hebd Seances Acad Sci D,* 262**,** 2543-5.

AZIZ, M. H., CUI, K., DAS, M., BROWN, K. E., ARDELL, C. L., FEBBRAIO, M., PLUSKOTA, E., HAN, J., WU, H., BALLANTYNE, C. M., SMITH, J. D., CATHCART, M. K. & YAKUBENKO, V. P. 2017. The Upregulation of Integrin α(D)β(2) (CD11d/CD18) on Inflammatory Macrophages Promotes Macrophage Retention in Vascular Lesions and Development of Atherosclerosis. *J Immunol,* 198**,** 4855-4867.

AZIZI, E., CARR, A. J., PLITAS, G., CORNISH, A. E., KONOPACKI, C., PRABHAKARAN, S., NAINYS, J., WU, K., KISELIOVAS, V., SETTY, M., CHOI, K., FROMME, R. M., DAO, P., MCKENNEY, P. T., WASTI, R. C., KADAVERU, K., MAZUTIS, L., RUDENSKY, A. Y. & PE'ER, D. 2018. Single-Cell Map of Diverse Immune Phenotypes in the Breast Tumor Microenvironment. *Cell,* 174**,** 1293-1308.e36.

BAGHDADI, M., WADA, H., NAKANISHI, S., ABE, H., HAN, N., PUTRA, W. E., ENDO, D., WATARI, H., SAKURAGI, N., HIDA, Y., KAGA, K., MIYAGI, Y., YOKOSE, T., TAKANO, A., DAIGO, Y. & SEINO, K. I. 2016. Chemotherapy-Induced IL34 Enhances Immunosuppression by Tumor-Associated Macrophages and Mediates Survival of Chemoresistant Lung Cancer Cells. *Cancer Res,* 76**,** 6030-6042.

BELTRAMINELLI, T. & DE PALMA, M. 2020. Biology and therapeutic targeting of tumour-associated macrophages. *J Pathol,* 250**,** 573-592.

BENNER, B., SCARBERRY, L., SUAREZ-KELLY, L. P., DUGGAN, M. C., CAMPBELL, A. R., SMITH, E., LAPURGA, G., JIANG, K., BUTCHAR, J. P., TRIDANDAPANI, S., HOWARD, J. H., BAIOCCHI, R. A., MACE, T. A. & CARSON, W. E., 3RD 2019. Generation of monocyte-derived tumor-associated macrophages using tumor-conditioned media provides a novel method to study tumor-associated macrophages in vitro. *J Immunother Cancer,* 7**,** 140.

BERG, J., WEINSTEIN, M. J., SPRINGFIELD, D. S. & RAND, W. M. 1995. Results of surgery and doxorubicin chemotherapy in dogs with osteosarcoma. *J Am Vet Med Assoc,* 206**,** 1555-60.

BERGMAN, P. J., MACEWEN, E. G., KURZMAN, I. D., HENRY, C. J., HAMMER, A. S., KNAPP, D. W., HALE, A., KRUTH, S. A., KLEIN, M. K., KLAUSNER, J., NORRIS, A. M., MCCAW, D., STRAW, R. C. & WITHROW, S. J. 1996. Amputation and carboplatin for treatment of dogs with osteosarcoma: 48 cases (1991 to 1993). *J Vet Intern Med,* 10**,** 76-81.

BEURY, D. W., PARKER, K. H., NYANDJO, M., SINHA, P., CARTER, K. A. & OSTRAND-ROSENBERG, S. 2014. Cross-talk among myeloid-derived suppressor cells, macrophages, and tumor cells impacts the inflammatory milieu of solid tumors. *J Leukoc Biol,* 96**,** 1109-18.

BIENIASZ-KRZYWIEC, P., MARTÍN-PÉREZ, R., EHLING, M., GARCÍA-CABALLERO, M., PINIOTI, S., PRETTO, S., KROES, R., ALDENI, C., DI MATTEO, M., PRENEN, H., TRIBULATTI, M. V., CAMPETELLA, O., SMEETS, A., NOEL, A., FLORIS, G., VAN GINDERACHTER, J. A. & MAZZONE, M. 2019. Podoplanin-Expressing Macrophages Promote Lymphangiogenesis and Lymphoinvasion in Breast Cancer. *Cell Metab,* 30**,** 917-936.e10.

BONNETT, B. N., EGENVALL, A., OLSON, P. & HEDHAMMAR, A. 1997. Mortality in insured Swedish dogs: rates and causes of death in various breeds. *Vet Rec,* 141**,** 40-4.

BOSTON, S. E., EHRHART, N. P., DERNELL, W. S., LAFFERTY, M. & WITHROW, S. J. 2006. Evaluation of survival time in dogs with stage III osteosarcoma that undergo treatment: 90 cases (1985-2004). *J Am Vet Med Assoc,* 228**,** 1905-8.

BRODEY, R. S. 1979. The Use of Naturally Occurring Cancer in Domestic Animals for Research into Human Cancer: General Considerations and a Review of Canine Skeletal Osteosarcoma. *Yale J Biol Med,* 52**,** 345–361.

BRODEY, R. S. & ABT, D. A. 1976. Results of surgical treatment in 65 dogs with osteosarcoma. *J Am Vet Med Assoc,* 168**,** 1032-5.

BRODEY, R. S., MC, G. J. & REYNOLDS, H. 1959. A clinical and radiological study of canine bone neoplasms. I. *J Am Vet Med Assoc,* 134**,** 53-71.

BRODEY, R. S. & RISER, W. H. 1969. Canine osteosarcoma. A clinicopathologic study of 194 cases. *Clin Orthop Relat Res,* 62**,** 54-64.

BRODEY, R. S., SAUER, R. M. & MEDWAY, W. 1963. Canine Bone Neoplasms. *J Am Vet Med Assoc,* 143**,** 471-95.

BRULAND, O., FODSTAD, O., FUNDERUD, S. & PIHL, A. 1985. Potential Application of a New Monoclonal-Antibody Highly Specific for Human Sarcomas. *British Journal of Cancer,* 52**,** 661-661.

BRULAND, O., FODSTAD, O., FUNDERUD, S. & PIHL, A. 1986. New Monoclonal-Antibodies Specific for Human Sarcomas. *Int J Cancer,* 38**,** 27-31.

BRULAND, O. S., FODSTAD, O., STENWIG, A. E. & PIHL, A. 1988. Expression and characteristics of a novel human osteosarcoma-associated cell surface antigen. *Cancer Res,* 48**,** 5302-9.

BRULAND, O. S., HOIFODT, H., SAETER, G., SMELAND, S. & FODSTAD, O. 2005. Hematogenous micrometastases in osteosarcoma patients. *Clin Cancer Res,* 11**,** 4666-73.

BRYNIARSKI, K., SZCZEPANIK, M., PTAK, M., ZEMELKA, M. & PTAK, W. 2009. Influence of cyclophosphamide and its metabolic products on the activity of peritoneal macrophages in mice. *Pharmacol Rep,* 61**,** 550-7.

BU, P., CHEN, K. Y., XIANG, K., JOHNSON, C., CROWN, S. B., RAKHILIN, N., AI, Y., WANG, L., XI, R., ASTAPOVA, I., HAN, Y., LI, J., BARTH, B. B., LU, M., GAO, Z., MINES, R., ZHANG, L., HERMAN, M., HSU, D., ZHANG, G. F. & SHEN, X. 2018. Aldolase B-Mediated Fructose Metabolism Drives Metabolic Reprogramming of Colon Cancer Liver Metastasis. *Cell Metab,* 27**,** 1249-1262.e4.

BURTON, J. & KHANNA, C. 2014. The role of clinical trials in veterinary oncology. *Vet Clin North Am Small Anim Pract,* 44**,** 977-87.

CAI, J., XIA, L., LI, J., NI, S., SONG, H. & WU, X. 2019. Tumor-Associated Macrophages Derived TGF-β–Induced Epithelial to Mesenchymal Transition in Colorectal Cancer Cells through Smad2,3-4/Snail Signaling Pathway. *Cancer Res Treat,* 51**,** 252-266.

CAO, X., YAKALA, G. K., VAN DEN HIL, F. E., COCHRANE, A., MUMMERY, C. L. & ORLOVA, V. V. 2019. Differentiation and Functional Comparison of Monocytes and Macrophages from hiPSCs with Peripheral Blood Derivatives. *Stem Cell Reports,* 12**,** 1282-1297.

CASANOVA-ACEBES, M., DALLA, E., LEADER, A. M., LEBERICHEL, J., NIKOLIC, J., MORALES, B. M., BROWN, M., CHANG, C., TRONCOSO, L., CHEN, S. T., SASTRE-PERONA, A., PARK, M. D., TABACHNIKOVA, A., DHAINAUT, M., HAMON, P., MAIER, B., SAWAI, C. M., AGULLÓ-PASCUAL, E., SCHOBER, M., BROWN, B. D., REIZIS, B., MARRON, T., KENIGSBERG, E., MOUSSION, C., BENAROCH, P., AGUIRRE-GHISO, J. A. & MERAD, M. 2021. Tissue-resident macrophages provide a pro-tumorigenic niche to early NSCLC cells. *Nature,* 595**,** 578-584.

CASSETTA, L., FRAGKOGIANNI, S., SIMS, A. H., SWIERCZAK, A., FORRESTER, L. M., ZHANG, H., SOONG, D. Y. H., COTECHINI, T., ANUR, P., LIN, E. Y., FIDANZA, A., LOPEZ-YRIGOYEN, M., MILLAR, M. R., URMAN, A., AI, Z., SPELLMAN, P. T., HWANG, E. S., DIXON, J. M., WIECHMANN, L., COUSSENS, L. M., SMITH, H. O. & POLLARD, J. W. 2019. Human Tumor-Associated Macrophage and Monocyte Transcriptional Landscapes Reveal Cancer-Specific Reprogramming, Biomarkers, and Therapeutic Targets. *Cancer Cell,* 35**,** 588-602.e10.

CAVALCANTI, J. N., AMSTALDEN, E. M. I., GUERRA, J. L. & MAGNA, L. C. 2004a. Osteosarcoma in dogs: clinical-morphological study and prognostic correlation. *Brazilian Journal of Veterinary Research and Animal Science,* 41**,** 299-305.

CAVALCANTI, J. N., AMSTALDEN, E. M. I., GUERRA, J. L. & MAGNA, L. C. 2004b. Osteosarcoma in dogs: clinical-morphological study and prognostic correlation. *Braz J Vet Res Anim Sci,* 41**,** 299-305.

CENDROWICZ, E., SAS, Z., BREMER, E. & RYGIEL, T. P. 2021. The Role of Macrophages in Cancer Development and Therapy. *Cancers (Basel),* 13.

CHAKAROV, S., LIM, H. Y., TAN, L., LIM, S. Y., SEE, P., LUM, J., ZHANG, X. M., FOO, S., NAKAMIZO, S., DUAN, K., KONG, W. T., GENTEK, R., BALACHANDER, A., CARBAJO, D., BLERIOT, C., MALLERET, B., TAM, J. K. C., BAIG, S., SHABEER, M., TOH, S. E. S., SCHLITZER, A., LARBI, A., MARICHAL, T., MALISSEN, B., CHEN, J., POIDINGER, M., KABASHIMA, K., BAJENOFF, M., NG, L. G., ANGELI, V. & GINHOUX, F. 2019. Two distinct interstitial macrophage populations coexist across tissues in specific subtissular niches. *Science,* 363.

CHEN, J., YAO, Y., GONG, C., YU, F., SU, S., CHEN, J., LIU, B., DENG, H., WANG, F. & LIN, L. 2011a. CCL18 from tumor-associated macrophages promotes breast cancer metastasis via PITPNM3. *Cancer Cell,* 19.

CHEN, Q., ZHANG, X. H. & MASSAGUÉ, J. 2011b. Macrophage binding to receptor VCAM-1 transmits survival signals in breast cancer cells that invade the lungs. *Cancer Cell,* 20**,** 538-49.

CHEN, S., SO, E. C., STROME, S. E. & ZHANG, X. 2015. Impact of Detachment Methods on M2 Macrophage Phenotype and Function. *J Immunol Methods,* 426**,** 56-61.

CHEN, Y., SONG, Y., DU, W., GONG, L., CHANG, H. & ZOU, Z. 2019. Tumor-associated macrophages: an accomplice in solid tumor progression. *Journal of Biomedical Science,* 26**,** 78.

CHEVRIER, S., LEVINE, J. H., ZANOTELLI, V. R. T., SILINA, K., SCHULZ, D., BACAC, M., RIES, C. H., AILLES, L., JEWETT, M. A. S., MOCH, H., VAN DEN BROEK, M., BEISEL, C., STADLER, M. B., GEDYE, C., REIS, B., PE'ER, D. & BODENMILLER, B. 2017. An Immune Atlas of Clear Cell Renal Cell Carcinoma. *Cell,* 169**,** 736-749.e18.

CHIODA, M., PERANZONI, E., DESANTIS, G., PAPALINI, F., FALISI, E., SOLITO, S., MANDRUZZATO, S. & BRONTE, V. 2011. Myeloid cell diversification and complexity: an old concept with new turns in oncology. *Cancer Metastasis Rev,* 30**,** 27-43.

COENYE, T. 2021. Do results obtained with RNA-sequencing require independent verification? *Biofilm,* 3**,** 100043.

COLEGIO, O. R., CHU, N. Q., SZABO, A. L., CHU, T., RHEBERGEN, A. M., JAIRAM, V., CYRUS, N., BROKOWSKI, C. E., EISENBARTH, S. C., PHILLIPS, G. M., CLINE, G. W., PHILLIPS, A. J. & MEDZHITOV, R. 2014. Functional polarization of tumour-associated macrophages by tumour-derived lactic acid. *Nature,* 513**,** 559-63.

COOLEY, D. M., BERANEK, B. C., SCHLITTLER, D. L., GLICKMAN, N. W., GLICKMAN, L. T. & WATERS, D. J. 2002. Endogenous gonadal hormone exposure and bone sarcoma risk. *Cancer Epidemiol Biomarkers Prev,* 11**,** 1434-40.

CORDELL, J. L., FALINI, B., ERBER, W. N., GHOSH, A. K., ABDULAZIZ, Z., MACDONALD, S., PULFORD, K. A., STEIN, H. & MASON, D. Y. 1984. Immunoenzymatic labeling of monoclonal antibodies using immune complexes of alkaline phosphatase and monoclonal anti-alkaline phosphatase (APAAP complexes). *J Histochem Cytochem,* 32**,** 219-29.

CORZO, C. A., CONDAMINE, T., LU, L., COTTER, M. J., YOUN, J. I., CHENG, P., CHO, H. I., CELIS, E., QUICENO, D. G., PADHYA, T., MCCAFFREY, T. V., MCCAFFREY, J. C. & GABRILOVICH, D. I. 2010. HIF-1α regulates function and differentiation of myeloid-derived suppressor cells in the tumor microenvironment. *J Exp Med,* 207**,** 2439-53.

COSSARIZZA, A., CHANG, H. D., RADBRUCH, A., ABRIGNANI, S., ADDO, R., AKDIS, M., ANDRÄ, I., ANDREATA, F., ANNUNZIATO, F., ARRANZ, E., BACHER, P., BARI, S., BARNABA, V., BARROS-MARTINS, J., BAUMJOHANN, D., BECCARIA, C. G., BERNARDO, D., BOARDMAN, D. A., BORGER, J., BÖTTCHER, C., BROCKMANN, L., BURNS, M., BUSCH, D. H., CAMERON, G., CAMMARATA, I., CASSOTTA, A., CHANG, Y., CHIRDO, F. G., CHRISTAKOU, E., ČIČIN-ŠAIN, L., COOK, L., CORBETT, A. J., CORNELIS, R., COSMI, L., DAVEY, M. S., DE BIASI, S., DE SIMONE, G., DEL ZOTTO, G., DELACHER, M., DI ROSA, F., DI SANTO, J., DIEFENBACH, A., DONG, J., DÖRNER, T., DRESS, R. J., DUTERTRE, C. A., ECKLE, S. B. G., EEDE, P., EVRARD, M., FALK, C. S., FEUERER, M., FILLATREAU, S., FIZ-LOPEZ, A., FOLLO, M., FOULDS, G. A., FRÖBEL, J., GAGLIANI, N., GALLETTI, G., GANGAEV, A., GARBI, N., GARROTE, J. A., GEGINAT, J., GHERARDIN, N. A., GIBELLINI, L., GINHOUX, F., GODFREY, D. I., GRUARIN, P., HAFTMANN, C., HANSMANN, L., HARPUR, C. M., HAYDAY, A. C., HEINE, G., HERNÁNDEZ, D. C., HERRMANN, M., HOELSKEN, O., HUANG, Q., HUBER, S., HUBER, J. E., HUEHN, J., HUNDEMER, M., HWANG, W. Y. K., IANNACONE, M., IVISON, S. M., JÄCK, H. M., JANI, P. K., KELLER, B., KESSLER, N., KETELAARS, S., KNOP, L., KNOPF, J., KOAY, H. F., KOBOW, K., KRIEGSMANN, K., KRISTYANTO, H., KRUEGER, A., KUEHNE, J. F., KUNZE-SCHUMACHER, H., KVISTBORG, P., KWOK, I., LATORRE, D., et al. 2021. Guidelines for the use of flow cytometry and cell sorting in immunological studies (third edition). *Eur J Immunol,* 51**,** 2708-3145.

COSTA-SILVA, B., AIELLO, N. M., OCEAN, A. J., SINGH, S., ZHANG, H., THAKUR, B. K., BECKER, A., HOSHINO, A., MARK, M. T., MOLINA, H., XIANG, J., ZHANG, T., THEILEN, T. M., GARCIA-SANTOS, G., WILLIAMS, C., ARARSO, Y., HUANG, Y., RODRIGUES, G., SHEN, T. L., LABORI, K. J., LOTHE, I. M., KURE, E. H., HERNANDEZ, J., DOUSSOT, A., EBBESEN, S. H., GRANDGENETT, P. M., HOLLINGSWORTH, M. A., JAIN, M., MALLYA, K., BATRA, S. K., JARNAGIN, W. R., SCHWARTZ, R. E., MATEI, I., PEINADO, H., STANGER, B. Z., BROMBERG, J. & LYDEN, D. 2015. Pancreatic cancer exosomes initiate pre-metastatic niche formation in the liver. *Nat Cell Biol,* 17**,** 816-26.

CURIEL, T. J., COUKOS, G., ZOU, L., ALVAREZ, X., CHENG, P., MOTTRAM, P., EVDEMON-HOGAN, M., CONEJO-GARCIA, J. R., ZHANG, L., BUROW, M., ZHU, Y., WEI, S., KRYCZEK, I., DANIEL, B., GORDON, A., MYERS, L., LACKNER, A., DISIS, M. L., KNUTSON, K. L., CHEN, L. & ZOU, W. 2004. Specific recruitment of regulatory T cells in ovarian carcinoma fosters immune privilege and predicts reduced survival. *Nat Med,* 10**,** 942-9.

CZYSTOWSKA-KUZMICZ, M., SOSNOWSKA, A., NOWIS, D., RAMJI, K., SZAJNIK, M., CHLEBOWSKA-TUZ, J., WOLINSKA, E., GAJ, P., GRAZUL, M., PILCH, Z., ZERROUQI, A., GRACZYK-JARZYNKA, A., SOROCZYNSKA, K., CIERNIAK, S., KOKTYSZ, R., ELISHAEV, E., GRUCA, S., STEFANOWICZ, A., BLASZCZYK, R., BOREK, B., GZIK, A., WHITESIDE, T. & GOLAB, J. 2019. Small extracellular vesicles containing arginase-1 suppress T-cell responses and promote tumor growth in ovarian carcinoma. *Nat Commun,* 10**,** 3000.

DANILENKO, D. M., ROSSITTO, P. V., VAN DER VIEREN, M., LE TRONG, H., MCDONOUGH, S. P., AFFOLTER, V. K. & MOORE, P. F. 1995. A novel canine leukointegrin, alpha d beta 2, is expressed by specific macrophage subpopulations in tissue and a minor CD8+ lymphocyte subpopulation in peripheral blood. *J Immunol,* 155**,** 35-44.

DAVIS, G. J., KAPATKIN, A. S., CRAIG, L. E., HEINS, G. S. & WORTMAN, J. A. 2002. Comparison of radiography, computed tomography, and magnetic resonance imaging for evaluation of appendicular osteosarcoma in dogs. *J Am Vet Med Assoc,* 220**,** 1171-6.

DAY, C. P., MERLINO, G. & VAN DYKE, T. 2015. Preclinical mouse cancer models: a maze of opportunities and challenges. *Cell,* 163**,** 39-53.

DE, M. S. C. H., TOLEDO-PIZA, E., AMORIN, R., BARBOZA, A. & TOBIAS, K. M. 2009. Inflammatory mammary carcinoma in 12 dogs: clinical features, cyclooxygenase-2 expression, and response to piroxicam treatment. *Can Vet J,* 50**,** 506-10.

DEBACKER, J. M., GONDRY, O., LAHOUTTE, T., KEYAERTS, M. & HUVENNE, W. 2021. The Prognostic Value of CD206 in Solid Malignancies: A Systematic Review and Meta-Analysis. *Cancers (Basel),* 13.

DEEP, G., JAIN, A., KUMAR, A., AGARWAL, C., KIM, S., LEEVY, W. M. & AGARWAL, R. 2020. Exosomes secreted by prostate cancer cells under hypoxia promote matrix metalloproteinases activity at pre-metastatic niches. *Mol Carcinog,* 59**,** 323-332.

DENARDO, D. G., BARRETO, J. B., ANDREU, P., VASQUEZ, L., TAWFIK, D., KOLHATKAR, N. & COUSSENS, L. M. 2009. CD4(+) T cells regulate pulmonary metastasis of mammary carcinomas by enhancing protumor properties of macrophages. *Cancer Cell,* 16.

DEVITA, V. T., JR. & CHU, E. 2008. A history of cancer chemotherapy. *Cancer Res,* 68**,** 8643-53.

DOLLT, C., BECKER, K., MICHEL, J., MELCHERS, S., WEIS, C. A., SCHLEDZEWSKI, K., KREWER, A., KLOSS, L., GEBHARDT, C., UTIKAL, J. & SCHMIEDER, A. 2017. The shedded ectodomain of Lyve-1 expressed on M2-like tumor-associated macrophages inhibits melanoma cell proliferation. *Oncotarget,* 8**,** 103682-103692.

DOMCKE, S., SINHA, R., LEVINE, D. A., SANDER, C. & SCHULTZ, N. 2013. Evaluating cell lines as tumour models by comparison of genomic profiles. *Nat Commun,* 4**,** 2126.

DOMÍNGUEZ-SOTO, A., SIERRA-FILARDI, E., PUIG-KRÖGER, A., PÉREZ-MACEDA, B., GÓMEZ-AGUADO, F., CORCUERA, M. T., SÁNCHEZ-MATEOS, P. & CORBÍ, A. L. 2011. Dendritic cell-specific ICAM-3-grabbing nonintegrin expression on M2-polarized and tumor-associated macrophages is macrophage-CSF dependent and enhanced by tumor-derived IL-6 and IL-10. *J Immunol,* 186**,** 2192-200.

DONG, Q., LIU, X., CHENG, K., SHENG, J., KONG, J. & LIU, T. 2021. Pre-metastatic Niche Formation in Different Organs Induced by Tumor Extracellular Vesicles. *Front Cell Dev Biol,* 9**,** 733627.

DORFMAN, S. K., HURVITZ, A. I. & PATNAIK, A. K. 1977. Primary and secondary bone tumours in the dog. *J Small Anim Pract,* 18**,** 313-26.

DOW, S. 2019. A Role for Dogs in Advancing Cancer Immunotherapy Research. *Front Immunol,* 10**,** 2935.

DOW, S., ELMSLIE, R., KURZMAN, I., MACEWEN, G., PERICLE, F. & LIGGITT, D. 2005. Phase I study of liposome-DNA complexes encoding the interleukin-2 gene in dogs with osteosarcoma lung metastases. *Hum Gene Ther,* 16**,** 937-46.

DUWEB, A., GAISER, A. K., STILTZ, I., EL GAAFARY, M., SIMMET, T. & SYROVETS, T. 2022. The SC cell line as an in vitro model of human monocytes. *J Leukoc Biol,* 112**,** 659-668.

EGENVALL, A., NODTVEDT, A. & VON EULER, H. 2007. Bone tumors in a population of 400 000 insured Swedish dogs up to 10 y of age: incidence and survival. *Can J Vet Res,* 71**,** 292-9.

EHRHART, N. R., SD; FAN, TM. 2013. Tumors of the Skeletal System. *Withrow and MacEwen's Small Animal Clinical Oncology.* 5th ed. St. Louis, Missouri: Saunders, Elsevier.

ERRENI, M., MANTOVANI, A. & ALLAVENA, P. 2011. Tumor-associated Macrophages (TAM) and Inflammation in Colorectal Cancer. *Cancer Microenviron,* 4**,** 141-54.

FANG, T., LV, H., LV, G., LI, T., WANG, C., HAN, Q., YU, L., SU, B., GUO, L., HUANG, S., CAO, D., TANG, L., TANG, S., WU, M., YANG, W. & WANG, H. 2018. Tumor-derived exosomal miR-1247-3p induces cancer-associated fibroblast activation to foster lung metastasis of liver cancer. *Nat Commun,* 9**,** 191.

FEDERMAN, N., BERNTHAL, N., EILBER, F. C. & TAP, W. D. 2009. The multidisciplinary management of osteosarcoma. *Curr Treat Options Oncol,* 10**,** 82-93.

FENG, Y., YE, Z., SONG, F., HE, Y. & LIU, J. 2022. The Role of TAMs in Tumor Microenvironment and New Research Progress. *Stem Cells Int,* 2022**,** 5775696.

FERRANTE, C. J., PINHAL-ENFIELD, G., ELSON, G., CRONSTEIN, B. N., HASKO, G., OUTRAM, S. & LEIBOVICH, S. J. 2013. The adenosine-dependent angiogenic switch of macrophages to an M2-like phenotype is independent of interleukin-4 receptor alpha (IL-4Rα) signaling. *Inflammation,* 36**,** 921-31.

FIDLER, I. J., SONE, S., FOGLER, W. E. & BARNES, Z. L. 1981. Eradication of spontaneous metastases and activation of alveolar macrophages by intravenous injection of liposomes containing muramyl dipeptide. *Proc Natl Acad Sci U S A,* 78**,** 1680-4.

FINOTELLO, R., WHYBROW, K., SCARIN, G. & RESSEL, L. 2021. Correlation between Tumour Associated Macrophage (TAM) Infiltration and Mitotic Activity in Canine Soft Tissue Sarcomas. *Animals (Basel),* 11.

FONG, M. Y., ZHOU, W., LIU, L., ALONTAGA, A. Y., CHANDRA, M., ASHBY, J., CHOW, A., O'CONNOR, S. T., LI, S., CHIN, A. R., SOMLO, G., PALOMARES, M., LI, Z., TREMBLAY, J. R., TSUYADA, A., SUN, G., REID, M. A., WU, X., SWIDERSKI, P., REN, X., SHI, Y., KONG, M., ZHONG, W., CHEN, Y. & WANG, S. E. 2015. Breast-cancer-secreted miR-122 reprograms glucose metabolism in premetastatic niche to promote metastasis. *Nat Cell Biol,* 17**,** 183-94.

FOSSMARK, R., BALTO, T. M., MARTINSEN, T. C., GRØNBECH, J. E., MUNKVOLD, B., MJØNES, P. G. & WALDUM, H. L. 2019. Hepatic micrometastases outside macrometastases are present in all patients with ileal neuroendocrine primary tumour at the time of liver resection. *Scand J Gastroenterol,* 54**,** 1003-1007.

FOURNIER, K., SCHILLER, A., PERRY, R. R. & LARONGA, C. 2004. Micrometastasis in the sentinel lymph node of breast cancer does not mandate completion axillary dissection. *Ann Surg,* 239**,** 859-63; discussion 863-5.

FRANK, A. C., EBERSBERGER, S., FINK, A. F., LAMPE, S., WEIGERT, A., SCHMID, T., EBERSBERGER, I., SYED, S. N. & BRÜNE, B. 2019. Apoptotic tumor cell-derived microRNA-375 uses CD36 to alter the tumor-associated macrophage phenotype. *Nat Commun,* 10**,** 1135.

GAO, Y., BADO, I., WANG, H., ZHANG, W., ROSEN, J. M. & ZHANG, X. H. 2019. Metastasis Organotropism: Redefining the Congenial Soil. *Dev Cell,* 49**,** 375-391.

GEORGOUDAKI, A. M., PROKOPEC, K. E., BOURA, V. F., HELLQVIST, E., SOHN, S., ÖSTLING, J., DAHAN, R., HARRIS, R. A., RANTALAINEN, M., KLEVEBRING, D., SUND, M., BRAGE, S. E., FUXE, J., ROLNY, C., LI, F., RAVETCH, J. V. & KARLSSON, M. C. 2016. Reprogramming Tumor-Associated Macrophages by Antibody Targeting Inhibits Cancer Progression and Metastasis. *Cell Rep,* 15**,** 2000-11.

GHOSHAL, A., RODRIGUES, L. C., GOWDA, C. P., ELCHEVA, I. A., LIU, Z., ABRAHAM, T. & SPIEGELMAN, V. S. 2019. Extracellular vesicle-dependent effect of RNA-binding protein IGF2BP1 on melanoma metastasis. *Oncogene,* 38**,** 4182-4196.

GIBSON, W. E., GONZALEZ, R. S., CATES, J. M. M., LIU, E. & SHI, C. 2018. Hepatic micrometastases are associated with poor prognosis in patients with liver metastases from neuroendocrine tumors of the digestive tract. *Hum Pathol,* 79**,** 109-115.

GILLANDERS, W. E., MIKHITARIAN, K., HEBERT, R., MAULDIN, P. D., PALESCH, Y., WALTERS, C., URIST, M. M., MANN, G. B., DOHERTY, G., HERRMANN, V. M., HILL, A. D., EREMIN, O., EL-SHEEMY, M., ORR, R. K., VALLE, A. A., HENDERSON, M. A., DEWITTY, R. L., SUGG, S. L., FRYKBERG, E., YEH, K., BELL, R. M., METCALF, J. S., ELLIOTT, B. M., BROTHERS, T., ROBISON, J., MITAS, M. & COLE, D. J. 2004. Molecular detection of micrometastatic breast cancer in histopathology-negative axillary lymph nodes correlates with traditional predictors of prognosis: an interim analysis of a prospective multi-institutional cohort study. *Ann Surg,* 239**,** 828-37; discussion 837-40.

GILLOT, L., BAUDIN, L., ROUAUD, L., KRIDELKA, F. & NOËL, A. 2021. The pre-metastatic niche in lymph nodes: formation and characteristics. *Cell Mol Life Sci,* 78**,** 5987-6002.

GILROY, D. W., COLVILLE-NASH, P. R., WILLIS, D., CHIVERS, J., PAUL-CLARK, M. J. & WILLOUGHBY, D. A. 1999. Inducible cyclooxygenase may have anti-inflammatory properties. *Nat Med,* 5**,** 698-701.

GOODSPEED, A., HEISER, L. M., GRAY, J. W. & COSTELLO, J. C. 2016. Tumor-Derived Cell Lines as Molecular Models of Cancer Pharmacogenomics. *Mol Cancer Res,* 14**,** 3-13.
GORDON, S. 2007. The macrophage: past, present and future. *Eur J Immunol,* 37 Suppl 1**,** S9-17.
GORDON, S. & MARTINEZ-POMARES, L. 2017. Physiological roles of macrophages. *Pflugers Arch,* 469**,** 365-374.
GORDON, S., PLÜDDEMANN, A. & MARTINEZ ESTRADA, F. 2014. Macrophage heterogeneity in tissues: phenotypic diversity and functions. *Immunol Rev,* 262**,** 36-55.
GRANGE, C., TAPPARO, M., COLLINO, F., VITILLO, L., DAMASCO, C., DEREGIBUS, M. C., TETTA, C., BUSSOLATI, B. & CAMUSSI, G. 2011. Microvesicles released from human renal cancer stem cells stimulate angiogenesis and formation of lung premetastatic niche. *Cancer Res,* 71**,** 5346-56.
GRUGAN, K. D., MCCABE, F. L., KINDER, M., GREENPLATE, A. R., HARMAN, B. C., EKERT, J. E., VAN ROOIJEN, N., ANDERSON, G. M., NEMETH, J. A., STROHL, W. R., JORDAN, R. E. & BREZSKI, R. J. 2012. Tumor-associated macrophages promote invasion while retaining Fc-dependent anti-tumor function. *J Immunol,* 189**,** 5457-66.
GUO, Y., FENG, Y., CUI, X., WANG, Q. & PAN, X. 2019. Autophagy inhibition induces the repolarisation of tumour-associated macrophages and enhances chemosensitivity of laryngeal cancer cells to cisplatin in mice. *Cancer Immunol Immunother,* 68**,** 1909-1920.
GUPTA, G. P., NGUYEN, D. X., CHIANG, A. C., BOS, P. D., KIM, J. Y., NADAL, C., GOMIS, R. R., MANOVA-TODOROVA, K. & MASSAGUÉ, J. 2007. Mediators of vascular remodelling co-opted for sequential steps in lung metastasis. *Nature,* 446**,** 765-70.
HAINES, D. M. & BRULAND, O. S. 1989. Immunohistochemical detection of osteosarcoma-associated antigen in canine osteosarcoma. *Anticancer Res,* 9**,** 903-7.
HAN, S. J., KWON, S. & KIM, K. S. 2021. Challenges of applying multicellular tumor spheroids in preclinical phase. *Cancer Cell Int,* 21**,** 152.
HANSEN, M. T., FORST, B., CREMERS, N., QUAGLIATA, L., AMBARTSUMIAN, N., GRUM-SCHWENSEN, B., KLINGELHÖFER, J., ABDUL-AL, A., HERRMANN, P., OSTERLAND, M., STEIN, U., NIELSEN, G. H., SCHERER, P. E., LUKANIDIN, E., SLEEMAN, J. P. & GRIGORIAN, M. 2015. A link between inflammation and metastasis: serum amyloid A1 and A3 induce metastasis, and are targets of metastasis-inducing S100A4. *Oncogene,* 34**,** 424-35.

HARTANA, C. A., KINN, J., ROSENBLATT, R., ANANIA, S., ALAMDARI, F., GLISE, H., SHERIF, A. & WINQVIST, O. 2016. Detection of micrometastases by flow cytometry in sentinel lymph nodes from patients with renal tumours. *Br J Cancer,* 115**,** 957-966.

HASHIMOTO, K., TAKAHASHI, T. & SUZUKI, C. 1976. Micrometastasis in resected lungs of lung cancer patients. *Gann = Gan,* 67**,** 717-723.

HE, L., JHONG, J. H., CHEN, Q., HUANG, K. Y., STRITTMATTER, K., KREUZER, J., DERAN, M., WU, X., LEE, T. Y., SLAVOV, N., HAAS, W. & MARNEROS, A. G. 2021. Global characterization of macrophage polarization mechanisms and identification of M2-type polarization inhibitors. *Cell Rep,* 37**,** 109955.

HEATH, O., BERLATO, C., MANIATI, E., LAKHANI, A., PEGRUM, C., KOTANTAKI, P., ELORBANY, S., BÖHM, S., BARRY, S. T., ANNIBALDI, A., BARTON, D. P. & BALKWILL, F. R. 2021. Chemotherapy Induces Tumor-Associated Macrophages that Aid Adaptive Immune Responses in Ovarian Cancer. *Cancer Immunol Res,* 9**,** 665-681.

HEINRICH, F., LEHMBECKER, A., RADDATZ, B. B., KEGLER, K., TIPOLD, A., STEIN, V. M., KALKUHL, A., DESCHL, U., BAUMGARTNER, W., ULRICH, R. & SPITZBARTH, I. 2017. Morphologic, phenotypic, and transcriptomic characterization of classically and alternatively activated canine blood-derived macrophages in vitro. *PLoS One,* 12**,** e0183572.

HERRMANN, I., GOTOVINA, J., FAZEKAS-SINGER, J., FISCHER, M. B., HUFNAGL, K., BIANCHINI, R. & JENSEN-JAROLIM, E. 2018. Canine macrophages can like human macrophages be in vitro activated toward the M2a subtype relevant in allergy. *Dev Comp Immunol,* 82**,** 118-127.

HEYMAN, S. J., DIEFENDERFER, D. L., GOLDSCHMIDT, M. H. & NEWTON, C. D. 1992. Canine axial skeletal osteosarcoma. A retrospective study of 116 cases (1986 to 1989). *Vet Surg,* 21**,** 304-10.

HIRATSUKA, S., ISHIBASHI, S., TOMITA, T., WATANABE, A., AKASHI-TAKAMURA, S., MURAKAMI, M., KIJIMA, H., MIYAKE, K., ABURATANI, H. & MARU, Y. 2013. Primary tumours modulate innate immune signalling to create pre-metastatic vascular hyperpermeability foci. *Nat Commun,* 4**,** 1853.

HIRATSUKA, S., WATANABE, A., ABURATANI, H. & MARU, Y. 2006. Tumour-mediated upregulation of chemoattractants and recruitment of myeloid cells predetermines lung metastasis. *Nat Cell Biol,* 8**,** 1369-75.

HIRATSUKA, S., WATANABE, A., SAKURAI, Y., AKASHI-TAKAMURA, S., ISHIBASHI, S., MIYAKE, K., SHIBUYA, M., AKIRA, S., ABURATANI, H. & MARU, Y. 2008. The S100A8-serum amyloid A3-TLR4 paracrine cascade establishes a pre-metastatic phase. *Nat Cell Biol,* 10**,** 1349-55.

HNASKO, T. S. & HNASKO, R. M. 2015. The Western Blot. *Methods Mol Biol,* 1318**,** 87-96.

HOSHINO, A., COSTA-SILVA, B., SHEN, T. L., RODRIGUES, G., HASHIMOTO, A., TESIC MARK, M., MOLINA, H., KOHSAKA, S., DI GIANNATALE, A., CEDER, S., SINGH, S., WILLIAMS, C., SOPLOP, N., URYU, K., PHARMER, L., KING, T., BOJMAR, L., DAVIES, A. E., ARARSO, Y., ZHANG, T., ZHANG, H., HERNANDEZ, J., WEISS, J. M., DUMONT-COLE, V. D., KRAMER, K., WEXLER, L. H., NARENDRAN, A., SCHWARTZ, G. K., HEALEY, J. H., SANDSTROM, P., LABORI, K. J., KURE, E. H., GRANDGENETT, P. M., HOLLINGSWORTH, M. A., DE SOUSA, M., KAUR, S., JAIN, M., MALLYA, K., BATRA, S. K., JARNAGIN, W. R., BRADY, M. S., FODSTAD, O., MULLER, V., PANTEL, K., MINN, A. J., BISSELL, M. J., GARCIA, B. A., KANG, Y., RAJASEKHAR, V. K., GHAJAR, C. M., MATEI, I., PEINADO, H., BROMBERG, J. & LYDEN, D. 2015. Tumour exosome integrins determine organotropic metastasis. *Nature,* 527**,** 329-35.

HOURANI, T., HOLDEN, J. A., LI, W., LENZO, J. C., HADJIGOL, S. & O'BRIEN-SIMPSON, N. M. 2021. Tumor Associated Macrophages: Origin, Recruitment, Phenotypic Diversity, and Targeting. *Front Oncol,* 11**,** 788365.

HU, B., WANG, Z., ZENG, H., QI, Y., CHEN, Y., WANG, T., WANG, J., CHANG, Y., BAI, Q., XIA, Y., WANG, Y., LIU, L., ZHU, Y., DAI, B., GUO, J., XU, L., ZHANG, W. & XU, J. 2020. Blockade of DC-SIGN(+) Tumor-Associated Macrophages Reactivates Antitumor Immunity and Improves Immunotherapy in Muscle-Invasive Bladder Cancer. *Cancer Res,* 80**,** 1707-1719.

HUANG, Y., SONG, N., DING, Y., YUAN, S., LI, X., CAI, H., SHI, H. & LUO, Y. 2009. Pulmonary vascular destabilization in the premetastatic phase facilitates lung metastasis. *Cancer Res,* 69**,** 7529-37.

HUME, D. A., IRVINE, K. M. & PRIDANS, C. 2019. The Mononuclear Phagocyte System: The Relationship between Monocytes and Macrophages. *Trends Immunol,* 40**,** 98-112.

HUVOS, A. G., HUTTER, R. V. & BERG, J. W. 1971. Significance of axillary macrometastases and micrometastases in mammary cancer. *Ann Surg,* 173**,** 44-6.

HÄYRY, V., KÅGEDAL, Å., HJALMARSSON, E., NEVES DA SILVA, P. F., DRAKSKOG, C., MARGOLIN, G., GEORÉN, S. K., MUNCK-WIKLAND, E., WINQVIST, O. & CARDELL, L. O. 2018. Rapid nodal staging of head and neck cancer surgical specimens with flow cytometric analysis. *Br J Cancer,* 118**,** 421-427.

IM, K., MARENINOV, S., DIAZ, M. F. P. & YONG, W. H. 2019. An Introduction to Performing Immunofluorescence Staining. *Methods Mol Biol,* 1897**,** 299-311.

INOHARA, N., OGURA, Y., FONTALBA, A., GUTIERREZ, O., PONS, F., CRESPO, J., FUKASE, K., INAMURA, S., KUSUMOTO, S., HASHIMOTO, M., FOSTER, S. J., MORAN, A. P., FERNANDEZ-LUNA, J. L. & NUÑEZ, G. 2003. Host recognition of bacterial muramyl dipeptide mediated through NOD2. Implications for Crohn's disease. *J Biol Chem,* 278**,** 5509-12.

INOUE, M., HASEGAWA, A., HOSOI, Y. & SUGIURA, K. 2015. A current life table and causes of death for insured dogs in Japan. *Prev Vet Med,* 120**,** 210-218.

INTLEKOFER, A. M. & THOMPSON, C. B. 2013. At the bench: preclinical rationale for CTLA-4 and PD-1 blockade as cancer immunotherapy. *J Leukoc Biol,* 94**,** 25-39.

ITO, M., MINAMIYA, Y., KAWAI, H., SAITO, S., SAITO, H., IMAI, K. & OGAWA, J. 2005. Intraoperative detection of lymph node micrometastasis with flow cytometry in non-small cell lung cancer. *J Thorac Cardiovasc Surg,* 130**,** 753-8.

IWICKA, E., HAJTUCH, J., DZIERZBICKA, K. & INKIELEWICZ-STEPNIAK, I. 2022. Muramyl dipeptide-based analogs as potential anticancer compounds: Strategies to improve selectivity, biocompatibility, and efficiency. *Front Oncol,* 12**,** 970967.

JAGER, N. A., WALLIS DE VRIES, B. M., HILLEBRANDS, J. L., HARLAAR, N. J., TIO, R. A., SLART, R. H., VAN DAM, G. M., BOERSMA, H. H., ZEEBREGTS, C. J. & WESTRA, J. 2016. Distribution of Matrix Metalloproteinases in Human Atherosclerotic Carotid Plaques and Their Production by Smooth Muscle Cells and Macrophage Subsets. *Mol Imaging Biol,* 18**,** 283-91.

JAMIYAN, T., KURODA, H., YAMAGUCHI, R., ABE, A. & HAYASHI, M. 2020. CD68- and CD163-positive tumor-associated macrophages in triple negative cancer of the breast. *Virchows Arch,* 477**,** 767-775.

JETTEN, N., VERBRUGGEN, S., GIJBELS, M. J., POST, M. J., DE WINTHER, M. P. & DONNERS, M. M. 2014. Anti-inflammatory M2, but not pro-inflammatory M1 macrophages promote angiogenesis in vivo. *Angiogenesis,* 17**,** 109-18.

JI, Q., ZHOU, L., SUI, H., YANG, L., WU, X., SONG, Q., JIA, R., LI, R., SUN, J., WANG, Z., LIU, N., FENG, Y., SUN, X., CAI, G., FENG, Y., CAI, J., CAO, Y., CAI, G., WANG, Y. & LI, Q. 2020. Primary tumors release ITGBL1-rich extracellular vesicles to promote distal metastatic tumor growth through fibroblast-niche formation. *Nat Commun,* 11**,** 1211.

JIN, M. Z. & JIN, W. L. 2020. The updated landscape of tumor microenvironment and drug repurposing. *Signal Transduct Target Ther,* 5**,** 166.

JINUSHI, M., CHIBA, S., YOSHIYAMA, H., MASUTOMI, K., KINOSHITA, I., DOSAKA-AKITA, H., YAGITA, H., TAKAOKA, A. & TAHARA, H. 2011. Tumor-associated macrophages regulate tumorigenicity and anticancer drug responses of cancer stem/initiating cells. *Proc Natl Acad Sci U S A,* 108**,** 12425-30.

KALLA, D., KIND, A. & SCHNIEKE, A. 2020. Genetically Engineered Pigs to Study Cancer. *Int J Mol Sci,* 21.

KALLIS, M. P., MALONEY, C., BLANK, B., SOFFER, S. Z., SYMONS, M. & STEINBERG, B. M. 2020. Pharmacological prevention of surgery-accelerated metastasis in an animal model of osteosarcoma. *J Transl Med,* 18**,** 183.

KAMAT, K., KRISHNAN, V. & DORIGO, O. 2022. Macrophage-derived CCL23 upregulates expression of T-cell exhaustion markers in ovarian cancer. *Br J Cancer,* 127**,** 1026-1033.

KANNO, S., HIRANO, S., SAKAMOTO, T., FURUYAMA, A., TAKASE, H., KATO, H., FUKUTA, M. & AOKI, Y. 2020. Scavenger receptor MARCO contributes to cellular internalization of exosomes by dynamin-dependent endocytosis and macropinocytosis. *Sci Rep,* 10**,** 21795.

KAPLAN, R. N., RIBA, R. D., ZACHAROULIS, S., BRAMLEY, A. H., VINCENT, L., COSTA, C., MACDONALD, D. D., JIN, D. K., SHIDO, K., KERNS, S. A., ZHU, Z., HICKLIN, D., WU, Y., PORT, J. L., ALTORKI, N., PORT, E. R., RUGGERO, D., SHMELKOV, S. V., JENSEN, K. K., RAFII, S. & LYDEN, D. 2005. VEGFR1-positive haematopoietic bone marrow progenitors initiate the pre-metastatic niche. *Nature,* 438**,** 820-7.

KARNIK, K. S., SAMII, V. F., WEISBRODE, S. E., LONDON, C. A. & GREEN, E. M. 2012. Accuracy of computed tomography in determining lesion size in canine appendicular osteosarcoma. *Vet Radiol Ultrasound,* 53**,** 273-9.

KATO, Y., MURAKAMI, M., HOSHINO, Y., MORI, T., MARUO, K., HIRATA, A., NAKAGAWA, T. L., YANAI, T. & SAKAI, H. 2013. The class A macrophage scavenger receptor CD204 is a useful immunohistochemical marker of canine histiocytic sarcoma. *J Comp Pathol,* 148**,** 188-96.

KATZENELENBOGEN, Y., SHEBAN, F., YALIN, A., YOFE, I., SVETLICHNYY, D., JAITIN, D. A., BORNSTEIN, C., MOSHE, A., KEREN-SHAUL, H., COHEN, M., WANG, S. Y., LI, B., DAVID, E., SALAME, T. M., WEINER, A. & AMIT, I. 2020. Coupled scRNA-Seq and Intracellular Protein Activity Reveal an Immunosuppressive Role of TREM2 in Cancer. *Cell,* 182**,** 872-885.e19.

KERBER, M., REISS, Y., WICKERSHEIM, A., JUGOLD, M., KIESSLING, F., HEIL, M., TCHAIKOVSKI, V., WALTENBERGER, J., SHIBUYA, M., PLATE, K. H. & MACHEIN, M. R. 2008. Flt-1 signaling in macrophages promotes glioma growth in vivo. *Cancer Res,* 68**,** 7342-51.

KHANNA, C., HASZ, D. E., KLAUSNER, J. S. & ANDERSON, P. M. 1996. Aerosol delivery of interleukin 2 liposomes is nontoxic and biologically effective: canine studies. *Clin Cancer Res,* 2**,** 721-34.

KIEU, T. Q., TAZAWA, K., KAWASHIMA, N., NODA, S., FUJII, M., NARA, K., HASHIMOTO, K., HAN, P. & OKIJI, T. 2022. Kinetics of LYVE-1-positive M2-like macrophages in developing and repairing dental pulp in vivo and their pro-angiogenic activity in vitro. *Sci Rep,* 12**,** 5176.

KIRPENSTEIJN, J., KIK, M., TESKE, E. & RUTTEMAN, G. R. 2008. TP53 gene mutations in canine osteosarcoma. *Vet Surg,* 37**,** 454-60.

KNAPP, D. W., RUPLE-CZERNIAK, A., RAMOS-VARA, J. A., NAUGHTON, J. F., FULKERSON, C. M. & HONKISZ, S. I. 2016. A Nonselective Cyclooxygenase Inhibitor Enhances the Activity of Vinblastine in a Naturally-Occurring Canine Model of Invasive Urothelial Carcinoma. *Bladder Cancer,* 2**,** 241-250.

KNAPP, D. W. & WATERS, D. J. 1997. Naturally occurring cancer in pet dogs: important models for developing improved cancer therapy for humans. *Mol Med Today,* 3**,** 8-11.

KOGA, Y. & OCHIAI, A. 2019. Systematic Review of Patient-Derived Xenograft Models for Preclinical Studies of Anti-Cancer Drugs in Solid Tumors. *Cells,* 8.

KONDO, H., NARUKE, T., TSUCHIYA, R., GOYA, T., SUEMASU, K., YAMAGISHI, K., KISHI, K. & NOGUCHI, M. 1989. Pleural lavage cytology immediately after thoracotomy as a prognostic factor for patients with lung cancer. *Jpn J Cancer Res,* 80**,** 233-7.

KOTAS, M. E. & MEDZHITOV, R. 2015. Homeostasis, inflammation, and disease susceptibility. *Cell,* 160**,** 816-827.

KRAEGEL, S. A., MADEWELL, B. R., SIMONSON, E. & GREGORY, C. R. 1991. Osteogenic sarcoma and cisplatin chemotherapy in dogs: 16 cases (1986-1989). *J Am Vet Med Assoc,* 199**,** 1057-9.

KUANG, D. M., ZHAO, Q., PENG, C., XU, J., ZHANG, J. P., WU, C. & ZHENG, L. 2009. Activated monocytes in peritumoral stroma of hepatocellular carcinoma foster immune privilege and disease progression through PD-L1. *J Exp Med,* 206.

KUBOTA, K., MORIYAMA, M., FURUKAWA, S., RAFIUL, H., MARUSE, Y., JINNO, T., TANAKA, A., OHTA, M., ISHIGURO, N., YAMAUCHI, M., SAKAMOTO, M., MAEHARA, T., HAYASHIDA, J. N., KAWANO, S., KIYOSHIMA, T. & NAKAMURA, S. 2017. CD163(+)CD204(+) tumor-associated macrophages contribute to T cell regulation via interleukin-10 and PD-L1 production in oral squamous cell carcinoma. *Sci Rep,* 7**,** 1755.

KUKURBA, K. R. & MONTGOMERY, S. B. 2015. RNA Sequencing and Analysis. *Cold Spring Harb Protoc,* 2015**,** 951-69.

KURAHARA, H., SHINCHI, H., MATAKI, Y., MAEMURA, K., NOMA, H., KUBO, F., SAKODA, M., UENO, S., NATSUGOE, S. & TAKAO, S. 2011. Significance of M2-polarized tumor-associated macrophage in pancreatic cancer. *J Surg Res,* 167**,** e211-9.

LA FLEUR, L., BOTLING, J., HE, F., PELICANO, C., ZHOU, C., HE, C., PALANO, G., MEZHEYEUSKI, A., MICKE, P., RAVETCH, J. V., KARLSSON, M. C. I. & SARHAN, D. 2021. Targeting MARCO and IL37R on Immunosuppressive Macrophages in Lung Cancer Blocks Regulatory T Cells and Supports Cytotoxic Lymphocyte Function. *Cancer Res,* 81**,** 956-967.

LAPLANE, L., DULUC, D., LARMONIER, N., PRADEU, T. & BIKFALVI, A. 2018. The Multiple Layers of the Tumor Environment. *Trends Cancer,* 4**,** 802-809.

LARIONOVA, I., CHERDYNTSEVA, N., LIU, T., PATYSHEVA, M., RAKINA, M. & KZHYSHKOWSKA, J. 2019. Interaction of tumor-associated macrophages and cancer chemotherapy. *Oncoimmunology,* 8**,** 1596004.

LASCELLES, B. D., DERNELL, W. S., CORREA, M. T., LAFFERTY, M., DEVITT, C. M., KUNTZ, C. A., STRAW, R. C. & WITHROW, S. J. 2005. Improved survival associated with postoperative wound infection in dogs treated with limb-salvage surgery for osteosarcoma. *Ann Surg Oncol,* 12**,** 1073-83.

LAVIN, Y., KOBAYASHI, S., LEADER, A., AMIR, E. D., ELEFANT, N., BIGENWALD, C., REMARK, R., SWEENEY, R., BECKER, C. D., LEVINE, J. H., MEINHOF, K., CHOW, A., KIM-SHULZE, S., WOLF, A., MEDAGLIA, C., LI, H., RYTLEWSKI, J. A., EMERSON, R. O., SOLOVYOV, A., GREENBAUM, B. D., SANDERS, C., VIGNALI, M., BEASLEY, M. B., FLORES, R., GNJATIC, S., PE'ER, D., RAHMAN, A., AMIT, I. & MERAD, M. 2017. Innate Immune Landscape in Early Lung Adenocarcinoma by Paired Single-Cell Analyses. *Cell,* 169**,** 750-765.e17.

LEE, H. W., CHOI, H. J., HA, S. J., LEE, K. T. & KWON, Y. G. 2013. Recruitment of monocytes/macrophages in different tumor microenvironments. *Biochim Biophys Acta,* 1835**,** 170-9.

LEE, W. J., LEE, M. H., KIM, H. T., WON, C. H., LEE, M. W., CHOI, J. H. & CHANG, S. E. 2019. Prognostic significance of CD163 expression and its correlation with cyclooxygenase-2 and vascular endothelial growth factor expression in cutaneous melanoma. *Melanoma Res,* 29**,** 501-509.

LEWIS, J. S., LANDERS, R. J., UNDERWOOD, J. C., HARRIS, A. L. & LEWIS, C. E. 2000. Expression of vascular endothelial growth factor by macrophages is up-regulated in poorly vascularized areas of breast carcinomas. *J Pathol,* 192**,** 150-8.

LI, H., HAN, Y., GUO, Q., ZHANG, M. & CAO, X. 2009. Cancer-expanded myeloid-derived suppressor cells induce anergy of NK cells through membrane-bound TGF-beta 1. *J Immunol,* 182**,** 240-9.

LIM, H. Y., LIM, S. Y., TAN, C. K., THIAM, C. H., GOH, C. C., CARBAJO, D., CHEW, S. H. S., SEE, P., CHAKAROV, S., WANG, X. N., LIM, L. H., JOHNSON, L. A., LUM, J., FONG, C. Y., BONGSO, A., BISWAS, A., GOH, C., EVRARD, M., YEO, K. P., BASU, R., WANG, J. K., TAN, Y., JAIN, R., TIKOO, S., CHOONG, C., WENINGER, W., POIDINGER, M., STANLEY, R. E., COLLIN, M., TAN, N. S., NG, L. G., JACKSON, D. G., GINHOUX, F. & ANGELI, V. 2018. Hyaluronan Receptor LYVE-1-Expressing Macrophages Maintain Arterial Tone through Hyaluronan-Mediated Regulation of Smooth Muscle Cell Collagen. *Immunity,* 49**,** 326-341.e7.

LIM, S. Y., YUZHALIN, A. E., GORDON-WEEKS, A. N. & MUSCHEL, R. J. 2016. Tumor-infiltrating monocytes/macrophages promote tumor invasion and migration by upregulating S100A8 and S100A9 expression in cancer cells. *Oncogene,* 35**,** 5735-5745.

LING, G. V., MORGAN, J. P. & POOL, R. R. 1974. Primary bone rumors in the dog: a combined clinical, radiographic, and histologic approach to early diagnosis. *J Am Vet Med Assoc,* 165**,** 55-67.

LIU, C. Y., XU, J. Y., SHI, X. Y., HUANG, W., RUAN, T. Y., XIE, P. & DING, J. L. 2013. M2-polarized tumor-associated macrophages promoted epithelial-mesenchymal transition in pancreatic cancer cells, partially through TLR4/IL-10 signaling pathway. *Lab Invest,* 93**,** 844-54.

LIU, J., ZHANG, N., LI, Q., ZHANG, W., KE, F., LENG, Q., WANG, H., CHEN, J. & WANG, H. 2011. Tumor-associated macrophages recruit CCR6+ regulatory T cells and promote the development of colorectal cancer via enhancing CCL20 production in mice. *PLoS One,* 6**,** e19495.

LIU, S., JIANG, M., ZHAO, Q., LI, S., PENG, Y., ZHANG, P. & HAN, M. 2014. Vascular endothelial growth factor plays a critical role in the formation of the pre-metastatic niche via prostaglandin E2. *Oncol Rep,* 32**,** 2477-84.

LIU, Y. & CAO, X. 2016. Characteristics and Significance of the Pre-metastatic Niche. *Cancer Cell,* 30**,** 668-681.

LOO, J. M., SCHERL, A., NGUYEN, A., MAN, F. Y., WEINBERG, E., ZENG, Z., SALTZ, L., PATY, P. B. & TAVAZOIE, S. F. 2015. Extracellular metabolic energetics can promote cancer progression. *Cell,* 160**,** 393-406.

LOUKOPOULOS, P., ROZMANEC, M. & SUTTON, R. H. 2005. Cytological versus histopathological diagnosis in canine osteosarcoma. *Vet Rec,* 157**,** 784.

LUQUE-MARTIN, R., MANDER, P. K., LEENEN, P. J. M. & WINTHER, M. P. J. 2021. Classic and new mediators for in vitro modelling of human macrophages. *J Leukoc Biol,* 109**,** 549-560.

MA, W. T., GAO, F., GU, K. & CHEN, D. K. 2019. The Role of Monocytes and Macrophages in Autoimmune Diseases: A Comprehensive Review. *Front Immunol,* 10**,** 1140.

MACEWEN, E. G. 1990. Spontaneous tumors in dogs and cats: models for the study of cancer biology and treatment. *Cancer Metastasis Rev,* 9**,** 125-36.

MACEWEN, E. G., KURZMAN, I. D., ROSENTHAL, R. C., SMITH, B. W., MANLEY, P. A., ROUSH, J. K. & HOWARD, P. E. 1989. Therapy for osteosarcoma in dogs with intravenous injection of liposome-encapsulated muramyl tripeptide. *J Natl Cancer Inst,* 81**,** 935-8.

MAGAKI, S., HOJAT, S. A., WEI, B., SO, A. & YONG, W. H. 2019. An Introduction to the Performance of Immunohistochemistry. *Methods Mol Biol,* 1897**,** 289-298.

MANTOVANI, A. & ALLAVENA, P. 2015. The interaction of anticancer therapies with tumor-associated macrophages. *J Exp Med,* 212**,** 435-45.

MANTOVANI, A., SICA, A., SOZZANI, S., ALLAVENA, P., VECCHI, A. & LOCATI, M. 2004. The chemokine system in diverse forms of macrophage activation and polarization. *Trends Immunol,* 25**,** 677-86.

MARKO, T. A., DIESSNER, B. J. & SPECTOR, L. G. 2016. Prevalence of Metastasis at Diagnosis of Osteosarcoma: An International Comparison. *Pediatr Blood Cancer,* 63**,** 1006-11.

MARTINEZ, F. O. & GORDON, S. 2014. The M1 and M2 paradigm of macrophage activation: time for reassessment. *F1000Prime Rep,* 6**,** 13.

MASON, D. Y. & SAMMONS, R. 1978a. Alkaline phosphatase and peroxidase for double immunoenzymatic labelling of cellular constituents. *J Clin Pathol,* 31**,** 454-60.
MASON, D. Y. & SAMMONS, R. 1978b. Rapid preparation of peroxidase: anti-peroxidase complexes for immunocytochemical use. *J Immunol Methods,* 20**,** 317-24.
MASON, N. J., GNANANDARAJAH, J. S., ENGILES, J. B., GRAY, F., LAUGHLIN, D., GAURNIER-HAUSSER, A., WALLECHA, A., HUEBNER, M. & PATERSON, Y. 2016. Immunotherapy with a HER2-Targeting Listeria Induces HER2-Specific Immunity and Demonstrates Potential Therapeutic Effects in a Phase I Trial in Canine Osteosarcoma. *Clin Cancer Res,* 22**,** 4380-90.
MATHENGE, E. G., DEAN, C. A., CLEMENTS, D., VAGHAR-KASHANI, A., PHOTOPOULOS, S., COYLE, K. M., GIACOMANTONIO, M., MALUETH, B., NUNOKAWA, A., JORDAN, J., LEWIS, J. D., GUJAR, S. A., MARCATO, P., LEE, P. W. & GIACOMANTONIO, C. A. 2014. Core needle biopsy of breast cancer tumors increases distant metastases in a mouse model. *Neoplasia,* 16**,** 950-60.
MATOS, L. L., TRUFELLI, D. C., DE MATOS, M. G. & DA SILVA PINHAL, M. A. 2010. Immunohistochemistry as an important tool in biomarkers detection and clinical practice. *Biomark Insights,* 5**,** 9-20.
MAULDIN, G. N., MATUS, R. E., WITHROW, S. J. & PATNAIK, A. K. 1988. Canine osteosarcoma. Treatment by amputation versus amputation and adjuvant chemotherapy using doxorubicin and cisplatin. *J Vet Intern Med,* 2**,** 177-80.
MAZUMDAR, A., URDINEZ, J., BORO, A., ARLT, M. J. E., EGLI, F. E., NIEDERÖST, B., JAEGER, P. K., MOSCHINI, G., MUFF, R., FUCHS, B., SNEDEKER, J. G. & GVOZDENOVIC, A. 2020a. Exploring the Role of Osteosarcoma-Derived Extracellular Vesicles in Pre-Metastatic Niche Formation and Metastasis in the 143-B Xenograft Mouse Osteosarcoma Model. *Cancers (Basel),* 12.
MAZUMDAR, A., URDINEZ, J., BORO, A., MIGLIAVACCA, J., ARLT, M. J. E., MUFF, R., FUCHS, B., SNEDEKER, J. G. & GVOZDENOVIC, A. 2020b. Osteosarcoma-Derived Extracellular Vesicles Induce Lung Fibroblast Reprogramming. *Int J Mol Sci,* 21.
MCKINNON, K. M. 2018. Flow Cytometry: An Overview. *Curr Protoc Immunol,* 120**,** 5.1.1-5.1.11.
MENDOZA, S., KONISHI, T., DERNELL, W. S., WITHROW, S. J. & MILLER, C. W. 1998. Status of the p53, Rb and MDM2 genes in canine osteosarcoma. *Anticancer Res,* 18**,** 4449-53.

MERTENS, C., AKAM, E. A., REHWALD, C., BRÜNE, B., TOMAT, E. & JUNG, M. 2016. Intracellular Iron Chelation Modulates the Macrophage Iron Phenotype with Consequences on Tumor Progression. *PLoS One,* 11**,** e0166164.

MEYERS, P. A. & CHOU, A. J. 2014. Muramyl tripeptide-phosphatidyl ethanolamine encapsulated in liposomes (L-MTP-PE) in the treatment of osteosarcoma. *Adv Exp Med Biol,* 804**,** 307-21.

MILLS, C. D., KINCAID, K., ALT, J. M., HEILMAN, M. J. & HILL, A. M. 2000. M-1/M-2 macrophages and the Th1/Th2 paradigm. *J Immunol,* 164**,** 6166-73.

MISAGHI, A., GOLDIN, A., AWAD, M. & KULIDJIAN, A. A. 2018. Osteosarcoma: a comprehensive review. *Sicot j,* 4**,** 12.

MISDORP, W. & HART, A. A. 1979. Some prognostic and epidemiologic factors in canine osteosarcoma. *J Natl Cancer Inst,* 62**,** 537-45.

MITSI, E., KAMNG'ONA, R., RYLANCE, J., SOLÓRZANO, C., JESUS REINÉ, J., MWANDUMBA, H. C., FERREIRA, D. M. & JAMBO, K. C. 2018. Human alveolar macrophages predominately express combined classical M1 and M2 surface markers in steady state. *Respir Res,* 19**,** 66.

MIYASATO, Y., SHIOTA, T., OHNISHI, K., PAN, C., YANO, H., HORLAD, H., YAMAMOTO, Y., YAMAMOTO-IBUSUKI, M., IWASE, H., TAKEYA, M. & KOMOHARA, Y. 2017. High density of CD204-positive macrophages predicts worse clinical prognosis in patients with breast cancer. *Cancer Sci,* 108**,** 1693-1700.

MIYAZAKI, Y., VIEIRA-DE-ABREU, A., HARRIS, E. S., SHAH, A. M., WEYRICH, A. S., CASTRO-FARIA-NETO, H. C. & ZIMMERMAN, G. A. 2014. Integrin αDβ2 (CD11d/CD18) is expressed by human circulating and tissue myeloid leukocytes and mediates inflammatory signaling. *PLoS One,* 9**,** e112770.

MONTEIRO, L. N., RODRIGUES, M. A., GOMES, D. A., SALGADO, B. S. & CASSALI, G. D. 2018. Tumour-associated macrophages: Relation with progression and invasiveness, and assessment of M1/M2 macrophages in canine mammary tumours. *Vet J,* 234**,** 119-125.

MOORE, K. J., SHEEDY, F. J. & FISHER, E. A. 2013. Macrophages in atherosclerosis: a dynamic balance. *Nat Rev Immunol,* 13**,** 709-21.

MOREIRA, M. L., DORNELES, E. M., SOARES, R. P., MAGALHÃES, C. P., COSTA-PEREIRA, C., LAGE, A. P., TEIXEIRA-CARVALHO, A., MARTINS-FILHO, O. A. & ARAÚJO, M. S. 2015. Cross-reactivity of commercially available anti-human monoclonal antibodies with canine cytokines: establishment of a reliable panel to detect the functional profile of peripheral blood lymphocytes by intracytoplasmic staining. *Acta Vet Scand,* 57**,** 51.

MOTTOLESE, M., MORELLI, L., AGRIMI, U., BENEVOLO, M., SCIARRETTA, F., ANTONUCCI, G. & NATALI, P. G. 1994. Spontaneous canine mammary tumors. A model for monoclonal antibody diagnosis and treatment of human breast cancer. *Lab Invest,* 71**,** 182-7.

MUELLER, F., FUCHS, B. & KASER-HOTZ, B. 2007. Comparative biology of human and canine osteosarcoma. *Anticancer Res,* 27**,** 155-64.

MURRAY, P. J. 2017. Macrophage Polarization. *Annu Rev Physiol,* 79**,** 541-566.

MURRAY, P. J., ALLEN, J. E., BISWAS, S. K., FISHER, E. A., GILROY, D. W., GOERDT, S., GORDON, S., HAMILTON, J. A., IVASHKIV, L. B., LAWRENCE, T., LOCATI, M., MANTOVANI, A., MARTINEZ, F. O., MEGE, J. L., MOSSER, D. M., NATOLI, G., SAEIJ, J. P., SCHULTZE, J. L., SHIREY, K. A., SICA, A., SUTTLES, J., UDALOVA, I., VAN GINDERACHTER, J. A., VOGEL, S. N. & WYNN, T. A. 2014. Macrophage activation and polarization: nomenclature and experimental guidelines. *Immunity,* 41**,** 14-20.

MUSSER, M. L., BERGER, E. P., TRIPP, C. D., CLIFFORD, C. A., BERGMAN, P. J. & JOHANNES, C. M. 2021. Safety evaluation of the canine osteosarcoma vaccine, live Listeria vector. *Vet Comp Oncol,* 19**,** 92-98.

MÜLLER, A., HOMEY, B., SOTO, H., GE, N., CATRON, D., BUCHANAN, M. E., MCCLANAHAN, T., MURPHY, E., YUAN, W., WAGNER, S. N., BARRERA, J. L., MOHAR, A., VERÁSTEGUI, E. & ZLOTNIK, A. 2001. Involvement of chemokine receptors in breast cancer metastasis. *Nature,* 410**,** 50-6.

NA, Y. R., YOON, Y. N., SON, D., JUNG, D., GU, G. J. & SEOK, S. H. 2015. Consistent inhibition of cyclooxygenase drives macrophages towards the inflammatory phenotype. *PLoS One,* 10**,** e0118203.

NAKAGOMI, D., SUZUKI, K., MEGURO, K., HOSOKAWA, J., TAMACHI, T., TAKATORI, H., SUTO, A., MATSUE, H., OHARA, O., NAKAYAMA, T., SHIMADA, S. & NAKAJIMA, H. 2015. Matrix metalloproteinase 12 is produced by M2 macrophages and plays important roles in the development of contact hypersensitivity. *J Allergy Clin Immunol,* 135**,** 1397-400.

NAKAJIMA, T., HARASHIMA, S., HIRATA, M. & KAJITANI, T. 1978. Prognostic and therapeutic values of peritoneal cytology in gastric cancer. *Acta Cytol,* 22**,** 225-9.

NAKAMURA, K. & SMYTH, M. J. 2020. TREM2 marks tumor-associated macrophages. *Signal Transduct Target Ther,* 5**,** 233.

NAKANE, P. K. 1968. Simultaneous localization of multiple tissue antigens using the peroxidase-labeled antibody method: a study on pituitary glands of the rat. *J Histochem Cytochem,* 16**,** 557-60.

NAKANE, P. K. & PIERCE, G. B., JR. 1966. Enzyme-labeled antibodies: preparation and application for the localization of antigens. *J Histochem Cytochem,* 14**,** 929-31.
NANKO, M., SHIMADA, H., YAMAOKA, H., TANAKA, K., MASUI, H., MATSUO, K., IKE, H., OKI, S. & HARA, M. 1998. Micrometastatic colorectal cancer lesions in the liver. *Surg Today,* 28**,** 707-13.
NEIHAUS, S. A., LOCKE, J. E., BARGER, A. M., BORST, L. B. & GORING, R. L. 2011. A novel method of core aspirate cytology compared to fine-needle aspiration for diagnosing canine osteosarcoma. *J Am Anim Hosp Assoc,* 47**,** 317-23.
NGAMBENJAWONG, C., GUSTAFSON, H. H. & PUN, S. H. 2017. Progress in tumor-associated macrophage (TAM)-targeted therapeutics. *Adv Drug Deliv Rev,* 114**,** 206-221.
NIELSEN, M. C., ANDERSEN, M. N. & MØLLER, H. J. 2020. Monocyte isolation techniques significantly impact the phenotype of both isolated monocytes and derived macrophages in vitro. *Immunology,* 159**,** 63-74.
OGAWA, C., LIU, Y. J. & KOBAYASHI, K. S. 2011. Muramyl dipeptide and its derivatives: peptide adjuvant in immunological disorders and cancer therapy. *Curr Bioact Compd,* 7**,** 180-197.
OH, S. A. & LI, M. O. 2013. TGF-β: guardian of T cell function. *J Immunol,* 191**,** 3973-9.
OHTAKI, Y., ISHII, G., NAGAI, K., ASHIMINE, S., KUWATA, T., HISHIDA, T., NISHIMURA, M., YOSHIDA, J., TAKEYOSHI, I. & OCHIAI, A. 2010. Stromal macrophage expressing CD204 is associated with tumor aggressiveness in lung adenocarcinoma. *J Thorac Oncol,* 5**,** 1507-15.
OISHI, S., TAKANO, R., TAMURA, S., TANI, S., IWAIZUMI, M., HAMAYA, Y., TAKAGAKI, K., NAGATA, T., SETO, S., HORII, T., OSAWA, S., FURUTA, T., MIYAJIMA, H. & SUGIMOTO, K. 2016. M2 polarization of murine peritoneal macrophages induces regulatory cytokine production and suppresses T-cell proliferation. *Immunology,* 149**,** 320-328.
OKAMI, J., DOHNO, K., SAKON, M., IWAO, K., YAMADA, T., YAMAMOTO, H., FUJIWARA, Y., NAGANO, H., UMESHITA, K., MATSUURA, N., NAKAMORI, S. & MONDEN, M. 2000. Genetic detection for micrometastasis in lymph node of biliary tract carcinoma. *Clin Cancer Res,* 6**,** 2326-32.
OLSON, B., LI, Y., LIN, Y., LIU, E. T. & PATNAIK, A. 2018. Mouse Models for Cancer Immunotherapy Research. *Cancer Discov,* 8**,** 1358-1365.
OWEN, L. N., BOSTOCK, D. E. & LAVELLE, R. B. 1975. Studies on chemotherapy and immunotherapy in canine lymphosarcoma and osteosarcoma. *Bibl Haematol***,** 522-3.

PADILLA, L., DAKHEL, S., ADAN, J., MASA, M., MARTINEZ, J. M., ROQUE, L., COLL, T., HERVAS, R., CALVIS, C., LLINAS, L., BUENESTADO, S., CASTELLSAGUE, J., MESSEGUER, R., MITJANS, F. & HERNANDEZ, J. L. 2017. S100A7: from mechanism to cancer therapy. *Oncogene,* 36**,** 6749-6761.

PAGE, R. L., GARG, P. K., GARG, S., ARCHER, G. E., BRULAND, O. S. & ZALUTSKY, M. R. 1994. PET imaging of osteosarcoma in dogs using a fluorine-18-labeled monoclonal antibody Fab fragment. *J Nucl Med,* 35**,** 1506-13.

PAGET, S. 1889. The distribution of secondary growths in cancer of the breast. *The Lancet,* 1**,** 571-573.

PALAZON, A., TYRAKIS, P. A., MACIAS, D., VELIÇA, P., RUNDQVIST, H., FITZPATRICK, S., VOJNOVIC, N., PHAN, A. T., LOMAN, N., HEDENFALK, I., HATSCHEK, T., LÖVROT, J., FOUKAKIS, T., GOLDRATH, A. W., BERGH, J. & JOHNSON, R. S. 2017. An HIF-1α/VEGF-A Axis in Cytotoxic T Cells Regulates Tumor Progression. *Cancer Cell,* 32**,** 669-683.e5.

PARISI, F., TESI, M., MILLANTA, F., GNOCCHI, M. & POLI, A. 2021. M1 and M2 tumour-associated macrophages subsets in canine malignant mammary tumours: An immunohistochemical study. *Res Vet Sci,* 136**,** 32-38.

PARK, J. A. & SHIN, H. Y. 2016. Influence of genetic polymorphisms in the folate pathway on toxicity after high-dose methotrexate treatment in pediatric osteosarcoma. *Blood Res,* 51**,** 50-7.

PARK, J. S., WITHERS, S. S., MODIANO, J. F., KENT, M. S., CHEN, M., LUNA, J. I., CULP, W. T. N., SPARGER, E. E., REBHUN, R. B., MONJAZEB, A. M., MURPHY, W. J. & CANTER, R. J. 2016. Canine cancer immunotherapy studies: linking mouse and human. *J Immunother Cancer,* 4**,** 97.

PAULUS, P., STANLEY, E. R., SCHÄFER, R., ABRAHAM, D. & AHARINEJAD, S. 2006. Colony-stimulating factor-1 antibody reverses chemoresistance in human MCF-7 breast cancer xenografts. *Cancer Res,* 66**,** 4349-56.

PEINADO, H., ALECKOVIC, M., LAVOTSHKIN, S., MATEI, I., COSTA-SILVA, B., MORENO-BUENO, G., HERGUETA-REDONDO, M., WILLIAMS, C., GARCIA-SANTOS, G., GHAJAR, C., NITADORI-HOSHINO, A., HOFFMAN, C., BADAL, K., GARCIA, B. A., CALLAHAN, M. K., YUAN, J., MARTINS, V. R., SKOG, J., KAPLAN, R. N., BRADY, M. S., WOLCHOK, J. D., CHAPMAN, P. B., KANG, Y., BROMBERG, J. & LYDEN, D. 2012. Melanoma exosomes educate bone marrow progenitor cells toward a pro-metastatic phenotype through MET. *Nat Med,* 18**,** 883-91.

PELLIZZARI, G., HOSKIN, C., CRESCIOLI, S., MELE, S., GOTOVINA, J., CHIARUTTINI, G., BIANCHINI, R., ILIEVA, K., BAX, H. J., PAPA, S., LACY, K. E., JENSEN-JAROLIM, E., TSOKA, S., JOSEPHS, D. H., SPICER, J. F. & KARAGIANNIS, S. N. 2019. IgE re-programs alternatively-activated human macrophages towards pro-inflammatory anti-tumoural states. *EBioMedicine,* 43**,** 67-81.

PETTY, A. J., DAI, R., LAPALOMBELLA, R., BAIOCCHI, R. A., BENSON, D. M., LI, Z., HUANG, X. & YANG, Y. 2021. Hedgehog-induced PD-L1 on tumor-associated macrophages is critical for suppression of tumor-infiltrating CD8+ T cell function. *JCI Insight,* 6.

PILLAI, S. R., DAMAGHI, M., MARUNAKA, Y., SPUGNINI, E. P., FAIS, S. & GILLIES, R. J. 2019. Causes, consequences, and therapy of tumors acidosis. *Cancer Metastasis Rev,* 38**,** 205-222.

PLEBANEK, M. P., ANGELONI, N. L., VINOKOUR, E., LI, J., HENKIN, A., MARTINEZ-MARIN, D., FILLEUR, S., BHOWMICK, R., HENKIN, J., MILLER, S. D., IFERGAN, I., LEE, Y., OSMAN, I., THAXTON, C. S. & VOLPERT, O. V. 2017. Pre-metastatic cancer exosomes induce immune surveillance by patrolling monocytes at the metastatic niche. *Nat Commun,* 8**,** 1319.

POMBO ANTUNES, A. R., SCHEYLTJENS, I., LODI, F., MESSIAEN, J., ANTORANZ, A., DUERINCK, J., KANCHEVA, D., MARTENS, L., DE VLAMINCK, K., VAN HOVE, H., KJØLNER HANSEN, S. S., BOSISIO, F. M., VAN DER BORGHT, K., DE VLEESCHOUWER, S., SCIOT, R., BOUWENS, L., VERFAILLIE, M., VANDAMME, N., VANDENBROUCKE, R. E., DE WEVER, O., SAEYS, Y., GUILLIAMS, M., GYSEMANS, C., NEYNS, B., DE SMET, F., LAMBRECHTS, D., VAN GINDERACHTER, J. A. & MOVAHEDI, K. 2021. Single-cell profiling of myeloid cells in glioblastoma across species and disease stage reveals macrophage competition and specialization. *Nat Neurosci,* 24**,** 595-610.

POON, S. & AILLES, L. E. 2022. Modeling the Role of Cancer-Associated Fibroblasts in Tumor Cell Invasion. *Cancers (Basel),* 14.

POPOVIC, P. J., ZEH, H. J., 3RD & OCHOA, J. B. 2007. Arginine and immunity. *J Nutr,* 137**,** 1681s-1686s.

PORCELLATO, I., SFORNA, M., LO GIUDICE, A., BOSSI, I., MUSI, A., TOGNOLONI, A., CHIARADIA, E., MECHELLI, L. & BRACHELENTE, C. 2022. Tumor-Associated Macrophages in Canine Oral and Cutaneous Melanomas and Melanocytomas: Phenotypic and Prognostic Assessment. *Front Vet Sci,* 9**,** 878949.

PRIER, J. E. & BRODEY, R. S. 1963. CANINE NEOPLASIA. A PROTOTYPE FOR HUMAN CANCER STUDY. *Bull World Health Organ,* 29**,** 331-44.

PROSCHOWSKY, H. F., RUGBJERG, H. & ERSBØLL, A. K. 2003. Mortality of purebred and mixed-breed dogs in Denmark. *Prev Vet Med,* 58**,** 63-74.

PU, J., XU, Z., NIAN, J., FANG, Q., YANG, M., HUANG, Y., LI, W., GE, B., WANG, J. & WEI, H. 2021. M2 macrophage-derived extracellular vesicles facilitate CD8+T cell exhaustion in hepatocellular carcinoma via the miR-21-5p/YOD1/YAP/β-catenin pathway. *Cell Death Discov,* 7**,** 182.
QIAN, B. Z. & POLLARD, J. W. 2010. Macrophage diversity enhances tumor progression and metastasis. *Cell,* 141.
QUAIL, D. F. & JOYCE, J. A. 2013. Microenvironmental regulation of tumor progression and metastasis. *Nat Med,* 19.
RANA, S., MALINOWSKA, K. & ZÖLLER, M. 2013. Exosomal tumor microRNA modulates premetastatic organ cells. *Neoplasia,* 15**,** 281-95.
RAPOSO, T. P., PIRES, I., CARVALHO, M. I., PRADA, J., ARGYLE, D. J. & QUEIROGA, F. L. 2015. Tumour-associated macrophages are associated with vascular endothelial growth factor expression in canine mammary tumours. *Vet Comp Oncol,* 13**,** 464-74.
RAUSCH, M., BLANC, L., DE SOUZA SILVA, O., DORMOND, O., GRIFFIOEN, A. W. & NOWAK-SLIWINSKA, P. 2021. Characterization of Renal Cell Carcinoma Heterotypic 3D Co-Cultures with Immune Cell Subsets. *Cancers (Basel),* 13.
REGAN, D. P., ESCAFFI, A., COY, J., KURIHARA, J. & DOW, S. W. 2017. Role of monocyte recruitment in hemangiosarcoma metastasis in dogs. *Vet Comp Oncol,* 15**,** 1309-1322.
REIMEGÅRD, J., TARBIER, M., DANIELSSON, M., SCHUSTER, J., BASKARAN, S., PANAGIOTOU, S., DAHL, N., FRIEDLÄNDER, M. R. & GALLANT, C. J. 2021. A combined approach for single-cell mRNA and intracellular protein expression analysis. *Commun Biol,* 4**,** 624.
RENNERT, K., NITSCHKE, M., WALLERT, M., KEUNE, N., RAASCH, M., LORKOWSKI, S. & MOSIG, A. S. 2017. Thermo-responsive cell culture carrier: Effects on macrophage functionality and detachment efficiency. *J Tissue Eng,* 8**,** 2041731417726428.
RIABOV, V., GUDIMA, A., WANG, N., MICKLEY, A., OREKHOV, A. & KZHYSHKOWSKA, J. 2014. Role of tumor associated macrophages in tumor angiogenesis and lymphangiogenesis. *Front Physiol,* 5**,** 75.
RIBATTI, D., NICO, B., CRIVELLATO, E. & VACCA, A. 2007. Macrophages and tumor angiogenesis. *Leukemia,* 21**,** 2085-9.
ROBERTSON, D., SAVAGE, K., REIS-FILHO, J. S. & ISACKE, C. M. 2008. Multiple immunofluorescence labelling of formalin-fixed paraffin-embedded (FFPE) tissue. *BMC Cell Biol,* 9**,** 13.

RODRIGUES, G., HOSHINO, A., KENIFIC, C. M., MATEI, I. R., STEINER, L., FREITAS, D., KIM, H. S., OXLEY, P. R., SCANDARIATO, I., CASANOVA-SALAS, I., DAI, J., BADWE, C. R., GRIL, B., TEŠIĆ MARK, M., DILL, B. D., MOLINA, H., ZHANG, H., BENITO-MARTIN, A., BOJMAR, L., ARARSO, Y., OFFER, K., LAPLANT, Q., BUEHRING, W., WANG, H., JIANG, X., LU, T. M., LIU, Y., SABARI, J. K., SHIN, S. J., NARULA, N., GINTER, P. S., RAJASEKHAR, V. K., HEALEY, J. H., MEYLAN, E., COSTA-SILVA, B., WANG, S. E., RAFII, S., ALTORKI, N. K., RUDIN, C. M., JONES, D. R., STEEG, P. S., PEINADO, H., GHAJAR, C. M., BROMBERG, J., DE SOUSA, M., PISAPIA, D. & LYDEN, D. 2019. Tumour exosomal CEMIP protein promotes cancer cell colonization in brain metastasis. *Nat Cell Biol,* 21**,** 1403-1412.

RODRIGUEZ, P. C., QUICENO, D. G. & OCHOA, A. C. 2007. L-arginine availability regulates T-lymphocyte cell-cycle progression. *Blood,* 109**,** 1568-73.

RU, G., TERRACINI, B. & GLICKMAN, L. T. 1998. Host related risk factors for canine osteosarcoma. *Vet J,* 156**,** 31-9.

RUAN, C., MENG, Y. & SONG, H. 2022. CD36: an emerging therapeutic target for cancer and its molecular mechanisms. *J Cancer Res Clin Oncol,* 148**,** 1551-1558.

RUFFELL, B., CHANG-STRACHAN, D., CHAN, V., ROSENBUSCH, A., HO, C. M., PRYER, N., DANIEL, D., HWANG, E. S., RUGO, H. S. & COUSSENS, L. M. 2014. Macrophage IL-10 blocks CD8+ T cell-dependent responses to chemotherapy by suppressing IL-12 expression in intratumoral dendritic cells. *Cancer Cell,* 26**,** 623-37.

SABATTINI, E., BISGAARD, K., ASCANI, S., POGGI, S., PICCIOLI, M., CECCARELLI, C., PIERI, F., FRATERNALI-ORCIONI, G. & PILERI, S. A. 1998. The EnVision++ system: a new immunohistochemical method for diagnostics and research. Critical comparison with the APAAP, ChemMate, CSA, LABC, and SABC techniques. *J Clin Pathol,* 51**,** 506-11.

SABATTINI, S., RENZI, A., BURACCO, P., DEFOURNY, S., GARNIER-MOIROUX, M., CAPITANI, O. & BETTINI, G. 2017. Comparative Assessment of the Accuracy of Cytological and Histologic Biopsies in the Diagnosis of Canine Bone Lesions. *J Vet Intern Med,* 31**,** 864-871.

SAHARINEN, P., EKLUND, L., PULKKI, K., BONO, P. & ALITALO, K. 2011. VEGF and angiopoietin signaling in tumor angiogenesis and metastasis. *Trends Mol Med,* 17**,** 347-62.

SAJJAD, H., IMTIAZ, S., NOOR, T., SIDDIQUI, Y. H., SAJJAD, A. & ZIA, M. 2021. Cancer models in preclinical research: A chronicle review of advancement in effective cancer research. *Animal Model Exp Med,* 4**,** 87-103.

SANJURJO, L., ARAN, G., TÉLLEZ, É., AMÉZAGA, N., ARMENGOL, C., LÓPEZ, D., PRATS, C. & SARRIAS, M. R. 2018. CD5L Promotes M2 Macrophage Polarization through Autophagy-Mediated Upregulation of ID3. *Front Immunol,* 9**,** 480.

SAPIERZYŃSKI, R. & CZOPOWICZ, M. 2017. The animal-dependent risk factors in canine osteosarcomas. *Pol J Vet Sci,* 20**,** 293-298.

SAWANO, A., IWAI, S., SAKURAI, Y., ITO, M., SHITARA, K., NAKAHATA, T. & SHIBUYA, M. 2001. Flt-1, vascular endothelial growth factor receptor 1, is a novel cell surface marker for the lineage of monocyte-macrophages in humans. *Blood,* 97**,** 785-91.

SCENEAY, J., CHOW, M. T., CHEN, A., HALSE, H. M., WONG, C. S., ANDREWS, D. M., SLOAN, E. K., PARKER, B. S., BOWTELL, D. D., SMYTH, M. J. & MÖLLER, A. 2012. Primary tumor hypoxia recruits CD11b+/Ly6Cmed/Ly6G+ immune suppressor cells and compromises NK cell cytotoxicity in the premetastatic niche. *Cancer Res,* 72**,** 3906-11.

SCHIFFMAN, J. D. & BREEN, M. 2015. Comparative oncology: what dogs and other species can teach us about humans with cancer. *Philos Trans R Soc Lond B Biol Sci,* 370.

SCHOOK, L. B., COLLARES, T. V., HU, W., LIANG, Y., RODRIGUES, F. M., RUND, L. A., SCHACHTSCHNEIDER, K. M., SEIXAS, F. K., SINGH, K., WELLS, K. D., WALTERS, E. M., PRATHER, R. S. & COUNTER, C. M. 2015. A Genetic Porcine Model of Cancer. *PLoS One,* 10**,** e0128864.

SEGERITZ, C.-P. & VALLIER, L. 2017. Chapter 9 - Cell Culture: Growing Cells as Model Systems In Vitro. *In:* JALALI, M., SALDANHA, F. Y. L. & JALALI, M. (eds.) *Basic Science Methods for Clinical Researchers.* Boston: Academic Press.

SELMIC, L. E., BURTON, J. H., THAMM, D. H., WITHROW, S. J. & LANA, S. E. 2014. Comparison of carboplatin and doxorubicin-based chemotherapy protocols in 470 dogs after amputation for treatment of appendicular osteosarcoma. *J Vet Intern Med,* 28**,** 554-63.

SEUNG, B. J., LIM, H. Y., SHIN, J. I., KIM, H. W., CHO, S. H., KIM, S. H. & SUR, J. H. 2018. CD204-Expressing Tumor-Associated Macrophages Are Associated With Malignant, High-Grade, and Hormone Receptor-Negative Canine Mammary Gland Tumors. *Vet Pathol,* 55**,** 417-424.

SHAO, X. J., XIANG, S. F., CHEN, Y. Q., ZHANG, N., CAO, J., ZHU, H., YANG, B., ZHOU, Q., YING, M. D. & HE, Q. J. 2019. Inhibition of M2-like macrophages by all-trans retinoic acid prevents cancer initiation and stemness in osteosarcoma cells. *Acta Pharmacol Sin,* 40**,** 1343-1350.

SHARMA, S. K., CHINTALA, N. K., VADREVU, S. K., PATEL, J., KARBOWNICZEK, M. & MARKIEWSKI, M. M. 2015. Pulmonary alveolar macrophages contribute to the premetastatic niche by suppressing antitumor T cell responses in the lungs. *J Immunol,* 194**,** 5529-38.

SHARMA, S. V., HABER, D. A. & SETTLEMAN, J. 2010. Cell line-based platforms to evaluate the therapeutic efficacy of candidate anticancer agents. *Nat Rev Cancer,* 10**,** 241-53.
SHARPLESS, N. E. & DEPINHO, R. A. 2006. The mighty mouse: genetically engineered mouse models in cancer drug development. *Nat Rev Drug Discov,* 5**,** 741-54.
SHIAO, S. L., RUFFELL, B., DENARDO, D. G., FADDEGON, B. A., PARK, C. C. & COUSSENS, L. M. 2015. TH2-Polarized CD4(+) T Cells and Macrophages Limit Efficacy of Radiotherapy. *Cancer Immunol Res,* 3**,** 518-25.
SHIMIZU, K., IYODA, T., OKADA, M., YAMASAKI, S. & FUJII, S. I. 2018. Immune suppression and reversal of the suppressive tumor microenvironment. *Int Immunol,* 30**,** 445-454.
SHIOZAWA, Y., EBER, M. R., BERRY, J. E. & TAICHMAN, R. S. 2015. Bone marrow as a metastatic niche for disseminated tumor cells from solid tumors. *Bonekey Rep,* 4**,** 689.
SHREE, T., OLSON, O. C., ELIE, B. T., KESTER, J. C., GARFALL, A. L., SIMPSON, K., BELL-MCGUINN, K. M., ZABOR, E. C., BROGI, E. & JOYCE, J. A. 2011. Macrophages and cathepsin proteases blunt chemotherapeutic response in breast cancer. *Genes Dev,* 25**,** 2465-79.
SHU, S., YANG, Y., ALLEN, C. L., MAGUIRE, O., MINDERMAN, H., SEN, A., CIESIELSKI, M. J., COLLINS, K. A., BUSH, P. J., SINGH, P., WANG, X., MORGAN, M., QU, J., BANKERT, R. B., WHITESIDE, T. L., WU, Y. & ERNSTOFF, M. S. 2018. Metabolic reprogramming of stromal fibroblasts by melanoma exosome microRNA favours a pre-metastatic microenvironment. *Sci Rep,* 8**,** 12905.
SIMPSON, S., DUNNING, M. D., DE BROT, S., GRAU-ROMA, L., MONGAN, N. P. & RUTLAND, C. S. 2017. Comparative review of human and canine osteosarcoma: morphology, epidemiology, prognosis, treatment and genetics. *Acta Vet Scand,* 59**,** 71-81.
SINGLETARY, S. E., ALLRED, C., ASHLEY, P., BASSETT, L. W., BERRY, D., BLAND, K. I., BORGEN, P. I., CLARK, G., EDGE, S. B., HAYES, D. F., HUGHES, L. L., HUTTER, R. V., MORROW, M., PAGE, D. L., RECHT, A., THERIAULT, R. L., THOR, A., WEAVER, D. L., WIEAND, H. S. & GREENE, F. L. 2002. Revision of the American Joint Committee on Cancer staging system for breast cancer. *J Clin Oncol,* 20**,** 3628-36.
SKORUPSKI, K. A., UHL, J. M., SZIVEK, A., ALLSTADT FRAZIER, S. D., REBHUN, R. B. & RODRIGUEZ, C. O., JR. 2016. Carboplatin versus alternating carboplatin and doxorubicin for the adjuvant treatment of canine appendicular osteosarcoma: a randomized, phase III trial. *Vet Comp Oncol,* 14**,** 81-7.

SLOANE, J. P., ORMEROD, M. G. & NEVILLE, A. M. 1980. Potential pathological application of immunocytochemical methods to the detection of micrometastases. *Cancer Res,* 40**,** 3079-82.
SMITH, T. D., TSE, M. J., READ, E. L. & LIU, W. F. 2016. Regulation of macrophage polarization and plasticity by complex activation signals. *Integr Biol (Camb),* 8**,** 946-55.
SOARES, M. P. & HAMZA, I. 2016. Macrophages and Iron Metabolism. *Immunity,* 44**,** 492-504.
SOLINAS, G., SCHIAREA, S., LIGUORI, M., FABBRI, M., PESCE, S., ZAMMATARO, L., PASQUALINI, F., NEBULONI, M., CHIABRANDO, C., MANTOVANI, A. & ALLAVENA, P. 2010. Tumor-conditioned macrophages secrete migration-stimulating factor: a new marker for M2-polarization, influencing tumor cell motility. *J Immunol,* 185**,** 642-52.
SPODNICK, G. J., BERG, J., RAND, W. M., SCHELLING, S. H., COUTO, G., HARVEY, H. J., HENDERSON, R. A., MACEWEN, G., MAULDIN, N., MCCAW, D. L. & ET AL. 1992. Prognosis for dogs with appendicular osteosarcoma treated by amputation alone: 162 cases (1978-1988). *J Am Vet Med Assoc,* 200**,** 995-9.
SPOLSKI, R., LI, P. & LEONARD, W. J. 2018. Biology and regulation of IL-2: from molecular mechanisms to human therapy. *Nat Rev Immunol,* 18**,** 648-659.
STREMMEL, C., SCHUCHERT, R., WAGNER, F., THALER, R., WEINBERGER, T., PICK, R., MASS, E., ISHIKAWA-ANKERHOLD, H. C., MARGRAF, A., HUTTER, S., VAGNOZZI, R., KLAPPROTH, S., FRAMPTON, J., YONA, S., SCHEIERMANN, C., MOLKENTIN, J. D., JESCHKE, U., MOSER, M., SPERANDIO, M., MASSBERG, S., GEISSMANN, F. & SCHULZ, C. 2018. Yolk sac macrophage progenitors traffic to the embryo during defined stages of development. *Nat Commun,* 9**,** 75.
SUN, L., KEES, T., ALMEIDA, A. S., LIU, B., HE, X. Y., NG, D., HAN, X., SPECTOR, D. L., MCNEISH, I. A., GIMOTTY, P., ADAMS, S. & EGEBLAD, M. 2021. Activating a collaborative innate-adaptive immune response to control metastasis. *Cancer Cell,* 39**,** 1361-1374.e9.
TACCONI, C., UNGARO, F., CORREALE, C., ARENA, V., MASSIMINO, L., DETMAR, M., SPINELLI, A., CARVELLO, M., MAZZONE, M., OLIVEIRA, A. I., RUBBINO, F., GARLATTI, V., SPANÒ, S., LUGLI, E., COLOMBO, F. S., MALESCI, A., PEYRIN-BIROULET, L., VETRANO, S., DANESE, S. & D'ALESSIO, S. 2019. Activation of the VEGFC/VEGFR3 Pathway Induces Tumor Immune Escape in Colorectal Cancer. *Cancer Res,* 79**,** 4196-4210.

TAICHMAN, R. S., COOPER, C., KELLER, E. T., PIENTA, K. J., TAICHMAN, N. S. & MCCAULEY, L. K. 2002. Use of the stromal cell-derived factor-1/CXCR4 pathway in prostate cancer metastasis to bone. *Cancer Res,* 62**,** 1832-7.

TALMADGE, J. E., SINGH, R. K., FIDLER, I. J. & RAZ, A. 2007. Murine models to evaluate novel and conventional therapeutic strategies for cancer. *Am J Pathol,* 170**,** 793-804.

TAMURA, R., TANAKA, T., YAMAMOTO, Y., AKASAKI, Y. & SASAKI, H. 2018. Dual role of macrophage in tumor immunity. *Immunotherapy,* 10**,** 899-909.

THAM, M., KHOO, K., YEO, K. P., KATO, M., PREVOST-BLONDEL, A., ANGELI, V. & ABASTADO, J. P. 2015. Macrophage depletion reduces postsurgical tumor recurrence and metastatic growth in a spontaneous murine model of melanoma. *Oncotarget,* 6**,** 22857-68.

THIJSSEN, V. L., PAULIS, Y. W., NOWAK-SLIWINSKA, P., DEUMELANDT, K. L., HOSAKA, K., SOETEKOUW, P. M., CIMPEAN, A. M., RAICA, M., PAUWELS, P., VAN DEN OORD, J. J., TJAN-HEIJNEN, V. C., HENDRIX, M. J., HELDIN, C. H., CAO, Y. & GRIFFIOEN, A. W. 2018. Targeting PDGF-mediated recruitment of pericytes blocks vascular mimicry and tumor growth. *J Pathol,* 246**,** 447-458.

THOMPSON, J. P. & FUGENT, M. J. 1992. Evaluation of survival times after limb amputation, with and without subsequent administration of cisplatin, for treatment of appendicular osteosarcoma in dogs: 30 cases (1979-1990). *J Am Vet Med Assoc,* 200**,** 531-3.

THRALL, D. E., WITHROW, S. J., POWERS, B. E., STRAW, R. C., PAGE, R. L., HEIDNER, G. L., RICHARDSON, D. C., BISSONNETTE, K. W., BETTS, C. W., DEYOUNG, D. J. & ET AL. 1990. Radiotherapy prior to cortical allograft limb sparing in dogs with osteosarcoma: a dose response assay. *Int J Radiat Oncol Biol Phys,* 18**,** 1351-7.

TOMITA, T., SAKURAI, Y., ISHIBASHI, S. & MARU, Y. 2010. Imbalance of Clara cell-mediated homeostatic inflammation is involved in lung metastasis. *Oncogene,* 30.

TRIPEPI, G., JAGER, K. J., DEKKER, F. W. & ZOCCALI, C. 2010. Selection bias and information bias in clinical research. *Nephron Clin Pract,* 115**,** c94-9.

TURNER, R. J., GERAGHTY, N. J., WILLIAMS, J. G., LY, D., BRUNGS, D., CAROLAN, M. G., GUY, T. V., WATSON, D., DE LEON, J. F. & SLUYTER, R. 2020. Comparison of peripheral blood mononuclear cell isolation techniques and the impact of cryopreservation on human lymphocytes expressing CD39 and CD73. *Purinergic Signal,* 16**,** 389-401.

UMEZU, D., OKADA, N., SAKODA, Y., ADACHI, K., OJIMA, T., YAMAUE, H., ETO, M. & TAMADA, K. 2019. Inhibitory functions of PD-L1 and PD-L2 in the regulation of anti-tumor immunity in murine tumor microenvironment. *Cancer Immunol Immunother,* 68**,** 201-211.

VADREVU, S. K., CHINTALA, N. K., SHARMA, S. K., SHARMA, P., CLEVELAND, C., RIEDIGER, L., MANNE, S., FAIRLIE, D. P., GORCZYCA, W., ALMANZA, O., KARBOWNICZEK, M. & MARKIEWSKI, M. M. 2014. Complement c5a receptor facilitates cancer metastasis by altering T-cell responses in the metastatic niche. *Cancer Res,* 74**,** 3454-65.

VAIL, D. M. & MACEWEN, E. G. 2000. Spontaneously occurring tumors of companion animals as models for human cancer. *Cancer Invest,* 18**,** 781-92.

VAIL, D. M., MACEWEN, E. G., KURZMAN, I. D., DUBIELZIG, R. R., HELFAND, S. C., KISSEBERTH, W. C., LONDON, C. A., OBRADOVICH, J. E., MADEWELL, B. R., RODRIGUEZ, C. O., JR. & ET AL. 1995. Liposome-encapsulated muramyl tripeptide phosphatidylethanolamine adjuvant immunotherapy for splenic hemangiosarcoma in the dog: a randomized multi-institutional clinical trial. *Clin Cancer Res,* 1**,** 1165-70.

VALETA-MAGARA, A., GADI, A., VOLTA, V., WALTERS, B., ARJU, R., GIASHUDDIN, S., ZHONG, H. & SCHNEIDER, R. J. 2019. Inflammatory Breast Cancer Promotes Development of M2 Tumor-Associated Macrophages and Cancer Mesenchymal Cells through a Complex Chemokine Network. *Cancer Res,* 79**,** 3360-3371.

VAN DALEN, F. J., VAN STEVENDAAL, M., FENNEMANN, F. L., VERDOES, M. & ILINA, O. 2018. Molecular Repolarisation of Tumour-Associated Macrophages. *Molecules,* 24.

VAN OVERMEIRE, E., STIJLEMANS, B., HEYMANN, F., KEIRSSE, J., MORIAS, Y., ELKRIM, Y., BRYS, L., ABELS, C., LAHMAR, Q., ERGEN, C., VEREECKE, L., TACKE, F., DE BAETSELIER, P., VAN GINDERACHTER, J. A. & LAOUI, D. 2016. M-CSF and GM-CSF Receptor Signaling Differentially Regulate Monocyte Maturation and Macrophage Polarization in the Tumor Microenvironment. *Cancer Res,* 76**,** 35-42.

VANDENBORRE, K., VAN GOOL, S. W., KASRAN, A., CEUPPENS, J. L., BOOGAERTS, M. A. & VANDENBERGHE, P. 1999. Interaction of CTLA-4 (CD152) with CD80 or CD86 inhibits human T-cell activation. *Immunology,* 98**,** 413-21.

VASILJEVA, O., PAPAZOGLOU, A., KRÜGER, A., BRODOEFEL, H., KOROVIN, M., DEUSSING, J., AUGUSTIN, N., NIELSEN, B. S., ALMHOLT, K., BOGYO, M., PETERS, C. & REINHECKEL, T. 2006. Tumor cell-derived and macrophage-derived cathepsin B promotes progression and lung metastasis of mammary cancer. *Cancer Res,* 66**,** 5242-50.

VÁZQUEZ, S., VALLEJO, R., ESPINOSA, J., ARTECHE, N., VEGA, J. A. & PÉREZ, V. 2021. Immunohistochemical Characterization of Tumor-Associated Macrophages in Canine Lymphomas. *Animals,* 11**,** 2301.

WAGNER, J., RAPSOMANIKI, M. A., CHEVRIER, S., ANZENEDER, T., LANGWIEDER, C., DYKGERS, A., REES, M., RAMASWAMY, A., MUENST, S., SOYSAL, S. D., JACOBS, A., WINDHAGER, J., SILINA, K., VAN DEN BROEK, M., DEDES, K. J., RODRÍGUEZ MARTÍNEZ, M., WEBER, W. P. & BODENMILLER, B. 2019. A Single-Cell Atlas of the Tumor and Immune Ecosystem of Human Breast Cancer. *Cell,* 177**,** 1330-1345.e18.

WANG, H., NAGHAVI, M., ALLEN, C., BARBER, R. M., BHUTTA, Z. A., CARTER, A., CASEY, D. C., CHARLSON, F. J., CHEN, A. Z., COATES, M. M., COGGESHALL, M., DANDONA, L., DICKER, D. J., ERSKINE, H. E., FERRARI, A. J., FITZMAURICE, C., FOREMAN, K., FOROUZANFAR, M. H., FRASER, M. S., FULLMAN, N., GETHING, P. W., GOLDBERG, E. M., GRAETZ, N., HAAGSMA, J. A., HAY, S. I., HUYNH, C., JOHNSON, C. O., KASSEBAUM, N. J., KINFU, Y., KULIKOFF, X. R., KUTZ, M., KYU, H. H., LARSON, H. J., LEUNG, J., LIANG, X., LIM, S. S., LIND, M., LOZANO, R., MARQUEZ, N., MENSAH, G. A., MIKESELL, J., MOKDAD, A. H., MOONEY, M. D., NGUYEN, G., NSOESIE, E., PIGOTT, D. M., PINHO, C., ROTH, G. A., SALOMON, J. A., SANDAR, L., SILPAKIT, N., SLIGAR, A., SORENSEN, R. J. D., STANAWAY, J., STEINER, C., TEEPLE, S., THOMAS, B. A., TROEGER, C., VANDERZANDEN, A., VOLLSET, S. E., WANGA, V., WHITEFORD, H. A., WOLOCK, T., ZOECKLER, L., ABATE, K. H., ABBAFATI, C., ABBAS, K. M., ABD-ALLAH, F., ABERA, S. F., ABREU, D. M. X., ABU-RADDAD, L. J., ABYU, G. Y., ACHOKI, T., ADELEKAN, A. L., ADEMI, Z., ADOU, A. K., ADSUAR, J. C., AFANVI, K. A., AFSHIN, A., AGARDH, E. E., AGARWAL, A., AGRAWAL, A., KIADALIRI, A. A., AJALA, O. N., AKANDA, A. S., AKINYEMI, R. O., AKINYEMIJU, T. F., AKSEER, N., LAMI, F. H. A., ALABED, S., AL-ALY, Z., ALAM, K., ALAM, N. K. M., ALASFOOR, D., ALDHAHRI, S. F., ALDRIDGE, R. W., ALEGRETTI, M. A., ALEMAN, A. V., ALEMU, Z. A., ALEXANDER, L. T., et al. 2016a. Global, regional, and national life expectancy, all-cause mortality, and cause-specific mortality for 249 causes of death, 1980–2015: a systematic analysis for the Global Burden of Disease Study 2015. *The Lancet,* 388**,** 1459-1544.

WANG, H., PAN, J., BARSKY, L., JACOB, J. C., ZHENG, Y., GAO, C., WANG, S., ZHU, W., SUN, H., LU, L., JIA, H., ZHAO, Y., BRUNS, C., VAGO, R., DONG, Q. & QIN, L. 2021. Characteristics of pre-metastatic niche: the landscape of molecular and cellular pathways. *Mol Biomed,* 2**,** 3.

WANG, J., LI, D., CANG, H. & GUO, B. 2019. Crosstalk between cancer and immune cells: Role of tumor-associated macrophages in the tumor microenvironment. *Cancer Med,* 8**,** 4709-4721.

WANG, Z., XIONG, S., MAO, Y., CHEN, M., MA, X., ZHOU, X., MA, Z., LIU, F., HUANG, Z., LUO, Q. & OUYANG, G. 2016b. Periostin promotes immunosuppressive premetastatic niche formation to facilitate breast tumour metastasis. *J Pathol,* 239**,** 484-95.

WATSON, A. L., CARLSON, D. F., LARGAESPADA, D. A., HACKETT, P. B. & FAHRENKRUG, S. C. 2016. Engineered Swine Models of Cancer. *Front Genet,* 7**,** 78.

WCULEK, S. K. & MALANCHI, I. 2015. Neutrophils support lung colonization of metastasis-initiating breast cancer cells. *Nature,* 528**,** 413-7.

WEN, S. W., SCENEAY, J., LIMA, L. G., WONG, C. S., BECKER, M., KRUMEICH, S., LOBB, R. J., CASTILLO, V., WONG, K. N., ELLIS, S., PARKER, B. S. & MÖLLER, A. 2016. The Biodistribution and Immune Suppressive Effects of Breast Cancer-Derived Exosomes. *Cancer Res,* 76**,** 6816-6827.

WITHERS, S. S., SKORUPSKI, K. A., YORK, D., CHOI, J. W., WOOLARD, K. D., LAUFER-AMORIM, R., SPARGER, E. E., RODRIGUEZ, C. O., MCSORLEY, S. J., MONJAZEB, A. M., MURPHY, W. J., CANTER, R. J. & REBHUN, R. B. 2019a. Association of macrophage and lymphocyte infiltration with outcome in canine osteosarcoma. *Vet Comp Oncol,* 17**,** 49-60.

WITHERS, S. S., YORK, D., CHOI, J. W., WOOLARD, K. D., LAUFER-AMORIM, R., SPARGER, E. E., BURTON, J. H., MCSORLEY, S. J., MONJAZEB, A. M., MURPHY, W. J., CANTER, R. J. & REBHUN, R. B. 2019b. Metastatic immune infiltrates correlate with those of the primary tumour in canine osteosarcoma. *Vet Comp Oncol,* 17**,** 242-252.

WITHROW, S. J., POWERS, B. E., STRAW, R. C. & WILKINS, R. M. 1991. Comparative aspects of osteosarcoma. Dog versus man. *Clin Orthop Relat Res***,** 159-68.

WITHROW, S. J. & WILKINS, R. M. 2010. Cross talk from pets to people: translational osteosarcoma treatments. *Ilar j,* 51**,** 208-13.

WU, H., HAN, Y., RODRIGUEZ SILLKE, Y., DENG, H., SIDDIQUI, S., TREESE, C., SCHMIDT, F., FRIEDRICH, M., KEYE, J., WAN, J., QIN, Y., KÜHL, A. A., QIN, Z., SIEGMUND, B. & GLAUBEN, R. 2019. Lipid droplet-dependent fatty acid metabolism controls the immune suppressive phenotype of tumor-associated macrophages. *EMBO Mol Med,* 11**,** e10698.

WU, X., ZHOU, Z., XU, S., LIAO, C., CHEN, X., LI, B., PENG, J., LI, D. & YANG, L. 2020. Extracellular vesicle packaged LMP1-activated fibroblasts promote tumor progression via autophagy and stroma-tumor metabolism coupling. *Cancer Lett,* 478**,** 93-106.

WU, Z., WEI, D., GAO, W., XU, Y., HU, Z., MA, Z., GAO, C., ZHU, X. & LI, Q. 2015. TPO-Induced Metabolic Reprogramming Drives Liver Metastasis of Colorectal Cancer CD110+ Tumor-Initiating Cells. *Cell Stem Cell,* 17**,** 47-59.

XIANG, W., SHI, R., KANG, X., ZHANG, X., CHEN, P., ZHANG, L., HOU, A., WANG, R., ZHAO, Y., ZHAO, K., LIU, Y., MA, Y., LUO, H., SHANG, S., ZHANG, J., HE, F., YU, S., GAN, L., SHI, C., LI, Y., YANG, W., LIANG, H. & MIAO, H. 2018. Monoacylglycerol lipase regulates cannabinoid receptor 2-dependent macrophage activation and cancer progression. *Nat Commun,* 9**,** 2574.

XING, F., LIU, Y., WU, S. Y., WU, K., SHARMA, S., MO, Y. Y., FENG, J., SANDERS, S., JIN, G., SINGH, R., VIDI, P. A., TYAGI, A., CHAN, M. D., RUIZ, J., DEBINSKI, W., PASCHE, B. C., LO, H. W., METHENY-BARLOW, L. J., D'AGOSTINO, R. B., JR. & WATABE, K. 2018. Loss of XIST in Breast Cancer Activates MSN-c-Met and Reprograms Microglia via Exosomal miRNA to Promote Brain Metastasis. *Cancer Res,* 78**,** 4316-4330.

XU, J., ESCAMILLA, J., MOK, S., DAVID, J., PRICEMAN, S., WEST, B., BOLLAG, G., MCBRIDE, W. & WU, L. 2013. CSF1R signaling blockade stanches tumor-infiltrating myeloid cells and improves the efficacy of radiotherapy in prostate cancer. *Cancer Res,* 73**,** 2782-94.

XU, X., YE, J., HUANG, C., YAN, Y. & LI, J. 2019. M2 macrophage-derived IL6 mediates resistance of breast cancer cells to hedgehog inhibition. *Toxicol Appl Pharmacol,* 364**,** 77-82.

YAN, H. H., PICKUP, M., PANG, Y., GORSKA, A. E., LI, Z., CHYTIL, A., GENG, Y., GRAY, J. W., MOSES, H. L. & YANG, L. 2010. Gr-1+CD11b+ myeloid cells tip the balance of immune protection to tumor promotion in the premetastatic lung. *Cancer Res,* 70**,** 6139-49.

YANG, M., LIU, J., SHAO, J., QIN, Y., JI, Q., ZHANG, X. & DU, J. 2014. Cathepsin S-mediated autophagic flux in tumor-associated macrophages accelerate tumor development by promoting M2 polarization. *Mol Cancer,* 13**,** 43.

YANG, M., MCKAY, D., POLLARD, J. W. & LEWIS, C. E. 2018. Diverse Functions of Macrophages in Different Tumor Microenvironments. *Cancer Res,* 78**,** 5492-5503.

YANG, W. W., YANG, L. Q., ZHAO, F., CHEN, C. W., XU, L. H., FU, J., LI, S. L. & GE, X. Y. 2017. Epiregulin Promotes Lung Metastasis of Salivary Adenoid Cystic Carcinoma. *Theranostics,* 7**,** 3700-3714.

YAO, R. R., LI, J. H., ZHANG, R., CHEN, R. X. & WANG, Y. H. 2018. M2-polarized tumor-associated macrophages facilitated migration and epithelial-mesenchymal transition of HCC cells via the TLR4/STAT3 signaling pathway. *World J Surg Oncol,* 16**,** 9.

YIN, Y., YAO, S., HU, Y., FENG, Y., LI, M., BIAN, Z., ZHANG, J., QIN, Y., QI, X., ZHOU, L., FEI, B., ZOU, J., HUA, D. & HUANG, Z. 2017. The Immune-microenvironment Confers Chemoresistance of Colorectal Cancer through Macrophage-Derived IL6. *Clin Cancer Res,* 23**,** 7375-7387.

YU, Z., ZHAO, S., REN, L., WANG, L., CHEN, Z., HOFFMAN, R. M. & ZHOU, J. 2017. Pancreatic cancer-derived exosomes promote tumor metastasis and liver pre-metastatic niche formation. *Oncotarget,* 8**,** 63461-63483.

ZENG, Z., LI, Y., PAN, Y., LAN, X., SONG, F., SUN, J., ZHOU, K., LIU, X., REN, X., WANG, F., HU, J., ZHU, X., YANG, W., LIAO, W., LI, G., DING, Y. & LIANG, L. 2018. Cancer-derived exosomal miR-25-3p promotes pre-metastatic niche formation by inducing vascular permeability and angiogenesis. *Nat Commun,* 9**,** 5395.

ZHANG, X. W., YANG, H. Y., FAN, P., YANG, L. & CHEN, G. Y. 2005. Detection of micrometastasis in peripheral blood by multi-sampling in patients with colorectal cancer. *World J Gastroenterol,* 11**,** 436-8.

ZHAO, J., SCHLÖßER, H. A., WANG, Z., QIN, J., LI, J., POPP, F., POPP, M. C., ALAKUS, H., CHON, S. H., HANSEN, H. P., NEISS, W. F., JAUCH, K. W., BRUNS, C. J. & ZHAO, Y. 2019. Tumor-Derived Extracellular Vesicles Inhibit Natural Killer Cell Function in Pancreatic Cancer. *Cancers (Basel),* 11.

ZHAO, X., WU, Q., GONG, X., LIU, J. & MA, Y. 2021. Osteosarcoma: a review of current and future therapeutic approaches. *Biomed Eng Online,* 20**,** 24.

ZHAO, X., XU, Z. & LI, H. 2017. NSAIDs Use and Reduced Metastasis in Cancer Patients: results from a meta-analysis. *Sci Rep,* 7**,** 1875.

ZHENG, P., CHEN, L., YUAN, X., LUO, Q., LIU, Y., XIE, G., MA, Y. & SHEN, L. 2017. Exosomal transfer of tumor-associated macrophage-derived miR-21 confers cisplatin resistance in gastric cancer cells. *J Exp Clin Cancer Res,* 36**,** 53.

ZHOU, W., FONG, M. Y., MIN, Y., SOMLO, G., LIU, L., PALOMARES, M. R., YU, Y., CHOW, A., O'CONNOR, S. T., CHIN, A. R., YEN, Y., WANG, Y., MARCUSSON, E. G., CHU, P., WU, J., WU, X., LI, A. X., LI, Z., GAO, H., REN, X., BOLDIN, M. P., LIN, P. C. & WANG, S. E. 2014. Cancer-secreted miR-105 destroys vascular endothelial barriers to promote metastasis. *Cancer Cell,* 25**,** 501-15.

ZHU, X., SHEN, H., YIN, X., LONG, L., CHEN, X., FENG, F., LIU, Y., ZHAO, P., XU, Y., LI, M., XU, W. & LI, Y. 2017. IL-6R/STAT3/miR-204 feedback loop contributes to cisplatin resistance of epithelial ovarian cancer cells. *Oncotarget,* 8**,** 39154-39166.

ZILIONIS, R., ENGBLOM, C., PFIRSCHKE, C., SAVOVA, V., ZEMMOUR, D., SAATCIOGLU, H. D., KRISHNAN, I., MARONI, G., MEYEROVITZ, C. V., KERWIN, C. M., CHOI, S., RICHARDS, W. G., DE RIENZO, A., TENEN, D. G., BUENO, R., LEVANTINI, E., PITTET, M. J. & KLEIN, A. M. 2019. Single-Cell Transcriptomics of Human and Mouse Lung Cancers Reveals Conserved Myeloid Populations across Individuals and Species. *Immunity,* 50**,** 1317-1334.e10.

ZOSO, A., MAZZA, E. M., BICCIATO, S., MANDRUZZATO, S., BRONTE, V., SERAFINI, P. & INVERARDI, L. 2014. Human fibrocytic myeloid-derived suppressor cells express IDO and promote tolerance via Treg-cell expansion. *Eur J Immunol,* 44**,** 3307-19.

ÖREN, B., UROSEVIC, J., MERTENS, C., MORA, J., GUIU, M., GOMIS, R. R., WEIGERT, A., SCHMID, T., GREIN, S., BRÜNE, B. & JUNG, M. 2016. Tumour stroma-derived lipocalin-2 promotes breast cancer metastasis. *J Pathol,* 239**,** 274-85.

7 Papers I-III

I Paper I

Acta Veterinaria Scandinavica

RESEARCH Open Access

Early immunohistochemical detection of pulmonary micrometastases in dogs with osteosarcoma

Mikael Kerboeuf[1*], Erling Olaf Koppang[2], Anita Haug Haaland[1], Frode Lingaas[2], Øyvind Sverre Bruland[3], Jon Teige[2] and Lars Moe[1]

Abstract

Background: Despite decades of research, the early phases of metastatic development are still not fully understood. Canine osteosarcoma (OS) is a highly aggressive cancer, with a high metastatic rate (> 90%), despite a low overt metastatic prevalence at initial diagnosis (< 15%). Canine OS is generally regarded as a good clinically relevant model for human OS. The aim of this hypothesis-generating study was to evaluate a method to detect pulmonary micrometastases and study their prevalence in dogs with OS without macroscopic metastases. We prospectively enrolled dogs with OS that received no cancer-specific treatment (n = 12) and control dogs without cancer (n = 2). Dogs were necropsied and sampled immediately after euthanasia. The OS dogs were classified as having macroscopic metastases (n = 2) or not (n = 10). We immunohistochemically stained one tissue sample from each of the seven lung lobes from each dog with a monoclonal antibody (TP-3) to identify micrometastases (defined as clusters of 5–50 tumour cells), microscopic metastases (> 50 tumour cells) and TP-3 positive single cells (< 5 tumour cells).

Results: We showed that pulmonary micrometastases easily overseen on routine histology could be detected with TP-3. Pulmonary micrometastases and microscopic metastases were present in two dogs with OS without macroscopic metastases (20%). Micrometastases were visualised in three (43%) and four (57%) of seven samples from these two dogs, with a mean of 0.6 and 1.7 micrometastases per sample. Microscopic metastases were present in one (14%) and four (57%) of seven samples from the same two dogs, with a mean of 0.14 and 1.0 microscopic metastases per sample. There were four (57%) and two (29%) samples with neither microscopic metastases nor micrometastases for each of these two dogs. The prevalence of pulmonary micrometastases (20%) was significantly lower than expected (> 90%) based on commonly expected metastatic rates after amputation ($P < 0.0001$). There was no statistically significant difference in the number of TP-3 positive single cells in between groups ($P = 0.85$).

Conclusions: Pulmonary micrometastases could be detected with TP-3 immunohistochemistry in a subset of dogs with OS before macroscopic metastases had developed. We propose that dogs with spontaneous OS represent clinically relevant models to study early micrometastatic disease.

Keywords: Bone cancer, Canine, Lung metastasis, Metastasis model, Pulmonary metastasis

Background

Cancer is currently ranked as a major leading cause of death in humans and dogs, mainly due to metastatic disease [1–6]. Historically, murine cancer models have proven useful in understanding many of the underlying mechanisms of cancer, albeit with some limitations [7].

*Correspondence: mikael.mathias.kerboeuf@nmbu.no
[1] Department of Companion Animal Clinical Sciences, Faculty of Veterinary Medicine, Norwegian University of Life Sciences, Elizabeth Stephansens vei 15, 1433 Ås, Norway
Full list of author information is available at the end of the article

This is especially true when developing new therapeutics, as the majority have failed to reach the clinic. Micrometastases have been studied in some spontaneous canine cancer forms [8–12]. Their presence in lymph nodes, peripheral blood and bone marrow has been investigated in dogs with mammary carcinoma, as well as in lymph nodes of dogs with some other carcinomas and mast cell tumours. In humans, micrometastases have been studied in lymph nodes, bone marrow, lungs, liver, pleural or peritoneal cavities and peripheral blood in several forms of cancer [13–22].

Spontaneous canine osteosarcoma (OS) is considered a good model for human OS [23–30]. Most dogs with OS succumb to the disease, with the majority dying or being euthanized due to metastatic disease [31]. Although radiographically detectable metastases are uncommon at presentation (< 15–17%), most dogs eventually develop metastatic disease (> 90%) [31–35]. A question that remains unanswered is where the disseminated cells reside before macroscopic metastases develop. The main target organs for metastatic OS, both in humans and dogs, are the lungs and bones [29, 31, 34–37]. Bruland et al. found tumour cells in the bone marrow in 63% of human OS patients at presentation [14]. Amongst those presenting with overt metastases, the prevalence of tumour cells in the bone marrow was 92%. To our knowledge, micrometastases in the lungs have not been prospectively investigated either in human or canine OS.

The monoclonal antibody TP-3 binds selectively to a sarcoma-associated cell surface membrane antigen related to osteoblastic differentiation [38, 39]. The antigen is a monomeric polypeptide with alkaline phosphatase activity and a molecular weight of 80 kDa. TP-3 has been shown to bind to all evaluated OS cases in dogs [40, 41]. Similarly, various human sarcomas express the antigen, including all human OS cases examined [38, 39].

The aim of this hypothesis-generating study was to evaluate the use of TP-3 immunohistochemistry (IHC) on frozen tissue sections as a tool to detect pulmonary micrometastases and to study their prevalence in dogs with spontaneous OS before the development of macroscopic metastasis.

Methods

Study population

This study was conducted as a prospective case series of necropsied dogs with OS (OS+) and control dogs without OS (OS−). All cases were privately owned dogs presented to the Veterinary Teaching Hospital and private practices. Owners signed a participation consent form before the dogs were euthanized and necropsied. Dogs included in the OS + group could be of any breed, sex and age, had to have an appendicular primary tumour location and a confirmed histopathological OS diagnosis. Dogs that had undergone surgical treatment, except for diagnostic incisional biopsies, or other treatments except for pain-relieving drugs (opioids and NSAIDs), were excluded. For inclusion into the OS− group, dogs could be of any breed, sex and age, and had to have been euthanized for non-cancer-related disease. Hence, dogs with a previous history of cancer or a histopathological cancer diagnosis at necropsy were excluded from the OS− group.

Necropsy and tissue collection

According to our protocol, all dogs had to be necropsied within two hours after euthanasia. Standard necropsy procedure was followed, with all organ systems being inspected macroscopically. Based on necropsy results, dogs in the OS + group were further classified as having macroscopic pulmonary metastases (OS + /Met +) or not (OS + /Met−). Tissue samples from all major organ systems (kidneys, lungs, liver, spleen, adrenal glands, myocardium, skeletal muscles and intestines) and any lesions suspected of being metastatic or neoplastic were collected and formalin-fixed. All formalin-fixed paraffin-embedded samples were stained with haematoxylin & eosin (H&E) and examined microscopically. Four tissue samples (sample size of approximately 1 × 1 × 1 cm) were taken from each of the seven lung lobes from each dog. Two were taken from the peripheral areas of the lobes, where only small bronchi were present, and two from the central, close to the main stem bronchi. Samples from all areas were collected for both formalin fixation and snap freezing in cold isopropanol (− 20 °C), quickly followed by submersion in liquid nitrogen and storage at − 80 °C. For dogs in the OS + /Met + group, samples for IHC analysis were taken from the same anatomical regions while avoiding macroscopic metastases. In addition, tissue samples from macroscopic metastases were formalin-fixed, stained with H&E and examined microscopically. Six of the seven samples from the peripheral areas and one of the seven from the central were picked at random, using an online random number generator (www.random.org) for further IHC analysis.

IHC staining

IHC TP-3 staining was performed on frozen tissue sections. Snap frozen samples were sliced into 7 µm sections with a cryostat at − 25 °C. The tissue sections were mounted on poly-lysin-coated slides (Superfrost™ Plus, Thermo Fisher Scientific, Oslo, Norway) and dried at room temperature for one hour. The slides were then stored at − 80 °C until further preparation. IHC sections were labelled using the peroxidase-conjugated immune-polymer method (EnVision™, Dako, Glostrup, Denmark).

The sections were first fixed in cold acetone (− 20 °C) for 10 min, followed by airdrying for 10 min. Endogenous peroxidase activity was inhibited by immersing the slides in a cold (4 °C) 0.3% H_2O_2 solution in phosphate-buffered saline (PBS) for 10 min. To prevent non-specific binding, the sections were blocked using a 1:50 solution of normal goat serum in 5% bovine serum albumin in tris-buffered saline (BSA/TBS) for 30 min. Sections were incubated with the purified IgG 2A monoclonal murine antibody (TP-3, 5 µg/mL, Norwegian Radiumhospital, Oslo, Norway), diluted in 1% BSA/TBS, for 60 min. The samples were then incubated with the secondary antibody (EnVision™, Dako, Glostrup, Denmark) for 30 min. Finally, immunolabelled tissues were developed using a 3-amino-9-ethylcarbazole (AEC) substrate chromogen (EnVision™, Dako, Glostrup, Denmark) incubated for 8 min, then counterstained with Mayer's haematoxylin. The slides were mounted with coverslips using a water-soluble mounting medium (Aquatex®, Merck, Darmstadt, Germany) and left to dry at room temperature overnight. Negative controls were stained without primary antibodies. All washing steps of the IHC procedure were done by immersing the slides in three changes of PBS, each for 5 min at room temperature. All incubations were done at room temperature in a moisture chamber placed on a rotation table. A section containing both micrometastases and macroscopic metastases was used as a positive control for each staining.

IHC analysis

Each slide was scanned for microscopic metastases, micrometastases and TP-3 positive single cells. Micrometastases were defined as clusters of ≥ 5 and ≤ 50 TP-3 positive cells. Clusters > 50 cells were defined as microscopic metastases, while clusters of < 5 TP-3 positive cells were defined as TP-3 positive single cells.

IHC stained slides were evaluated using a Zeiss AX10 microscope, equipped with a Zeiss axiocam 506 color camera, coupled with Zen pro 2012 (blue edition) image acquiring software (Carl Zeiss Microscopy GmbH, Jena, Germany). The total number of microscopic metastases and micrometastases, if present, were counted in the entire slide for each sample. The number of TP-3 positive single cells was counted in 10 high-power fields (HPF, defined as one field at 400x, equivalent to 0.196 mm^2 for the microscope used). Areas with folded up tissue were excluded from the analysis. Slides where staining was too weak to identify positive cells or significant unspecific staining was present, were also excluded.

Statistical analysis

All statistical analyses were performed using JMP pro 15.1.0 (SAS Institute Inc., Cary, NC). The mean number of TP-3 positive single cells per 10 HPF per lung lobe was compared between groups using Wilcoxon rank-sum tests for each pair and an unpaired Kruskal–Wallis test. The mean number of TP-3 positive single cells per 10 HPF for the different lung lobes (anatomical division) was compared between all the dogs combined and in between groups using Wilcoxon rank-sum tests for each pair and an unpaired Kruskal–Wallis test. The prevalence of micrometastases was tested against the expected prevalence (> 90%, based on the post-surgical metastatic rate) using a binomial test. P-values < 0.05 were considered statistically significant for statistical testing.

Results

Study population

Cases were enrolled and necropsied between 2012 and 2020. In total 14 dogs were included in the study, ten in the OS + /Met- group, two in the OS + /Met + group and two in the OS−/Met− group (see Tables 1 and 2). OS + cases were confirmed based on clinical signs, diagnostic imaging, and histopathologic examination after H&E staining. The mean age was 5.6 years (median six years, range 1–11 years). There were eight (57%) male and six (43%) female dogs. The mean time from clinical presentation to euthanasia due to OS was 33 days (median 9.5 days, range 1–155 days). No neoplastic disease other than OS was found at necropsy in any of the dogs. The only significant pathological changes in the lungs were the macroscopic metastases seen in the two OS + /Met + dogs (Fig. 1a) and microscopic metastases (Fig. 1b) and suspected micrometastases (Fig. 1c) in some of the OS + /Met- dogs.

Pulmonary micrometastases and microscopic metastases

A total of 98 lung samples underwent IHC TP-3 staining and histological evaluation, in addition to the positive and negative controls. Tumour cells throughout all micrometastases and microscopic metastases showed a strong and seemingly cytoplasmatic TP-3 staining, as seen in Fig. 2. Depending on their size, micrometastases were either found lodged within pulmonary arterioles (Fig. 2) or the capillaries of the alveolar septa. In larger metastatic lesions, TP-3 staining varied more. Here, cells in the periphery showed strong staining, while those towards the centre stained only weakly or not at all. Micrometastases were present in two dogs (20%) in the OS + /Met− group (Table 2), whereas we found none in the ten remaining cases (eight in the OS + /Met− and both in the OS + /Met + group) or the OS−/Met− group. Microscopic metastases were present in these same two dogs (Table 2). Micrometastases were found in three (43%) and four (57%) of the seven samples examined for each of the two dogs. The total number of micrometastases

Table 1 Overview of the clinical characteristics, final diagnosis and tumour location for the dogs necropsied with primary appendicular osteosarcoma based on haematoxylin & eosin staining and controls included in the prospective study

Case	Breed	Sex	Age -years	Final diagnosis	Location of primary tumour
1	Mixed breed	M	1	Osteosarcoma	Left distal radius
2	Schnauzer	F	8	Osteosarcoma, osteoblastic	Right distal radius
3	Newfoundland dog	M	8	Osteosarcoma	Left distal radius
4	Siberian husky	M	3	Osteosarcoma, fibroblastic	Left proximal humerus
5	Irish wolfhound	F	6	Osteosarcoma	Right distal tibia
6	English setter	M	8	Osteosarcoma	Right distal ulna
7	Pointer	F	4	Osteosarcoma	Left distal tibia
8	Shar Pei	M	11	Osteosarcoma	Right proximal humerus
9	Rottweiler	F	9	Osteosarcoma, osteoblastic	Left proximal humerus
10	German shepherd	F	3	Osteosarcoma, osteoblastic	Left distal radius
11	Flat-coated retriever	M	3	Osteosarcoma	Left distal radius
12	Leonberger	M	6	Osteosarcoma	Left distal radius
13	Dalmatian	M	8	Urolithiasis	N.A
14	Shetland Sheepdog	F	1	Behavioural problems	N.A

N.A Not applicable

Table 2 Overview of the TP-3 immunohistochemical findings for the dogs in Table 1

Group	Case	Microscopic metastases	Micrometastases	Days from presentation to euthanasia
OS+/Met+	1	No	No	36
	2	No	No	28
OS+/Met−	3	No	No	1
	4	No	No	5
	5	Yes	Yes	10
	6	No	No	4
	7	No	No	32
	8	No	No	3
	9	Yes	Yes	155
	10	No	No	106
	11	No	No	9
	12	No	No	4
OS−/Met−	13	No	No	N.A
	14	No	No	N.A

The dogs were divided into three groups,—with macroscopic metastases (OS+/Met+),—without macroscopic metastases (OS+/Met−) and—without osteosarcoma (OS−/Met−). The presence (yes) or absence (no) of microscopic metastases (cluster of > 50 TP-3 positive cells) and micrometastases (cluster of 5–50 TP-3 positive cells) was recorded for each dog. (*N.A* Not applicable)

in each dog was four and 12, respectively, with a mean of 0.6 (range 0–2) and 1.7 (range 0–6) micrometastases per sample. Microscopic metastases were found in one (14%) and four (57%) of the seven samples in the same two dogs. The total number of microscopic metastases was one and seven, respectively, with a mean of 0.14 (range 0–1) and 1.0 (range 0–3) microscopic metastases per sample. Figure 3 shows the distribution of metastases in each lung lobe. There were four (57%) and two (29%) samples for each of the two dogs with neither microscopic metastases nor micrometastases.

TP-3 positive single cells

TP-3 positive single cells were present in the lung parenchyma in all samples in all dogs. These were either scattered respiratory epithelial cells or metastatic OS cells. Most TP-3 positive single cells were identified as dislodged respiratory epithelium, based on cytoplasmatic morphology, staining pattern and nuclear characteristics (Fig. 4). They showed asymmetrical staining, which was stronger along the ciliated brush border and weaker on the opposite side of the cell. In addition, the majority had small to moderately sized eccentric nuclei and no visible nucleoli. In some cases, TP-3 positive single cells were more compatible with tumour cells, showing a strong and homogenous cytoplasmatic staining, with large nuclei and distinct nucleoli (Fig. 5). In most cases, we could not reliably distinguish the two cell populations, and as such, they were all counted as TP-3 positive single cells.

The mean number of TP-3 positive single cells per 10 HPF per sample was 6.5 (median 6.5, range 5.9–7) for the OS+/Met+group, 120.5 (median 15.2, range 3–941.9) for the OS+/Met- group and 17.9 (median 17.9, range 4.7–31.1) for the OS−/Met− group. There was no statistically significant difference in the mean number of TP-3 positive single cells per 10 HPF per sample between the groups (P = 0.85). There was no statistically significant difference between the means of the OS+/Met− group and the OS+/Met+(P = 0.75) or OS−/Met− (P = 0.75) group, nor between the OS+/Met+and OS−/

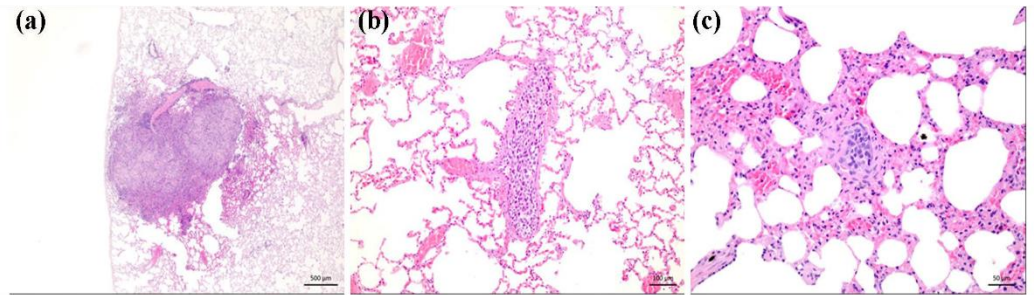

Fig. 1 **a** Section of lung tissue from a dog with osteosarcoma with macroscopic metastases (case 2) showing a macroscopic metastasis (25 × magnification). Section of lung tissue from a dog with osteosarcoma without macroscopic metastases (case 5) showing **b** a microscopic metastasis lodged within a pulmonary arteriole (100 × magnification), and **c** a presumed micrometastasis within the alveolar septa (200 × magnification). Formalin-fixed paraffin-embedded tissue, haematoxylin & eosin stain

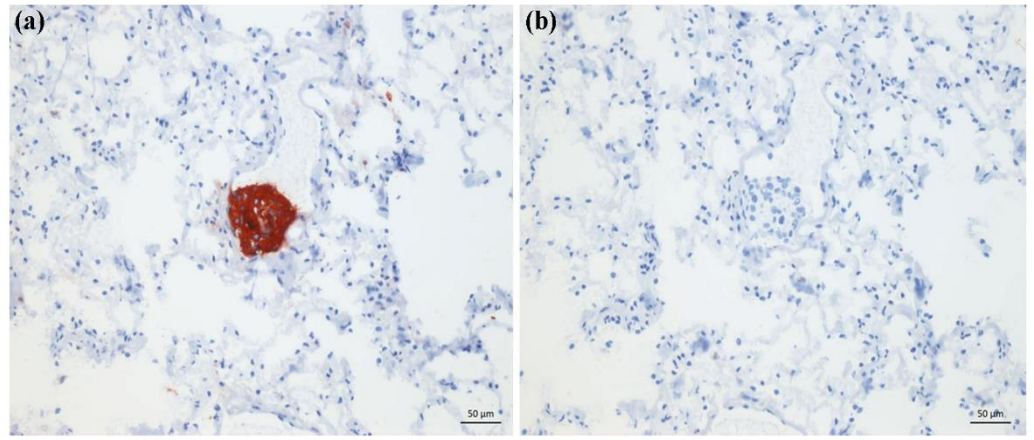

Fig. 2 **a** Section of lung tissue from a dog with osteosarcoma without macroscopic metastases (case 9) showing immunolabeling (red staining) with tumour protein-3 (TP-3) of a pulmonary micrometastasis (defined as a cluster of 5–50 TP-3 positive cells). The micrometastasis is lodged within a pulmonary arteriole. **b** Section of the same tissue as in **a**, but without TP-3 antibody (negative control). Snap frozen tissue, immunoperoxidase stain, TP-3, AEC chromogen and haematoxylin counterstain, 200 × magnification

Met− group (P = 1.0). There were no statistically significant differences in the mean number of TP-3 positive single cells per 10 HPF between any of the different lung lobes (anatomical division), neither when combining all the dogs (P = 0.96), nor within the different groups (for OS+/Met+, P = 0.82, OS+/Met−, P = 0.89 and OS−/Met−, P = 0.62).

Normal structures stained with TP-3

TP-3 staining was observed on the luminal side of the bronchial and bronchiolar epithelium in all dogs (Fig. 6). Staining of the epithelium in the terminal and respiratory bronchioles and alveolar ducts was more variable amongst dogs. In most cases, the staining was weak at the level of the terminal and respiratory bronchioles, with no visible staining towards the alveolar ducts. The columnar respiratory epithelium showed an asymmetrical staining pattern, as described for the dislodged respiratory epithelium (Fig. 6). The cuboidal epithelium of the respiratory and terminal bronchioles was more evenly stained throughout the cytoplasm and with a weaker intensity. Also, the bronchial seromucous glands showed asymmetrical cytoplasmatic staining in all dogs, with a stronger staining intensity towards the luminal side.

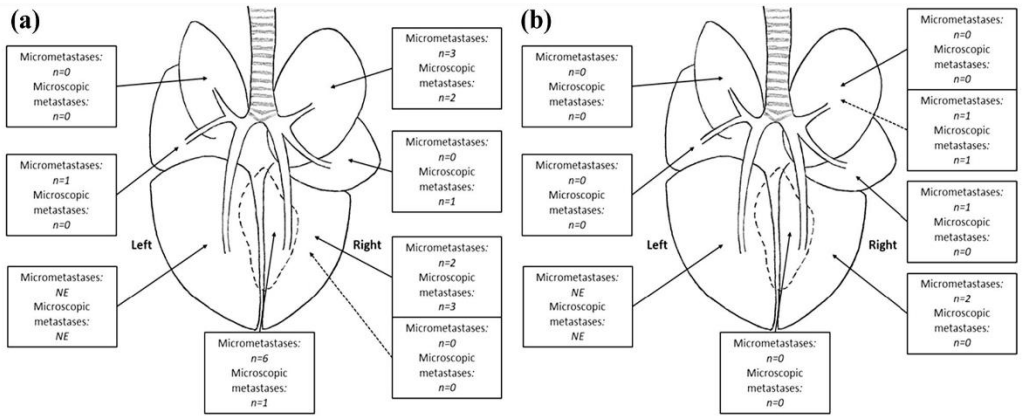

Fig. 3 Distribution and number of micrometastases (cluster of 5–50 TP-3 positive cells) and microscopic metastases (cluster of > 50 TP-3 positive cells) in two dogs with osteosarcoma without macroscopic metastases. **a** represents case 5 and **b** represents case 9. Each arrow and box correspond to a specific lung lobe, from the right top side and clockwise: Right cranial lobe, right medial lobe, right caudal lobe, accessory lobe, left caudal lobe, left medial lobe, and left cranial lobe. The solid arrows indicate samples from the peripheral lung tissue, while the dotted arrows indicate samples from the central lung tissue (*NE* Not examined)

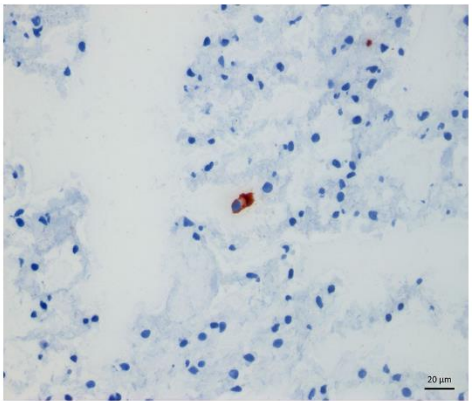

Fig. 4 Section of lung tissue from a dog without neoplastic disease (case 14) showing immunolabeling (red staining) with tumour protein-3 (TP-3) of a single cell. Based on staining pattern and intensity, as well as cytoplasmatic and nuclear morphology, the cell represents a dislodged respiratory epithelial cell. Snap frozen tissue, immunoperoxidase stain, TP-3, AEC chromogen and haematoxylin counterstain, 400 × magnification

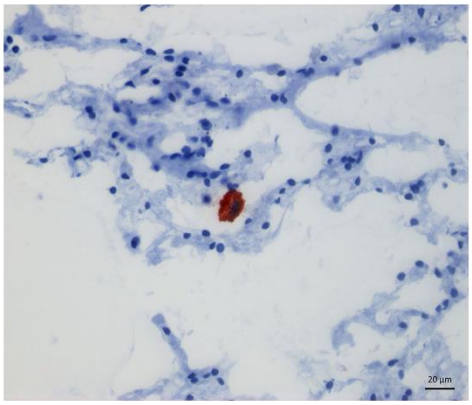

Fig. 5 Section of lung tissue from a dog with osteosarcoma without macroscopic metastases (case 5) showing immunolabeling (red staining) with tumour protein-3 (TP-3) of a single cell. Based on staining pattern and intensity, as well as cytoplasmatic and nuclear morphology, this cell may represent a tumour cell. Snap frozen tissue, immunoperoxidase stain, TP-3, AEC chromogen and haematoxylin counterstain, 400 × magnification

Discussion

To further improve OS treatment strategies and outcomes, it is essential to understand the pathogenesis of metastasis. In this hypothesis-generating study, we have shown that it is feasible to identify pulmonary micrometastases in dogs with OS using IHC with the monoclonal antibody TP-3. All cases of canine OS previously examined with TP-3 have shown positive staining of the primary tumour [40, 41]. In the present study, we found that pulmonary metastases, microscopic metastases and micrometastases also bind TP-3. We found pulmonary micrometastases and microscopic metastases in only

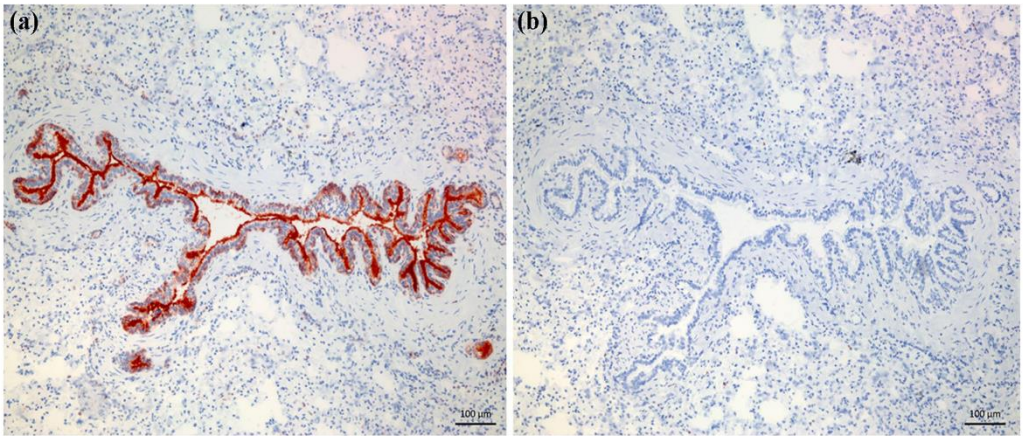

Fig. 6 **a** Section of lung tissue from a dog (case 3) showing immunolabeling (red staining) with tumour protein-3 (TP-3) of the respiratory bronchiolar epithelium. An asymmetrical staining pattern can be seen, with a stronger reaction towards the ciliated brush border. **b** Section of the same tissue as in **a**, but without TP-3 antibody (negative control). Snap frozen tissue, immunoperoxidase stain, TP-3, AEC chromogen and haematoxylin counterstain, 100 × magnification

20% of the dogs with OS before macroscopic metastases had developed. This was less than expected, seeing as most dogs with OS (> 90%) eventually develop pulmonary metastases, despite few having detectable metastases at presentation (< 15–17%) [31, 34, 35, 42].

One of the main concerns when using morphological methods such as IHC to detect micrometastases is that only a small portion of the entire lung can be examined. We found that micrometastases were present in three (43%) and four (57%) of the seven lung lobes examined. This finding seemingly indicates that the micrometastatic burden is relatively high once micrometastases have developed. However, our protocol might not be sensitive enough to identify dogs with a lower micrometastatic burden. It was not the scope of this study to examine the entire lung to find the true prevalence or distribution of micrometastasis. This would require the use of other methods of investigation. Without this information, we cannot evaluate the location from where tissue preferably should be sampled, nor the number of samples needed to reliably classify dogs as having micrometastases or not. Another possible explanation for the low incidence of pulmonary micrometastases could be that the lungs are not the primary site for metastatic dissemination during the early phases of metastasis in dogs with OS.

Among human patients with OS, the prevalence of tumour cells in the bone marrow at presentation was 63% and seemingly correlated with outcome [14, 43]. This is substantially higher than the prevalence of pulmonary micrometastases reported here in OS dogs. A possible explanation could be that the bone marrow serves as a temporary nest for metastasized cells until the subsequent dissemination of tumour cells to the lungs. Indeed, it has been shown that tumour cells of prostate and breast cancer in humans can disseminate to the bone marrow using mechanisms similar to those used by homing hematopoietic stem cells [44–47]. It has been suggested that these tumour cells can lay dormant in the bone marrow niche, where they remain quiescent for several years until metastases develop [48, 49]. Further studies investigating the presence of micrometastases in other organs in dogs with OS, such as the bone marrow, are therefore warranted.

We found no micrometastases or microscopic metastases in the two dogs in the OS + /Met + group (Table 2). Samples were taken from the same anatomical locations of the lungs as from the other dogs in the study, but specifically from tissues without macroscopic metastases. However, both dogs had a low metastatic burden (a total of 2 and 7 macroscopic metastases), which could indicate a less aggressive tumour phenotype. This might seem counterintuitive, as we might expect a higher micrometastatic burden once macroscopic metastases are present. However, the inhibitory effect of primary tumours on the growth of metastases is not an unknown phenomenon [50–52]. Whether overt lung metastases could exhibit a similar inhibitory effect on micrometastatic development is unknown, and further studies are needed to shed light on this. In a study evaluating the prevalence of micrometastases in seemingly unaffected areas of the lung in humans with primary lung cancer, the authors found that 47% had micrometastases [19]. Although they

investigated a different cancer disease, they used a morphological method as well. They found that only 7.7% of the examined microscopic slides contained micrometastases, emphasizing the need to evaluate several samples per patient. Similarly, the prevalence of hepatic micrometastases was investigated at metastasectomy in humans with ileal, small intestinal and pancreatic neuroendocrine tumours and colorectal cancer [20–22]. The authors found micrometastases in 100, 67, 32 and 56% of patients, respectively, in seemingly unaffected liver tissue. It appears that the presence of macroscopic metastases is no guaranty for finding micrometastases when using morphological methods to detect them.

TP-3 has not been commercially available since its discovery, and there is a limited number of studies that have used the antibody. In the veterinary field, there are only two [40, 41]. In contrast to the membrane staining seen in humans, we found that TP-3 staining of tumour cells also had a cytoplasmatic distribution [38]. The previously reported staining of the brush border of ciliated epithelial cells in the bronchi and lungs of dogs, not seen in humans, corresponded well with our observations [40]. The TP-3 staining of the seromucous glands has not been described previously. This lack of specificity was not an issue when detecting micrometastases and microscopic metastases. They were easily distinguishable from normal structures based on location, clustering of cells, nuclear and cytoplasmatic morphology and staining intensity.

The number of TP-3 positive single cells varied considerably between dogs. In one case, TP-3 staining of the epithelium was present from the bronchi to the alveolar ducts, resulting in high numbers of TP-3 positive single cells per 10 HPF (case 8). New sections from this dog were sliced and stained and with the same results. This staining variation, combined with the poor morphology and dislodgement of epithelium associated with frozen sections, makes TP-3 a poor IHC marker for pulmonary single-cell metastases in dogs with OS. In most cases, distinguishing single tumour cells from dislodged respiratory epithelial cells based on staining pattern and morphology was impossible. Formalin-fixed tissue would have offered better morphology, but formalin ablates the epitope of the TP-3 [38]. We have made several attempts to optimise a protocol for formalin-fixed paraffin embedded canine tissue, but with disappointing results. Most samples were chosen from the peripheral areas of the lung (6/7 samples) to reduce the amount of respiratory epithelium included. Since TP-3 stained the respiratory epithelium down to the bronchioles and sometimes into the smaller airways, this probably had no impact on the number of TP-3 staining non-tumour cells. There was no tendency towards higher numbers of TP-3 positive single cells in the OS + groups. However, the number of dogs included is too small to draw any definite conclusions, and other methods should be considered when studying single-cell metastases.

Another limitation of our study is that the primary tumour was not IHC evaluated with TP-3. It is thus possible that some of the OS cases were TP-3 negative, and consequently, so would the micrometastases and microscopic metastases. Hence, this may have resulted in an underestimation of the micrometastatic prevalence. However, in the previous report investigating canine OS using TP-3, 13/13 tumours were TP-3 positive [40]. Likewise, in a study evaluating the use of TP-3 Fab fragments for positron-emitting tomography imaging in dogs with OS, binding was documented in the primary tumour in the four cases included [41]. In humans, 15/15 and 31/31 cases of OS examined using IHC showed strong TP-3 staining [38, 39]. There were no suspected micrometastases or microscopic metastases which did not stain with TP-3 among our dogs after careful microscopic examination of all samples.

Historically, micrometastases have been defined in different ways depending on the method of investigation and organ. When using morphological methods to identify micrometastases in lymph nodes (histology or IHC), they are generally defined as tumour cell clusters of >0.2 mm but <2 mm in diameter [13, 53, 54]. Clusters <0.2 mm are usually classified as isolated (disseminated or circulating) tumour cells. Since there is no established definition for pulmonary micrometastases, we chose to define them as clusters of ≥ 5 and ≤ 50 tumour cells. Because IHC is a more sensitive method than H&E staining to identify micrometastases, we chose an upper limit of 50 cells. Clusters of >50 cells are more easily detectable in H&E stained lung tissue, and we classified those as microscopic metastases.

Metastasis has been extensively studied in laboratory animals and in vitro models. The limited translational value of these models when developing new therapeutics has inspired researchers to create new and more sophisticated cancer models [7, 55]. Dogs with cancer have proven to be reliable clinically relevant models for human cancer, also when developing new therapeutics [56]. Given the seemingly low prevalence of pulmonary micrometastases and the fact that most eventually develop metastases, dogs with OS should serve as excellent spontaneous cancer models to study premetastatic niche formation [57]. This might include studying immunological, metabolic, and extracellular matrix changes in the lungs before metastasis has occurred. Rigorous prospective study designs and relevant controls are needed to accomplish this. If findings from murine models can be verified in a naturally occurring spontaneous cancer model such as the dog, it would further support the underlying

mechanisms of premetastatic niche formation observed in mice. Since many owners decline cancer-specific treatment, a significant proportion of dogs are euthanized at an early disease stage. These dogs are excellent candidates to study distant metastatic target organs early in the disease process, to an extent not feasible in humans. Furthermore, by verifying findings from murine models, dogs could serve as a bridge between the preclinical models and humans for developing new therapies targeting premetastatic niche formation. We propose that dogs with spontaneous appendicular OS could represent clinically relevant models for studying early micrometastasis and premetastatic niche formation as an addition to murine models.

Conclusions

Our data shows that pulmonary micrometastases can be detected in dogs with OS by using TP-3 immunohistochemistry. The prevalence of pulmonary micrometastases was significantly lower than expected in dogs with OS before macroscopic metastases had developed. Once present, the micrometastatic burden was relatively high. This could indicate that pulmonary metastases do not originate directly from the primary tumour. However, it remains a hypothesis-generating study, and larger studies are needed to validate our findings.

Acknowledgements
The present study was partly funded by the faculty of veterinary medicine, Norwegian University of Life Sciences, as well as by Oncoinvent AS, Oslo, Norway, SVFs professional and scientific fund, Oslo, Norway and The Research fund for cancer in dogs, Oslo, Norway. TP-3 antibodies were generously provided by Oncoinvent AS.

Prior publication
Data have not been published previously.

Authors' contributions
MK participated in the collection of material, performed the immunohistochemical staining and examination of pulmonary tissue samples, analysed and interpreted the patient data and was a major contributor in writing the manuscript. EOK supervised the immunohistochemical staining, protocol validation, contributed to the study design and writing of the manuscript. AHH contributed to the study design and was a major contributor in writing of the manuscript. FL contributed to the study design, collection of material and writing of the manuscript. ØSB contributed to the conception, design and immunohistochemical staining protocol, as well as writing the manuscript. JT performed the histological examination of all primary tumours, metastases, and routine histology examination. LM contributed to the conception, design, interpretation of data and was a major contributor in writing of the manuscript. All authors have read and approved the final version of the manuscript.

Funding
The present study was partly funded by the faculty of veterinary medicine, Norwegian University of Life Sciences (which was also involved in design, collection of samples, analysis interpretation and writing of the manuscript), Oncoinvent AS, Oslo, Norway, SVFs professional and scientific fund, Oslo, Norway, and The Research fund for cancer in dogs, Oslo, Norway.

Availability of data and materials
The data that support the findings of this study are available from the corresponding author upon reasonable request.

Declarations

Ethics approval
This study did not require official or institutional ethical approval. The animals were handled according to high ethical standards and national legislation.

Consent for publication
Owners signed a participation consent form before the dogs were euthanized and necropsied, allowing for publication of anonymized research results.

Competing interests
The authors declare that they have no competing interests.

Author details
[1]Department of Companion Animal Clinical Sciences, Faculty of Veterinary Medicine, Norwegian University of Life Sciences, Elizabeth Stephansens vei 15, 1433 Ås, Norway. [2]Department of Preclinical Sciences and Pathology, Faculty of Veterinary Medicine, Norwegian University of Life Sciences, Elizabeth Stephansens vei 15, 1433 Ås, Norway. [3]Institute of Clinical Medicine &, Faculty of Medicine, Department of Oncology, The University of Oslo &, Norwegian Radium Hospital, Oslo University Hospital, Ullernchausseen 70, 0379 Oslo, Norway.

Received: 28 July 2021 Accepted: 19 October 2021
Published online: 03 November 2021

References

1. Wang H, Naghavi M, Allen C, Barber RM, Bhutta ZA, Carter A, Casey DC, Charlson FJ, Chen AZ, Coates MM, Coggeshall M. Global, regional, and national life expectancy, all-cause mortality, and cause-specific mortality for 249 causes of death, 1980–2015: a systematic analysis for the Global Burden of Disease Study 2015. Lancet. 2016;388:1459–544.
2. Adams VJ, Evans KM, Sampson J, Wood JLN. Methods and mortality results of a health survey of purebred dogs in the UK. J Small Anim Pract. 2010;51:512–24.
3. Inoue M, Hasegawa A, Hosoi Y, Sugiura K. A current life table and causes of death for insured dogs in Japan. Prev Vet Med. 2015;120:210–8.
4. Bonnett BN, Egenvall A, Olson P, Hedhammar A. Mortality in insured Swedish dogs: rates and causes of death in various breeds. Vet Rec. 1997;141:40–4.
5. Proschowsky HF, Rugbjerg H, Ersbøll AK. Mortality of purebred and mixed-breed dogs in Denmark. Prev Vet Med. 2003;58:63–74.
6. Dillekas H, Rogers MS, Straume O. Are 90% of deaths from cancer caused by metastases? Cancer Med. 2019;8:5574–6.
7. Ireson CR, Alavijeh MS, Palmer AM, Fowler ER, Jones HJ. The role of mouse tumour models in the discovery and development of anticancer drugs. Br J Cancer. 2019;121:101–8.
8. Matos AJ, Faustino AM, Lopes C, Rutteman GR, Gärtner F. Detection of lymph node micrometastases in malignant mammary tumours in dogs by cytokeratin immunostaining. Vet Rec. 2006;158:626–30.
9. Szczubiał M, Łopuszynski W. Prognostic value of regional lymph node status in canine mammary carcinomas. Vet Comp Oncol. 2011;9:296–303.
10. Weishaar KM, Thamm DH, Worley DR, Kamstock DA. Correlation of nodal mast cells with clinical outcome in dogs with mast cell tumour and a proposed classification system for the evaluation of node metastasis. J Comp Pathol. 2014;151:329–38.
11. Casey KM, Steffey MA, Affolter VK. Identification of occult micrometastases and isolated tumour cells within regional lymph nodes of previously diagnosed non-metastatic (stage 0) canine carcinomas. Vet Comp Oncol. 2017;15:785–92.
12. Marconato L, Facchinetti A, Zanardello C, Rossi E, Vidotto R, Capello K, et al. Detection and prognostic relevance of circulating and disseminated tumour cell in dogs with metastatic mammary carcinoma: a pilot study. Cancers. 2019;11:163–76.
13. Huvos AG, Hutter RV, Berg JW. Significance of axillary macrometastases and micrometastases in mammary cancer. Ann Surg. 1971;173:44–6.

14. Bruland OS, Hoifodt H, Saeter G, Smeland S, Fodstad O. Hematogenous micrometastases in osteosarcoma patients. Clin Cancer Res. 2005;11:4666–73.
15. Sloane JP, Ormerod MG, Neville AM. Potential pathological application of immunocytochemical methods to the detection of micrometastases. Cancer Res. 1980;40:3079–82.
16. Zhang XW, Yang HY, Fan P, Yang L, Chen GY. Detection of micrometastasis in peripheral blood by multi-sampling in patients with colorectal cancer. World J Gastroenterol. 2005;11:436–8.
17. Nakajima T, Harashima S, Hirata M, Kajitani T. Prognostic and therapeutic values of peritoneal cytology in gastric cancer. Acta Cytol. 1978;22:225–9.
18. Kondo H, Naruke T, Tsuchiya R, Goya T, Suemasu K, Yamagishi K, et al. Pleural lavage cytology immediately after thoracotomy as a prognostic factor for patients with lung cancer. Jpn J Cancer Res Gann. 1989;80:233–7.
19. Hashimoto K, Takahashi T, Suzuki C. Micrometastasis in resected lungs of lung cancer patients. Gann. 1976;67:717–23.
20. Nanko M, Shimada H, Yamaoka H, Tanaka K, Masui H, Matsuo K, et al. Micrometastatic colorectal cancer lesions in the liver. Surg Today. 1998;28:707–13.
21. Gibson WE, Gonzalez RS, Cates JMM, Liu E, Shi C. Hepatic micrometastases are associated with poor prognosis in patients with liver metastases from neuroendocrine tumors of the digestive tract. Hum Pathol. 2018;79:109–15.
22. Fossmark R, Balto TM, Martinsen TC, Grønbech JE, Munkvold B, Mjønes PG, et al. Hepatic micrometastases outside macrometastases are present in all patients with ileal neuroendocrine primary tumour at the time of liver resection. Scand J Gastroenterol. 2019;54:1003–7.
23. Morello E, Martano M, Buracco P. Biology, diagnosis and treatment of canine appendicular osteosarcoma: similarities and differences with human osteosarcoma. Vet J (Lond, Engl). 1997;2011(189):268–77.
24. Withrow SJ, Powers BE, Straw RC, Wilkins RM. Comparative aspects of osteosarcoma. Dog versus man. Clin Orthop Relat Res. 1991;270:159–68.
25. Simpson S, Dunning MD, de Brot S, Grau-Roma L, Mongan NP, Rutland CS. Comparative review of human and canine osteosarcoma: morphology, epidemiology, prognosis, treatment and genetics. Acta Vet Scand. 2017;59:71–81.
26. Brodey RS. The use of naturally occurring cancer in domestic animals for research into human cancer: general considerations and a review of canine skeletal osteosarcoma. Yale J Biol Med. 1979;52:345–61.
27. Mueller F, Fuchs B, Kaser-Hotz B. Comparative biology of human and canine osteosarcoma. Anticancer Res. 2007;27:155–64.
28. Withrow SJ, Wilkins RM. Cross talk from pets to people: translational osteosarcoma treatments. ILAR J. 2010;51:208–13.
29. Brodey RS, Riser WH. Canine osteosarcoma. A clinicopathologic study of 194 cases. Clin Orthop Relat Res. 1969;62:54–64.
30. Guijarro MV, Ghivizzani SC, Gibbs CP. Animal models in osteosarcoma. Front Oncol. 2014;4:189–95.
31. Spodnick GJ, Berg J, Rand WM, Schelling SH, Couto G, Harvey HJ, et al. Prognosis for dogs with appendicular osteosarcoma treated by amputation alone: 162 cases (1978–1988). J Am Vet Med Assoc. 1992;200:995–9.
32. Selmic LE, Burton JH, Thamm DH, Withrow SJ, Lana SE. Comparison of carboplatin and doxorubicin-based chemotherapy protocols in 470 dogs after amputation for treatment of appendicular osteosarcoma. J Vet Intern Med. 2014;28:554–63.
33. Skorupski KA, Uhl JM, Szivek A, Allstadt Frazier SD, Rebhun RB, Rodriguez CO Jr. Carboplatin versus alternating carboplatin and doxorubicin for the adjuvant treatment of canine appendicular osteosarcoma: a randomized, phase III trial. Vet Comp Oncol. 2016;14:81–7.
34. Cavalcanti JN, Amstalden EMI, Guerra JL, Magna LC. Osteosarcoma in dogs: clinical-morphological study and prognostic correlation. Braz J Vet Res Anim Sci. 2004;41:299–305.
35. Ling GV, Morgan JP, Pool RR. Primary bone rumors in the dog: a combined clinical, radiographic, and histologic approach to early diagnosis. J Am Vet Med Assoc. 1974;165:55–67.
36. Brodey RS, Sauer RM, Medway W. Canine bone neoplasms. J Am Vet Med Assoc. 1963;143:471–95.
37. Federman N, Bernthal N, Eilber FC, Tap WD. The multidisciplinary management of osteosarcoma. Curr Treat Options Oncol. 2009;10:82–93.
38. Bruland OS, Fodstad O, Stenwig AE, Pihl A. Expression and characteristics of a novel human osteosarcoma-associated cell surface antigen. Cancer Res. 1988;48:5302–9.
39. Bruland O, Fodstad O, Funderud S, Pihl A. New Monoclonal-Antibodies Specific for Human Sarcomas. Int J Cancer. 1986;38:27-31
40. Haines DM, Bruland OS. Immunohistochemical detection of osteosarcoma-associated antigen in canine osteosarcoma. Anticancer Res. 1989;9:903–7.
41. Page RL, Garg PK, Garg S, Archer GE, Bruland OS, Zalutsky MR. PET imaging of osteosarcoma in dogs using a fluorine-18-labeled monoclonal antibody Fab fragment. J Nucl Med. 1994;35:1506–13.
42. Ehrhart NR, SD; Fan, TM. Tumors of the skeletal system. Withrow and MacEwen's small animal clinical oncology, 5th edn. St. Louis, Missouri: Saunders, Elsevier; 2013. p. 463–503.
43. Bruland ØS, Høifødt H, Hall KS, Smeland S, Fodstad Ø. Bone marrow micrometastases studied by an immunomagnetic isolation procedure in extremity localized non-metastatic osteosarcoma patients. Cancer Treat Res. 2009;152:509–15.
44. Taichman RS, Cooper C, Keller ET, Pienta KJ, Taichman NS, McCauley LK. Use of the stromal cell-derived factor-1/CXCR4 pathway in prostate cancer metastasis to bone. Cancer Res. 2002;62:1832–7.
45. Müller A, Homey B, Soto H, Ge N, Catron D, Buchanan ME, et al. Involvement of chemokine receptors in breast cancer metastasis. Nature. 2001;410:50–6.
46. Allocca G, Hughes R, Wang N, Brown HK, Ottewell PD, Brown NJ, et al. The bone metastasis niche in breast cancer-potential overlap with the haematopoietic stem cell niche in vivo. J Bone Oncol. 2019;17:100244.
47. Shiozawa Y, Eber MR, Berry JE, Taichman RS. Bone marrow as a metastatic niche for disseminated tumor cells from solid tumors. Bonekey Rep. 2015;4:689.
48. Aguirre-Ghiso JA. Models, mechanisms and clinical evidence for cancer dormancy. Nat Rev Cancer. 2007;7:834–46.
49. Páez D, Labonte MJ, Bohanes P, Zhang W, Benhanim L, Ning Y, et al. Cancer dormancy: a model of early dissemination and late cancer recurrence. Clin Cancer Res. 2012;18:645–53.
50. Demicheli R, Retsky MW, Hrushesky WJ, Baum M, Gukas ID. The effects of surgery on tumor growth: a century of investigations. Ann Oncol. 2008;19:1821–8.
51. Kaya M, Wada T, Nagoya S, Kawaguchi S, Isu K, Yamashita T. Concomitant tumour resistance in patients with osteosarcoma. A clue to a new therapeutic strategy. J Bone Joint Surg Br. 2004;86:143–7.
52. Tsunemi T, Nagoya S, Kaya M, Kawaguchi S, Wada T, Yamashita T, et al. Postoperative progression of pulmonary metastasis in osteosarcoma. Clin Orthop Relat Res. 2003;407:159–66.
53. Benson JR, Querci Della Rovere G. Classification of isolated tumor cells and micrometastasis. CancerAm Cancer Soc. 2000;89:707–9 (**author reply 11**).
54. Giuliano AE, Connolly JL, Edge SB, Mittendorf EA, Rugo HS, Solin LJ, et al. Breast Cancer-major changes in the American Joint Committee on Cancer eighth edition cancer staging manual. CA Cancer J Clin 2017; 67:290–303.
55. Yin L, Wang XJ, Chen DX, Liu XN, Wang XJ. Humanized mouse model: a review on preclinical applications for cancer immunotherapy. Am J Cancer Res. 2020;10:4568–84.
56. Dow S. A role for dogs in advancing cancer immunotherapy research. Front Immunol. 2020;10:89–96.
57. Doglioni G, Parik S, Fendt SM. Interactions in the (Pre)metastatic niche support metastasis formation. Front Oncol. 2019;9:219.

Publisher's Note

II Paper II

Canine *in vitro* generated tumor-conditioned macrophages display an M2-skewed phenotype

Mikael Kerboeuf[1], Anita Haug Haaland[1], Lars Moe[1], David Argyle[2], Seda Ozaydin[2], Maciej Parys[2] and Preben Boysen[3]

Institutions: [1] Department of Companion Animal Clinical Sciences, Faculty of Veterinary Medicine, Norwegian University of Life Sciences, [2] The Royal (Dick) School of Veterinary Studies and Roslin Institute, University of Edinburgh, [3] Department of Preclinical Sciences and Pathology, Faculty of Veterinary Medicine, Norwegian University of Life Sciences.

Abstract

Tumor-associated macrophages (TAMs) are heterogeneous and abundantly present in the tumor stroma. They derive from tissue-resident macrophages and monocytes and play a central role in cancer. In murine models, TAMs promote invasion, intravasation, circulatory survival, and extravasation of tumor cells. TAMs promote tumor progression and angiogenesis, remodel the tumor microenvironment, and modulate the adaptive immune system. Historically, dogs have proven to be reliable cancer models. We hypothesized that canine tumor-conditioned monocyte-derived macrophages (TCMΦ) are similar to anti-inflammatory M2 (M-CSF+IL4) macrophages and have a tumor-promoting phenotype, as in humans. We collected blood from healthy dogs, isolated monocytes, and differentiated them *in vitro* using tumor-conditioned media from three canine cancer cell lines. Three TCMΦ populations were generated and compared with *in vitro*-generated M1 and M2 macrophages. We assessed the macrophages using multicolor flow cytometry and RNA sequencing. All TCMΦ showed an increased expression of two M2 markers (CD209 and FcεRI), while 2 out of 3 TCMΦ populations had increased expression of two additional M2 markers (CD206 and CD11d). Transcriptomically, several M2-associated surface markers, cytokines, and chemokines were upregulated in TCMΦ, while M1-associated genes were downregulated. In conclusion, canine TCMΦ share many similarities with human TCMΦ, further warranting the use of dogs as cancer models.

Introduction

Tumor-associated macrophages (TAMs) play a central role in regulating the tumor microenvironment (TME) (1). The TME is highly heterogenous and composed of several compartments, one being the immune microenvironment (2). In addition to cancer cells, the TME contains several immune cell subsets and stromal cells. TAMs are abundantly present in most tumors and represent one of the main cellular constituents of the TME (3). They can promote tumor progression, remodel the TME extracellular matrix, promote angiogenesis, regulate tumor metabolism, and have an immunomodulatory effect on the adaptive immune response (3, 4). Furthermore, TAMs can facilitate invasion, intravasation, lymphoinvasion, survival in circulation, and extravasation of cancer cells (3). High numbers of TAMs correlate with poor clinical outcomes in most human cancers, and TAMs can contribute to chemotherapy and radiotherapy resistance (4, 5, 6).

Mills et al. introduced the concept of M1 (classically activated) and M2 (alternatively activated) macrophages in association with the pro-inflammatory Th1 and anti-inflammatory Th2 responses (7). M1 macrophages can be generated *in vitro* when stimulated with IFN-γ and lipopolysaccharides (LPS), while M2 when stimulated with IL-4. However, this M1/M2 dichotomy is oversimplified and does not fully reflect *in vivo* polarization (8). Macrophages are highly plastic cells that can exhibit different phenotypes within the same microenvironment. Canine *in vitro*-generated, monocyte-derived macrophages show similar characteristics to human and murine macrophages (9, 10). Phenotypical macrophage markers can vary between species and are not directly translatable from mice or humans to dogs (11). Typical murine or human M1 markers, such as inducible nitric oxide synthase (iNOS), CD16, CD32, CD80, CD86, or MHCII, and the M2 markers Arg-1 and CD163 are not differentially expressed in canine M1 and M2 macrophages (9, 10). However, canine M2 macrophages have a high expression of CD206 and FcεRI compared to M1.

In humans and mice, TAMs have a predominantly M2-skewed phenotype, meaning they are anti-inflammatory and tumor-permissive (3, 12). Most TAMs express the M2-associated markers CD163 and CD206, secret anti-inflammatory cytokines such as IL-10, PGE2, and TGF-β, and express checkpoint ligands such as PD-L1, CD80/CD86, FasL, and TRAIL (3, 12). They can produce arginase-1 (Arg-1) and chemokines CCL5, CCL20, and CCL22, which inhibit T cell-mediated antitumor responses and result in Treg-recruitment. TAMs can exhibit characteristics of both M1 and M2 macrophages, and single-cell RNA-Seq of tumors

has shown TAMs cannot be classified within the M1/M2 dichotomy (12, 13, 14). Monteiro et al. showed that TAMs of malignant canine mammary carcinomas (MC) were almost exclusively $CD206^{+}$, supporting the notion that most canine TAMs are also M2-skewed *in vivo* (15).

Preclinical murine cancer models are instrumental in exploring mechanistic aspects of cancer development and progression. However, they have limited translational value when assessing new cancer drugs, as they have a poor success rate when moving into the clinic (16). Dogs with cancer are excellent models for human cancer, especially the highly malignant osteosarcoma (OS) (17, 18, 19). Dogs develop cancer naturally, are immunocompetent, live in the same environments as humans, and have an educated microbiome and immune system. Most importantly, their tumors develop within a host with the same genetic makeup, meaning there is a natural interaction between the cancer cells and the TME.

Despite being excellent cancer models, our knowledge about the interactions in TME in dogs is limited. This study therefore aimed to characterize *in vitro*-generated canine tumor-conditioned macrophages (TCMΦ) and provide a new *in vitro* model system to study canine TAMs. We wanted to compare their expression of phenotypical markers and transcriptomic profiles with M1 and M2 macrophages. These results may provide tools for further research into canine TAMs, shed light on their role in cancer, and identify new therapeutic targets.

Methods

Study population

Blood from six healthy dogs was collected for peripheral blood monocyte isolation and macrophage cultivation. Dogs were recruited from the Veterinary Teaching Hospital at the Norwegian University of Life Sciences (Ås, Norway). A complete medical history was recorded, and each dog underwent a clinical examination and had a hematology and biochemistry panel, including C-reactive protein, analyzed. The blood for monocyte isolation (10 mL) was collected in ethylenediamine tetraacetic acid (EDTA) coated tubes. Dogs included in the study had to have a body weight of >10kg and be clinically healthy. Dogs were excluded if they had clinical signs or laboratory findings indicative of systemic inflammatory disease, infections, allergies, or neoplastic disease. Dogs with a previous history of neoplasia or allergy were also excluded. Dogs receiving treatment with

immunomodulating drugs (glucocorticoids, chemotherapy, antipruritic drugs) were also excluded. Relevant clinical characteristics and leukocyte counts of the included dogs are summarized in Table 1. The dog owners had to sign a written consent form before inclusion in the study. Ethical approval was granted by the Norwegian Food Safety Authority (FOTS id nr. 24314).

Generation of tumor conditioned media

The osteosarcoma cell lines D17 and KTOSA5 and the mammary carcinoma line REM134 were kindly gifted from Dr. D. Argyle, University of Edinburgh. D17 and REM134 were maintained in Minimum Essential Medium (MEM) with GlutaMAX™ supplementation (Gibco), and KTOSA in Dulbecco's Modified Eagle Medium (DMEM) with GlutaMAX™ supplementation (Gibco), all supplemented with 10% fetal bovine serum (FBS) (Gibco) and 1% penicillin/streptomycin (P/S) (Gibco) (20, 21). Tumor-conditioned media (TCM) was generated by culturing the three cell lines in RPMI-1640 with GlutaMAX™ (Gibco), supplemented with 10% FBS and 1% P/S until reaching 70-80% confluence (Fig. 1a). Then, the medium was completely removed, and fresh medium was added and incubated for another 24 hours. The TCM was harvested and centrifuged at 1,200xg for 10 minutes to remove remaining cells and debris, then stored at -80°C until further use. Cell lines were maintained in standard culture conditions (5% CO2 and 37°C) and inspected daily, with media change every 2-3 days.

Isolation of peripheral blood monocytes

The general steps of monocyte isolation are summarized in Fig. 1b. Peripheral blood mononuclear cells (PBMCs) were isolated from EDTA blood samples using density gradient centrifugation as performed by Heinrich et al. with several modifications (9). Briefly, the blood was diluted 1:2 in dPBS (Gibco) containing 2% FBS and 1% P/S, then transferred to a SepMate™ tube (StemCell Technologies) containing 15 mL of room-tempered Lymphoprep (1.077 g/mL; StemCell Technologies) and centrifuged for 10 minutes, 1,200xg at 20°C. PBMCs were harvested by pouring the top layer off the SepMate™ tube, then washed twice using dPBS containing 2% FBS and 1% P/S, followed by centrifugation for 10 minutes, 400xg at 20°C. The remaining red blood cells were lysed using cold (4°C) distilled water for

30 seconds. Monocytes were isolated from PBMCs using MACS CD14 MicroBeads (130-050-201, Miltenyi Biotec), MACS LS columns (Miltenyi Biotec), and MidiMACS™ separator (Miltenyi Biotec) according to the manufacturer's instructions. Briefly, PBMCs were resuspended in 80 µL MACS buffer (dPBS containing 0.5% bovine serum albumin (BSA) and 2mM EDTA) per 10^7 cells and incubated with 20 µL MACS CD14 MicroBeads per 10^7 cells for 15 minutes on ice. The mix was then washed with MACS buffer, centrifuged at 300x g for 10 minutes, and resuspended in 500 µL MACS buffer. The cells were strained thru a 70 µm cell strainer (Falcon), then transferred onto a pre-rinsed MACS LS column placed in the MidiMACS™ separator. The column was then washed three times with MACS buffer. The flow thru was discarded, and $CD14^+$ cells were collected from the MACS LS column and washed twice with dPBS containing 2% FBS and 1% P/S, followed by centrifugation for 10 minutes, 400xg at 20°C. Monocytes were resuspended in RPMI-1640 with GlutaMAX™ containing 10% FBS and 1 % P/S (complete medium).

Generation of macrophages and polarization

Peripheral blood monocytes were seeded onto 12-well Nunc™ Multidishes with UpCell™ Surface (Thermo Fisher Scientific) at 5 x 10^5 cells per well in 1.2 mL medium. Monocytes were cultured over seven days to generate and polarize monocyte-derived macrophages. Cells were grown in complete medium with various hematopoietic growth factors, interleukins, and TCM to generate five different macrophage phenotypes (Fig. 1c). M1 and M2 macrophages were differentiated according to the protocol used by Heinrich et al. (9). M1 macrophages were differentiated over five days with recombinant canine granulocyte-macrophage colony-stimulating factor (GM-CSF, 5 ng/mL; R&D Systems), followed by stimulation with lipopolysaccharide (LPS, 100ng/mL; *Escherichia coli* O55:B5, Sigma-Aldrich), recombinant canine interferon-gamma (INFγ, 20 ng/mL; R&D Systems) and GM-CSF for two days. M2 macrophages were differentiated over five days with recombinant human macrophage colony-stimulating factor (M-CSF, 25 ng/mL; PeproTech), followed by stimulation with recombinant canine interleukin 4 (IL-4, 20 ng/mL; R&D Systems) and M-CSF for two days. The three TCMΦ populations (TAM(D17), TAM(KTOSA5), and TAM(REM134)) were generated using M-CSF (25 ng/mL) and TCM (1:1 with complete medium) over seven days. Half of the culture medium was replaced every 2-3 days, along with fresh growth factors. Cells were cultured under standard conditions (5% CO2, 37°C) and inspected daily.

157

158 **Staining and flow cytometry analysis**

159 After seven days of culture, the medium was removed, and the wells were washed with dPBS
160 for 30 seconds to remove any dead cells and debris. The wells were then filled with 1.2 mL
161 complete medium and placed at room temperature for 30 minutes to detach the cells from the
162 temperature-responsive surface. Cells were harvested by gently repeated pipetting and
163 transferred to separate tubes. After harvesting, 1 x10^5 cells per condition were transferred to a
164 96-well u-bottom plate for staining. First, dead cells were stained using the LIVE/DEAD™
165 fixable yellow staining kit (Invitrogen) according to the manufacturer's instructions. Briefly,
166 1 µL of LIVE/DEAD dye stock solution was diluted 1:500 in dPBS containing 2mM EDTA,
167 and cells were incubated with the dye for 10 minutes on ice. Cells were washed with dPBS
168 containing 2mM EDTA, then centrifuged at 800xg for one minute at 4°C. Cells were
169 incubated with canine Fc-receptor binding inhibitor (Invitrogen), 5µL per reaction diluted in
170 flow buffer (dPBS containing 0.5% BSA and 0.005% sodium azide) for 20 minutes on ice to
171 inhibit unspecific antibody binding. Cells were stained with fluorochrome-conjugated
172 antibodies for 20 minutes on ice in the dark. The following antibodies to were used to label
173 the macrophages: Pacific blue anti-CD14 1:100 (clone TÜK4, MCA1568PB, BioRad), FITC
174 anti-LYVE-1 1:50 (polyclonal, NB100-725F, Novus Biologicals), APC anti-CD11d 1:50
175 (clone CA11.8H2, NB100-65292APC, Novus Biologicals), Pacific blue anti-FcεRI 1:50
176 (clone MAR-1, 134314, Nordic BioSite), PE/Cy7 anti-CD206 1:50 (clone 15-2, 321120,
177 Nordic BioSite) and PE-anti-CD209a 1:50 (clone MMD3, 833004, Nordic BioSite). The
178 purity of macrophages was assessed by anti-CD14 staining (Fig. 1d and 1e). Fluorescence
179 minus one (FMO) controls were used to set the gates and control for non-specific binding.
180 UltraComp eBeads™ (Invitrogen) were used for single staining controls to adjust
181 compensation. Unstained samples were also included to record autofluorescence. Isotype
182 controls were run as part of the protocol optimization. After two washing steps with flow
183 buffer, the cells were fixed using 1x BD FACS™ Lysing Solution (BD Biosciences) for 10
184 minutes on ice, then washed again with flow buffer before analysis. At least 10,000 gated
185 events were recorded for each staining using the Gallios flow cytometer (Beckman Coulter),
186 coupled with the Kaluza G software, and analyzed with Kaluza software v.2.1 (Beckman
187 Coulter). The Δ mean fluorescent intensity (MFI) was calculated for each reading by
188 subtracting the FMO control MFI from the measure MFI of a given population.

RNA sequencing and transcriptomic analysis

Total RNA was isolated using the RNeasy Mini Kit (Qiagen) according to the manufacturer's instructions. After removing the medium from the wells, the cells were rinsed with dPBS for 30 seconds. Cells were lysed directly in the wells using 350 µL buffer RLT containing 40mM/mL dithiothreitol. The cell lysate was homogenized using QIAshredder spin columns (Qiagen) and centrifuged at max speed for 2 minutes. One volume of 70% ethanol was added to the lysate before being transferred to an RNeasy spin column. After 15 seconds of centrifugation at ≥8,000xg, the flowthrough was discarded, and the column was washed with 350 µL buffer RW1 and centrifugation at ≥8,000xg for 15 seconds. On-column DNA digestion was done by adding 80 µL DNase I onto the column for 15 minutes at room temperature before being washed with 350 µL buffer RW1 and centrifugation at ≥8,000xg for 15 seconds. The column was washed twice with buffer RPE, then dried out by centrifugation at full speed for two minutes. Total RNA was then eluted into a new tube using 30 µL of RNAse-free water by centrifugation at ≥8,000xg for 15 seconds. RNA integrity was assessed using the Agilent 2200 Tape station system (Agilent) coupled with the 2200 TapeStation Controller Software. Library prep and sequencing were performed at a commercial laboratory (The Norwegian Sequencing Centre, Oslo). Briefly, cDNA libraries were generated using the TruSeq stranded mRNA prep kit (Illumina) according to the manufacturer's instructions. Samples were sequenced on the NovaSeq 6000 (Illumina) using a NovaSeq 6000 SP flow cell (Illumina) with resulting 100bp single-end reads.

Raw RNA sequences were assessed for quality using FastQC v.0.11.9. Low-quality regions were removed, and adapters were trimmed using Trimmomatic v.0.39. High-quality reads were mapped using Kallisto v.0.44.0 using reference transcriptome ROS_Cfam_1.0 (GCA_014441545.1) with a k-mer length of 31 (Broad Institute, Cambridge, MA, released June 2021; downloaded from Ensemble release 105). Differentially expressed gene (DEG) analysis was performed using Degust v.4.1.1 and R v.4.2.2 to compare gene expression between conditions.

Statistical analysis

All statistical analyses for flow cytometry data were performed using JMP pro 15.1.0 (SAS Institute Inc., Cary, NC). Groups were compared using one-way ANOVA, with post hoc testing using Tukey tests for comparison between groups. Differentially expressed gene (DEG) analysis was performed using Degust v.4.1.1 and R v.4.2.2 to compare gene expression between conditions. The significance level was set at P=.05.

Results

Canine tumor conditioned macrophages have a heterogenous morphological appearance

After seven days of culture, M1 and M2 macrophages displayed different morphological characteristics (Fig. 2), as previously described by Heinrich et al. (9). M1 macrophages were dominated by amoeboid cells with protruding fibrillary cytoplasmatic processes, with low numbers of small round cells. There were some spindeloid cells, but these were rare, and no large flat cells were visible. In M2 macrophage cultures, there were primarily amoeboid, spindeloid, and large flat cells in equal numbers and low numbers of small round cells.

For the OS-conditioned macrophages, TAM(D17) and TAM(KTOSA5), cells showed a heterogenous morphology comparable to M2 macrophages (Fig. 2). There were primarily amoeboid, spindeloid, and large flat cells, with low numbers of small round cells. MC-conditioned macrophages, TAM(REM134), showed a mixed morphology between M1 and M2 macrophages. There were moderate to high numbers of amoeboid cells, low numbers of spindeloid and large flat cells, and low numbers of small round cells.

Canine M2 macrophages have a higher expression of CD206, FcεRI, CD209, CD11d and LYVE-1 compared to M1 macrophages

To assess the validity of the M2 markers in dogs, we compared the ΔMFI of canine monocyte-derived M1 and M2 macrophages for all markers (Fig. 3). For CD206 and FcεRI, the ΔMFI was significantly higher for M2 macrophages compared to M1 macrophages (P<.0001 and P=.0011, respectively). This is in line with previous findings from Heinrich et al. and Hermann et al. (9, 10). Furthermore, the ΔMFI for CD209, CD11d, and Lymphatic Vessel Endothelial Receptor-1 (LYVE-1) were also significantly higher for M2 macrophages,

compared to M1 macrophages (P=.0002, P<.0001, and P=.0022, respectively). The mean ΔMFIs for each marker are summarized in Table 2.

Canine tumor conditioned macrophages have an increased expression of the M2 markers CD209 and FcεRI

Both OS-conditioned macrophages TAM(D17) and TAM(KTOSA5) and MC-conditioned macrophages TAM(REM134) had a high expression of CD209 and FcεRI (Fig. 4a). The ΔMFI for CD209 was significantly higher for TAM(D17), TAM(KTOSA5) and TAM(REM134) than for M1 macrophages (P<.0001, P<.0001, and P=.0002, respectively). However, ΔMFI for CD209 was not significantly different between the TCMΦ and the M2 macrophages. Similarly, the ΔMFI for FcεRI was significantly higher for TAM(D17), TAM(KTOSA5) and TAM(REM134) compared to the M1 macrophages (P<.0001, P<.0001, and P=.0003, respectively). Again, ΔMFI for FcεRI was not significantly different between the TCMΦ and M2 macrophages. The mean ΔMFIs for each marker are summarized in Table 2.

Canine osteosarcoma conditioned macrophages have an intermediately high expression of CD11d, CD206 and a high expression of LYVE-1

Both TAM(D17) and TAM(KTOSA5) macrophages had an intermediately high expression of CD11d (Fig. 4b). The ΔMFI for CD11d was significantly higher for TAM(D17) and TAM(KTOSA5) than for M1 (P=.0016 and P=.0039 respectively) but significantly lower than for M2 (P=.0051 and P=.0021, respectively).

Similarly, TAM(KTOSA5) and TAM(D17) had an intermediately high expression of CD206 (Fig. 4b). However, the ΔMFI for CD206 was only significantly higher for TAM(KTOSA5) when compared to M1 (P=.0397), whereas TAM(D17) did not reach statistical significance (P=.055). Both TAM(D17) and TAM(KTOSA5) had a significantly lower ΔMFI for CD206 than M2 macrophages (P=.0002 and P=.0002, respectively).

Only TAM(KTOSA5) had an increased expression of LYVE-1, which was significantly higher than for the M1 macrophages (P=.0292) (Fig. 4b). The ΔMFI for LYVE-1 in TAM(D17) was not significantly different from M1 macrophages (P=.2295). ΔMFI for

LYVE-1 was not significantly different between either TAM(D17) or TAM(KTOSA5) compared to the M2 macrophages. The mean ΔMFIs for each marker are summarized in Table 2.

Transcriptomic analysis of *in vitro* generated macrophages

In the multidimensional scaling (MDS) plot, the transcriptomes of all TCMΦ clustered together, while M1 and M2 macrophages each formed separate clusters (Fig. 5). After controlling for false discovery rates (FDR, $P<.05$), there were 423 differentially expressed genes with a $\log_2$ fold change ≥ 2 between groups (see supplementary file). In TCMΦ, pathways associated with "apoptosis", "inflammation of lung", "inflammation of body cavity", "inflammation of organs", and "immune-mediated inflammation" were upregulated (Fig. 6). Pathways associated with "differentiation of Th2 cells", "response to antigen presentation", "fatty acid metabolism", and "activation of myeloid cells" were downregulated in TCMΦ. In the DEG analysis, the M1-associated pro-inflammatory cytokines TNFα, IL1a, IL6, IL15, IL27, and IL34 were downregulated in TCMΦ. Similarly, the M1-associated chemokines CCL4, CCL5, and CCL22 were downregulated in TCMΦ. The M2-associated cytokines and chemokines TGF-β, CCL23, and MMP9 were upregulated in TCMΦ. Additionally, S100A8, S100A9, S100A13, α4 integrin, and CTLA-4 receptor CD86 were upregulated in TCMΦ compared to M1 and M2 macrophages. An overview of the top 50 differentially expressed genes can be seen in Table 3.

FcεRI and CD209 were upregulated in TCMΦ and M2 vs. M1 as measured on flow cytometry. On the other hand, CD11d, CD206, and LYVE-1 were not upregulated in TCMΦ. The surface receptors CD36, CD163, and CD204 were upregulated in TCMΦ and M2 vs. M1, while TREM2 and MARCO were upregulated in TCMΦ vs. M1 and M2.

Discussion

Despite the increasing interest in TAMs and their role in the TME in humans, TAMs in canine cancers remain poorly characterized. Here, we show that canine *in vitro*-generated TAMs have a high expression of several M2-associated markers, such as CD209 and FcεRI, as well as CD11d and CD206 for the osteosarcoma-conditioned TAMs. We also identified several new M2-associated canine macrophage markers. Previous work from Herman et al.

and Heinrich et al. showed that CD206 and FcεRI were highly expressed in canine M2 macrophages (9, 10). We additionally showed that CD209, CD11d, and LYVE-1 expression was higher among canine M2 macrophages than M1.

The dendritic cell-specific C-type lectin (DC-SIGN), or CD209, was initially described as a surface receptor on dendritic cells (DC) (22). M2 macrophages, *in vitro*-generated TCMΦ, and TAMs in several human tumors, such as breast cancer and OS, also have a high CD209 expression (23, 24, 25, 26, 27). We found that canine TCMΦ exhibited similar CD209 expression to M2 macrophages on flow cytometry and at the transcriptomic level. The high-affinity IgE receptor FcεRI was also similarly expressed among the TCMΦ and the M2 macrophages. The expression of FcεRI on different macrophage subsets is poorly characterized in humans, but as in dogs, human *in vitro*-generated monocyte-derived M2 macrophages have an increased FcεRI expression (10, 28).

The mannose receptor CD206 is a well-established M2 marker in humans and mice, and most TAMs express it (12, 29, 30, 31). Similarly, CD206 expression is high in canine *in vitro*-generated M2 macrophages, and virtually all TAMs in dogs with malignant mammary tumors express CD206 (9, 15). We found that osteosarcoma-conditioned macrophages had an intermediately high expression of CD206, which was significantly higher than in M1 yet lower than in M2 macrophages. The mammary carcinoma-conditioned macrophages did not show the same pattern and had a CD206 expression similar to M1 macrophages. On the transcriptomic level, CD206 was not significantly upregulated in TCMΦ. The expression of CD11d was immediately high among the osteosarcoma-conditioned macrophages but not in mammary carcinoma-conditioned macrophages. CD11d was not upregulated in either M2 macrophages or TCMΦ on RNA-seq. CD11d is a β2-integrin expressed on a subset of bone marrow macrophages, splenic red pulp macrophages, and lymph node medullary macrophages, as well as a subset of $CD8^+$ lymphocytes in dogs (32). The expression of CD11d by different macrophage phenotypes is poorly characterized. In mice, M1 macrophages express a higher level of CD11d than M2 macrophages and macrophages within atherosclerotic lesions express CD11d (33). However, most macrophages within atherosclerotic lesions also express CD206, usually associated with M2 macrophages, further showing the poor overlap between *in vivo* phenotypes and *in vitro* M1/M2 macrophages (34).

Furthermore, CD11d expression in normal tissues varies between humans, mice, and dogs, suggesting differences in its biological functions (32, 35). Although LYVE-1 expression was higher in M2 macrophages than in M1, the expression on TCMΦ was more variable both on flow cytometry and RNA-seq. In murine models, tissue-resident macrophages expressing M2-associated markers (CD163 and CD206) also express LYVE-1 (36, 37). Furthermore, *in vitro*-generated murine M2 macrophages have a high expression of LYVE-1, and so do TAMs in melanoma (38, 39).

In addition to the surface markers evaluated by flow cytometry, CD36, CD163, and CD204 transcripts were upregulated in M2 and TCMΦ, compared to M1 macrophages. CD36 is upregulated in several human cancers, highly expressed by TAMs, and participates in tumor growth regulation, metastasis, and drug resistance through several mechanisms (40). CD163 is a well-established M2 marker in humans and is highly expressed by human TAMs and similarly by TAMs in canine melanoma (6, 41). CD204 is also highly expressed in human M2-like TAMs in several types of cancers and canine melanoma and osteosarcoma (41, 42, 43, 44, 45). Triggering-Receptor-Expressed on Myeloid cells 2 (TREM2) is a marker for immunosuppressive Arg-1 positive TAMs and tumor-infiltrating monocytes but not for Arg-1 negative myeloid cells within tumor tissues (46, 47). Similarly, macrophage receptor with collagenous structure (MARCO) is highly expressed by human immunosuppressive TAMs and TCMΦ (48). TREM2 and MARCO were both upregulated in our TCMΦ compared to M1 and M2 macrophages.

The immunosuppressive cytokine TGF-β was upregulated in M2 and TCMΦ compared to M1. TGF-β can inhibit $CD8^+$ and $CD4^+$ T-cell functions and induce and recruit Tregs that can inhibit effector T-cells. Furthermore, CCL23 was upregulated in TCMΦ, which can induce exhausted T-cell phenotypes with a high expression of immune checkpoint proteins (CTLA-4, PD-1, TIGIT, TIM-3, and LAG-3) and cancer cell migration in ovarian cancer (49). The CTLA-4 ligand CD86 was also upregulated in TCMΦ, which can inhibit cytotoxic T-cell functions (50). Additionally, MMP9 was upregulated in TCMΦ as well as in M2 macrophages. MMP9 can modify cell-to-cell junctions, disrupt basal membranes, and promotes cancer cell migration, invasion, and metastasis (6). Lastly, the α4 integrin was upregulated in TCMΦ compared to M1 and M2 macrophages, which in murine models can promote survival and extravasation of tumor cells (51).

The M1-associated pro-inflammatory interleukins and chemokines were downregulated in TCMΦ and M2 macrophages. In humans, TNFα, IL1b, IL6, and several pro-inflammatory chemokines are produced by TAMs and contribute to angiogenesis, tumor cell migration, invasion metastasis, and immunosuppression (6). However, the pro-inflammatory mediators S100A8 and S100A9 were upregulated in TCMΦ compared to M1 and M2 macrophages. Both can promote tumor invasion and migration and are central in pre-metastatic niche formation (6, 52). Canine TCMΦ generally exhibited more M2-skewed phenotypes than *in vivo* TAMs in humans, which have a heterogeneous specter of polarization.

Despite the guidelines introduced by Murray et al. in 2014, the old M1/M2 classification is still widely used in the literature (11). Phenotypically, there is a significant overlap between *in vitro* generated classically (M1, LPS+IFN-γ) activated macrophages and *in vivo* M1 macrophages (3). However, there is limited overlap between *in vivo* M2 and *in vitro* alternatively (M2, IL-4) activated macrophages. This M1/M2 dichotomy represents only two extremes of a complex and dynamic spectrum of macrophage polarization (11, 53). *In vitro* studies should therefore be interpreted carefully, and results validated in an *in situ* or *in vivo* setting.

When performing *in vitro* macrophage research, the experimental setup can significantly impact the study outcomes. Firstly, the starting material for generating macrophages can result in differences in phenotypical and functional traits (11). Macrophage-monocyte cell lines, such as the human THP-1 or SC lines, showed significant deviations in surface marker expression and cytokine production compared to monocyte-derived macrophages (54). Similarly, canine histiocytic cell line DH82-derived macrophages have different phenotypical surface marker expression and cytokine production than monocyte-derived macrophages (10). Macrophages can also be generated from bone marrow-derived cells and induced pluripotent stem cells (iPSCs) (55, 56). Phenotypically and functionally, these cells are more similar to monocyte-derived macrophages than cell line-derived macrophages, although they exhibit some transcriptomic and functional differences. However, bone marrow and iPSC-derived macrophages require more invasive sampling and are considerably more time-consuming and costly to generate than monocyte-derived macrophages. Despite the technical challenges and high cost, iPSC-derived macrophages have some benefits. They are transcriptomically similar to tissue-resident macrophages, can easily be genetically

409 manipulated, and expand *in vitro* (55). We chose to use blood-derived monocytes since they
410 are readily obtainable from healthy dogs and more representative of *in vivo* macrophages than
411 cell line-derived macrophages. Furthermore, many TAMs are monocyte-derived, which
412 supports their use for modeling TAMs *in vitro* (12).

413

414 Monocyte isolation technique can also impact the phenotype of the resulting macrophages
415 (57). Plastic adhesion results in M1-skewing of macrophages, while negative selection results
416 in M2-skewing. Positive selection using $CD14^+$ paramagnetic beads interferes the least with
417 macrophage phenotype and results in higher monocyte purity. We used positive selection in
418 our study, while previous studies on canine monocyte-derived macrophages have used plastic
419 adhesion (9, 10). Detachment methods can also impact phenotypical surface markers on
420 macrophages (58). Enzymatic detachment methods such as trypsin or Accutase™ can result
421 in cleavage and loss of M2-associated surface markers and phagocytic capabilities. We used
422 thermo-responsive surface plastic, which permits gentle detachment of macrophages and high
423 viability compared to mechanical cell detachment. Thermo-responsive plastic interferes little
424 with macrophage phenotypes and functionality (59). Despite the benefits of thermo-
425 responsive plastic, it results in rapid morphological changes in macrophages when taken out
426 of the incubator. Previously, canine monocyte-derived macrophages displayed distinctive
427 morphological characteristics depending on phenotype (9, 10). Although we observed similar
428 morphological differences, we were not able to image and quantify morphological differences
429 before the morphology of the cells changed due to falling temperatures. Finally, we applied
430 an Fc-blocker, which prevents the unspecific binding of antibodies to Fc-receptors expressing
431 cells, such as macrophages (60). Including Fc-blockers, or species-specific IgG or serum, can
432 impact results and should be used when assessing macrophages.

433

434 Previous studies of *in vitro*-generated TAMs in humans have used similar differentiation
435 protocols as we used. Most studies combine TCM with M-CSF (61, 62, 63). Since the
436 differentiation of monocytes into macrophages is driven mainly by M-CSF within tumor
437 tissues, and only a few examined human cancer cell lines (2/16) secrete M-CSF *in vitro*, it is
438 essential to add it to ensure that they differentiate (61). Other cytokines, such as IL-4 and IL-
439 10, have also been combined with M-SCF and TCM to generate macrophages more similar to
440 TAMs (62). We chose to use TCM and M-CSF in our study, as we wanted to assess the effect

of tumor cells on macrophage phenotype, and adding IL-4 and IL-10 would induce an M2 phenotype regardless of the effects of TCM. Our results may also provide new markers to study pre-metastatic niche formation in dogs since future sites of metastatic dissemination are conditioned by secreted factors and extracellular vesicles, which are also present in the TCM (52, 64).

In conclusion, canine *in vitro* generated TCMΦ express several M2-associated surface markers, such as CD209, FcεRI, and in some cases, CD206 and CD11d. The M2-associated markers CD36, CD163, and CD204 were also transcriptomically upregulated in TCMΦ. Furthermore, TREM2 and MARCO were transcriptomically upregulated in TCMΦ compared to M1 and M2 macrophages. Additionally, M1-associated cytokines and chemokines were downregulated in TCMΦ, while some M2-associated ones, such as TGF-B, CCL23, and MMP9, were upregulated. These results suggest that canine *in vitro*-generated TAMs express many of the same phenotypical markers and share several immunological functions with human TAMs. Given the high translational value of dogs with cancer, they may represent excellent models to assess TAM-repolarizing drugs.

Acknowledgements

The authors would like to acknowledge the technical assistance provided by the laboratory staff (Grethe Marie Johansen) at the Immunology unit, *Department of Preclinical Sciences and Pathology,* for providing technical guidance for cell culture techniques.

Competing interest

The authors declared no potential conflicts of interest with respect to the research, authorship, and/or publication of this article.

Data availability

The data that support the findings of this study are available from the corresponding author upon reasonable request.

Funding

The present study was funded by the Faculty of Veterinary Medicine, Norwegian University of Life Sciences, the Research Fund for Cancer in Dogs, Norway, the Small Animal Practice Veterinary Association's (SVFs) Scientific and Professional Fund (project number 19-209), Norway, the Astri and Birger Torsteds Foundation (project number 2021/22), Norway, and Agria and the Swedish Kennel Klub (SKK) Research Fund (project number N2020-0061), Sweden.

Authors' contributions

MK collected the blood samples used in this study. MK performed the isolation of monocytes, *in vitro* differentiation of macrophages, flow cytometric analysis, and RNA isolation. PB and MK analysed the flow cytometric data. SO and MP performed the bioinformatic analyses. MK, AHH, LM, DA and PB interpretated data. MK, AHH, LM, DA, SO, MP, and PB contributed to writing the manuscript. All authors have read and approved the final version of the manuscript.

References

1. Feng Y, Ye Z, Song F, He Y, Liu J. The Role of TAMs in Tumor Microenvironment and New Research Progress. Stem Cells Int. 2022;2022:5775696.
2. Jin MZ, Jin WL. The updated landscape of tumor microenvironment and drug repurposing. Signal Transduct Target Ther. 2020;5(1):166.
3. Cendrowicz E, Sas Z, Bremer E, Rygiel TP. The Role of Macrophages in Cancer Development and Therapy. Cancers. 2021;13(8).
4. Beltraminelli T, De Palma M. Biology and therapeutic targeting of tumour-associated macrophages. J Pathol. 2020;250(5):573-92.
5. Larionova I, Cherdyntseva N, Liu T, Patysheva M, Rakina M, Kzhyshkowska J. Interaction of tumor-associated macrophages and cancer chemotherapy. Oncoimmunology. 2019;8(7):1596004.
6. Chen Y, Song Y, Du W, Gong L, Chang H, Zou Z. Tumor-associated macrophages: an accomplice in solid tumor progression. Journal of Biomedical Science. 2019;26(1):78.
7. Mills CD, Kincaid K, Alt JM, Heilman MJ, Hill AM. M-1/M-2 macrophages and the Th1/Th2 paradigm. J Immunol. 2000;164(12):6166-73.

8. Murray PJ, Wynn TA. Obstacles and opportunities for understanding macrophage polarization. J Leukoc Biol. 2011;89(4):557-63.
9. Heinrich F, Lehmbecker A, Raddatz BB, Kegler K, Tipold A, Stein VM, et al. Morphologic, phenotypic, and transcriptomic characterization of classically and alternatively activated canine blood-derived macrophages in vitro. Plos One. 2017;12(8):e0183572.
10. Herrmann I, Gotovina J, Fazekas-Singer J, Fischer MB, Hufnagl K, Bianchini R, et al. Canine macrophages can like human macrophages be in vitro activated toward the M2a subtype relevant in allergy. Dev Comp Immunol. 2018;82:118-27.
11. Murray PJ, Allen JE, Biswas SK, Fisher EA, Gilroy DW, Goerdt S, et al. Macrophage activation and polarization: nomenclature and experimental guidelines. Immunity. 2014;41(1):14-20.
12. Hourani T, Holden JA, Li W, Lenzo JC, Hadjigol S, O'Brien-Simpson NM. Tumor Associated Macrophages: Origin, Recruitment, Phenotypic Diversity, and Targeting. Front Oncol. 2021;11:788365.
13. Zilionis R, Engblom C, Pfirschke C, Savova V, Zemmour D, Saatcioglu HD, et al. Single-Cell Transcriptomics of Human and Mouse Lung Cancers Reveals Conserved Myeloid Populations across Individuals and Species. Immunity. 2019;50(5):1317-34.e10.
14. Azizi E, Carr AJ, Plitas G, Cornish AE, Konopacki C, Prabhakaran S, et al. Single-Cell Map of Diverse Immune Phenotypes in the Breast Tumor Microenvironment. Cell. 2018;174(5):1293-308.e36.
15. Monteiro LN, Rodrigues MA, Gomes DA, Salgado BS, Cassali GD. Tumour-associated macrophages: Relation with progression and invasiveness, and assessment of M1/M2 macrophages in canine mammary tumours. Veterinary journal (London, England : 1997). 2018;234:119-25.
16. Day CP, Merlino G, Van Dyke T. Preclinical mouse cancer models: a maze of opportunities and challenges. Cell. 2015;163(1):39-53.
17. Park JS, Withers SS, Modiano JF, Kent MS, Chen M, Luna JI, et al. Canine cancer immunotherapy studies: linking mouse and human. J Immunother Cancer. 2016;4:97.
18. Schiffman JD, Breen M. Comparative oncology: what dogs and other species can teach us about humans with cancer. Philos Trans R Soc Lond B Biol Sci. 2015;370(1673).
19. Mason NJ. Comparative Immunology and Immunotherapy of Canine Osteosarcoma. Adv Exp Med Biol. 2020;1258:199-221.
20. Else RW, Norval M, Neill WA. The characteristics of a canine mammary carcinoma cell line, REM 134. Br J Cancer. 1982;46(4):675-81.

21. Pang LY, Gatenby EL, Kamida A, Whitelaw BA, Hupp TR, Argyle DJ. Global gene expression analysis of canine osteosarcoma stem cells reveals a novel role for COX-2 in tumour initiation. Plos One. 2014;9(1):e83144.
22. Geijtenbeek TB, Kwon DS, Torensma R, van Vliet SJ, van Duijnhoven GC, Middel J, et al. DC-SIGN, a dendritic cell-specific HIV-1-binding protein that enhances trans-infection of T cells. Cell. 2000;100(5):587-97.
23. Domínguez-Soto A, Sierra-Filardi E, Puig-Kröger A, Pérez-Maceda B, Gómez-Aguado F, Corcuera MT, et al. Dendritic cell-specific ICAM-3-grabbing nonintegrin expression on M2-polarized and tumor-associated macrophages is macrophage-CSF dependent and enhanced by tumor-derived IL-6 and IL-10. J Immunol. 2011;186(4):2192-200.
24. He L, Jhong JH, Chen Q, Huang KY, Strittmatter K, Kreuzer J, et al. Global characterization of macrophage polarization mechanisms and identification of M2-type polarization inhibitors. Cell Rep. 2021;37(5):109955.
25. Valeta-Magara A, Gadi A, Volta V, Walters B, Arju R, Giashuddin S, et al. Inflammatory Breast Cancer Promotes Development of M2 Tumor-Associated Macrophages and Cancer Mesenchymal Cells through a Complex Chemokine Network. Cancer Res. 2019;79(13):3360-71.
26. Hu B, Wang Z, Zeng H, Qi Y, Chen Y, Wang T, et al. Blockade of DC-SIGN(+) Tumor-Associated Macrophages Reactivates Antitumor Immunity and Improves Immunotherapy in Muscle-Invasive Bladder Cancer. Cancer Res. 2020;80(8):1707-19.
27. Shao XJ, Xiang SF, Chen YQ, Zhang N, Cao J, Zhu H, et al. Inhibition of M2-like macrophages by all-trans retinoic acid prevents cancer initiation and stemness in osteosarcoma cells. Acta Pharmacol Sin. 2019;40(10):1343-50.
28. Pellizzari G, Hoskin C, Crescioli S, Mele S, Gotovina J, Chiaruttini G, et al. IgE re-programs alternatively-activated human macrophages towards pro-inflammatory anti-tumoural states. EBioMedicine. 2019;43:67-81.
29. Smith TD, Tse MJ, Read EL, Liu WF. Regulation of macrophage polarization and plasticity by complex activation signals. Integr Biol (Camb). 2016;8(9):946-55.
30. Mantovani A, Sica A, Sozzani S, Allavena P, Vecchi A, Locati M. The chemokine system in diverse forms of macrophage activation and polarization. Trends Immunol. 2004;25(12):677-86.
31. Yang M, McKay D, Pollard JW, Lewis CE. Diverse Functions of Macrophages in Different Tumor Microenvironments. Cancer Res. 2018;78(19):5492-503.
32. Danilenko DM, Rossitto PV, Van der Vieren M, Le Trong H, McDonough SP, Affolter VK, et al. A novel canine leukointegrin, alpha d beta 2, is expressed by specific macrophage subpopulations in

tissue and a minor CD8+ lymphocyte subpopulation in peripheral blood. J Immunol. 1995;155(1):35-44.
33. Aziz MH, Cui K, Das M, Brown KE, Ardell CL, Febbraio M, et al. The Upregulation of Integrin α(D)β(2) (CD11d/CD18) on Inflammatory Macrophages Promotes Macrophage Retention in Vascular Lesions and Development of Atherosclerosis. J Immunol. 2017;198(12):4855-67.
34. Lin P, Ji HH, Li YJ, Guo SD. Macrophage Plasticity and Atherosclerosis Therapy. Front Mol Biosci. 2021;8:679797.
35. Miyazaki Y, Vieira-de-Abreu A, Harris ES, Shah AM, Weyrich AS, Castro-Faria-Neto HC, et al. Integrin αDβ2 (CD11d/CD18) is expressed by human circulating and tissue myeloid leukocytes and mediates inflammatory signaling. Plos One. 2014;9(11):e112770.
36. Lim HY, Lim SY, Tan CK, Thiam CH, Goh CC, Carbajo D, et al. Hyaluronan Receptor LYVE-1-Expressing Macrophages Maintain Arterial Tone through Hyaluronan-Mediated Regulation of Smooth Muscle Cell Collagen. Immunity. 2018;49(2):326-41.e7.
37. Chakarov S, Lim HY, Tan L, Lim SY, See P, Lum J, et al. Two distinct interstitial macrophage populations coexist across tissues in specific subtissular niches. Science. 2019;363(6432).
38. Kieu TQ, Tazawa K, Kawashima N, Noda S, Fujii M, Nara K, et al. Kinetics of LYVE-1-positive M2-like macrophages in developing and repairing dental pulp in vivo and their pro-angiogenic activity in vitro. Sci Rep. 2022;12(1):5176.
39. Dollt C, Becker K, Michel J, Melchers S, Weis CA, Schledzewski K, et al. The shedded ectodomain of Lyve-1 expressed on M2-like tumor-associated macrophages inhibits melanoma cell proliferation. Oncotarget. 2017;8(61):103682-92.
40. Ruan C, Meng Y, Song H. CD36: an emerging therapeutic target for cancer and its molecular mechanisms. J Cancer Res Clin Oncol. 2022;148(7):1551-8.
41. Porcellato I, Sforna M, Lo Giudice A, Bossi I, Musi A, Tognoloni A, et al. Tumor-Associated Macrophages in Canine Oral and Cutaneous Melanomas and Melanocytomas: Phenotypic and Prognostic Assessment. Front Vet Sci. 2022;9:878949.
42. Kurahara H, Shinchi H, Mataki Y, Maemura K, Noma H, Kubo F, et al. Significance of M2-polarized tumor-associated macrophage in pancreatic cancer. J Surg Res. 2011;167(2):e211-9.
43. Ohtaki Y, Ishii G, Nagai K, Ashimine S, Kuwata T, Hishida T, et al. Stromal macrophage expressing CD204 is associated with tumor aggressiveness in lung adenocarcinoma. J Thorac Oncol. 2010;5(10):1507-15.
44. Miyasato Y, Shiota T, Ohnishi K, Pan C, Yano H, Horlad H, et al. High density of CD204-positive macrophages predicts worse clinical prognosis in patients with breast cancer. Cancer Sci. 2017;108(8):1693-700.

45. Withers SS, Skorupski KA, York D, Choi JW, Woolard KD, Laufer-Amorim R, et al. Association of macrophage and lymphocyte infiltration with outcome in canine osteosarcoma. Vet Comp Oncol. 2019;17(1):49-60.
46. Katzenelenbogen Y, Sheban F, Yalin A, Yofe I, Svetlichnyy D, Jaitin DA, et al. Coupled scRNA-Seq and Intracellular Protein Activity Reveal an Immunosuppressive Role of TREM2 in Cancer. Cell. 2020;182(4):872-85.e19.
47. Nakamura K, Smyth MJ. TREM2 marks tumor-associated macrophages. Signal Transduct Target Ther. 2020;5(1):233.
48. La Fleur L, Botling J, He F, Pelicano C, Zhou C, He C, et al. Targeting MARCO and IL37R on Immunosuppressive Macrophages in Lung Cancer Blocks Regulatory T Cells and Supports Cytotoxic Lymphocyte Function. Cancer Res. 2021;81(4):956-67.
49. Kamat K, Krishnan V, Dorigo O. Macrophage-derived CCL23 upregulates expression of T-cell exhaustion markers in ovarian cancer. Br J Cancer. 2022;127(6):1026-33.
50. Vandenborre K, Van Gool SW, Kasran A, Ceuppens JL, Boogaerts MA, Vandenberghe P. Interaction of CTLA-4 (CD152) with CD80 or CD86 inhibits human T-cell activation. Immunology. 1999;98(3):413-21.
51. Chen Q, Zhang XH, Massagué J. Macrophage binding to receptor VCAM-1 transmits survival signals in breast cancer cells that invade the lungs. Cancer Cell. 2011;20(4):538-49.
52. Liu Y, Cao X. Characteristics and Significance of the Pre-metastatic Niche. Cancer Cell. 2016;30(5):668-81.
53. Martinez FO, Gordon S. The M1 and M2 paradigm of macrophage activation: time for reassessment. F1000Prime Rep. 2014;6:13.
54. Duweb A, Gaiser AK, Stiltz I, El Gaafary M, Simmet T, Syrovets T. The SC cell line as an in vitro model of human monocytes. J Leukoc Biol. 2022;112(4):659-68.
55. Cao X, Yakala GK, van den Hil FE, Cochrane A, Mummery CL, Orlova VV. Differentiation and Functional Comparison of Monocytes and Macrophages from hiPSCs with Peripheral Blood Derivatives. Stem Cell Reports. 2019;12(6):1282-97.
56. Luque-Martin R, Mander PK, Leenen PJM, Winther MPJ. Classic and new mediators for in vitro modelling of human macrophages. J Leukoc Biol. 2021;109(3):549-60.
57. Nielsen MC, Andersen MN, Møller HJ. Monocyte isolation techniques significantly impact the phenotype of both isolated monocytes and derived macrophages in vitro. Immunology. 2020;159(1):63-74.
58. Chen S, So EC, Strome SE, Zhang X. Impact of Detachment Methods on M2 Macrophage Phenotype and Function. J Immunol Methods. 2015;426:56-61.

59. Rennert K, Nitschke M, Wallert M, Keune N, Raasch M, Lorkowski S, et al. Thermo-responsive cell culture carrier: Effects on macrophage functionality and detachment efficiency. J Tissue Eng. 2017;8:2041731417726428.
60. Andersen MN, Al-Karradi SN, Kragstrup TW, Hokland M. Elimination of erroneous results in flow cytometry caused by antibody binding to Fc receptors on human monocytes and macrophages. Cytometry A. 2016;89(11):1001-9.
61. Solinas G, Schiarea S, Liguori M, Fabbri M, Pesce S, Zammataro L, et al. Tumor-conditioned macrophages secrete migration-stimulating factor: a new marker for M2-polarization, influencing tumor cell motility. J Immunol. 2010;185(1):642-52.
62. Benner B, Scarberry L, Suarez-Kelly LP, Duggan MC, Campbell AR, Smith E, et al. Generation of monocyte-derived tumor-associated macrophages using tumor-conditioned media provides a novel method to study tumor-associated macrophages in vitro. J Immunother Cancer. 2019;7(1):140.
63. Grugan KD, McCabe FL, Kinder M, Greenplate AR, Harman BC, Ekert JE, et al. Tumor-associated macrophages promote invasion while retaining Fc-dependent anti-tumor function. J Immunol. 2012;189(11):5457-66.
64. Dong Q, Liu X, Cheng K, Sheng J, Kong J, Liu T. Pre-metastatic Niche Formation in Different Organs Induced by Tumor Extracellular Vesicles. Front Cell Dev Biol. 2021;9:733627.

Table 1 Overview of clinical characteristics, white blood cell and monocyte counts of the dogs used to isolate blood monocytes and generate macrophages *in vitro*.

Dog nr	Age (years)	Sex	breed	Body weight (kg)	Neutered (Y/N)	White blood cell count/L	Monocyte count/L
1	7	F	English setter	19.2	N	5.7 x10^9	0.3 x10^9
2	1	F	English setter	16.3	N	9.6 x10^9	0.4 x10^9
3	2	F	Labrador retriever	22.8	Y	8.7 x10^9	0.2 x10^9
4	4	F	Labrador retriever	28.1	Y	7.1 x10^9	0.3 x10^9
5	8	M	Labrador retriever	25.4	N	5.8 x10^9	0.2 x10^9
6	1	M	Labrador retriever	28.5	N	9.0 x10^9	0.5 x10^9

Table 2 Overview of the mean Δ median fluorescent intensity (Δ MFI, measured MFI minus fluorescence minus one (FMO) FMI) for the five different macrophage phenotypes (M1, M2, TAM(D17), TAM(KTOSA5), and TAM(REM134)) for each surface marker as measured by flow cytometry.

Phenotype	ΔMFI CD209a	ΔMFI FcεRI	ΔMFI CD11d	ΔMFI CD206	ΔMFI LYVE-1
M1	60140	45209	4893	9607	10048
M2	87375	59330	16104	45473	14056
TAM(D17)	93620	65574	10831	21965	12024
TAM(KTOSA5)	92278	63170	10322	22631	13002
TAM(REM134)	86788	61307	7190	8159	9064

Table 3 Overview of the top 50 differentially expressed genes between the five different macrophage phenotypes (M1, M2, TAM(D17), TAM(KTOSA5), and TAM(REM134). Values are shown in log2 fold change.

Gene name	Gene id	M1	M2	TAM(D17)	TAM(KTOSA5)	TAM(REM134)	P value
TGFB2	00845049765.1	-0,839	3,032	-0,826	-0,885	-0,483	4,55E-10
IL13RA2	00845029028.1	-2,143	4,569	-0,682	-1,339	-0,405	1,14E-09
NHLH1	00845054095.1	-0,583	2,389	-0,598	-0,582	-0,626	7,69E-09
HEYL	00845020794.1	2,890	-0,258	-0,973	-0,823	-0,836	1,09E-08
VTA1	00845019706.1	3,947	-1,455	-0,157	-0,815	-1,520	1,37E-08
SCN4B	00845004942.1	-0,684	2,488	-0,492	-0,601	-0,711	1,77E-08
LPGAT1	00845006230.1	1,422	-0,685	-0,352	-0,201	-0,184	2,99E-08
WARS1	00845007763.1	2,434	-0,037	-0,901	-0,904	-0,593	4,54E-08
CALD1	00845017561.1	-1,501	3,837	-0,900	-0,850	-0,587	3,74E-08
STEAP2	00845019734.1	-2,468	0,732	0,527	0,313	0,896	4,35E-08
LOC480601	00845015842.1	-2,172	2,752	-0,335	-0,133	-0,113	7,12E-08
CALD1	00845017611.1	-0,665	2,413	-0,529	-0,758	-0,461	7,00E-08
CCL17	00845005907.1	0,900	6,599	-2,051	-2,167	-3,282	1,28E-07
EVI2B	00845025541.1	-2,599	0,571	0,638	0,775	0,616	1,82E-07
IL13RA2	00845028771.1	-0,832	2,934	-1,011	-0,411	-0,680	2,25E-07
TFEC	00845011203.1	2,609	-0,621	-0,658	-0,643	-0,687	2,73E-07
GALR1	00845000409.1	-1,725	3,041	-0,441	-0,594	-0,281	2,97E-07
C3	00845018110.1	1,270	3,362	-1,683	-1,402	-1,548	3,43E-07
PIK3CG	00845047153.1	-0,612	1,374	-0,324	-0,339	-0,099	3,34E-07
CHI3L1	00845025239.1	2,260	-1,377	-0,147	0,248	-0,984	4,14E-07
PTGES	00845041265.1	2,784	-3,353	0,161	-1,440	1,848	4,65E-07
ARHGAP35	00845005376.1	-2,198	-0,149	0,857	0,841	0,650	5,27E-07
LAPTM5	00845013024.1	-1,039	-0,131	0,439	0,426	0,305	5,55E-07
SLC24A3	00845051965.1	2,572	-0,998	-0,463	-0,338	-0,772	5,84E-07
ST7	00845014923.1	1,148	-1,657	0,223	0,082	0,204	6,32E-07
TIMMDC1	00845029675.1	-2,162	1,716	0,908	0,823	-1,285	6,25E-07
EPHX2	00845020014.1	2,414	-0,751	-0,534	-0,668	-0,461	6,73E-07
DIXDC1	00845003169.1	2,042	0,327	-1,495	-0,745	-0,129	7,75E-07
LOC608975	00845027160.1	1,315	-2,727	0,465	0,427	0,520	8,82E-07
YEATS4	00845030877.1	1,456	-0,318	-1,722	0,004	0,579	9,23E-07
TEK	00845031961.1	-2,127	-1,593	1,353	1,448	0,918	8,43E-07
ASGR2	00845032057.1	-0,352	1,644	-0,426	-0,411	-0,455	8,97E-07
OCSTAMP	00845034148.1	-1,022	2,220	-0,162	-0,511	-0,525	9,21E-07
GLUL	00845007242.1	2,037	-0,895	-0,407	-0,229	-0,507	9,62E-07
C17orf99	00845026656.1	2,095	3,417	-1,858	-1,691	-1,963	9,83E-07
CXCR2	00845046624.1	-0,941	2,574	-0,491	-0,548	-0,595	1,14E-06
SLC45A3	00845047974.1	-1,056	2,000	-0,312	-0,321	-0,311	1,16E-06
TMEM150C	00845034122.1	3,227	-1,123	-0,769	-0,258	-1,077	1,27E-06
C3	00845017821.1	0,750	2,802	-1,018	-1,414	-1,120	1,4E-06
CR1L	00845004111.1	2,809	0,523	-1,613	-0,611	-1,109	1,52E-06
ACVR1B	00845048330.1	-0,369	-1,284	0,539	0,415	0,698	1,72E-06
IL34	00845009386.1	3,734	-0,874	-1,066	-0,988	-0,806	1,99E-06
OMG	00845025558.1	-2,242	0,695	0,496	0,608	0,443	2,02E-06
UST	00845031673.1	-1,169	2,740	-0,821	-0,668	-0,083	2,23E-06
RBP4	00845034407.1	-1,944	-1,079	1,003	0,924	1,096	2,24E-06
DNM1	00845052062.1	-2,716	0,753	0,639	0,777	0,546	2,27E-06
NUPR1	00845004014.1	1,596	-0,317	-0,428	-0,304	-0,546	2,46E-06
FGL2	00845037473.1	-1,886	0,467	0,357	0,469	0,593	3,11E-06
CD180	00845020654.1	-2,860	0,171	0,504	0,928	1,257	3,2E-06
SCG5	00845055326.1	-1,017	3,015	-0,332	-0,901	-0,766	3,3E-06

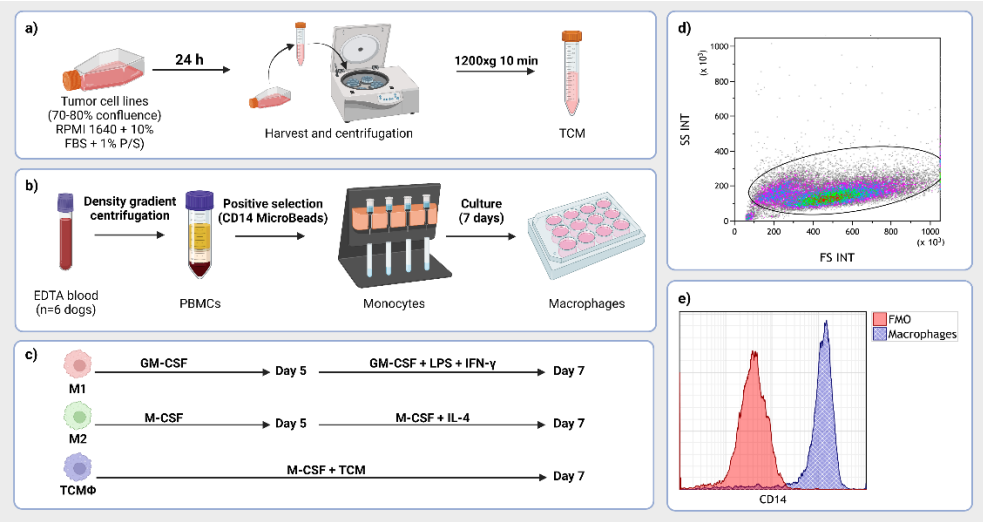

Fig. 1 Schematic representation showing how canine monocyte-derived macrophages were differentiated *in vitro*. **a)** Tumor-conditioned media (TCM) was generated from three different canine cancer cell lines (D17, KTOSA5, and REM134) by incubating cells at 70-80% confluence with fresh medium for 24 hours. TCM was then harvested, centrifuged, and stored at -80ºC. **b)** Peripheral blood mononuclear cells (PBMCs) were isolated from peripheral blood by density gradient centrifugation. Monocytes were isolated from PBMCs using $CD14^+$ magnetic bead isolation on columns, then seeded on plates. **c)** Five distinct macrophage populations (M1, M2, TAM(D17), TAM(KTOSA5), and TAM(REM134)) were generated using different hematopoietic growth factors, cytokines, and TCM. **d)** Scatter-plot showing the resulting macrophages after seven days of differentiation. **e)** Histogram showing a high purity (>95%) of $CD14^+$ cells in the population gated in **d).** The blue histogram represents the anti-CD14 (pacific blue) stained macrophages, and red is the corresponding fluorescence minus one (FMO) control.

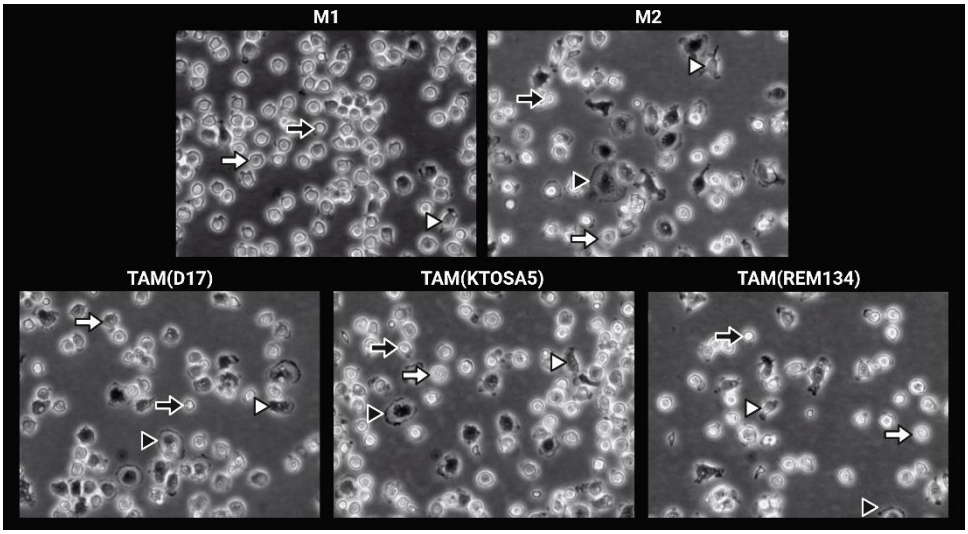

Fig. 2 Inverted microscopy pictures showing the morphologic appearance of the five different macrophage populations generated *in vitro*. Black arrows indicate small round macrophages, white arrows indicate amoeboid macrophages, black arrowheads indicate large flat macrophages and white arrowheads indicate spindeloid macrophages.

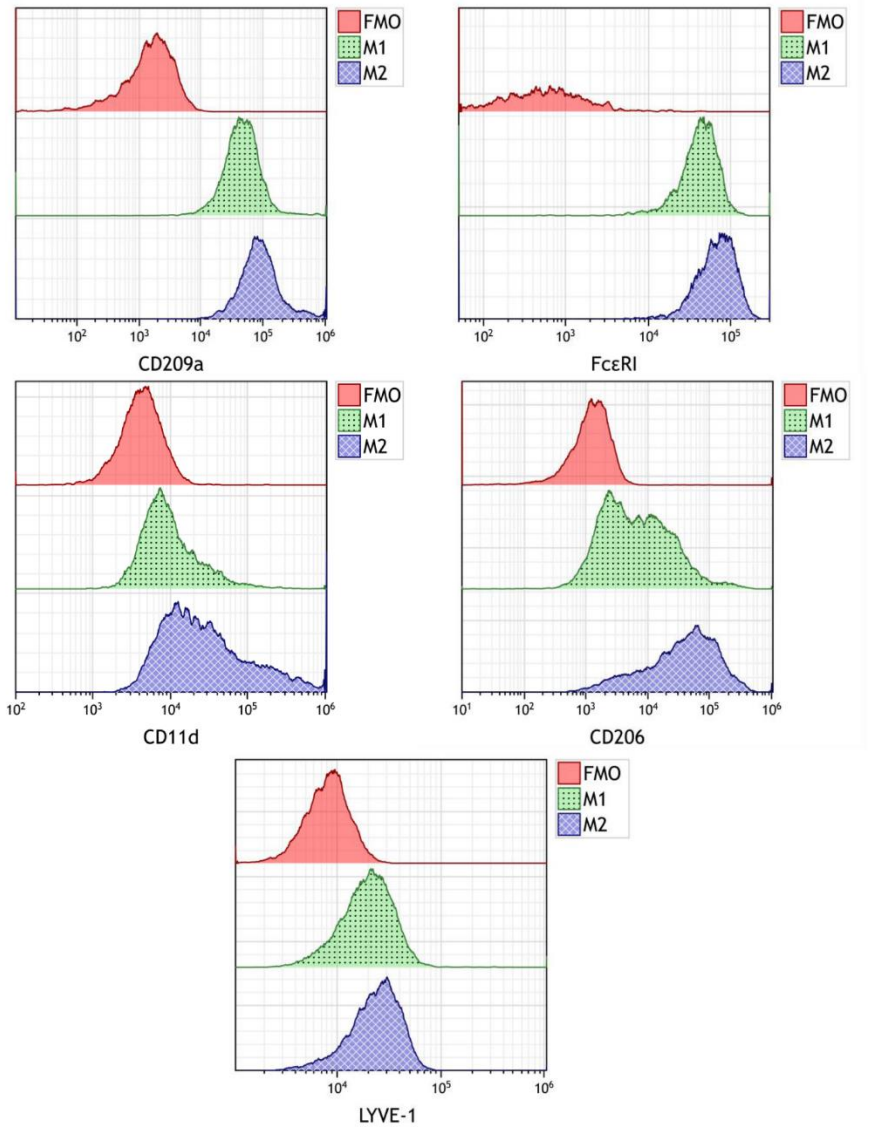

Fig. 3 Overlay of histograms showing the expression of five different surface markers (CD209a, FcεRI, CD11d, CD206, and LYVE-1) of M1 (green dotted) and M2 (blue gridded) macrophages and fluorescence minus one (FMO) controls (red). The Δ median fluorescent intensity (Δ MFI) for all five markers was significantly higher among M2 macrophages than in M1.

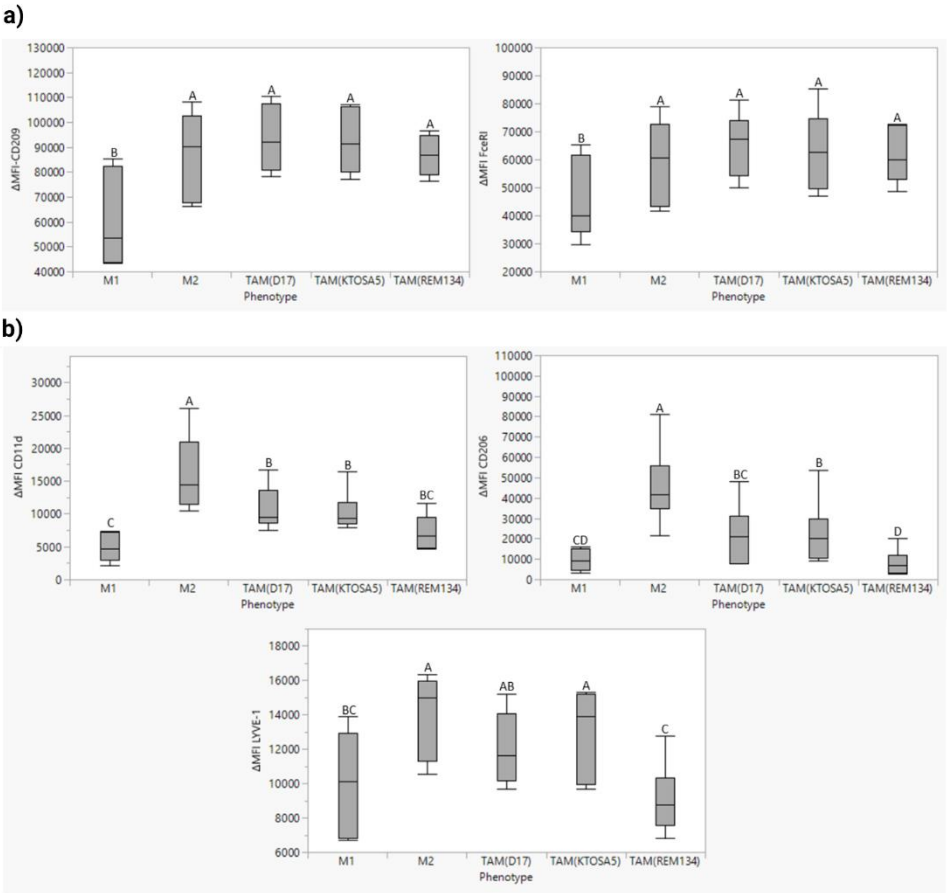

Fig. 4 Cat and whisker plots showing the differences in Δ median fluorescent intensity (Δ MFI, measured MFI minus fluorescence minus one (FMO) FMI) between the five different macrophage populations (M1, M2, TAM(D17), TAM(KTOSA5), and TAM(REM134)) for each surface marker. **a** shows the results for CD209a and FcεRI, while **b** shows the results for CD11d, CD206, and LYVE-1. Populations with different letters are significantly different from each other. Statistical testing was performed using one-way ANOVA followed by post hoc pairwise comparisons using Tukey tests, with P set at .05.

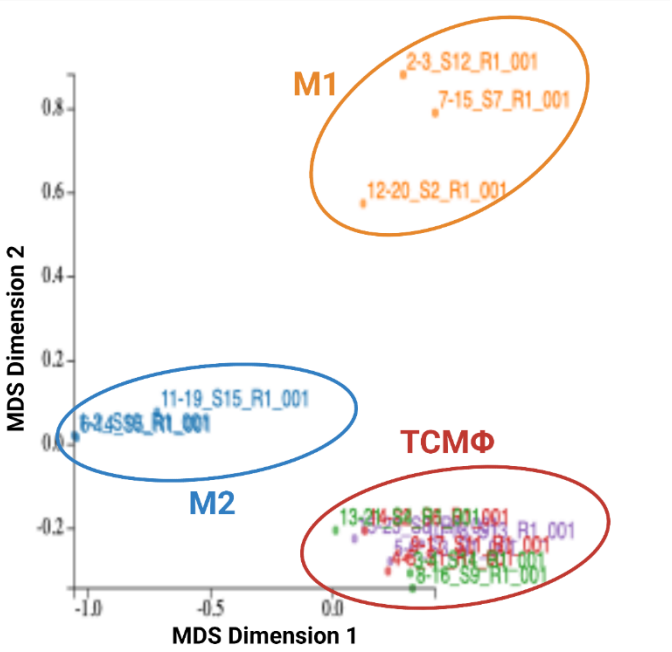

Fig. 5 Multidimensional scaling (MDS) plot showing the relation between the transcriptomes of the five different macrophage populations. M1 (orange, n=3) and M2 (blue, n=3) macrophages form distinct clusters, while the three tumor-conditioned macrophages (TCMΦ) populations (TAM(D17), n=3, TAM(KTOSA5), n=3, and TAM(REM134), n=3) form a third cluster together (red).

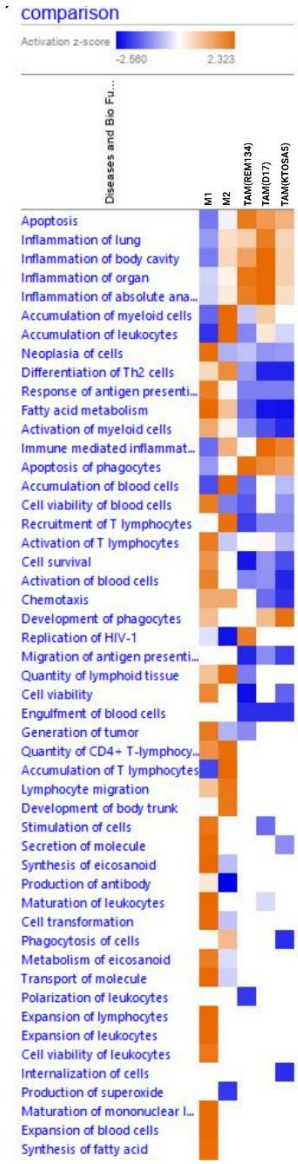

Fig. 6 Pathway analysis showing the 50 most differentially activated pathways between the five different macrophage populations (M1, M2, TAM(D17), TAM(KTOSA5), and TAM(REM134)).

III Paper III

Immunological pre-metastatic niche in dogs with naturally occurring osteosarcoma

Mikael Kerboeuf[1], Kristin Paaske Anfinsen[1], Erling Olaf Koppang[2], Frode Lingaas[2], David Argyle[3], John Teige[2], Bente Sævik[4] and Lars Moe[1]

Institutions: [1] Department of Companion Animal Clinical Sciences, Faculty of Veterinary Medicine, Norwegian University of Life Sciences, [2] Department of Preclinical Sciences and Pathology, Faculty of Veterinary Medicine, Norwegian University of Life Sciences, [3] The Royal (Dick) School of Veterinary Studies and Roslin Institute, University of Edinburgh, [4] AniCura Jeløy Small Animal Hospital (Norway).

Abstract

Pre-metastatic niche (PMN) formation is essential for metastatic development and drives organotropism. Tumor-derived extracellular vesicles and soluble factors remodel the microenvironment of distant metastatic organs before subsequent metastasis. Dogs with osteosarcoma (OS) have proven to be excellent disease models for their human companions. Here we show evidence of PMN formation in dogs with OS before metastasis. The numbers of $CD204^+$ macrophages, $CD206^+$ macrophages and monocytes, and $CD11d^+$ bone marrow-derived cells (BMDCs) are significantly higher in the pre-metastatic lung of dogs with OS than in control dogs. Similarly, the total nucleated cell density is higher before metastasis than in healthy lungs. Once metastases are established, the number of $CD11d^+$ cells is significantly lower than in the pre-metastatic lung. Our study provides evidence of PMN existence in a naturally occurring cancer model similar to those observed in pre-clinical murine models. Dogs with OS may represent ideal candidates for assessing new PMN-targeting therapies.

Introduction

Metastasis is the primary cause of death among cancer patients[1,2]. Different cancers exhibit specific metastatic patterns, a phenomenon first described by Dr. Steven Paget in his "Seed and Soil hypothesis"[3]. Over a century later, the concept of a pre-metastatic niche (PMN) was introduced by Kaplan *et al*, offering an underlying mechanism for the apparent organotropism of metastasis[4]. Since then, PMN-formation has been described in several cancers and different metastatic target organs[5-7]. The PMN is defined as the metastasis-supporting microenvironmental changes that occur in a distant target organ before metastasis[7]. These microenvironmental changes include angiogenesis and vascular permeability, lymphangiogenesis, stromal and metabolic reprogramming, inflammation, and immunosuppression[7]. The primary tumor releases soluble factors and extracellular vesicles (EVs) containing proteins, lipids, mRNA, miRNA, and DNA that remodel the microenvironment at the metastatic sites[5,7]. Tumor-derived EVs show distinctive organotropism and induce PMN-formation in organs that subsequently develop metastasis[8-10]. Metastasis can, to some extent, be blocked when mice are pre-treated with EVs from non-metastatic tumors before tumor transplantation[8-10]. The lungs are a common predilection site for metastasis and have been the focus of many PMN studies. The immunological changes here are attributed mainly to the recruitment of bone marrow-derived cells (BMDCs)[5,7]. Increased numbers of $CD11b^+$ BMDCs, myeloid-derived suppressor cells (MDSCs), $VEGFR1^+$ hematopoietic progenitor cells, monocytes, granulocytes, regulatory T-cells (Tregs), and macrophages have been observed before metastasis[7]. In addition, NK-cell dysfunction and a hampered cytotoxic T-cell response have been demonstrated. Despite findings in murine models, no studies have confirmed that distant PMN occurs in naturally occurring cancers in humans or animals apart from in tumor-draining lymph nodes[11].

Dogs with naturally occurring osteosarcoma (OS) are considered excellent models for their human counterparts[12-17]. OS is the most common primary bone tumor in humans and dogs, with remarkably similar clinical, pathological, molecular, and genetic features[13,14,18]. Furthermore, treatment strategies are the same between the two species, and the disease is more prevalent in dogs than humans. Despite the aggressive nature of OS, with most dogs (>90%) developing pulmonary metastasis after complete surgical excision of the primary tumor, only a small proportion of dogs have visible pulmonary metastases (<15%) or micrometastasis (20% of those without visible metastases) at clinical presentation[19-22].

Here, we show that dogs with naturally occurring OS exhibit similar immunological changes in the lungs before metastasis to those seen in murine PMN models. We provide evidence of PMN existence in a naturally occurring cancer model. The numbers of $CD11d^+$ bone marrow-derived myeloid cells, $CD204^+$ macrophages, and $CD206^+$ macrophages and monocytes are higher in the pre-metastatic lung of dogs with OS than in controls without cancer. Our results suggest that PMN formation occurs in dogs with OS and that they could serve as excellent models for further studies and as a bridge between pre-clinical models and humans.

Results

Clinical data

A total of 25 dogs were included in the study, euthanized, and necropsied between 2012 and 2022. Fifteen cases were included in the OS+ group, five had macroscopic metastases (OS+/Met+) (Supplementary Fig. 1b and 1d), and ten did not (OS+/Met-) (Supplementary Fig 1a and 1c). Ten dogs were included in the control group (OS-/Met-). An overview of clinical characteristics, cause of euthanasia, and time of sampling are summarized in Table 1. The mean age of the OS+/Met+, OS+/Met-, and OS-/Met- groups was 6.6 years (CI 2.6-10.6 years), 6.1 years (CI 4.1-8.1 years), and 4.3 years (CI 2.5-6.1 years) respectively. There were four (40%) females and six males (60%) in each of the OS+/Met- and OS-/Met- groups, and three females (60%) and two males (40%) in the OS+/Met+ group. There were no significant differences in age or sex distribution between groups.

Cases with OS have significantly higher numbers of $CD204^+$ and $CD206^+$ macrophages in the lungs before metastases than controls

The mean number of $CD204^+$ macrophages in the lungs in the OS+/Met- group (mean 78.6, CI 46.4-110.7) was significantly higher than in the OS-/Met- group (mean 41.2, CI 28.9-53.5) (Fig. 3b). However, when normalized to the total number of nucleated cells, the means were no longer significantly different (P=0.054) (Fig. 3c). The mean number of $CD204^+$ cells was not significantly different between the OS+/Met+ and the OS+/Met- or the OS-/Met- groups, nor when normalized to the total number of nucleated cells.

The mean number of $CD206^+$ macrophages was significantly higher in the OS+/Met- group (mean 84.0, CI 41.3-126.8) than in the OS-/Met- group (mean 38.1, CI 27.2-48.9) (Fig. 4b). This difference remained significant when normalized to the total number of nucleated cells (Fig. 4c). The mean number of $CD206^+$ cells was not significantly different between the

OS+/Met+ and the OS+/Met- or the OS-/Met- groups, nor between OS+/Met+ and OS+/Met- when normalized to the total number of nucleated cells. However, the normalized mean number of $CD206^+$ cells was significantly higher in the OS+/Met+ group than in the OS-/Met- group (Fig. 4c).

A subpopulation of $CD206^+$ cells did not express CD204. These $CD204^-CD206^+$ cells' morphology was consistent with interstitial macrophages or monocytes. All alveolar macrophages were $CD204^+$. The mean number of $CD204^-CD206^+$ cells was significantly higher in the OS+/Met- group (mean 14.2, CI 8.6-19.9) than in the OS-/Met- group (mean 4.7, CI 3.4-6.1) (Fig. 5b). This difference remained significant after normalizing to the total number of nucleated cells (Fig. 5c). The mean number of $CD204^-CD206^+$ cells was not significantly different between the OS+/Met+ and the OS+/Met- groups, nor when normalized to the total number of nucleated cells. However, the mean number of $CD204^-CD206^+$ cells was significantly higher in the OS+/Met+ group than in the OS-/Met- group (Fig. 5b), also when normalized to the total number of nucleated cells (Fig. 5c).

Cases with OS have significantly higher numbers of $CD11d^+$ myeloid cells in the lungs before metastasis than those with metastases and controls

The mean number of $CD11d^+$ myeloid cells in the lungs in the OS+/Met- group (mean 77.5, CI 34.7-120.3) was significantly higher than in the OS-/Met- group (mean 19.5, CI 0.0-41.5) (Fig. 6b). This was also the case when normalized to the total number of nucleated cells (Fig. 6c). The mean number of $CD11d^+$ cells was also significantly higher in the OS+/Met- group than in the OS+/Met+ (mean 14.8, CI 0.0-33.0) (Fig. 6b), also when normalized to the total number of nucleated cells (Fig. 6c). The number of $CD11d^+$ cells was not significantly different between the OS+/Met+ group and the OS-/Met- group, nor when normalized to the total number of nucleated cells. $CD11d^+$ cells were almost exclusively $CD206^-$.

The ratio of $CD206^+CD204^+/CD204^+$ macrophages in the lungs remains unchanged in OS cases, compared to controls

The ratio of $CD206^+CD204^+/CD204^+$ cells was similar among all three groups. The ratio in the OS+/Met- group was 0.83 (CI 0.77-0.89), which was not significantly different from the OS-/Met- group (0.76, CI 0.72-0.84), or the OS+/Met+ group (0.81, CI 0.66-0.96), nor was there any difference between the OS-/Met- and OS+/Met+ groups. These $CD206^+CD204^+$double-positive cells represented alveolar and interstitial macrophages.

Some $CD204^+$ cells were $CD206^-$, but there was no significant difference in the mean number between the OS+/Met- and OS-/Met- or the OS+/Met+ groups, nor between the OS+/Met+ and OS-/Met- groups. This was the same when normalized to the total number of nucleated cells.

The total nucleated cell density of the lung tissue is significantly higher in OS cases before metastasis than in controls

The mean number of total nucleated cells ($DAPI^+$ cells) per HPF was significantly higher in the OS+/Met- group (1106.0, CI 949.1-1263.0) than in the OS-/Met- group (778.1, CI 682.6-873.6) (Supplementary Fig. 2). There was, however, no significant difference in the mean number of total nucleated cells between the OS+/Met+ group and the OS+/Met- group or the OS-/Met- group.

Discussion

Despite many reports of PMN formation in distant metastatic target organs in murine models, none have reported evidence of its existence in naturally occurring cancer. Microenvironmental changes compatible with PMN formation have been described in tumor-draining lymph nodes of patients with malignant cancers such as melanoma, cervical cancer, breast cancer, lung cancer, and oral squamous carcinomas [23-28]. In the present study, we have found evidence supporting the existence of a pulmonary PMN in dogs with naturally occurring OS. Dogs with OS had significantly higher numbers of BMDCs, macrophages, and monocytes in the pre-metastatic lungs than dogs without cancer.

One of the main challenges when researching PMN in humans is accessing tissues from metastatic target organs before metastasis occurs. Furthermore, most tissues from human cancer patients have been exposed to treatments that could interfere with the niche. Results from pre-clinical research on new cancer drugs in murine models show a poor correlation with later clinical efficacy in human cancer patients[29,30]. Our findings are similar to those reported in murine xenograft OS models of PMN[31]. Dogs with cancer may therefore represent a unique opportunity, as many owners elect euthanasia over treatment due to financial or ethical reasons or a lack of standardized and effective treatment options. Therefore, many dogs do not receive treatment for their cancer which could affect the PMN.

Previous studies of pulmonary PMN formation have shown that several types of tumors can induce the recruitment of different immune cells to the lungs before metastasis[5,7]. One of the

most striking changes reported is the recruitment of $CD11b^+$ BMDCs[5,7]. In murine xenograft models of OS, most $CD11b^+$ cells also express Gr-1, suggesting they are either neutrophils or granulocytic MDSC[31]. Additionally, MDSC, VLA-4^+ BMDCs, $VEFFR1^+$ BMDCs, macrophages, monocytes, and Tregs are recruited to the lungs before metastasis[5,7]. We found an increased number of $CD11d^+$ cells in the pre-metastatic lung of dogs with OS, which are usually not present in healthy canine lungs[32]. These $CD11d^+$ BMDCs might also have been $CD11b^+$, but this epitope is destroyed by formalin fixation in canine tissues and could not be assessed. $CD11d^+$ is a β2-integrin first described in dogs and expressed by a subset of canine bone marrow macrophages, splenic red pulp macrophages, and lymph node medullary macrophages, as well as a small subset of circulating $CD8^+$ lymphocytes[32]. Canine granulocytic and dendritic cells do not express CD11d, which suggests these positive cells are not neutrophils. In humans, most myeloid cells express CD11d, including circulating monocytes, monocyte-derived macrophages, macrophages, dendritic cells, and neutrophilic granulocytes[33]. In addition, leukocytes in the alveoli and alveolar septa express CD11d under physiologic conditions in humans. Adoptive transfer of MDCS in mice showed that most Gr-1^+CD11b^+ MDSCs differentiate into $F4/80^+CD11b^+$ positive macrophages in tumor tissues[34]. Therefore, it might not be surprising that many BMDCs expressed CD11d in our cases after extravasation into the alveolar septa, as it is considered macrophage-specific in dogs.

We also found an increased number of $CD204^+$ macrophages in the pre-metastatic lung of dogs with OS. This is in line with findings from murine models of pancreatic cancer and salivary cystic carcinoma, where tumor-derived exosomes resulted in increased numbers of $F4/80^+$ macrophages in the liver and the lungs, respectively[35,36]. CD204 is a scavenger receptor expressed by tissue-resident and monocyte-derived macrophages in dogs[37,38]. Alveolar and interstitial macrophages express CD204 under physiologic conditions[37]. The increased number of $CD204^+$ cells reflects an increased total number of macrophages. Whether this increase is due to the local expansion of tissue-resident macrophages or recruited monocyte-derived macrophages is unclear.

The mannose receptor CD206 is a useful M2 macrophage phenotypical marker in humans and mice[39,40]. It has been well established that tumor-associated macrophages (TAMs) have a predominantly M2-skewed tumor-permissive phenotype, with high CD206 expression[41,42]. Similarly, CD206 is highly expressed in canine M2 macrophages, and most TAMs in dogs with malignant mammary tumors express CD206[43,44]. We found an increased number of $CD206^+$ macrophages in the lungs of dogs with OS, suggesting these macrophages have an

M2-skew phenotype and are immunosuppressive and tumor-permissive. Furthermore, dogs with OS had a higher number of $CD204^{-}CD206^{+}$ cells, with morphology compatible with undifferentiated monocytes. This suggests that the increased numbers are partly explained by monocyte recruitment and not due to the expansion of tissue-resident macrophages alone. There was, however, no significant difference in the ratio of $CD206^{+}/CD204^{+}$ cells between groups. As in humans, most alveolar and interstitial macrophages in healthy lungs express CD206 and are considered M2-skewed under physiologic conditions[45]. Furthermore, almost all TAMs in pulmonary metastases were $CD206^{+}$ (Supplementary Fig. 3).

The numbers of positive cells were normalized against the total number of nucleated cells to account for differences in tissue density between dogs. However, we also found that dogs with OS had significantly higher numbers of nucleated cells per HPF in the pre-metastatic lung than controls. The cell density varied more between the groups than between individual dogs. This increase in tissue density was of such a magnitude that it could not only be attributed to the increased numbers of $CD11d^{+}$ BMDCs, macrophages, and monocytes alone. Other leukocyte populations, such as granulocytes and Tregs, or stromal cell populations, such as fibroblasts, could explain the difference.

Interestingly, we found similar numbers of $CD206^{+}$ and $CD204^{+}$ cells in dogs with OS with and without established metastases. However, the number of $CD11d^{+}$ BMDCs was significantly higher among the dogs without metastases than those with established metastases. These results suggest that the recruitment of $CD11d^{+}$ cells might be a transient event necessary for metastatic development and ceases once metastases have developed.

Although we did not explore NK cell dysfunction and hampered cytotoxic $CD8^{+}$ T-cell responses, M2-skewed macrophages and tumor-conditioned macrophages are known to interfere with these responses[46-48]. Similarly, MDSCs in the PMN in mice have been shown to inhibit anti-tumor T-cell responses by expressing Th2 cytokines and reducing IFN-γ production[49]. In addition, MDCSs can inhibit NK-cell mediated cytotoxicity through TGF-β, antigen-presentation by dendritic cells and macrophages through IL-10, and convert effector T-cells into Tregs[50-52]. Since angiogenesis and vascular leakiness are challenging to study in a clinical setting in dogs, we could not explore these aspects of PMN formation. However, M2-skewed macrophages and TAMs secrete vascular endothelial growth factors and matrix metalloproteinase (MMPs) 1, 9, and 12, which can induce angiogenesis and increase vascular permeability [7,53-55].

When examining canine patients with naturally occurring cancer, there is more variation between cases than when performing controlled pre-clinical laboratory experiments. There is inter-tumor variation, host differences such as breed, age, and weight, and environmental and dietary differences. Furthermore, previous diseases or medications could have been missed during retrospective data collection or due to recollection bias in owners when recording the medical history. In addition, the dogs were necropsied and sampled at different time points in their disease progression. The fact that there were significant differences in a relatively small material supports the concept that PMN formation is a common phenomenon in OS.

Chemotherapy and surgery can influence the number of macrophages and their phenotype in the lungs[56-61]. Many chemotherapeutics will drive macrophages toward an M1 polarization, while surgery can increase the number of macrophages in the lungs and shift them toward an M2 polarization. None of the dogs had undergone surgery or received chemotherapy in the present study and not interfere with our results.

Evidence of PMN formation in dogs with OS supports their use as models to assess PMN-targeting drugs. The macrophage-repolarizing drug muramyl tripeptide (MTP) significantly improved survival in dogs with OS after surgical removal of the primary tumor (median survival time of 222 days vs. 77)[62]. MTP can repolarize alveolar macrophages from an M2-skewed phenotype towards an M1 phenotype *in vitro*[63,64]. These dogs received MTP at a time point in their disease process where only microscopic disease was present. A potential explanation for the clinical benefit could be MTP's ability to reprogram the immunosuppressive pulmonary PMN. MTP was also later found to improve survival in human pediatric patients with OS[65].

In conclusion, we found evidence supporting the existence of a PMN in dogs with OS. Furthermore, this is the first report of PMN in a distant metastatic target organ in an organism with naturally occurring cancer. Further studies investigating other aspects of pre-metastatic niche formation in dogs with OS and other highly metastatic cancers are therefore warranted. Dogs with OS may represent excellent candidates for assessing microenvironmental changes in metastatic target tissues and new PMN-targeting drugs.

Material and methods

Study population

The study was conducted as a prospective case series of dogs with OS (OS+) and retrospectively enrolled control dogs without OS (OS-). Dogs in the OS+ group could be of any breed, age, and sex and had to have a histopathological diagnosis of OS at an appendicular site. The dogs in the OS- group were selected retrospectively from the pathology archives. They could be of any breed, age, and sex and had to have been euthanized for another reason than cancer. Dogs were excluded from the study if they had any concurrent or previous neoplastic disease, concurrent systemic inflammatory disease, or clinically detectable atopic or allergic disease. In addition, dogs were excluded if they had received chemotherapy, immunomodulating drugs, radiotherapy, immunotherapy, or surgical treatment for their OS. All included cases were privately owned dogs, and owners had to sign a written consent form before euthanasia and necropsy.

Necropsy and tissue collection

All included dogs underwent standard necropsy after euthanasia. Organs were examined macroscopically, and routine tissue samples were collected (liver, kidneys, spleen, myocardium, and lungs). In addition, tissue samples were collected from any suspected pathological lesions. Dogs in the OS+ group were divided into those having macroscopic metastases (OS+/Met+) and those without (OS+/Met-). Formalin-fixed paraffin-embedded (FFPE) tissues were sectioned, stained with hematoxylin & eosin (H&E), and examined by a pathologist. Additional tissue samples were collected from the peripheral and central regions of each lung lobe from dogs in the OS+ groups. One of the peripheral lung samples was randomly chosen using an online random number generator (www.random.org) for use in this study. Only one tissue sample from the lungs was available from the OS- dogs and used in this study, routinely taken from the peripheral areas.

Immunohistochemical labelling

Tissues for immunohistochemical (IHC) labeling were sectioned from the FFPE blocks. Tissues were sectioned at 4 µm thickness using a microtome, mounted on poly-lysin-coated slides (SuperFrost™ Plus, Thermo Fisher Scientific, Oslo, Norway), and dried at room temperature for one hour. The sections were stored at 4°C for up to 14 days until further staining. IHC labeling was performed using the peroxidase-conjugated immune-polymer method (EnVision+™, Dako, Glostrup, Denmark). First, tissue sections were deparaffinized in xylene and rehydrated through an ethanol gradient using a standard protocol on an automated slide stainer. Next, heat-induced epitope retrieval was performed in a pressure

cooker at 110°C for 10 minutes using Diva Decloaked (Biocare Medical, Histolab, Gothenburg, Sweden). Endogenous peroxidase activity was inhibited by immersing the slides in a 3% H_2O_2 solution in methanol (4°C) for 10 minutes. The sections were blocked using a 1:50 solution of normal goat serum in 5% bovine serum albumin in tris-buffered saline (BSA/TBS) for 30 minutes to prevent unspecific labeling. Sections were incubated with primary antibodies against CD204 (1:100, mouse anti-human, IgG1, clone SRA-E5, Abnova), CD206 (1:1600, rabbit anti-human, IgG, polyclonal, Abcam), and CD11d (1:20, mouse anti-dog, IgG1, clone CA18.3C6, Leukocyte Antigen Laboratory UC Davis), diluted in 1% BSA/TBS for 60 minutes. The samples were incubated with secondary antibodies, polymer-HRP anti-mouse or polymer-HRP anti-rabbit (EnVision+™, Dako, Glostrup, Denmark), for 30 minutes. Immunolabelled tissues were developed using a 3-amino-9-ethyl carbazole (AEC) substrate chromogen (EnVision+™, Dako, Glostrup, Denmark) for 8-12 minutes and counterstained with Mayer's hematoxylin. The slides were mounted with coverslips using a water-soluble mounting medium (Aquatex®, Merck, Darmstadt, Germany) and left to dry at room temperature overnight. Negative controls were stained using the same protocol while omitting the primary antibodies. Washing between steps was done by immersing the slides in three changes of phosphate-buffered saline (PBS) each for 5 minutes at room temperature. All incubations were done at room temperature in a moisture chamber on a rotation table. A section containing pulmonary metastases was used as a positive control for each staining and compared with the immunofluorescent staining (Supplementary Fig. 4).

Immunofluorescent labelling

Tissues for immunofluorescent (IF) labeling were also sectioned from FFPE blocks. IF-labeled tissues were compared to IHC-labeled tissues to ensure similar labeling. Slides were sectioned, deparaffinized, and heat-induced epitope retrieval was performed as described above. The slides were blocked using a 1:50 solution of normal goat serum in 5% BSA/TBS for 30 minutes. Sections were incubated with the same primary antibodies against CD204 (1:100), CD206 (1:1600), and CD11d (1:50), diluted in immunofluorescent buffer (IFB, PBS + 1%BSA + 2% fetal bovine serum, filtered thru a 0.2 µm filter) for 60 minutes at room temperature, in the dark. The samples were incubated with secondary antibodies (1:1000, Alexa fluor 647 goat anti-mouse IgG1 and Alexa fluor 750 goat anti-rabbit IgG, Thermo Fisher), diluted in IFB for 60 minutes at room temperature, in the dark. The three last washing steps were performed by adding DAPI to the wash buffer (1.43 µM, 1:10.000 dilution) for nuclear staining. The slides were mounted with #1.5 coverslips using ProLong™

Diamond Antifade mounting media (Thermo Fisher Scientific, Oslo, Norway) and placed at 4°C until image acquisition within one week. Washing between steps was as described previously using PBS + 0.05% Tween 20. Negative controls were stained using the same protocol while omitting the primary antibodies. As part of the optimization protocol, fluorescent minus one (FMO) controls were labeled by omitting one of the primary antibodies or DAPI to ensure there was no spectral overlap between fluorophores. Single controls were labeled with only one of the primary antibodies or DAPI. In addition, single controls were labeled with single secondary antibodies or a mix of secondary antibodies to ensure there was no cross-reactivity between primary and secondary antibodies. Isotype controls were also run to ensure there was no unspecific labeling by primary antibodies. A positive control from healthy splenic tissue was labeled for each staining.

Microscopic and confocal evaluation

IHC labeled slides were evaluated and imaged using a Zeiss AX10 microscope, equipped with a Zeiss axiocam 506 color camera coupled with Zen pro-2012 (blue edition) image-acquiring software (Carl Zeiss Microscopy GmbH, Jena, Germany). IF-labeled slides were imaged using a Leica Stellaris 8 confocal microscope (Leica Microsystems, Wetzlar, Germany). Ten randomly selected high-power field images (HPF, 200x, equivalent to 0.276mm^2) were acquired from each IF-labeled slide, and immunolabeled cells were automatically quantified using ImageJ 1.51K (National Institute of Health, USA). Briefly, images were opened in ImageJ, converted to 8-bit grayscale, thresholded, inverted, and cells analyzed using the particle analysis tool (Supplementary Fig. 5). The number of CD204$^+$, CD206$^+$, CD11d$^+$, CD204$^-$CD206$^+$, CD204$^+$CD206$^-$ and CD204$^+$CD206$^+$ cells were recorded and normalized against the total number of nuclei in each field to account for variation in tissue density. For the DAPI channel, the fluorophore was exited using the 405 nm laser, and the detector was set to record between 410 and 480 nm. For Alexa fluor 647, the fluorophore was excited by setting the white laser to 645 nm, while the detector was set to record between 650 and 700 nm. In addition, Tau Gating was set to between 0.5 and 5 ns to remove unwanted autofluorescence. For Alexa fluor 750, the white laser was set to 685 nm, and the detector was to record between 750 and 800 nm.

Statistical analysis

All statistical analyses were performed using JMP pro 15.1.0 (SAS Institute Inc., Cary, NC). The mean number of CD204$^+$, CD206$^+$, CD204$^+$CD206$^-$, CD204$^+$CD206$^+$, CD204$^-$CD206$^+$,

CD11d$^+$, and DAPI positive cells per 10 HPF, as well as the number of positive cells normalized to the total nucleated cell count (DAPI positive), was compared between groups using Wilcoxon rank-sum tests for each pair and an unpaired Kruskal-Wallis test. The mean age was compared between groups using Student t-tests, while sex distribution was compared using a Chi-square test. P-values <0.05 were considered statistically significant for statistical testing.

Acknowledgements

The authors would like to acknowledge the technical assistance provided by the laboratory staff (Aleksandra Bodura Göksu, Mari Katharina Aas Ådland, Soheir Chahine Al Taoyl, and Sigbjørn Lunner) at the Unit of Pathology, Department of Preclinical Sciences and Pathology, in processing samples for immunohistochemical and immunofluorescent staining. We would also like to acknowledge Kjetil Dahl (deceased) for his contribution and Evidensia Oslo Animal Hospital for recruiting cases for the study.

Competing interest

The authors declared no potential conflicts of interest with respect to the research, authorship, and/or publication of this article.

Data availability

The data that support the findings of this study are available from the corresponding author upon reasonable request.

Funding

The present study was funded by the Faculty of Veterinary Medicine, Norwegian University of Life Sciences, the Research Fund for Cancer in Dogs, Norway, the Norwegian Research Council (project number 212831/o30), Norway, the Small Animal Practice Veterinary Association's (SVFs) Scientific and Professional Fund (project number 19-209), Norway, the Astri and Birger Torsteds Foundation (project number 2021/22), Norway, and Agria and the Swedish Kennel Klub (SKK) Research Fund (project number N2020-0061), Sweden.

Authors' contributions

MK, FL, BKS, and LM participated in the collection of material. JT performed the histological examination of all tissue samples. MK performed the immunofluorescent staining, image acquisition, and analysis. MK, KPA, EOK, FL, DA, and LM participated in

the interpretation of data. MK, KPA, EOK, FL, DA, JT, BKS, and LM contributed to writing the manuscript. All authors have read and approved the final version of the manuscript.

References

1 Dillekas, H., Rogers, M. S. & Straume, O. Are 90% of deaths from cancer caused by metastases? *Cancer Med* **8**, 5574-5576, doi:10.1002/cam4.2474 (2019).

2 Gupta, G. P. & Massagué, J. Cancer metastasis: building a framework. *Cell* **127**, 679-695, doi:10.1016/j.cell.2006.11.001 (2006).

3 Paget, S. The distribution of secondary growths in cancer of the breast. *The Lancet* **1**, 571-573 (1889).

4 Kaplan, R. N. *et al.* VEGFR1-positive haematopoietic bone marrow progenitors initiate the pre-metastatic niche. *Nature* **438**, 820-827, doi:10.1038/nature04186 (2005).

5 Dong, Q. *et al.* Pre-metastatic Niche Formation in Different Organs Induced by Tumor Extracellular Vesicles. *Front Cell Dev Biol* **9**, 733627, doi:10.3389/fcell.2021.733627 (2021).

6 Wang, H. *et al.* Characteristics of pre-metastatic niche: the landscape of molecular and cellular pathways. *Mol Biomed* **2**, 3, doi:10.1186/s43556-020-00022-z (2021).

7 Liu, Y. & Cao, X. Characteristics and Significance of the Pre-metastatic Niche. *Cancer Cell* **30**, 668-681, doi:10.1016/j.ccell.2016.09.011 (2016).

8 Peinado, H. *et al.* Melanoma exosomes educate bone marrow progenitor cells toward a pro-metastatic phenotype through MET. *Nat Med* **18**, 883-891, doi:10.1038/nm.2753 (2012).

9 Plebanek, M. P. *et al.* Pre-metastatic cancer exosomes induce immune surveillance by patrolling monocytes at the metastatic niche. *Nat Commun* **8**, 1319, doi:10.1038/s41467-017-01433-3 (2017).

10 Wen, S. W. *et al.* The Biodistribution and Immune Suppressive Effects of Breast Cancer-Derived Exosomes. *Cancer Res* **76**, 6816-6827, doi:10.1158/0008-5472.Can-16-0868 (2016).

11 Gillot, L., Baudin, L., Rouaud, L., Kridelka, F. & Noël, A. The pre-metastatic niche in lymph nodes: formation and characteristics. *Cell Mol Life Sci* **78**, 5987-6002, doi:10.1007/s00018-021-03873-z (2021).

12 Morello, E., Martano, M. & Buracco, P. Biology, diagnosis and treatment of canine appendicular osteosarcoma: similarities and differences with human osteosarcoma. *Veterinary journal (London, England : 1997)* **189**, 268-277, doi:10.1016/j.tvjl.2010.08.014 (2011).

13 Withrow, S. J., Powers, B. E., Straw, R. C. & Wilkins, R. M. Comparative aspects of osteosarcoma. Dog versus man. *Clin Orthop Relat Res*, 159-168 (1991).

14 Simpson, S. *et al.* Comparative review of human and canine osteosarcoma: morphology, epidemiology, prognosis, treatment and genetics. *Acta Vet Scand* **59**, 71-81, doi:10.1186/s13028-017-0341-9 (2017).

15 Brodey, R. S. The Use of Naturally Occurring Cancer in Domestic Animals for Research into Human Cancer: General Considerations and a Review of Canine Skeletal Osteosarcoma. *Yale J Biol Med* **52**, 345–361 (1979).

16 Mueller, F., Fuchs, B. & Kaser-Hotz, B. Comparative biology of human and canine osteosarcoma. *Anticancer Res* **27**, 155-164 (2007).

17 Withrow, S. J. & Wilkins, R. M. Cross talk from pets to people: translational osteosarcoma treatments. *ILAR journal* **51**, 208-213 (2010).

18 Federman, N., Bernthal, N., Eilber, F. C. & Tap, W. D. The multidisciplinary management of osteosarcoma. *Current treatment options in oncology* **10**, 82-93, doi:10.1007/s11864-009-0087-3 (2009).

19 Spodnick, G. J. *et al.* Prognosis for dogs with appendicular osteosarcoma treated by amputation alone: 162 cases (1978-1988). *J Am Vet Med Assoc* **200**, 995-999 (1992).

20 Cavalcanti, J. N., Amstalden, E. M. I., Guerra, J. L. & Magna, L. C. Osteosarcoma in dogs: clinical-morphological study and prognostic correlation. *Braz J Vet Res Anim Sci* **41**, 299-305 (2004).

21 Ling, G. V., Morgan, J. P. & Pool, R. R. Primary bone rumors in the dog: a combined clinical, radiographic, and histologic approach to early diagnosis. *J Am Vet Med Assoc* **165**, 55-67 (1974).

22 Kerboeuf, M. *et al.* Early immunohistochemical detection of pulmonary micrometastases in dogs with osteosarcoma. *Acta Vet Scand* **63**, 41, doi:10.1186/s13028-021-00608-9 (2021).

23 Gillot, L. *et al.* Periostin in lymph node pre-metastatic niches governs lymphatic endothelial cell functions and metastatic colonization. *Cell Mol Life Sci* **79**, 295, doi:10.1007/s00018-022-04262-w (2022).

24 Pucci, F. *et al.* SCS macrophages suppress melanoma by restricting tumor-derived vesicle-B cell interactions. *Science* **352**, 242-246, doi:10.1126/science.aaf1328 (2016).

25 Balsat, C. *et al.* A specific immune and lymphatic profile characterizes the pre-metastatic state of the sentinel lymph node in patients with early cervical cancer. *Oncoimmunology* **6**, e1265718, doi:10.1080/2162402x.2016.1265718 (2017).

26 Chung, M. K. *et al.* Lymphatic vessels and high endothelial venules are increased in the sentinel lymph nodes of patients with oral squamous cell carcinoma before the arrival of tumor cells. *Ann Surg Oncol* **19**, 1595-1601, doi:10.1245/s10434-011-2154-9 (2012).

27 Kawai, H., Minamiya, Y., Ito, M., Saito, H. & Ogawa, J. VEGF121 promotes lymphangiogenesis in the sentinel lymph nodes of non-small cell lung carcinoma patients. *Lung Cancer* **59**, 41-47, doi:10.1016/j.lungcan.2007.08.001 (2008).

28 Zhao, Y. C. *et al.* Tumor-derived VEGF-C, but not VEGF-D, promotes sentinel lymph node lymphangiogenesis prior to metastasis in breast cancer patients. *Med Oncol* **29**, 2594-2600, doi:10.1007/s12032-012-0205-0 (2012).

29 Day, C. P., Merlino, G. & Van Dyke, T. Preclinical mouse cancer models: a maze of opportunities and challenges. *Cell* **163**, 39-53, doi:10.1016/j.cell.2015.08.068 (2015).

30 Pan, E., Bogumil, D., Cortessis, V., Yu, S. & Nieva, J. A Systematic Review of the Efficacy of Preclinical Models of Lung Cancer Drugs. *Front Oncol* **10**, 591, doi:10.3389/fonc.2020.00591 (2020).

31 Mazumdar, A. *et al.* Exploring the Role of Osteosarcoma-Derived Extracellular Vesicles in Pre-Metastatic Niche Formation and Metastasis in the 143-B Xenograft Mouse Osteosarcoma Model. *Cancers* **12**, doi:10.3390/cancers12113457 (2020).

32 Danilenko, D. M. *et al.* A novel canine leukointegrin, alpha d beta 2, is expressed by specific macrophage subpopulations in tissue and a minor CD8+ lymphocyte subpopulation in peripheral blood. *J Immunol* **155**, 35-44 (1995).

33 Miyazaki, Y. *et al.* Integrin αDβ2 (CD11d/CD18) is expressed by human circulating and tissue myeloid leukocytes and mediates inflammatory signaling. *Plos One* **9**, e112770, doi:10.1371/journal.pone.0112770 (2014).

34 Corzo, C. A. *et al.* HIF-1α regulates function and differentiation of myeloid-derived suppressor cells in the tumor microenvironment. *J Exp Med* **207**, 2439-2453, doi:10.1084/jem.20100587 (2010).

35 Costa-Silva, B. *et al.* Pancreatic cancer exosomes initiate pre-metastatic niche formation in the liver. *Nature cell biology* **17**, 816-826, doi:10.1038/ncb3169 (2015).

36 Yang, W. W. *et al.* Epiregulin Promotes Lung Metastasis of Salivary Adenoid Cystic Carcinoma. *Theranostics* **7**, 3700-3714, doi:10.7150/thno.19712 (2017).

37 Kato, Y. *et al.* The class A macrophage scavenger receptor CD204 is a useful immunohistochemical marker of canine histiocytic sarcoma. *Journal of comparative pathology* **148**, 188-196, doi:10.1016/j.jcpa.2012.06.009 (2013).

38 Tomokiyo, R. *et al.* Production, characterization, and interspecies reactivities of monoclonal antibodies against human class A macrophage scavenger receptors. *Atherosclerosis* **161**, 123-132, doi:10.1016/s0021-9150(01)00624-4 (2002).

39 Smith, T. D., Tse, M. J., Read, E. L. & Liu, W. F. Regulation of macrophage polarization and plasticity by complex activation signals. *Integr Biol (Camb)* **8**, 946-955, doi:10.1039/c6ib00105j (2016).

40 Mantovani, A. *et al.* The chemokine system in diverse forms of macrophage activation and polarization. *Trends Immunol* **25**, 677-686, doi:10.1016/j.it.2004.09.015 (2004).

41 Hourani, T. *et al.* Tumor Associated Macrophages: Origin, Recruitment, Phenotypic Diversity, and Targeting. *Front Oncol* **11**, 788365, doi:10.3389/fonc.2021.788365 (2021).

42 Yang, M., McKay, D., Pollard, J. W. & Lewis, C. E. Diverse Functions of Macrophages in Different Tumor Microenvironments. *Cancer Res* **78**, 5492-5503, doi:10.1158/0008-5472.Can-18-1367 (2018).

43 Heinrich, F. *et al.* Morphologic, phenotypic, and transcriptomic characterization of classically and alternatively activated canine blood-derived macrophages in vitro. *Plos One* **12**, e0183572, doi:10.1371/journal.pone.0183572 (2017).

44 Monteiro, L. N., Rodrigues, M. A., Gomes, D. A., Salgado, B. S. & Cassali, G. D. Tumour-associated macrophages: Relation with progression and invasiveness, and assessment of M1/M2 macrophages in canine mammary tumours. *Veterinary journal (London, England : 1997)* **234**, 119-125, doi:10.1016/j.tvjl.2018.02.016 (2018).

45 Mitsi, E. *et al.* Human alveolar macrophages predominately express combined classical M1 and M2 surface markers in steady state. *Respir Res* **19**, 66, doi:10.1186/s12931-018-0777-0 (2018).

46 Benner, B. *et al.* Generation of monocyte-derived tumor-associated macrophages using tumor-conditioned media provides a novel method to study tumor-associated macrophages in vitro. *J Immunother Cancer* **7**, 140, doi:10.1186/s40425-019-0622-0 (2019).

47 Pu, J. *et al.* M2 macrophage-derived extracellular vesicles facilitate CD8+T cell exhaustion in hepatocellular carcinoma via the miR-21-5p/YOD1/YAP/β-catenin pathway. *Cell Death Discov* **7**, 182, doi:10.1038/s41420-021-00556-3 (2021).

48 Oishi, S. *et al.* M2 polarization of murine peritoneal macrophages induces regulatory cytokine production and suppresses T-cell proliferation. *Immunology* **149**, 320-328, doi:10.1111/imm.12647 (2016).

49 Yan, H. H. *et al.* Gr-1+CD11b+ myeloid cells tip the balance of immune protection to tumor promotion in the premetastatic lung. *Cancer Res* **70**, 6139-6149, doi:10.1158/0008-5472.Can-10-0706 (2010).

50 Li, H., Han, Y., Guo, Q., Zhang, M. & Cao, X. Cancer-expanded myeloid-derived suppressor cells induce anergy of NK cells through membrane-bound TGF-beta 1. *J Immunol* **182**, 240-249, doi:10.4049/jimmunol.182.1.240 (2009).

51 Beury, D. W. *et al.* Cross-talk among myeloid-derived suppressor cells, macrophages, and tumor cells impacts the inflammatory milieu of solid tumors. *J Leukoc Biol* **96**, 1109-1118, doi:10.1189/jlb.3A0414-210R (2014).

52 Zoso, A. *et al.* Human fibrocytic myeloid-derived suppressor cells express IDO and promote tolerance via Treg-cell expansion. *Eur J Immunol* **44**, 3307-3319, doi:10.1002/eji.201444522 (2014).

53 Jetten, N. *et al.* Anti-inflammatory M2, but not pro-inflammatory M1 macrophages promote angiogenesis in vivo. *Angiogenesis* **17**, 109-118, doi:10.1007/s10456-013-9381-6 (2014).

54 Nakagomi, D. *et al.* Matrix metalloproteinase 12 is produced by M2 macrophages and plays important roles in the development of contact hypersensitivity. *J Allergy Clin Immunol* **135**, 1397-1400, doi:10.1016/j.jaci.2014.10.055 (2015).

55 Jager, N. A. *et al.* Distribution of Matrix Metalloproteinases in Human Atherosclerotic Carotid Plaques and Their Production by Smooth Muscle Cells and Macrophage Subsets. *Mol Imaging Biol* **18**, 283-291, doi:10.1007/s11307-015-0882-0 (2016).

56 Bryniarski, K., Szczepanik, M., Ptak, M., Zemelka, M. & Ptak, W. Influence of cyclophosphamide and its metabolic products on the activity of peritoneal macrophages in mice. *Pharmacol Rep* **61**, 550-557, doi:10.1016/s1734-1140(09)70098-2 (2009).

57 Heath, O. *et al.* Chemotherapy Induces Tumor-Associated Macrophages that Aid Adaptive Immune Responses in Ovarian Cancer. *Cancer Immunol Res* **9**, 665-681, doi:10.1158/2326-6066.Cir-20-0968 (2021).

58 Mantovani, A. & Allavena, P. The interaction of anticancer therapies with tumor-associated macrophages. *J Exp Med* **212**, 435-445, doi:10.1084/jem.20150295 (2015).

59 Kallis, M. P. *et al.* Pharmacological prevention of surgery-accelerated metastasis in an animal model of osteosarcoma. *J Transl Med* **18**, 183, doi:10.1186/s12967-020-02348-2 (2020).

60 Mathenge, E. G. *et al.* Core needle biopsy of breast cancer tumors increases distant metastases in a mouse model. *Neoplasia* **16**, 950-960, doi:10.1016/j.neo.2014.09.004 (2014).

61 Tham, M. *et al.* Macrophage depletion reduces postsurgical tumor recurrence and metastatic growth in a spontaneous murine model of melanoma. *Oncotarget* **6**, 22857-22868, doi:10.18632/oncotarget.3127 (2015).

62 MacEwen, E. G. *et al.* Therapy for osteosarcoma in dogs with intravenous injection of liposome-encapsulated muramyl tripeptide. *J Natl Cancer Inst* **81**, 935-938, doi:10.1093/jnci/81.12.935 (1989).

63 Fidler, I. J., Sone, S., Fogler, W. E. & Barnes, Z. L. Eradication of spontaneous metastases and activation of alveolar macrophages by intravenous injection of liposomes containing muramyl dipeptide. *Proc Natl Acad Sci U S A* **78**, 1680-1684, doi:10.1073/pnas.78.3.1680 (1981).

64 Ogawa, C., Liu, Y. J. & Kobayashi, K. S. Muramyl dipeptide and its derivatives: peptide adjuvant in immunological disorders and cancer therapy. *Curr Bioact Compd* **7**, 180-197, doi:10.2174/157340711796817913 (2011).

65 Meyers, P. A. & Chou, A. J. Muramyl tripeptide-phosphatidyl ethanolamine encapsulated in liposomes (L-MTP-PE) in the treatment of osteosarcoma. *Adv Exp Med Biol* **804**, 307-321, doi:10.1007/978-3-319-04843-7_17 (2014).

Table 1 Overview of clinical characteristics and cause of euthanasia based on clinical records and necropsy findings.

Case	Group	Breed	Sex (M/F)	Age (years)	Year of sampling	Cause of euthanasia
1	OS+/MET+	Mixed breed	M	1	2012	Osteosarcoma, left distal radius
2	OS+/MET+	Giant Schnauzer	F	8	2013	Osteosarcoma, right distal radius
3	OS+/MET+	Irish wolfhound	F	7	2014	Osteosarcoma, right proximal humerus
4	OS+/MET+	Rottweiler	M	9	2013	Osteosarcoma, left distal ulna
5	OS+/MET+	Tervuren	F	8	2014	Osteosarcoma, left distal radius
6	OS+/MET-	Newfoundland dog	M	8	2018	Osteosarcoma, left distal radius
7	OS+/MET-	Siberian husky	M	3	2013	Osteosarcoma, left proximal humerus
8	OS+/MET-	Irish wolfhound	F	6	2013	Osteosarcoma, right distal tibia
9	OS+/MET-	English setter	M	8	2018	Osteosarcoma, right distal ulna
10	OS+/MET-	Pointer	F	4	2016	Osteosarcoma, left distal tibia
11	OS+/MET-	Shar Pei	M	11	2013	Osteosarcoma, right proximal humerus
12	OS+/MET-	Rottweiler	F	9	2015	Osteosarcoma, left proximal humerus
13	OS+/MET-	German shepherd	F	3	2013	Osteosarcoma, left distal radius
14	OS+/MET-	Flat-coated retriever	M	3	2015	Osteosarcoma, left distal radius
15	OS+/MET-	Leonberger	M	6	2016	Osteosarcoma, left distal radius
16	OS-/MET-	Dalmatian	M	8	2016	Urolithiasis
17	OS-/MET-	Shetland Sheepdog	F	1	2020	Behavioral problems
18	OS-/MET-	Chihuahua	M	7	2017	Idiopathic epilepsy
19	OS-/MET-	Jack Russell terrier	M	6	2018	Road traffic accident (hip fracture, tail fracture, perforation jejunum and rectum, perforation bladder)
20	OS-/MET-	Australian shepherd	F	1	2019	Behavioral problems
21	OS-/MET-	Dachshund	M	6	2014	Intervertebral disc disease
22	OS-/MET-	Malinois	M	4	2016	Intervertebral disc disease
23	OS-/MET-	Lagotto Romagnolo	M	1	2018	Vertebral fracture
24	OS-/MET-	Spanish Greyhound	F	4	2015	Behavioral problems
25	OS-/MET-	Dachshund	F	5	2014	Road traffic accident (multiple hip fractures, fracture of sacral bone, subcutaneous, intramuscular, and retroperitoneal bleeding)

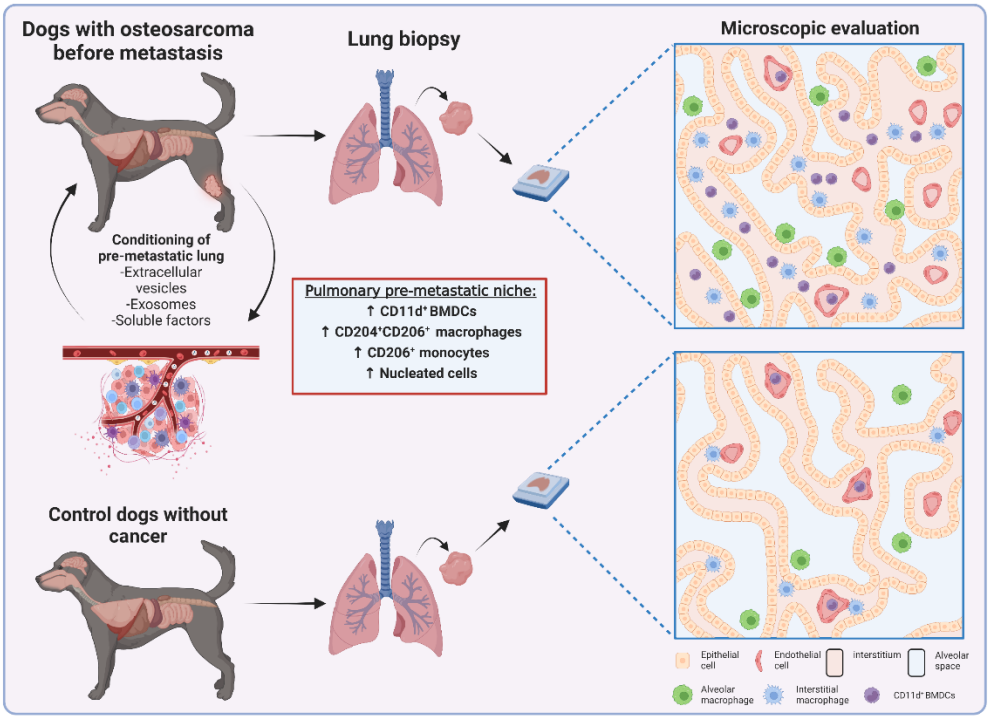

Fig. 1 Schematic representation of the study. Dogs with naturally occurring osteosarcoma (OS) were used as models to study pre-metastatic niche formation. Dogs were necropsied, and lung biopsies were collected from dogs with OS before metastasis had occurred. Dogs with established OS metastases and dogs without cancer were used as controls. There were significantly higher numbers of $CD204^+$ and $CD206^+$ macrophages, $CD206^+$ monocytes, and $CD11d^+$ bone marrow-derived cells (BMDCs) in the lungs before metastasis of OS than in controls without cancer. Furthermore, dogs with established metastases had fewer $CD11d^+$ BMDCs than those without metastases.

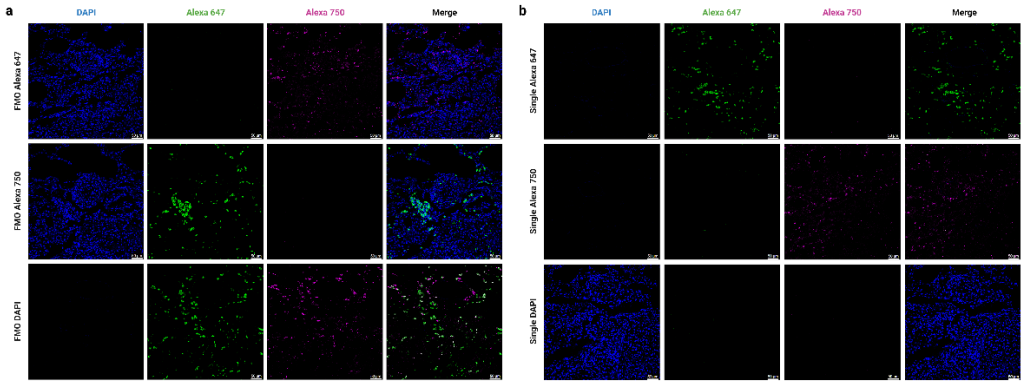

Fig. 2 Fluorescence minus one (FMO) controls and single controls for the antibody panel. **a** FMO controls for DAPI, Alexa fluor 647 (primary antibody mouse anti-CD204), and Alexa Fluor 750 (primary antibody rabbit anti-CD206). In each row, one of the secondary antibodies or DAPI have been omitted, while all primary antibodies have been included. There is no spectral overlap between the channels or unspecific binding of secondary antibodies. **b** Single control for DAPI, Alexa fluor 647 (primary antibody anti-CD204), and Alexa Fluor 750 (primary antibody anti-CD206). In each row, only one of the secondary antibodies or DAPI was used. There is no bleed-thru of signal between channels. Magnification: 200x. Scale bar: 50 µm.

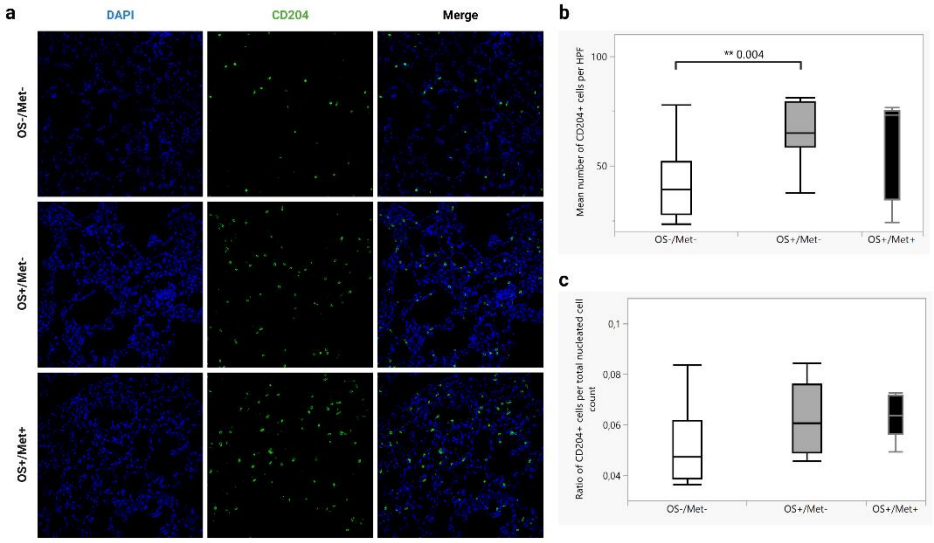

Fig. 3 Dogs with osteosarcoma (OS) have more $CD204^+$ cells in the lungs before metastasis than control dogs. **a** Immunofluorescent staining for CD204 of formalin-fixed paraffin-embedded lung tissue of dogs with OS with metastasis (OS+/Met-), without metastasis (OS+/Met-), and control dogs without cancer (OS-/Met-). Alexa fluor 647 (goat-anti mouse IgG1) was used as the secondary antibody. Magnification 200x. **b** Quantification of the mean number of $CD204^+$ cells per high power field (HPF, 200x magnification, equivalent to $0.276mm^2$) for each group in **a** (10 randomly selected HPF were counted for each dog). $^{**}P < 0.001$ calculated using Wilcoxon rank-sum tests (n= 5 in OS+/Met+, n=10 in OS+/Met-, and n=10 in OS-/Met-). Box plots show mean values and inter quartile ranges. **c** Mean ratios of the number of $CD204^+$ cells per HPF divided by the total number of nucleated cells in the same HPF for each group in **a.** Box plots show mean values and inter quartile ranges.

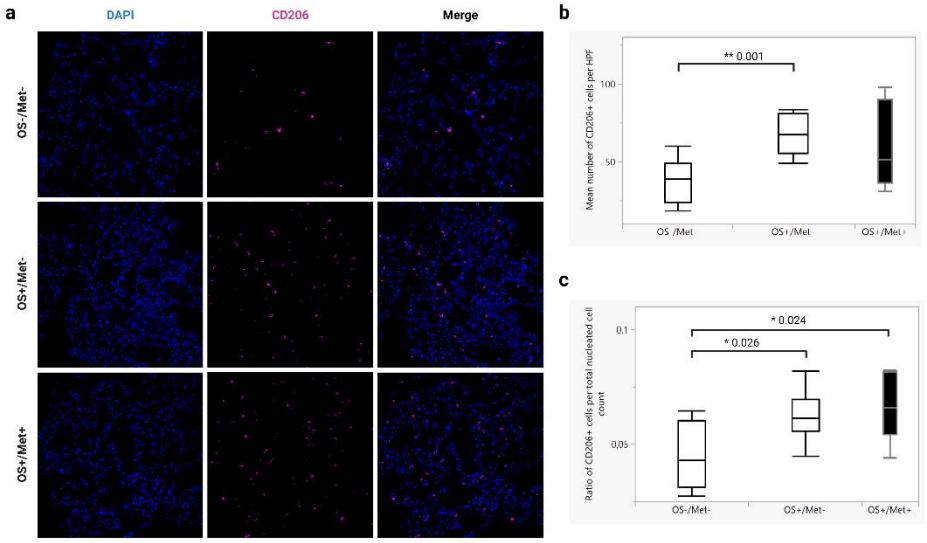

Fig. 4 Dogs with osteosarcoma (OS) have more $CD206^+$ cells in the lungs before metastasis than control dogs. **a** Immunofluorescent staining for CD206 of formalin-fixed paraffin-embedded lung tissue of dogs with OS with metastasis (OS+/Met-), without metastasis (OS+/Met-), and control dogs without cancer (OS-/Met-). Alexa fluor 750 (goat-anti rabbit IgG) was used as the secondary antibody. Magnification 200x. **b** Quantification of the mean number of $CD206^+$ cells per high power field (HPF, 200x magnification, equivalent to $0.276mm^2$) for each group in **a** (10 randomly selected HPF were counted for each dog). $^{**}P<0.001$ calculated using Wilcoxon rank-sum tests (n= 5 in OS+/Met+, n=10 in OS+/Met-, and n=10 in OS-/Met-). Box plots show mean values and inter quartile ranges. **c** Mean ratios of the number of $CD206^+$ cells per HPF divided by the total number of nucleated cells in the same HPF for each group in **a.** $^{*}P < 0.05$ calculated using Wilcoxon rank-sum tests (n= 5 in OS+/Met+, n=10 in OS+/Met-, and n=10 in OS-/Met-). Box plots show mean values and inter quartile ranges.

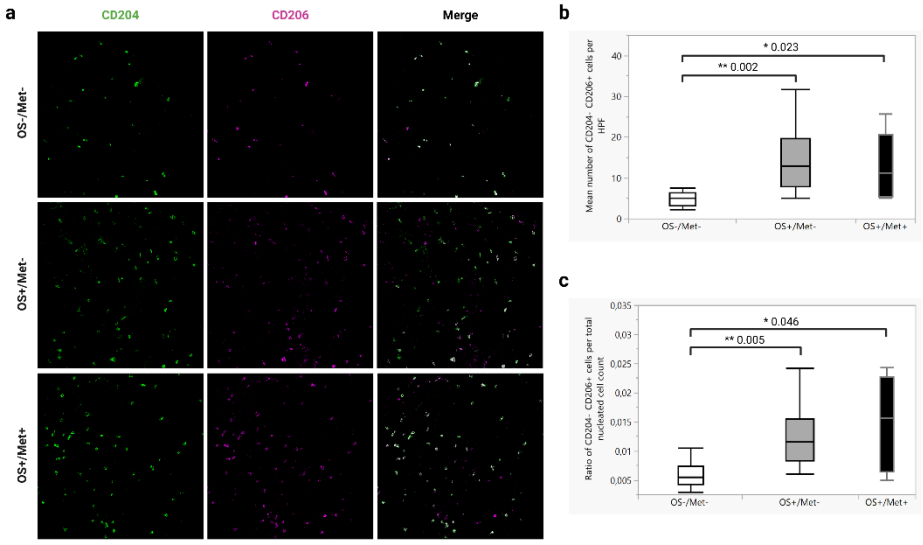

Fig. 5 Dogs with osteosarcoma (OS) have more $CD204^{-}CD206^{+}$ cells in the lungs before and after metastasis than control dogs. **a** Immunofluorescent staining for CD204 and CD206 of formalin-fixed paraffin-embedded lung tissue of dogs with OS with metastasis (OS+/Met-), without metastasis (OS+/Met-), and control dogs without cancer (OS-/Met-). Alexa fluor 647 (goat-anti mouse IgG1) was used as the secondary antibody for CD204 and Alexa fluor 750 (goat-anti rabbit IgG) for CD206. Magnification 200x. **b** Quantification of the mean number of $CD204^{-}CD206^{+}$ cells per high power field (HPF, 200x magnification, equivalent to $0.276mm^2$) for each group in **a** (10 randomly selected HPF were counted for each dog). $^{*}P < 0.05$ and $^{**}P<0.001$ calculated using Wilcoxon rank-sum tests (n= 5 in OS+/Met+, n=10 in OS+/Met-, and n=10 in OS-/Met-). Box plots show mean values and inter quartile ranges. **c** Mean ratios of the number of $CD204^{-}CD206^{+}$ cells per HPF divided by the total number of nucleated cells in the same HPF for each group in **a.** $^{*}P < 0.05$ and $^{**}P<0.001$ calculated using Wilcoxon rank-sum tests (n= 5 in OS+/Met+, n=10 in OS+/Met-, and n=10 in OS-/Met-). Box plots show mean values and inter quartile ranges.

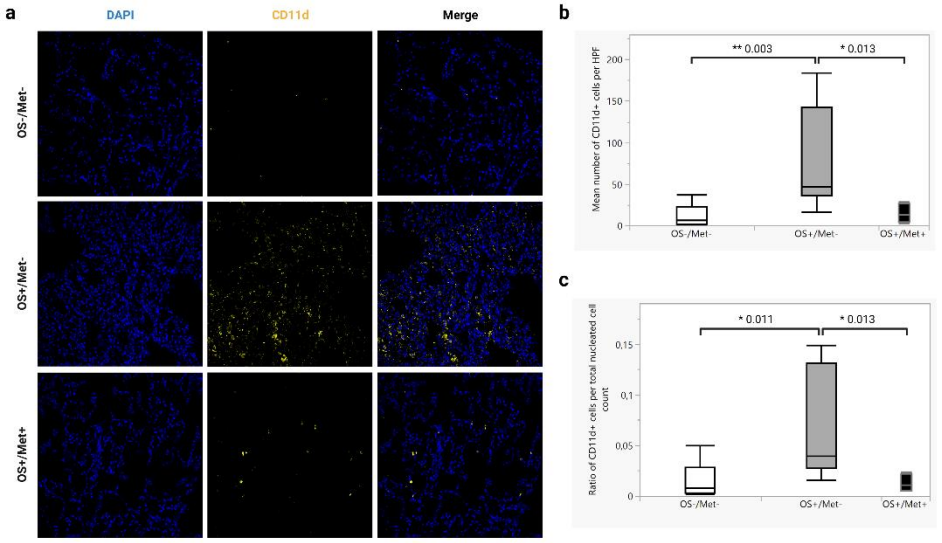

Fig. 6 Dogs with osteosarcoma (OS) have more CD11d$^+$ cells in the lungs before metastasis than those with established metastases and control dogs. **a** Immunofluorescent staining for CD11d of formalin-fixed paraffin-embedded lung tissue of dogs with OS with metastasis (OS+/Met-), without metastasis (OS+/Met-), and control dogs without cancer (OS-/Met-). Alexa fluor 647 (goat-anti mouse IgG1) was used as the secondary antibody. Magnification 200x. **b** Quantification of the mean number of CD11d$^+$ cells per high power field (HPF, 200x magnification, equivalent to 0.276mm^2) for each group in **a** (10 randomly selected HPF were counted for each dog). $^*P < 0.05$ and $^{**}P<0.001$ calculated using Wilcoxon rank-sum tests (n= 5 in OS+/Met+, n=10 in OS+/Met-, and n=10 in OS-/Met-). Box plots show mean values and inter quartile ranges. **c** Mean ratios of the number of CD11d$^+$ cells per HPF divided by the total number of nucleated cells in the same HPF for each group in **a.** $^*P < 0.05$ calculated using Wilcoxon rank-sum tests (n= 5 in OS+/Met+, n=10 in OS+/Met-, and n=10 in OS-/Met-). Box plots show mean values and inter quartile ranges.

Supplementary files

Immunological pre-metastatic niche in dogs with naturally occurring osteosarcoma

Mikael Kerboeuf*, Kristin Paaske Anfinsen, Erling Olaf Koppang, Frode Lingaas, David Argyle, Jon Teige, Bente Kristin Sævik, and Lars Moe*

*Corresponding authors.
E-mail: lars.moe@nmbu.no and
mikael.mathias.kerboeuf@nmbu.no

This PDF file includes:

Supplementary Figure 1-5

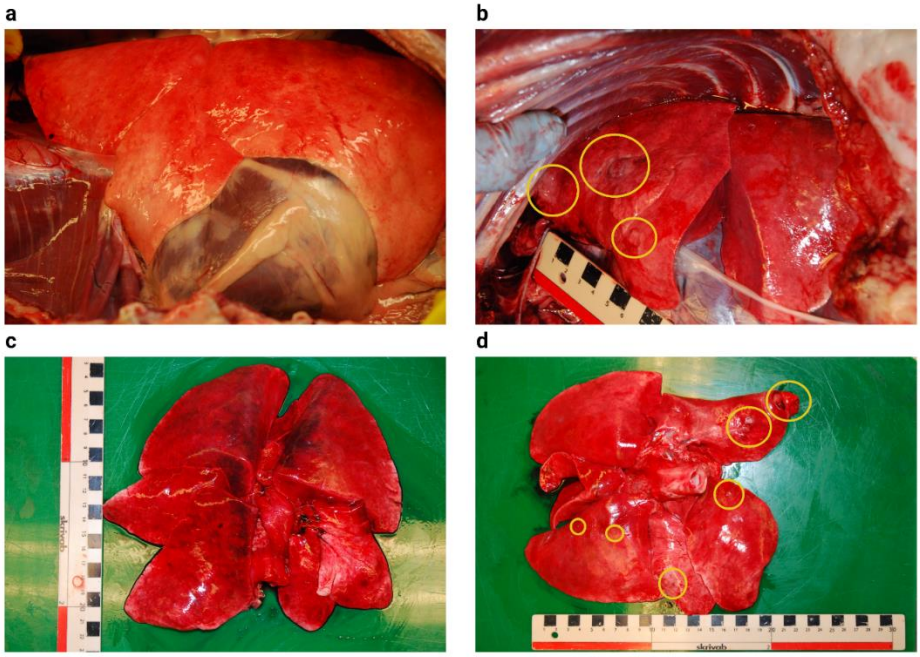

Supplementary Fig. 1 Macroscopic pictures of the lungs of dogs with osteosarcoma (OS) with and without metastasis. **a** Picture of the lungs *in situ* in the right thoracic cavity of a dog with OS without pulmonary metastases. **b** Picture of the lungs *in situ* in the left thoracic cavity of a dog with OS with pulmonary metastases. **c** Picture of the same lungs as in **a** after removal from the dog. **d** Picture of the same lungs as in **d** after removal from the dog. Metastases are shown with yellow circles.

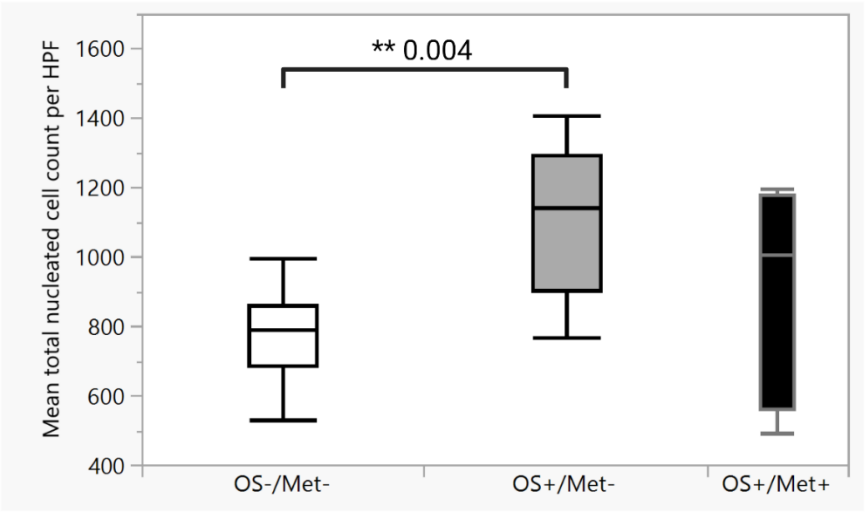

Supplementary Fig. 2 Dogs with osteosarcoma (OS) have a higher total nucleated cell density in the pre-metastatic lung than controls. Quantification of the mean number of $DAPI^+$ cells per high power field (HPF, 200x magnification, equivalent to $0.276mm^2$) for each group (10 randomly selected HPF were counted for each dog). $^{**}P < 0.001$ calculated using Wilcoxon rank-sum tests (n= 5 in OS+/Met+, n=10 in OS+/Met-, and n=10 in OS-/Met-). Box plots show mean values and inter quartile ranges.

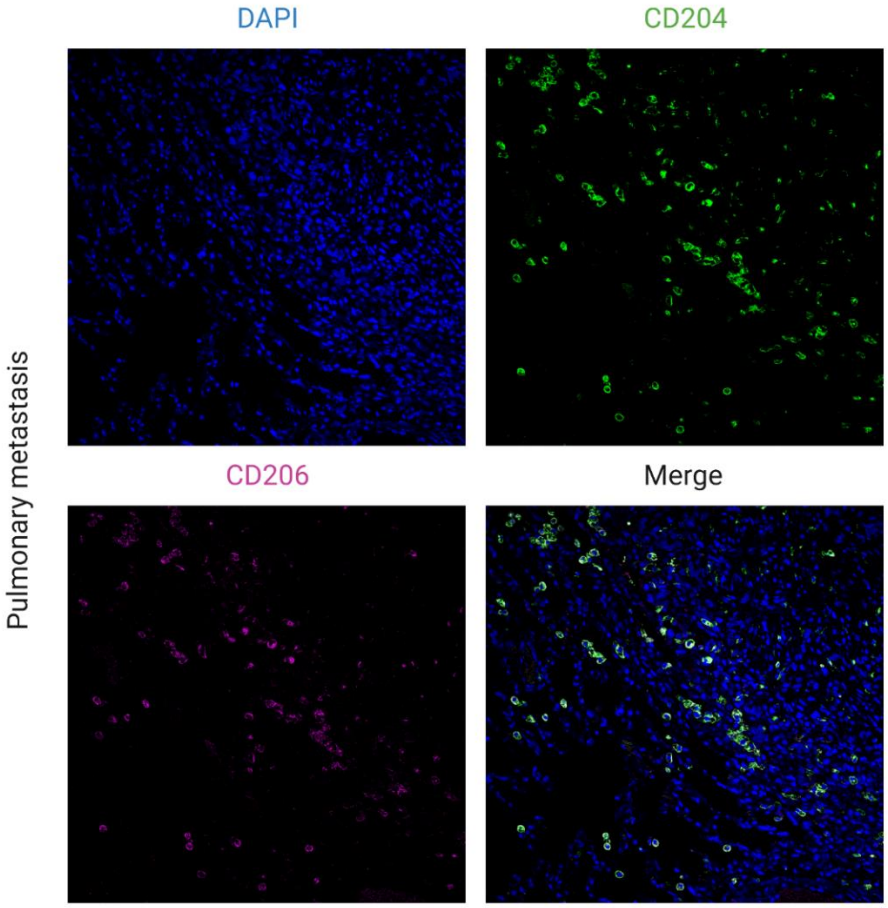

Supplementary Fig. 3 Tumor-associated macrophages (TAMs) within pulmonary metastases of osteosarcoma (OS) express the M2-associated marker CD206. Immunofluorescent staining for CD204, CD206, and DAPI of formalin-fixed paraffin-embedded lung tissue from a dog with OS with metastasis. Alexa fluor 647 (goat-anti mouse IgG1) was used as the secondary antibody for CD204 and Alexa fluor 750 (goat-anti rabbit IgG) for CD206. Magnification 200x. Virtually all TAMs express both CD204 and CD206.

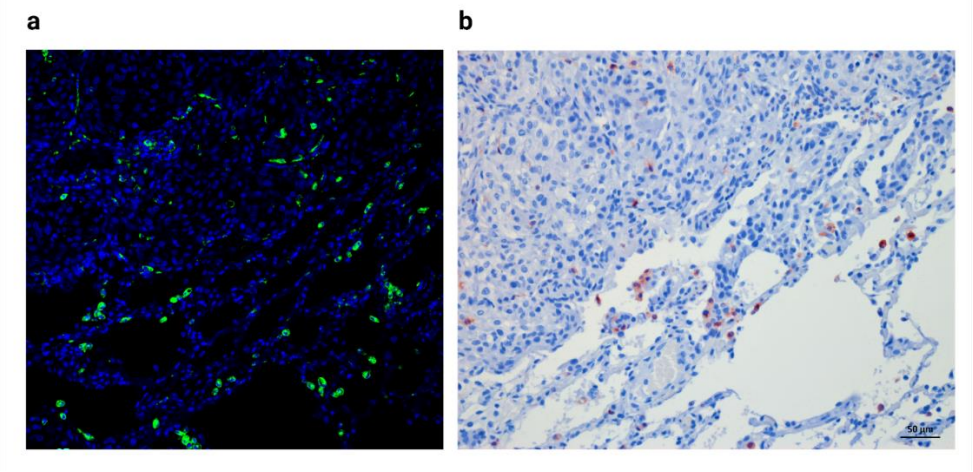

Supplementary Fig. 4 Comparison of immunofluorescence (IF) and chromogen immunohistochemical (IHC) staining for CD204. **a** IF staining for CD204 of formalin-fixed paraffin-embedded lung tissue of a dogs with osteosarcoma with metastasis. Alexa fluor 647 (goat-anti mouse IgG1) was used as the secondary antibody. Magnification 200x. **b** IHC staining for CD204 of the same tissue block. 3-amino-9-ethyl carbazole (AEC) chromogen and Meyer's hematoxylin counterstain. Magnification 200x.

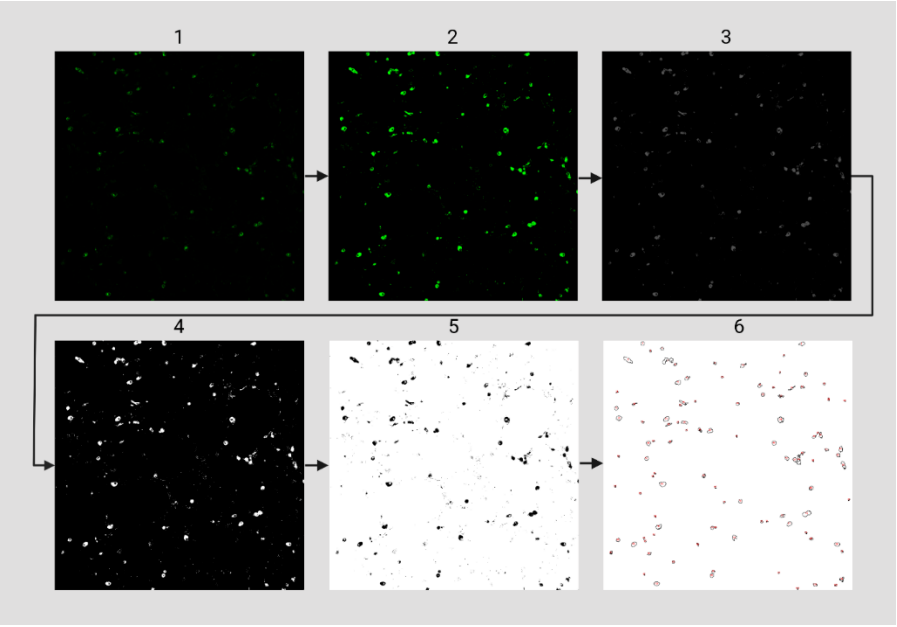

Supplementary Fig. 5 Visualization of automated positive cell quantification using ImageJ. **1** Images were opened in ImageJ and **2** image brightness was adjusted. **3** Images were then then converted to 8-bit grayscale, before **4** threshold was adjusted to remove background noise. **5** Images were then inverted, and holes filled, before **6** the number of positive cells were counted using the particle analysis tool counting particles with a size larger than 20 pixel units.

Errata

[content]

ISBN: 978-82-575-2078-6
ISSN: 1894-6402

Norwegian University
of Life Sciences

Postboks 5003
NO-1432 Ås, Norway
+47 67 23 00 00
www.nmbu.no

11829 / ANDVORDGRAFISK.NO